EXPLORING SELF-ASSEMBLED STILBENOID ARCHITECTURES IN THE PATHWAY FROM MOLECULES TO MATERIALS

THESIS SUBMITTED TO
THE UNIVERSITY OF KERALA
FOR THE DEGREE OF
DOCTOR OF PHILOSOPHY
IN CHEMISTRY
UNDER THE FACULTY OF SCIENCE

By

SHINTO VARGHESE

PHOTOSCIENCES AND PHOTONICS SECTION
CHEMICAL SCIENCES AND TECHNOLOGY DIVISION
NATIONAL INSTITUTE FOR INTERDISCIPLINARY SCIENCE
AND TECHNOLOGY (CSIR), TRIVANDRUM – 695 019
KERALA, INDIA

2010

DECLARATION

I hereby declare that the Ph. D. thesis entitled: *"Exploring Self-Assembled Stilbenoid Architectures in the Pathway from Molecules to Materials"* is an independent work carried out by me at the Photosciences and Photonics Section, Chemical Sciences and Technology Division, National Institute for Interdisciplinary Science and Technology (CSIR), Trivandrum under the supervision of Dr. Suresh Das and it has not been submitted elsewhere for any other degree, diploma or title.

In keeping with the general practice of reporting scientific observations, due acknowledgement has been made wherever the work described is based on the findings of other investigators.

<div align="right">

Shinto Varghese

</div>

National Institute for Interdisciplinary Science and Technology
Council of Scientific and Industrial Research (CSIR)
Industrial Estate P.O.,Trivandrum 695 019
Kerala, INDIA

sureshdas@niist.res.in
Tel.: +91-471-2515220
Fax: +91-471-2491712

Dr. Suresh Das, F. A. Sc.
Director

November 15, 2010

CERTIFICATE

This is to certify that the work embodied in the thesis entitled, *"Exploring Self-Assembled Stilbenoid Architectures in the Pathway from Molecules to Materials"* has been carried out by Mr. Shinto Varghese under my supervision and the same has not been submitted elsewhere for any other degree, diploma or title.

Suresh Das
Research Supervisor

ACKNOWLEDGEMENTS

I have great pleasure in placing on record my deep sense of gratitude to Dr. Suresh Das, my research supervisor, for suggesting the research problem and for his guidance, support and constant encouragement, leading to the successful completion of this work.

I would like to express my sincere thanks to Professor M. V. George for his constant encouragement and inspiration during the tenure of this work.

I thank present and former directors, Professor T. K. Chandrashekar and Dr. B. C. Pai, NIIST, Trivandrum for providing me the necessary facilities and infrastructure of the laboratory for carrying out this work.

My sincere thanks are also due to:

❖ Dr. A. Ajayaghosh, Dr. K. R. Gopidas, Dr. D. Ramaiah and Dr. K. George Thomas, Scientists of the Photosciences and Photonics Section, for all the help and support extended to me.

❖ Dr. Nigam P. Rath, Department of Chemistry, University of Missouri-St. Louis, USA for X-Ray crystallographic analysis, Dr. Krishna Prasad and Dr. Shankar Rao, Center for Liquid Crystal Research Institute, Bangalore for liquid crystalline characterization and Professor G. U. Kulkarni, Chemistry and Physics of Materials Unit, JNCASR, Bangalore for FE-SEM analysis.

❖ Dr. C. H. Suresh, Computational Modeling and Simulation Section, NIIST, Trivandrum for useful discussion regarding single crystal analysis and

CONTENTS

List of Tables

List of Figures

List of Abbreviations

1.	S_1	:	Singlet excited state
2.	S_0	:	Ground State
3.	P	:	Phantom state
4.	$^1p*$	:	Singlet phantom excited state
5.	DPH	:	Dihydrophenanthrene
6.	PICT	:	Planar intramolecular charge transfer state
7.	TICT	:	Twisted intramolecular charge transfer state
8.	ICT	:	Intramolecular charge transfer state
9.	FC	:	Franck Condon state

10.	LE	:	Locally excited state
11.	CD	:	Circular dichroism
12.	LED	:	Light emitting diode
13.	DSC	:	Differential scanning calorimetry
14.	POM	:	Polarized optical microscopy
15.	XRD	:	X-ray diffractometry
16.	Col_h	:	Hexagonal columnar phase
17.	Col_{ob}	:	Oblique columnar phase
18.	Col_r	:	Rectangular columnar phase
19.	TEM	:	Transmission electron microscopy
20.	SEM	:	Scanning electron microscopy
21.	LC	:	Liquid crystals
22.	FWHM	:	Full width at half maximum

PREFACE

The optical and electronic properties of π-conjugated oligomers have recently been the focus of interest mainly because of their potential for use as active elements in various electronic and optoelectronic devices. The photophysical properties of these materials in the bulk phase are not only influenced by the chemical structures of the constituent molecules but also to a large extent by the electronic interaction between the neighbouring molecules, which in turn are controlled by the nature of their intermolecular organization. Thus molecular organization plays a decisive role in defining the functional properties of these materials and the controlled self-assembly of molecules into desired structures within devices can lead to enhanced performances. One of the major challenges in this area of research is therefore to gain a fundamental understanding of the various molecular interactions which control the molecular ordering and the ability to harness them for the design of novel materials with desired molecular organization and functions. Stilbenoid compounds have been extensively investigated from the theoretical and experimental standpoint in view of their importance both as model compounds for polyenes and as functional materials. The photochemical properties of stilbenoid unit have been exploited for the construction of photoresponsive smart materials and the high sensitivity of the photophysical properties to the state of molecular organization provides an effective method to monitor the nature of the molecular packing involved in these materials. In this context, the emphasis of the work described in this thesis is on the investigation of the changes in the photophysical properties with the state of aggregation and on the exploration of the use of donor-acceptor substituted stilbenes as functional units for the construction of functional self-assembled materials. The thesis consists of four Chapters. Chapter 1 provides a brief overview on the photochemical and photophysical properties of stilbenoid

compounds and on their use in the construction of self-assembled soft materials. The role of molecular packing in controlling the photophysical properties of these materials in the self-assembled and solid state are also discussed.

The solid state photophysical properties of a series of donor-acceptor substituted stilbene derivatives with alkoxy groups as donors and the cyano group as the acceptor has been investigated and these studies are described in Chapter 2. The dialkoxy-cyano substituted stilbene derivatives show a red shift in their emission properties with increasing length of their alkyl chains. Since the chromophores in these derivatives are the same, the variation in optical properties with change in alkyl length can be attributed to variations in their molecular packing and these aspects were investigated in detail by single crystal analysis of the stilbene derivatives. A few of the derivatives exhibited a unique thermally induced crystal to crystal transition associated with drastic changes in their colour and photoemissive behaviour. This was attributed to planarization of the molecules followed by their reorganization which facilitated strong excitonic coupling between the nearest neighbour molecules.

Chapter 3 deals with the design, synthesis and investigation of the liquid crystalline and photophysical behaviour of a series of polycatenar mesogens. Polycatenar mesogens generally comprise of a rigid rod shaped core, functionalized with three or more terminal alkyl chains. Interest in these materials arises in view of the fact that inspite of their rod-like core, the mesomorphism of these derivatives is dominated by the formation of columnar phases. The chemical structure of the molecules consists of two alkoxy stilbenoid units attached to a central pyridine core through 1,3,4-oxadiazoles linkers in the 2,5- and 2,6-positions of the pyridine ring to form a rigid rod π-conjugated back bone resulting in a Donor-Acceptor-Donor architecture. These molecules exhibit stable columnar phases in both the heating and cooling cycles. These aspects as well as the photophysical properties of these derivatives have been investigated.

Chapter 4 describes a study involving the synthesis of novel trigonal oxadiazole derivatives and the self-assembly behaviour of these materials in the mesophase as well as their aggregates in solution. Few of the derivatives exhibited enantiontropic columnar discotic liquid crystalline phases with hexagonal as well as oblique two dimensional lattices. Their spontaneous concentration dependent hierarchical self-assembly in non-polar solvents from spheres to nano-fibers wherein the hexagonal columnar order observed in their mesophases was retained was also investigated. The high sensitivity of the luminescence properties of the stilbene chromophore to their state of aggregation provided an effective method to monitor the nature of the molecular packing involved in the various stages of the hierarchical self-assembly. These aspects as well as induction of chirality to the columnar stacks of these molecules and the concentration dependent reversal of chirality on the formation of coiled coil aggregates in solution has also been discussed.

An Introduction to Stilbenoid Materials

Photochemistry of Vision

Electronic Behaviour

Light Emitting Behaviour
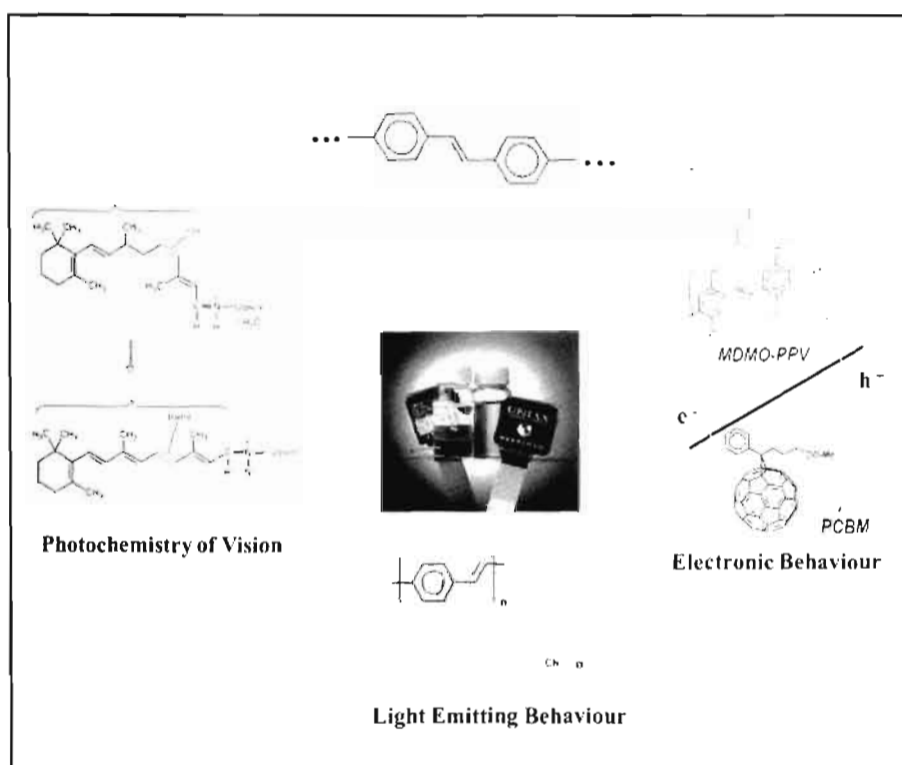
1.1. Abstract

Stilbenoid compounds constitute a major class of π-conjugated materials, which have been widely investigated from an academic as well as from a technological point of view due to their interesting photochemical, photophysical

and electronic properties. These investigations have shown that the major deactivation pathways for the excitation energy in stilbene are torsion induced non-radiative deactivation processes, fluorescence and photochemical processes such as photoisomerization and photodimerization. It has been shown that by suitably selecting the medium and also by suitable derivatization of the stilbenoid moiety, the deactivation processes can be selectively controlled to suit a particular application. In this Chapter, we describe the photochemical and photophysical process of stilbene and related systems. The utility of the stilbenoid systems in the construction of self-assembled materials and the changes in the photophysical properties on their self-assembly in few selected systems. Recent studies related to understanding the role of molecular packing in controlling the photophysical properties of stilbenoid systems in the solid state are also described.

1.2. Introduction

In the past few decades, π-conjugated oligomers and polymers have attracted considerable interest due to their potential applications in electronic and optoelectronic devices [Forrest *et al.* 2004; Schenning *et al.* 2005; Kelley *et al.* 2004; Venema 2008; Alves *et al.* 2008]. An attractive feature of these organic materials is the ability to fine-tune their optical and electronic properties by subtle manipulation of their basic molecular structure [Hoeben *et al.* 2005]. These materials also offer the possibility of developing light weight, low-cost, flexible

and easily processable devices by means of rather simple and low-energy demanding technologies. Prototype systems are currently available and the focus now is on improving device performance. Efficiencies in many of these devices are currently not satisfactory and there is considerable room for improvement. The orientation of π-conjugated molecules plays an important role in improving the performance of devices since anisotropic electronic coupling of organic molecules influences the electrical and optical properties of these materials. One of the reasons identified for the poor efficiency in organic electronics is the lack of long range order in most organic materials [Schenning *et al.* 2005; Hoeben *et al.* 2005]. Self-assembly offers new possibility for the construction of such ordered structures making use of weak intermolecular interactions [Zang *et al.* 2008; Wu *et al.* 2007; Che *et al.* 2007]. In view of this, a wide variety of well ordered π-conjugated materials have been synthesized and studied. Even in the best of materials thus designed, the possibility of formation of defects structures cannot be avoided, since self-assembly is governed by weak intermolecular forces. The challenge to obtain defect free long range ordered self-assembled π-conjugated materials which are of significant importance to the emerging field of organic electronics still remains unmet.
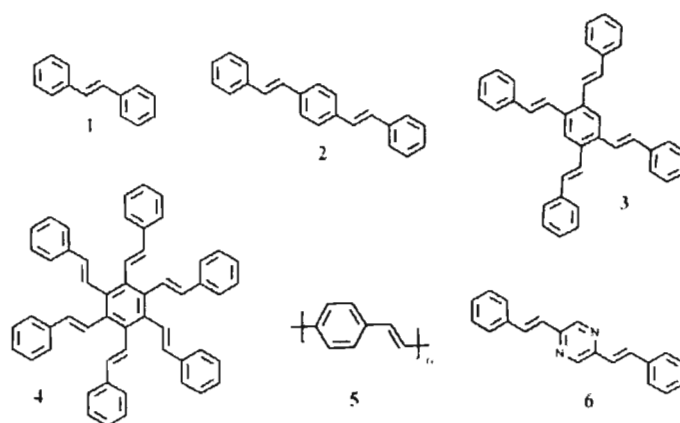
Chart 1.1

Stilbenoid compounds constitute a major class of such π-conjugated materials, which have been widely investigated from the academic as well as technological stand points due to their interesting photochemical, photophysical and electronic properties [Meier 1992]. Stilbenoid materials refer to the materials made up of stilbene units, including oligostyrylarenes (e.g., **2, 3** and **4**, Chart 1.1) and poly(phenylenevinylene)s (**5**, Chart 1.1) [Meier 1992]. Most of these compounds are associated with a strong absorption in the UV/Vis spectrum corresponding to the excitation of π-electrons of the conjugated double bond into π^* orbitals. Substituted chromophores as well as heteroatom substitution in the ring skeleton also fall within the definition of stilbenoid compounds, provided that their substitutions do not result in a completely different photophysical and photochemical character [Meier *et al.* 2008]. The way in which the stilbenoid derivatives respond to light makes them applicable widely as functional materials

in photoresist, imaging, optical switching and related applications [Likhtenshtein 2010]. The optical and electronic properties of stilbenoid compounds can be easily tuned for specific applications, making them one of the most promising molecules among π-conjugated materials and have been extensively used as active materials in electronic and optoelectronic devices [Schenning *et al.* 2005; Hoeben *et al.* 2005]. The latter applications are of emerging interest and the fabrication of cheap, flexible plastic devices using such materials is envisaged. Therefore, developing new stilbenoid materials and investigating their self-assembly behaviour with a view to understanding and manipulating their bulk optical and electronic properties remains an active area of research.

Due to the large number of examples in the literature, in this Chapter, we will discuss only the photochemical and photophysical properties of a selected group of stilbenoids and the influence of self-assembly on these properties. Special emphasis is also made on studies related to their solid state optical properties.

1.3. Photochemistry of Stilbenoid Derivatives

Cis-trans isomerization about a C=C double bond is efficiently used by Nature to trigger a response in biological processes such as in vision [Mathies 1997; Liu *et al.* 1986; Dugave *et al.* 2003]. In view of this, the study of stilbene photochemistry as model compounds for polyenes has attracted immense attention. Irradiation of (*E*)-stilbene chromophores can lead to different products

such as E/Z isomerization, cyclization, cyclodimerization and polymerization (Chart 1.2) [Meier 1992; Waldeck 1991; Likhtenshtein 2009].
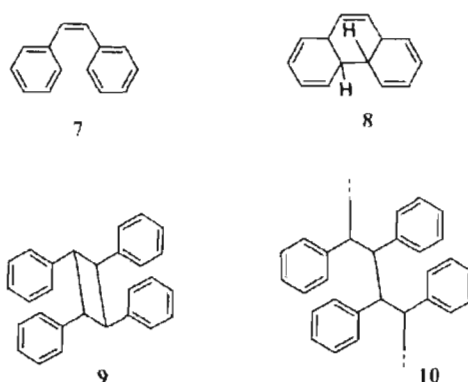
Chart 1.2

Photoisomerization

A schematic representation of the energy surfaces for the ground and excited singlet states of stilbene is shown in Figure 1.1. Upon direct excitation, the molecule reaches the electronically excited singlet state (S_1). This is followed by torsion around the central ethylene bond and rotation of the phenyl rings [Weigel *et al.* 2010; Saltiel *et al.* 1992; Syage *et al.* 1984]. This torsional motion proceeds until a 90° twisted geometry (Phantom singlet excited state) is reached, from which internal conversion to the ground state S_0 through conical intersection can occur. Since the phantom state has a perpendicular geometry, the formation of *trans* and *cis* isomers are of nearly equal probability when the molecule drops back to the S_0 state. Thus the control of their relative population in the

photostationary state depends on which ground state species is being selectively excited. This explains the transformation of the more stable *trans*-isomer to the less stable *cis*-isomer upon photoexcitation of the former.
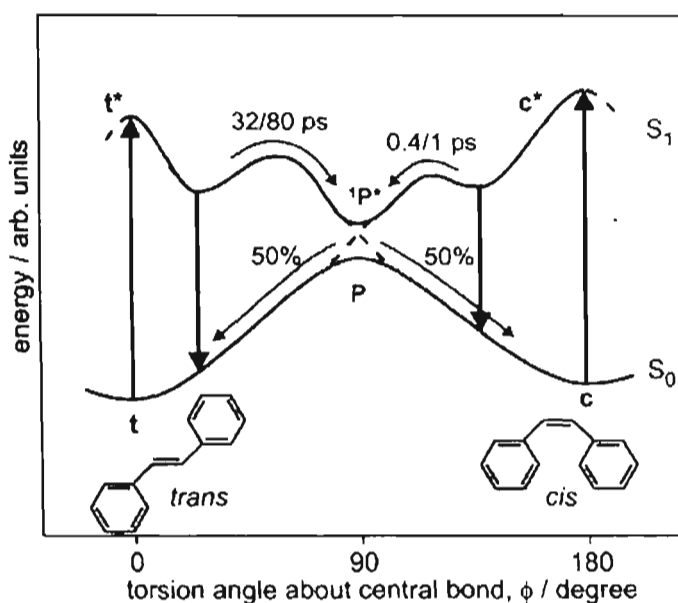
Figure 1.1. Simplified schematic diagram of the ground and excited state potential energy surfaces of stilbene along the reaction coordinate. Adapted from reference [Weigel *et al.* 2010].

For *trans*-stilbene, isomerization is hindered by an activation barrier of ~1200 cm^{-1} on the S_1 potential energy surface resulting in an excited state lifetime of the order of approximately 100 ps [Weigel *et al.* 2010; Saltiel *et al.* 1992; Rothenberger *et al.* 1983; Courtney *et al.* 1988]. In contrast, *cis*-stilbene exhibits only a shallow minimum in S_1 and conversion is complete after 1 ps [Weigel *et al.* 2010; Sumitani *et al.* 1979; Abrash *et al.* 1990; Sension *et al.* 1993; Todd *et al.*

1993; Repinec *et al.* 1991]. The outcome of an isomerization reaction is primed by the relaxation pathway on the excited state potential.

Photoisomerization can proceed either *via* the π, π^* singlet (S_1) or triplet (T_1) excited states and is driven by the properties of the molecule as well as the experimental conditions. However, the population of triplet states for *trans-* and *cis*-stilbene upon direct irradiation is negligible and thus the isomerization from a triplet excited state is normally observed only in the presence of triplet sensitizers. The influence of solvent, pressure and temperature as well as the nature and position of substituents which can strongly influence both the $Z:E$ ratio and isomerization kinetics have been investigated extensively [Saltiel *et al.* 1992; Rothenberger *et al.* 1983; Abrash *et al.* 1990; Todd *et al.* 1993; Yang *et al.* 2006]. The rate of isomerization of stilbene derivatives depends to a large extent upon the nature of the medium. For *trans*-stilbene, the quantum efficiency of photoisomerization generally decreases in constrained media and this can be attributed to torsional decay processes becoming more hindered with increasing solvent viscosity. In many diarylethylenes, photoisomerization of the *trans* isomer does not occur in frozen media because of the close packing of solvent molecules around the planar *trans* structure, resulting in a substantial reduction of the reaction free volume, making it difficult for the one-bond flip mechanism to operate [Yang *et al.* 2006]. The photoreactivity of the corresponding *cis* isomers, however, shows a different medium dependence, with the isomerization remaining

feasible in the frozen media. This can be attributed to less efficient packing of solvent molecules around the bent *cis* isomer, resulting in empty spaces around the molecule. As a result, photoisomerization becomes exclusively *cis* to *trans* in the frozen media [Liu *et al.* 1986; Liu *et al.* 2005; Ramamurthy 2003].

Photocyclization

The photocyclization of stilbene can lead to the formation of phenanthrene *via* the Z isomer, which can undergo electrocyclic ring closure involving six π-electrons leading to the formation of the coloured *trans*-dihydrophenanthrene (DHP) derivatives. The latter are generally unstable and can convert back to the corresponding Z isomers either photochemically or thermally by ring opening reactions. *Trans*-dihydrophenanthrene (DHP) can undergo dehydrogenation to form phenanthrenes in the presence of suitable oxidants such as iodine and oxygen (Scheme 1.1). It is reported that geometrical E/Z isomerization can occur in both the lowest excited states of singlet and triplet multiplicity (S_1 and T_1) while cyclization is known to occur only in the singlet manifold [Repinec *et al.* 1991; Caldwell *et al.* 1981]. The oxidative cyclization of stilbenoid compounds is employed widely for the synthesis of a variety of polycondensed arenes [Segura *et al.* 1992].
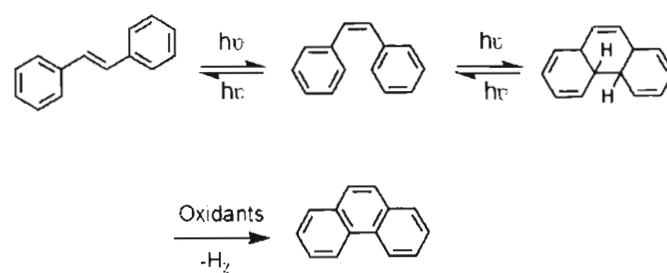
Scheme 1.1.

Photodimerization

The *trans*-stilbene derivatives undergo stereospecific cyclodimerization to yield four membered cyclobutane derivatives at higher concentrations. Upon excitation, the first excited singlet state S_1, undergoes a stereospecific $[2 + 2]$ cycloaddition by diffusion controlled formation of nonfluorescent singlet excimers. These excimers, which lie in the flat energy minima, transform to the minima D^* of doubly excited singlet state of the intermediate with a pericyclic geometry ("pericyclic minimum") which are rapidly deactivated to yield the ground state products as shown in Scheme 1.2 [Meier 1992; Letsinger *et al.* 1994; Brocklehurst *et al.* 1975].

Excimers and pericyclic minima determine the stereochemistry and in the asymmetrical case, also the regiochemistry. Predicting regiochemistry is difficult, since according to perturbation theory, the head-to-head adducts should give the most stable excimers and the head-to-tail adducts the most stable pericyclic

minima [Koutecky *et al.* 1987]. At lower concentrations, dimerization is restricted since the collision by diffusion of the molecules in the first excited singlet state with a dimerization partner is significantly reduced.

$$[\textit{Trans–Stilbene}] \longrightarrow [\textit{Trans–Stilbene}]\ S_1 + [\textit{Trans–Stilbene}]\ S_0$$

$$\longrightarrow [\textit{Trans–Stilbene*} ..... \textit{Trans–Stilbene}]\ S_1 \longrightarrow [\ D^*]$$

[67:33]
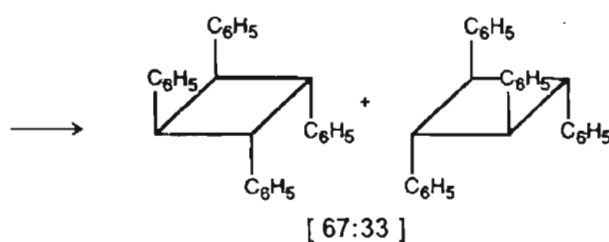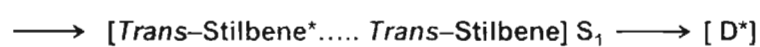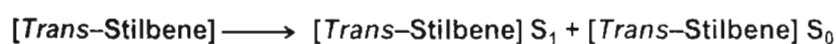
Scheme 1.2. Mechanism of cyclodimerization reaction in *trans*-stilbene. Adapted from reference [Meirer 1992].

Photopolymerization

Photopolymerization is observed in *trans*-stilbenes in condensed phases upon prolonged irradiation. Here the reaction is associated with a favourable arrangement of C=C double bond in the condensed phases. This topic is of significance to photo-crosslinking in polymers through the use of pendent stilbene units (Scheme 1. 3) [Dilling 1983]. The crosslinking can be applied for imaging applications as negative photoresists, because this process converts the soluble organic compounds to insoluble ones, as soon as a certain degree of crosslinking is reached.
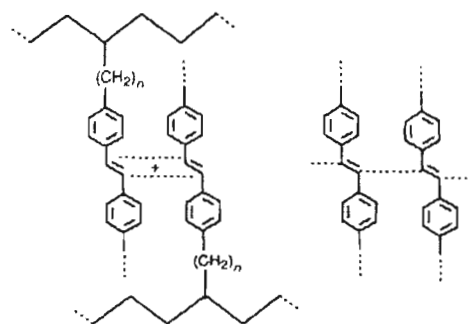
Scheme 1.3. Photo-crosslinking of polymers through stilbene units. Adapted form reference [Meirer 1992].

The possibility of these different photochemical reactions in stilbenoid derivatives is favourable for the construction of photoresponsive materials but act as a deterrent to their use as chromophores for the design of optoelectronic materials. From the point of view of developing optoelectronic materials, it would therefore be of interest to design stilbene based molecules wherein such processes are greatly controlled.

Fluorescence Properties

Deactivation of excited states through fluorescence emission in non-viscous solvents is generally inefficient in stilbene ($\Phi_f = 0.05$ in benzene. $\tau_f = 60$ ps) [Whitten 1993] and related compounds due to the competition with torsion induced non-radiative deactivation processes (Figure 1.1). For *trans*-stilbene, an increase in viscosity in dilute solution leads to an increase in fluorescence efficiency and lifetime with a concurrent decrease in the efficiency of *trans*-to-*cis* photoisomerization [Whitten 1993; Russell *et al.* 1980]. Fluorescence becomes

predominant when the torsional deactivation pathways of the stilbene molecules are restricted.

Figure 1.2. Schematic representation of geometries for PICT and TICT states for donor (D) acceptor (A) substituted conjugated systems. Adapted from reference [Yang *et al.* 2006].

Photoinduced Intramolecular Charge Transfer (ICT) often dictates the excited state behavior of strong electron donor (D)-acceptor (A) substituted conjugated systems such as *trans*-4-(N,N-dimethylamino)-4'-cyanostilbene [Grabowski *et al.* 2003; Pines *et al.* 2003; Lapouyade *et al.* 1992]. In donor-acceptor substituted stilbenes, the existence of two distinct potential minima namely the Planar Intramolecular Charge Transfer state (PICT) and the Twisted Intramolecular Charge Transfer State (TICT) which differ in their geometry and dynamics have been suggested (Figure 1.2.). In nonpolar solvents, it is conceivable that the ICT state dominates through D-A mesomeric interactions which favours a planar geometry (PICT). However, in polar solvents, the opposite extreme of ICT, referred to as TICT, where the D and A fragments are twisted and nearly electronically decoupled, might become energetically more favourable (Figure 1.2) [Yang *et al.* 2006; Zachariasse *et al.* 1996; Zachariasse 2000]. It is assumed that a TICT state allows a larger charge separation and thus possesses a

larger molecular dipole moment and in turn is better solvated in polar solvents (Figure 1.3). In principle, the radiative transition between the TICT and the ground states (S_0) is forbidden and the deactivation of the TICT state is mainly by heat and a lower fluorescence quantum yield for its decay is generally observed [Rettig *et al.* 2000].
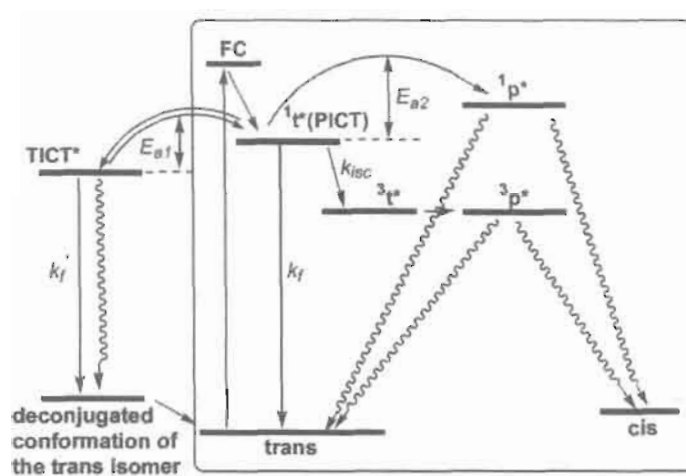
Figure 1.3. Simplified scheme for the formation and decay of the fluorescent ICT state of donor-acceptor substituted stilbenes, where the portion in the square corresponds to the conventional two-state (^{1}t* (PICT) and ^{1}p*) model. Adapted from reference [Yang *et al.* 2006].

Among stilbenoid systems, such TICT behaviour is observed in 4-N,N-dimethylamino-4-cyanostilbene and 4-N,N-dimethylamino-4-nitrostilbene in polar solvents [Yang *et al.* 2006]. Singh and co-workers investigated the fluorescence behaviour of a series of 1,2-diarylethenes and the derivative with CN group as the acceptor and two OMe groups as the donors exhibited solvent polarity-dependent

dual fluorescence, in which the short wavelength fluorescence band is due to the initially excited state, which is electronically delocalized and has a planar geometry [Singh *et al.* 2001]. The long wavelength fluorescence band is attributed to a non-planar TICT state possessing a dipolar character. The schematic representation of the plausible fluorescent excited state structures for dimethoxy-substituted cyano stilbene (11) is shown in Figure 1.4.
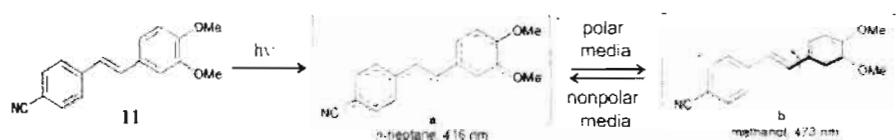
Figure. 1.4. Plausible fluorescent excited state structures for 11: a) Initially excited delocalized, planar state PICT, and b) non-planar TICT state. Adapted from reference [Singh *et al.* 2001].

1.4. Self-Assembled Stilbenoid Soft Materials

The term 'supramolecular' signifies that which is beyond the molecule and supramolecular concepts have had the greatest influence in the construction of complex architectures with well defined shape, size and functions, where the molecules self-assembles in an energetically favouarable way making use of weak intermolecular interactions [Lehn 1995]. The spontaneous self-assembly of molecules to form soft materials is currently a topic of great interest in areas that range from chemistry and biology to materials science. Upon self-assembly the functional properties of molecules are greatly altered and have structural features

and properties that are characteristic not of the molecules themselves but that of extended assemblies. Self-assembly of stilbene and its derivatives have been extensively investigated in order to gain insights on the properties of molecules in their aggregated state [Whitten *et al.* 1998; Song *et al.* 1998; Geiger *et al.* 1999; Wang *et al.* 2000]. The self-assembly behaviour of a large number of stilbenoid based materials have been investigated. Here we describe a few representative studies on such systems.

The aggregation of *trans*-stilbene amphiphiles in micellar media have been thoroughly investigated by Whitten and co-workers. These investigations showed the dependence of the stilbene chemistry on the exact location of the molecules in the micellar systems. Enhancement in fluorescence and a negligible isomerization quantum yield was observed when the stilbene chromophore was embedded in the lipid bilayer at low temperature or in gel phase [Whitten *et al.* 1998; Song *et al.* 1998; Geiger *et al.* 1999].

Whitten and co-workers investigated aggregation behaviour of a gelator containing a cholesterol group tethered to a *trans*-stilbene chromophore (12, Figure 1.5) [Wang *et al.* 2000]. The authors observed that as gel formation commenced, the solution dewetted from the surface, forming circular and elongated droplets, leaving an exposed substrate. Upon further development, fine fibers became dominant at the expense of the sol-phase droplets. The one-dimensional growth of individual fibers suggested continuous stacking of the

gelator molecules, which facilitated the sol-gel phase transition. Further condensation allowed combination of neighbouring fine fibers into thicker ones (Figure 1.5a-f). The one-dimensional helical stacking was evidenced from CD spectroscopic investigation and the schematic representation of the chromophore packing is as shown in Figure 1.5g.
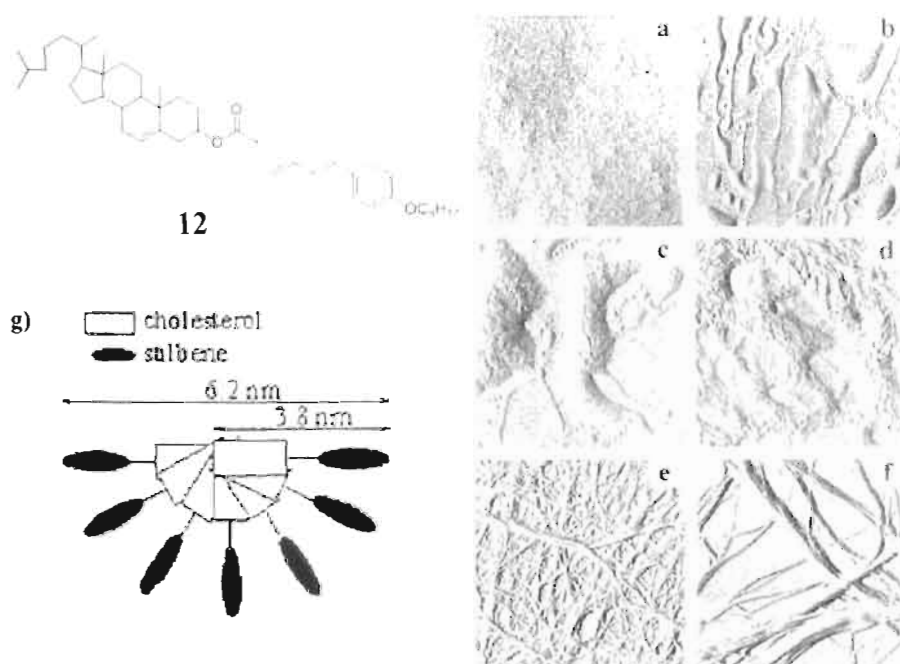
Figure 1.5. Time transient AFM images (in amplitude mode) of sol-gel phase transition. Images were acquired after the heated sol-phase solution (1.6%) was cooled to room temperature for (a) 0, (b) 10, (c) 15, (d) 18, (e) 21, and (f) 31 min. The scale of all the images is 12x12 μm. g) possible helical stacking model of the molecules in a unit fiber. Adapted from reference [Wang *et al.* 2000].

Ajayaghosh *et al.* reported the observation of thermoreversible gelation of fluorescent *p*-phenylenevinylene derivatives through cooperative hydrogen

bonding and π-stack induced self-assembly [Ajayaghosh *et al.* 2007, 2001; George *et al.* 2005]. The authors reported that H-bonding moieties played a crucial role in assisting π-stacking, resulting in room temperature gelation of *p*-phenylenevinylene at relatively low critical gelator concentrations. The schematic representation of the self-assembly in an OPV based gelator is shown in Figure 1.6. Later the same group described a wide variety of OPV derived organogelators and investigated the changes in optical properties on gelation. More recently these gel matrices have been used as scaffolds for facilitating energy transfer processes [Ajayaghosh *et al.* 2008].
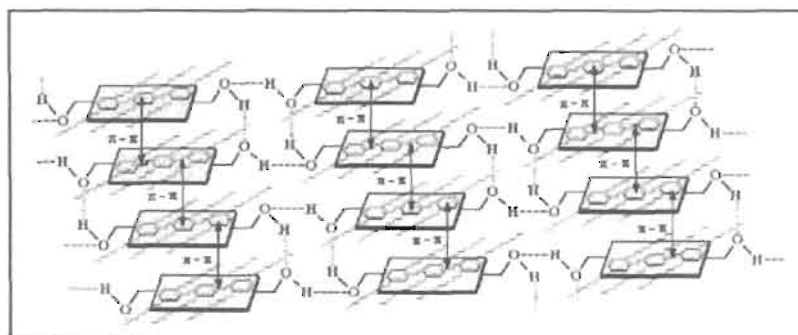
Figure 1.6. Proposed self-assembly of the *p*-phenylenevinylene gel in cyclohexane. Adapted from reference [Ajayaghosh *et al.* 2001].

Hydrogen-bond mediated self-assembly of OPV derivatives in the aggregated state has been extensively studied by Meijer and co-workers [Schenning *et al.* 2001; Jonkheijm *et al.* 2003]. These studies have unraveled many interesting properties of OPV aggregates, particularly related to their

morphological and optical properties [Hoeben *et al.* 2005 (a&b)]. The strategy was to introduce the quadruple hydrogen bonding in the OPV derivatives such as ureido-s-triazine and ureidopyrimidinone.
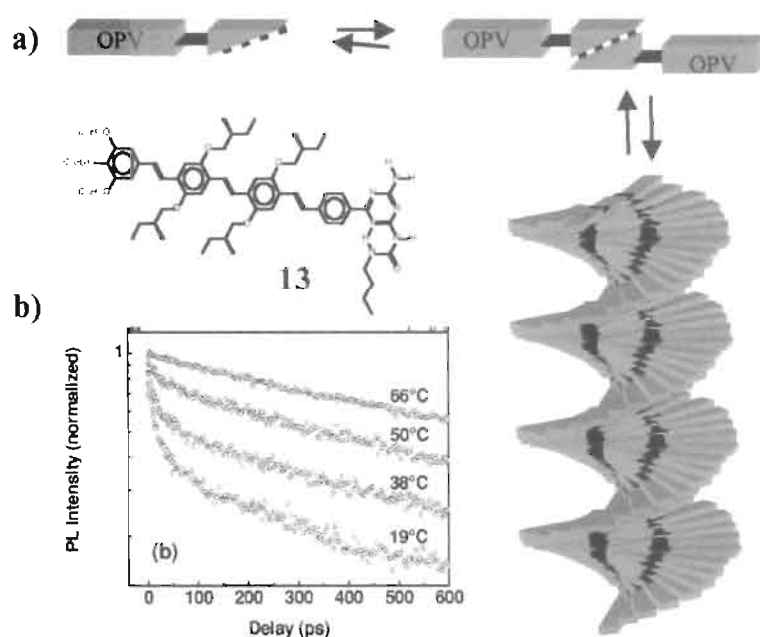
Figure 1.7. a) Schematic representation of the hierarchical organization of **13** in dodecane, b) photoluminescence decay dynamics at 2.226 eV at different temperatures. Adapted from references [Schenning *et al.* 2001, Herz *et al.* 2003].

In apolar solvents, quadruple hydrogen bonding between these groups resulted in a rod shaped π-conjugated structure which grow hierarchically into chiral stacks by solvophobic and π-π interactions (Figure 1.7a). This process was monitored by absorption, emission, CD and by morphological

investigations. Such formation of ordered chiral stacks of OPV molecules using hydrogen-bonding motifs lead to fast exciton diffusion along the stacking axis, as observed from fluorescence decay at variable temperatures (Figure 1.7b). The authors showed the electronic properties of the supramolecular OPV wires are intermediate between molecular crystals and disordered polymeric conductors, i.e., between collective excitation and hopping regimes [Herz *et al.* 2003; Hoeben *et al.* 2005 (a)].

Star-shaped stilbenoid zinc phthalocyanines with π-conjugated OPV (**14**) have been reported by Kimura and co-workers (Figure 1.8) [Kimura *et al.* 2002]. Fluorescence spectroscopy of the stilbenoid phthalocyanines provides evidence of an efficient photoinduced intramolecular energy transfer between the OPV side chains and the phthalocyanine core. OPVs with flexible hexyl tails induced liquid crystallinity in the bulk. Slow cooling from the isotropic phase yielded a hexagonal columnar mesophase driven by π-π and van der Waals interactions. UV/vis absorption spectra of a thin film of (**14**) at 130 °C revealed strong hypsochromic shifts compared to that in solution and X-ray diffraction revealed a stacking interdistance of 3.5 Å. These results confirm that (**14**) self-assembles into one-dimensional columns with a cofacial configuration as shown schematically in Figure 1.8.
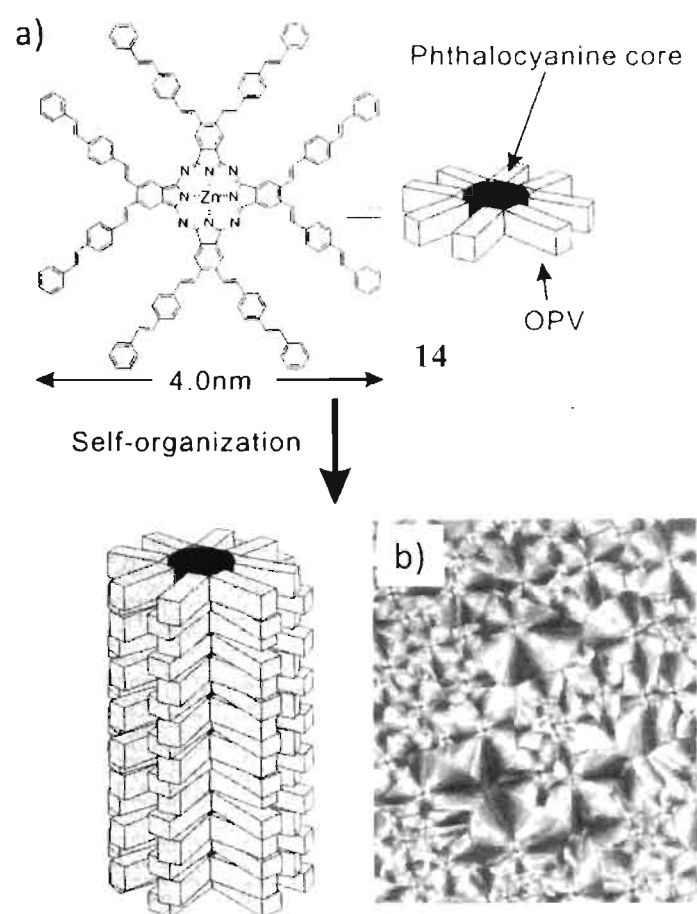
Figure 1.8. a) Schematic representation of the self-organization of stilbene-functionalized phthalocyanines **14** (general structure) into a liquid-crystalline mesophase, b) as visualized under the polarization microscope. Adapted from reference [Kimura *et al.* 2002].

1.5. Solid State Fluorescence of Stilbenoid Derivatives

In 1990, Friend and co-workers developed the first polymer based light emitting diode, which attracted a great deal of attention primarily because of the

enormous potential for the application of such materials in flexible and less energy demanding solid state light emitting devices [Burroughes *et al.* 1990]. In prototype polymer light emitting diodes (LEDs), polyphenylenevinylene (PPV) was used as active material. Ever since, a large number of oligomeric and polymeric stilbenoid derivatives have been synthesized and their photoemissive properties in solid state have been investigated [Shinar 2004]. Numerous studies over recent years have largely contributed to the design of new materials and devices. However, considerable improvement in performance is still required.

Organic materials are known to undergo drastic changes in their optical properties in the solid state compared to that in their solution. The change in optical properties on going from solvated molecules in solutions to aggregated molecules in macroscopic solids are mainly due to reduction of torsion induced non-radiative deactivation processes, migration of excitation energy to distortions, impurity traps or dopants and intermolecular coupling of electronic transition dipole moments. In many instances, it has been shown that solid state optical properties are strongly affected by intermolecular electronic interactions [Kumar *et al.* 2009; Kumar *et al.* 2008; Davis *et al.* 2008; Dong *et al.* 2009, Lewis *et al.* 1997].

For example, the quenching of radiative processes in the solid state often originate from π-π interactions encountered in the crystal lattice of planar conjugated molecules arranged in a cofacial fashion. This architecture leads to the

formation of H-aggregates in the ground state and excimer in the excited state,
which usually exhibit low photoluminescence efficiency [Siddiqui *et al.* 1999;
Cornil *et al.* 2001]. In view of this, development of strategies to prevent quenching
of luminescence efficiency is receiving increasing attention.
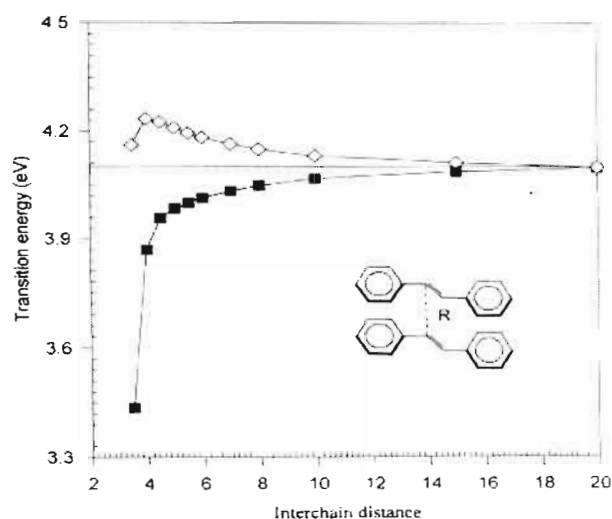
Figure 1.9. INDO/SCI-calculated transition energies of the lowest two optical transitions
of a cofacial dimer formed by two stilbene molecules as a function of the interchain
distance R (in Å). The horizontal line refers to the transition energy of the isolated
molecule. Adapted from reference [Cornil *et al.* 2000].

Extensive theoretical studies have addressed the effect of intermolecular
electronic coupling on charge carrier and photophysical properties of polymeric
and oligomeric molecules. Bredas and co-workers using AM1 semiempirical
treatment, investigated exciton splitting in stilbene dimers with respect to the
intermolecular distance and the effect of relative orientations on the energies and
oscillator strengths of the lowest excited states quantitatively (Figure 1.9).

Theoretical calculations on the cofacial dimer of stilbene molecules describes the evolution of the energy of the two lowest singlet excited states resulting from the interaction of the lowest excited state of isolated stilbene molecules with intermolecular packing distance varying from 20 Å down to 3.5 Å. The lowest excited state of the cofacial dimer (*H*-aggregates) is not optically coupled to the ground state, whatever the intermolecular distance; the oscillator strength is concentrated in the second excited state. When dealing with 'n' number of molecules in interaction in a cofacial configuration, the lowest excited state of the isolated molecule splits into 'n' states, the lowest of which is optically forbidden from the ground state. Thus, in cofacial configurations, strong intermolecular interactions lead to a blue shift of the lowest optically allowed transition with respect to the isolated molecule, as was observed experimentally for stilbene. The expected blue shift may sometime be masked due to the increased planarization of molecules in the solid state. The absence of optical coupling between the ground state and the lowest excited state of the cofacial arrangement usually reduces the luminescence quantum yield with respect to isolated chains. Thus theoretical calculations have shown that significant molecular interaction in a cofacial configuration at a distance less than that of 4 Å results in a considerable quenching in the luminescence efficiency [Cornil *et al.* 2000].

Focus was then made to promote a significant optical coupling between the ground state and the lowest excited state in solids with a view to reduce the

quenching of fluorescence. Calculations (INDO/SCI) were performed on a cofacial dimer with an intermolecular distance of 4 Å and translation and rotation operations were performed on the axis along the stacking direction and the long molecular axis. According to the calculations, the translation of a molecule over small distances along its long or short axis (Figure 1.10; case I or II) or rotation around the long molecular axis (Figure 1.10; case III) are insufficient operations for recovering a high fluorescence quantum yield in the solid state because such operations keep the superposition and parallelism of the long molecular axes. A much more successful approach is to promote a finite angle between the directions of the long molecular axes (Figure 1.10; case IV). As the amplitude of rotational angle increases, energy splitting between the lowest and the first excited states of the dimer reduces and a progressive transfer of the intensity from the second excited state to the first excited state takes place. As the configuration approaches a perpendicular stacking mode, the optical splitting vanishes and emission originate from the monomeric species. Misalignments in the molecular organization and the consequent reduced intermolecular π-overlap favours high luminescence quantum yields and at the same time results in a reduction of the charge transport properties.
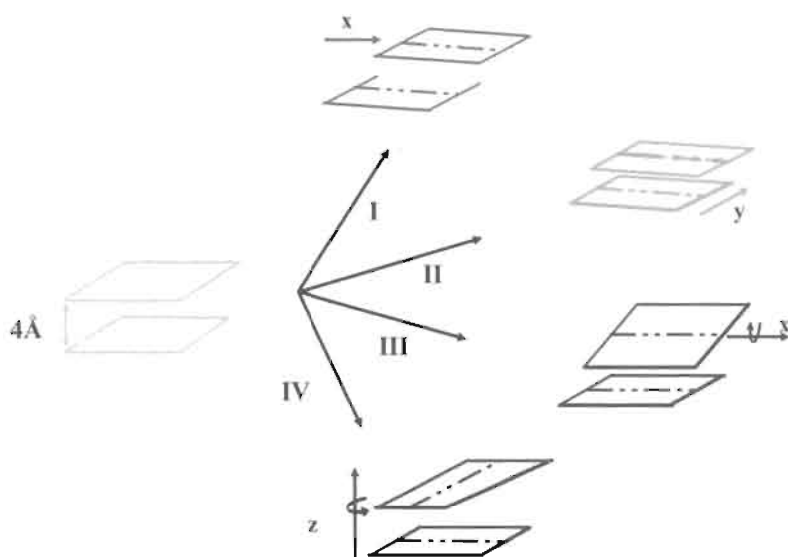
Figure 1.10. Sketch of the operations applied to a cofacial dimer formed by two stilbene molecules separated by 4 Å when investigating the role of positional disorder. The modifications are induced by (I) the translation of one molecule along the chain-axis direction, (II) the translation of one molecule along the in-plane transverse axis, (III) the rotation of one stilbene unit around its long axis, and (IV) the rotation of one stilbene molecule around the stacking axis while keeping the parallelism between the molecular planes. Adapted from reference [Cornil *et al.* 2001].

The crystalline state is considered as supramolecule *par excellence*, where reliable information on intermolecular interactions can be obtained through crystallography [Desiraju 1997]. Much of our knowledge on the dependence of solid state optical properties and intermolecular electronic interactions has been obtained from X-ray crystal structure analysis. OPV-based systems wherein adjacent molecules are arranged with their dipoles crossed, resulting in reduced π-π interaction and consequently highly fluorescent solids, have been reported by Ma

and co-workers [Xie *et al.* 2005]. 2,5-Diphenyl-1,4-distyrylbenzene with two *trans* double bonds (*trans*-15: Chart 1.3) tend to adopt a stable cross-stacking mode in the crystalline state. The crystal packing of *trans*-15 showed the molecules to be packed into one-dimensional molecular columns along the *b*-axis in which the central phenyl rings overlap. Each molecule was rotated relative to the other by an angle of 70° about an axis that passed through the centers of both the molecules (Figure 1.11).
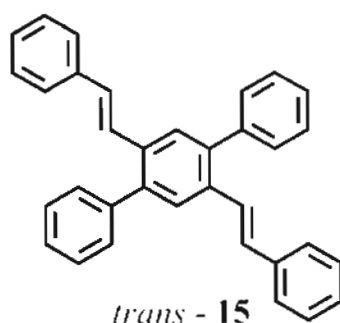
trans - **15**

Chart 1.3

The authors claimed that the molecular packing in the *trans*-15 single crystal was the first example of cross dipole stacking of conjugated molecules in the solid state, which resulted in enhancement of the solid state fluorescence as predicted theoretically by Brédas and co-workers [Cornil *et al.* 2001].

In the cross-stacked dimer, the energy difference between the excited states are reduced so that a progressive transfer of intensity from higher level to lower level occurs leading to a finite dipole moment between the ground state and lowest

excited state of clusters. As a result, a high fluorescence quantum yield was observed for this molecule in its crystalline state with the emission range very close to that of the monomer (blue region). Additionally, the overlapped central phenyl rings along one-dimensional molecular columns (*b* axis) can act as a channel for electron transport, producing high carrier mobility.
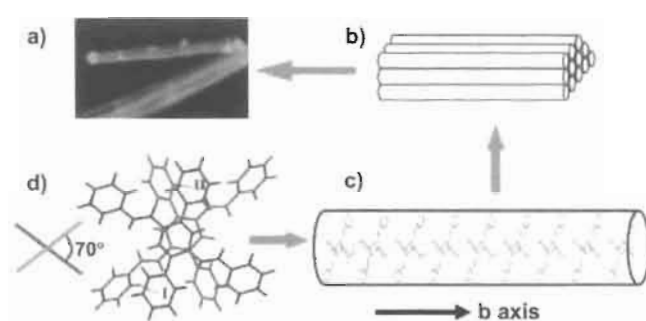
Figure 1.11. a) Crystals of *trans*-15 under UV light (365 nm), b) stacking of 1D molecular columns, c) cross-stacking molecules in 1D molecular column, d) schematic of the aromatic CH...π hydrogen bonds between two adjacent molecules. Adapted from reference [Xie *et al.* 2005]

The crystal of *trans*-15 possessed excellent thermal stability, good electron-transporting property and strong pure blue emission, which made this material a promising candidate for OLED and lasing applications.

Gierschner and co-workers investigated the consequences of the different packing motifs of a series of distyrylbenzene derivatives (**DSB (2)**, *t*-**Bu₄DSB** (**16**), **F₁₂DSB** (**17**) and 1:1 co-crystal of **DSB:F₁₂DSB**) on their optical and photophysical properties using absorption and fluorescence spectroscopy under time-resolved as well as angular resolved polarized conditions [Gierschner *et al.*

2005]. The solid state properties were studied using single crystals and nanoparticle suspensions. The absorption and fluorescence spectra of all molecules in solution were quite similar. However large differences in their solid state optical properties were observed. The differences of the optical properties in the solid state are essentially caused by different intermolecular organization.

DSB (2)

t-Bu₄DSB (16)

F₁₂DSB (17)
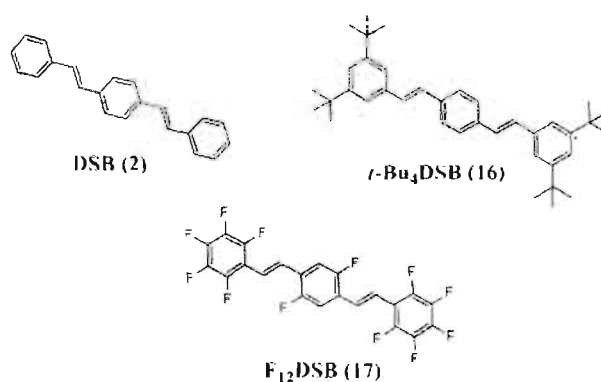
Chart 1.4.

t-**Bu₄DSB** did not show a long-range order of the constituting molecules due to the steric hindrance of the bulky *t*-butyl group. Concomitantly, its photophysical properties in the solid state are very similar to that observed in its solution due to the lack of electronic interactions between neighbouring molecules in the solid state. DSB organizes in a herringbone structure with an edge-to-face arrangement of the molecules, whereas **F₁₂DSB** as well as **DSB:F₁₂DSB** co-crystals organize in a face-to-face oriented molecules stacks. The layered structures with preferential parallel orientation of the molecular $S_0 \rightarrow S_1$ transition dipole moments promote *H*-aggregation for **DSB** as well as for **F₁₂DSB** and

DSB:F₁₂DSB and is indicated by the observed strong blue shifted absorption spectra and low radiative rate constants in these derivatives.
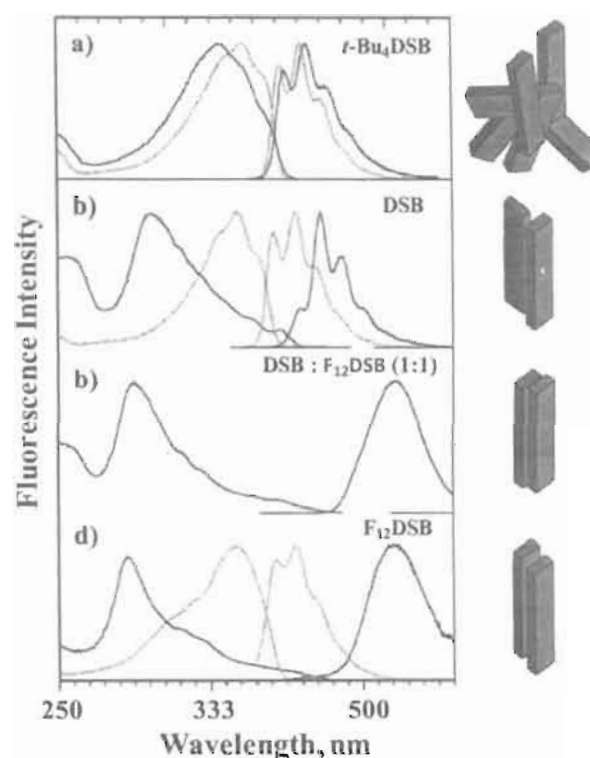
Figure.1.12. Fluorescence (right) and absorption spectra (left) of distyrylbenzene nanoparticles: a) *t*-Bu₄DSB, b) **DSB**, c) co-crystallized **DSB:F₁₂DSB** and d) **F₁₂DSB**. Spectra in hexane solution (dashed lines) are shown for comparison. A schematic representation of the respective condensed phase structures is given on the right. Adapted from reference [Gierschner *et al.* 2005]

The emission properties of these derivatives are significantly different, with herringbone structures showing well-resolved vibronic structuring, very similar to that in solution due to lack of significant contribution of intermolecular vibronic

coupling. In face-to- face stacked structures, a significant charge transfer character of the electronic transition was observed inducing efficient coupling of intermolecular vibrational modes. As a result strongly red shifted, unstructured excimer like emission spectrum was observed.
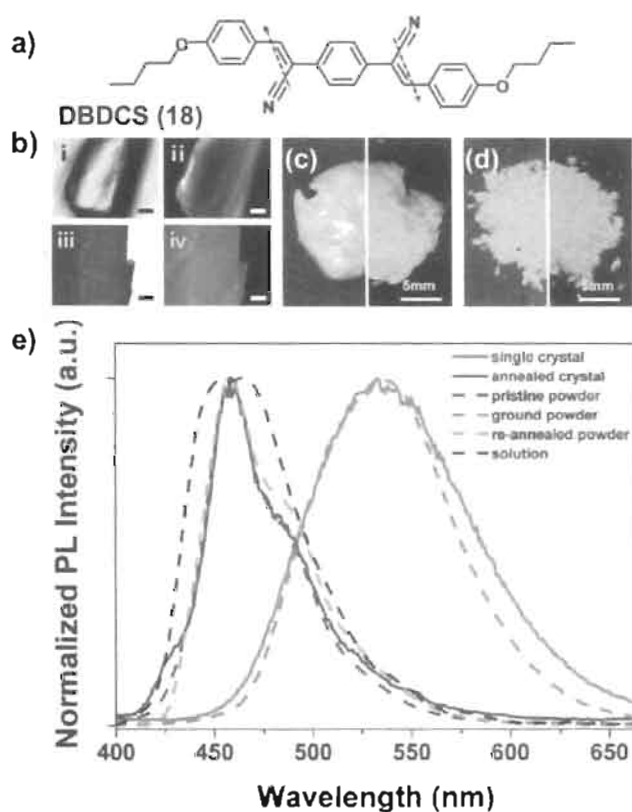
Figure 1.13. DBDCS material: (a) Molecular structure and its local dipoles (dashed arrows). (b) Photo of a single crystal: before annealing, under room light (i), and UV light (ii), and after annealing, under room light (iii), and UV light (iv) (scale bar = 0.2 mm). (c) Photo of the annealed powder under room (left) and UV light (right). (d) Photo of grinded powder under room light (left) and UV light (right). Adapted from reference [Yoon *et al.* 2010].

Park, Gierschner and co-workers have very recently investigated changes in fluorescence properties of cyano-distyrylbenzene (Figure 1.13a) [Yoon *et al.* 2010] when subjected to external stimuli such as temperature, pressure, solvent vapor which was earlier reported by Weder and co-workers [Crenshaw *et al.* 2005]. They were able to provide an explanation for the observed phenomena based on changes in intermolecular interactions between molecules brought about by the external stimulus.

Two distinct types of fluorescence behaviour were observed in **DBDCS (18)**. Single crystals grown from an ethyl acetate solution appeared yellow in colour and emitted green light (λ_{max} ~ 533 nm) under UV illumination. On heating the sample to 125 °C for an hour, however, the colour changed to pale green and the emission to blue (458 nm) , while the crystal appearance changed from transparent to opaque. The single crystal analysis of the green emitting material indicated the constituent molecules to be arranged in a slip-stacked arrangement along the long molecular axis (see Scheme 1.4) with a slip angle of 26.6° and an interlayer distance of about 3.67 Å. In this arrangement, the neighbouring molecules possessed substantial overlap of the π-systems (see Scheme 1.4), and the material exhibited an excimer-like emission centered at 533 nm. In the blue emitting material, powder XRD data showed the molecules to be slipped along the

long molecular axis at an angle of 62.8° with a head-to-tail coupling of the local dipoles in adjacent molecular sheets (see Scheme 1.4). In this case, the principal slip direction of the molecular sheets is along the shorter axis of the **DBDCS (18)** molecule to effectively offset the aromatic rings resulting in diminished excimer formation. The authors observed that the application of pressure to the blue emitting form could restore the original green emitting form.
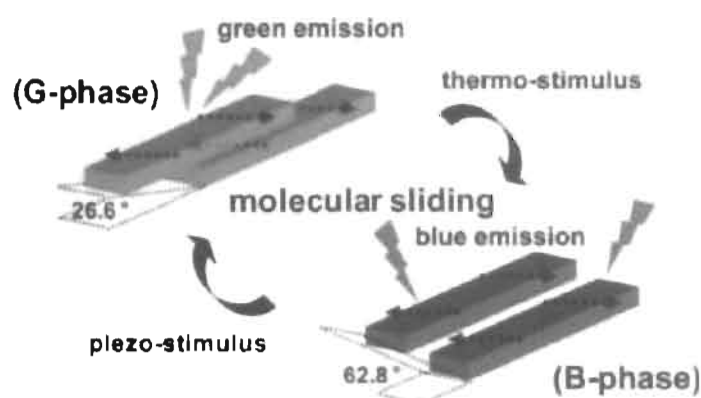
Scheme 1.4. Illustration of two different modes of slip-stacking in **DBDCS (18)** molecular sheets, dictated by different ways of antiparallel/head-to-tail coupling of local dipoles. Adapted from reference [Yoon *et al.* 2010]

In spite of the several investigations of the type reported in this Chapter, a clear understanding of the nature of the interactions that determine the packing of molecules in the solid state and how they affect the optical and electronic properties of these materials is still not available.

In this context, continued studies on stilbenoid derivatives can lead to a further understanding of structure property relationships, providing exciting prospects for the design and construction of novel materials with improved properties for applications in optoelectronic devices.

1.6. Objectives of the Present Work

The major focus of the present study is to synthesize and investigate the material properties of a few stilbenoid molecules and to monitor the changes in their photophysical properties on self-assembly. One of our objectives was to elucidate the correlation of solid state optical properties and molecular packing and to fine-tune these optical properties by bringing about subtle variations in their molecular packing by varying the nature of remote functional groups and also by using external stimulus such as heat. We have also investigated different functionalized stilbenoid units for the construction of self-assembled materials such as liquid crystals and gels and the effect of self-assembly on their optical properties in these condensed phases.

Synthesis and Study of Fluorescence Properties of Alkoxy-Cyano Substituted Stilbene Derivatives in Solution and Crystalline Phase
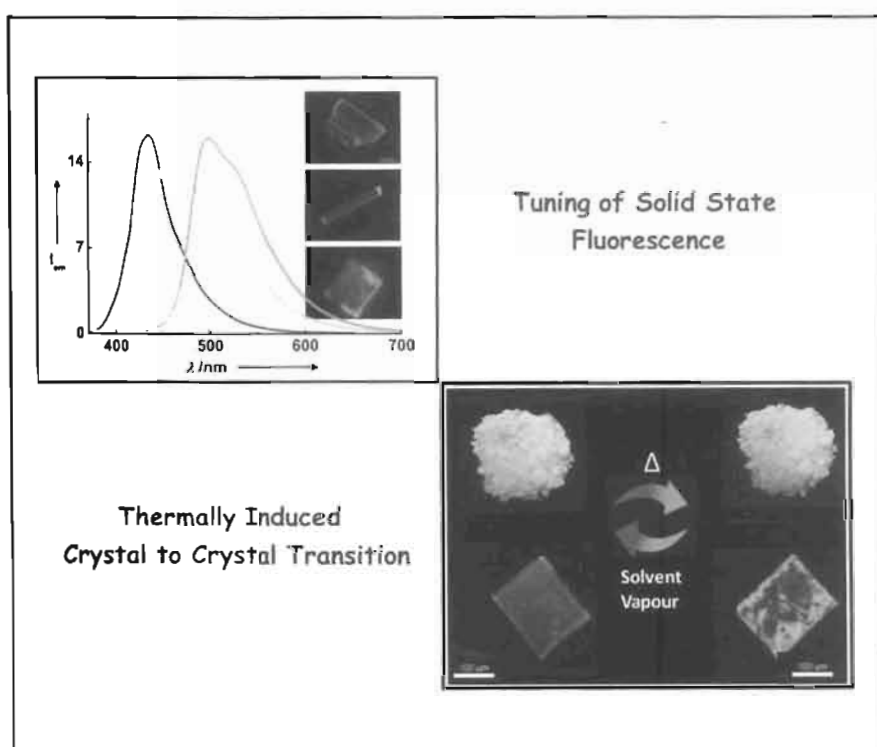
Objective: To understand the role of molecular packing in controlling the optical properties of stilbene derivatives in solid state and to fine-tune their molecular organization for obtaining materials with desired optical properties.

2.1. Abstract

*The synthesis and photoluminescence properties of a series of donor-acceptor substituted stilbene derivatives wherein alkoxy group as donor and cyano group as the acceptor are described. All the derivatives showed weak fluorescence in the solution state whereas they exhibited strong fluorescence in the solid state. Moreover, in these stilbene derivatives the nature of the solid state fluorescence properties was observed to be very sensitive to the length of the alkyl substituent. Derivatives with short alkyl chains (**DS1-DS4**) emitted in the blue region, while derivatives with intermediate alkyl chain length (**DS5-DS7**) emitted in the bluish green region and that with a long alkyl chain (**DS8**) emitted in the green region. The role of molecular packing in controlling the solid state fluorescence was investigated by studying the crystal structure of these molecules. Single crystal X-ray analyses of the crystals of these derivatives indicated that the nature of the molecular packing was controlled by the length of the alkyl substituents. A strong correlation could be observed between the nature of the molecular packing and the solid state optical properties of these materials. A few of the derivatives (**DS10** and **DS12**) exhibited a unique thermally induced crystal to crystal transition associated with drastic changes in their colour and photoemissive behaviour, which could be attributed to planarization and rotation of the molecules leading to changes in the relative orientations of the neighbouring molecules resulting in strong excitonic coupling between them.*

2.2. Introduction

Organic π-conjugated oligomers have recently been the focus of interest mainly because of their potential for use as active elements in various electronic and optoelectronic devices [Forrest *et al.* 2004; Schenning *et al.* 2005: Hide *et al.* 1997; Montali *et al.* 1998]. To achieve successful incorporation of such conjugated materials into functional devices, it is necessary to understand and to be able to manipulate their solid state electronic interactions which in turn control exciton migration, charge transport as well as the optical properties [Cornil *et al.* 2001; Sun *et al.* 2003]. Molecular organization plays a decisive role in defining the functional properties of these materials and the controlled self-assembly of molecules into desired structures within devices can lead to enhanced performances [Lim *et al.* 2009; Antony *et al.* 2006; Antony *et al.* 2007]. The structure-property relationships of organic π-conjugated materials are fairly well established at the molecular level but the factors that control their bulk properties are still not fully understood.

In the solid state, photophysical properties are mainly affected by intermolecular coupling of electronic transition dipole moments, reduction of torsion induced non-radiative deactivation processes and migration of excitation energy to distortions, impurity traps or dopants. The interplay of these factors complicate the understanding of the exact reasons for the changes in the luminescence properties on going from solution to solids. Out of these parameters,

intermolecular coupling of electronic transition dipole moments is more important which in turn is decided by the relative orientations of the neighbouring molecules and the resultant excitonic interactions [Lewis *et al.* 1996; Lewis *et al.* 1997; Gierschner *et al.* 2005; Spano 2003; Sheikh-Ali *et al.* 1994]. The relative alignments of these molecules are controlled by weak intermolecular forces involving both π-conjugated units as well as remote functional groups which are not in conjugation. Variations of molecular packing by introducing remote functional groups can therefore be utilized as an effective strategy to fine-tune the solid state photophysical properties of a particular chromophore [Davis *et al.* 2008; Kumar *et al.* 2008; Kumar *et al.* 2009; Jayanty *et al.* 2004; Radhakrishnan *et al.* 2008; Prakash *et al.* 2006; Mizobe *et al.* 2005; Dong *et al.* 2009]. Alternatively, the molecular packing of chromophores in the bulk can be altered by external stimuli such as heat [Davis *et al.* 2005; Mutai *et al.* 2005; Crenshaw *et al.* 2005; Chandrasekharan *et al.* 2001; Mutai *et al.* 2008; Kunzelman *et al.* 2008], light [Chung *et al.* 2009; Papaefstathiou *et al.* 2006], pressure [Kunzelman *et al.* 2008; Sagara *et al.* 2007; Mizukami *et al.* 2005; Ito *et al.* 2008; Mizuguchi *et al.* 2003; Sagara *et al.* 2009], and chemicals [Fei *et al.* 2003]. Materials which can respond to external stimuli in such a manner can provide valuable information about the nature of molecular packing that controls the optical properties and also have significant potential for application as smart materials.

In this Chapter, we describe our detailed investigations on the solid state photophysical properties of novel donor-acceptor substituted stilbene derivatives (Chart 2.1). Stilbene derivatives possessing a cyano group as the acceptor and dialkoxy group as the donor, with varying alkyl chain lengths (DS1-DS12) were synthesized and have been characterized. In these stilbene derivatives, the nature of the solid state fluorescence properties were observed to be very sensitive to the length of the alkyl substituent, derivatives with short alkyl chains (DS1- DS4) emitting in the blue region, while derivatives with intermediate alkyl chain lengths emitting in the bluish green region (DS5-DS7) and the derivative with a long alkyl chain emitting in the green region (DS8). The role of molecular packing in controlling the solid state fluorescence of these derivatives was elucidated by studying their crystal structure. Few of these stilbene derivatives exhibited thermally induced crystal to crystal transformation with drastic changes in their optical properties. The role of the modification of molecular packing on heating in controlling optical properties of the material has been investigated.

DS1, R = CH$_3$;   DS2, R = C$_2$H$_5$;

DS3, R = C$_3$H$_7$;   DS4, R C$_4$H$_9$;

DS5, R ~ C$_5$H$_{11}$;   DS6, R = C$_6$H$_{13}$;

DS7, R C$_7$H$_{15}$;   DS8, R C$_8$H$_1$-;

DS10, R =C$_{10}$H$_{21}$;   DS12, R = C$_{12}$H$_{25}$.
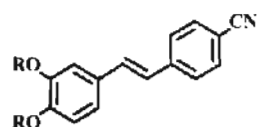
Dialkoxy – Cyano Stilbene Derivatives (DS)

Chart 2.1

2.3. Results and Discussion

2.3.1. Synthesis of Stilbene Derivatives

The alkoxy-cyano substituted stilbene derivatives shown in the Chart 2.1 were synthesized in high yields by the Wittig-Horner reaction between diethyl 4-cyanobenzylphosphonate and the corresponding alkoxy substituted benzaldehydes using sodium hydride as base and tetrahydrofuran as solvent (Scheme 2.1).
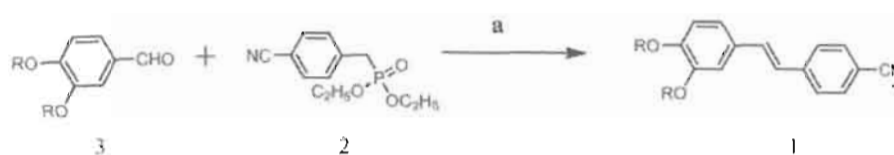
Reagents and Conditions: a) NaH, THF. 25 °C, 3h.

<div align="center">

Scheme 2.1.

</div>

The structures of these stilbene derivatives were established by FT-IR, ^{1}H, ^{13}C NMR spectroscopy and mass spectrometry. ^{1}H NMR spectroscopic analysis revealed that the compounds existed as their *E* isomers. The detailed synthetic procedure and spectral characterization data of these derivatives are provided in the Experimental Section 2.5.

2.3.2. Photophysical Properties in Solutions

The absorption and fluorescence properties of the dialkoxy-cyano substituted stilbene derivative (**DS12**) in different solvents of varying polarity are summarized in Table 2.1. The absorption spectra (λ_{max} 350 nm) were found to be

practically independent of the nature of the solvent indicating that the dipole moments of its ground and excited states are nearly the same. The stilbene derivatives exhibited a very weak fluorescence in solution and the fluorescence maximum underwent a bathochromic shift with increase in solvent polarity. It is interesting to note that the absorption spectra of the alkoxy-cyano substituted stilbenes was not affected by solvent polarity indicating that there is not much difference between the dipole moments of the ground and excited states, while the red shift in the fluorescence spectra with increase in solvent polarity suggests a significant enhancement in the dipole moment of the excited state compared to the ground state. In order to explain this contradiction, it must be assumed that the Franck-Condon (FC) excited state and the emitting states are different. Upon direct excitation, these molecules reach into a locally excited (LE) state, which subsequently transforms into a polar intra-molecular charge transfer (ICT) state [Singh *et al.* 2001; Rettig *et al.* 1994; Davis *et al.* 2001]. The absorption and fluorescence spectra of the dodecyloxy-cyano substituted stilbene derivative **DS12** are shown in Figure 2.1. In a particular solvent, change in length of the alkyl group did not bring about any change in its absorption or emission properties. Since at the molecular level, optical properties are decided by the intramolecular electronic interactions and the variations in the length of the alkyl group is not expected to bring about substantial changes in these interactions.
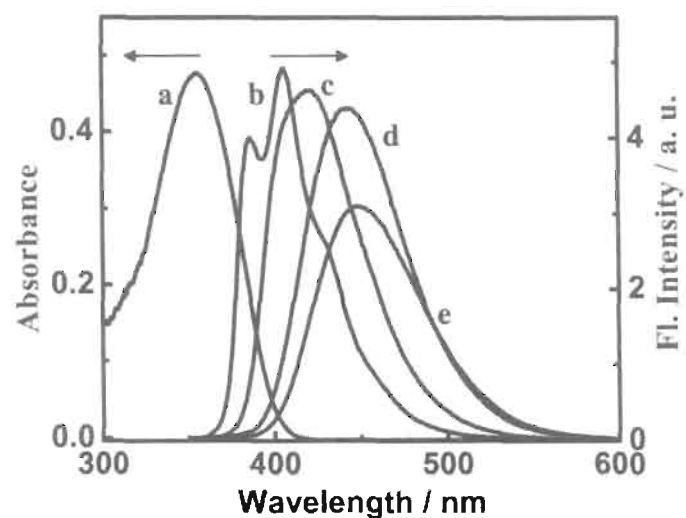
Figure 2.1. Absorption and fluorescence spectra of **DS12**; (a) absorption spectrum in hexane; fluorescence spectra in (b) hexane, (c) toluene, (d) dichloromethane and (e) benzonitrile (Excitation: 340 nm).

Table 2.1. Absorption and fluorescence data of (E)-4-(3,4-bis(dodecyloxy)styryl)benzonitrile (**DS12**) in solvents of varying polarity.

Solvent	**DS12**		
	Abs.$_{\lambda max}$ (nm)	Ems.$_{\lambda max}$ (nm)	(ϕ_F)
Hexane	348	405	0.012
Toluene	350	421	0.014
DCM	353	443	0.018
THF	351	443	0.020
BCN	356	450	0.021

2.3.3. Photophysical Properties in the Solid State

The solid state fluorescence behaviour of the alkoxy-cyano substituted stilbene derivatives was distinctly different from that of their solutions. All the derivatives exhibited significant enhancement in fluorescence quantum yields in the solid state, compared to that in their solutions. The enhancement in emission in the solid state may be attributed to restricted molecular motion as well as to formation of exciton coupled aggregates in the solid state. Table 2.2 summarizes the emission characteristics of dialkoxy-cyano substituited stilbene derivatives in their crystalline state.

Table 2.2. Absorption maxima, emission maxima and quantum yields of fluorescence (Φ_f) of **DS** series in solid state.

Sample Code	Abs.$_{\lambda max}$ (nm)[a]	Ems.$_{\lambda max}$ (nm)	FWHM [cm^{-1}]	Φ_f
DS1	440	415	2885	0.64
DS2	440	411	2135	0.66
DS3	443	405	2302	0.60
DS4	435	394	2545	0.58
DS5	474	416	3554	0.68
DS6	472	415	3800	0.71
DS7	472	430	4034	0.66
DS8	500	460	2924	0.41

[a] As obtained from excitation spectrum.
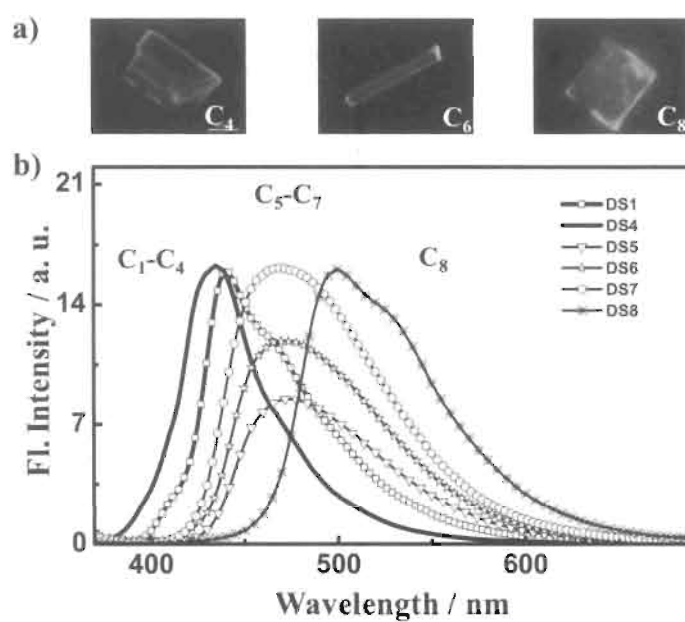
Figure 2.2. a) Fluorescence images of the crystals upon excitation with 360 nm light of **DS4, DS6** and **DS8,** respectively and b) fluorescence spectra of dialkoxy-cyano substituted stilbene derivatives in crystals.

The fluorescence properties of dialkoxy-cyano substituted stilbene derivatives in solid state were observed to be highly sensitive to the length of the alkyl chain. The fluorescence properties of these materials were classified into three distinct types, based on the region of fluorescence emission. Upon excitation with 360 nm light, the crystals of **DS1** to **DS4** emitted in the blue region (λ_{max} ~440 nm), while **DS5** to **DS7** emitted in the bluish green region (λ_{max}~470 nm), and **DS8** emitted in the green region (λ_{max} ~500 nm). The solid state emission spectra and the representative photographs of the crystals emitting in three different regions upon excitation with 360 nm light are shown in Figure 2.2.

The colours of the stilbene derivatives were also dependent on the length of the alkyl chains, indicating a red shift in their absorption with increasing alkyl chain length. The excitation spectra also reflected this red shift with increasing alkyl chain lengths. The blue emitting derivatives (**DS1-DS4**) were white transparent solids, the bluish green emitters (**DS5-DS7**) appeared light green in colour and the green emitting **DS8** was yellow coloured. Figure 2.3 depicts the representative examples that show the changes in the excitation spectra with increase in alkyl chain lengths.
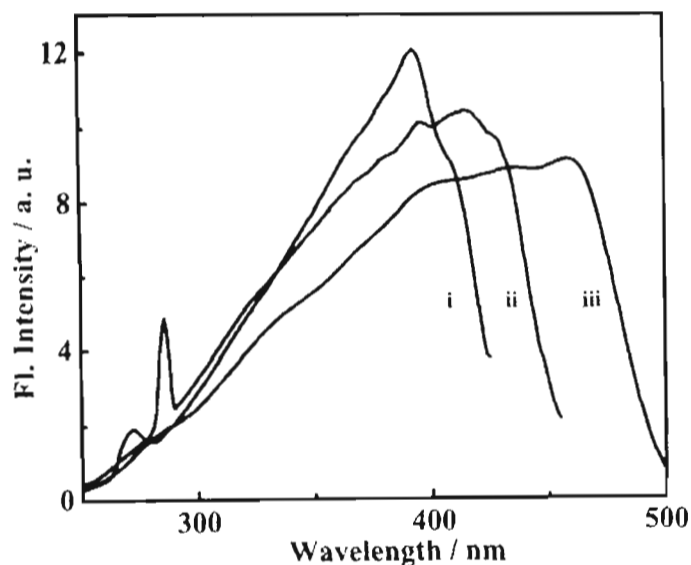
Figure 2.3. Fluorescence excitation spectra of i) **DS4**, ii) **DS6** and iii) **DS8** in crystals (Emission collected at their corresponding emission maximum; 440, 470 and 500 nm respectively).

The fluorescence lifetimes in the crystals of these derivatives were measured by exciting at a wavelength of 375 nm and collecting the emission at their

corresponding emission maxima (See Table 2.2). In their solutions. all the derivatives exhibited extremely short lifetimes, well within the instrument response limit, whereas in the solid state the lifetimes were considerably larger. It must be recognized that generally interpretation of solid state luminescence lifetimes can be complicated due to the inhomogenities that can exist in the crystals, which could lead to aggregates differing slightly in their configurations. However, some general trends can be perceived and this is discussed below.
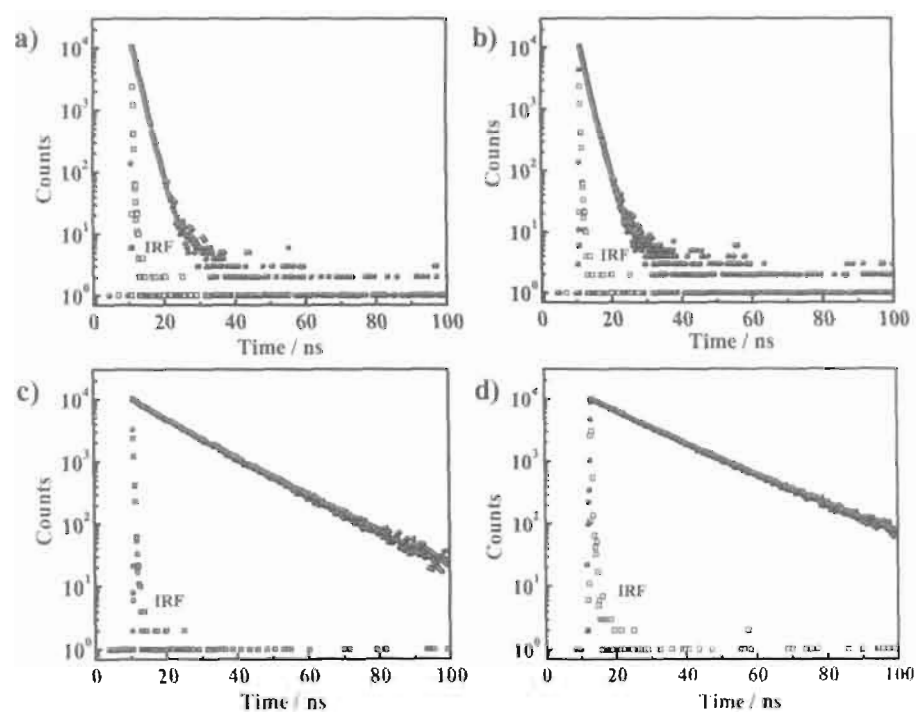
Figure 2.4. Fluorescence lifetime decay profile of the representative examples of dialkoxy-cyano substituted stilbene derivatives in crystals: a) **DS1**, b) **DS4**, c) **DS6**, d) **DS8** (λ_{ex} 375 nm).

Table 2.3. Fluorescence lifetime data of dialkoxy-cyano substituted stilbene derivatives.

Sample Code	τ_1 / ns (F_1%)	τ_2 / ns (F_2%)	χ^2
DS1	3.87 (73.29)	1.57 (26.71)	1.02
DS2	1.20 (72.91)	1.13 (27.09)	1.07
DS3	2.54 (24.94)	0.63 (75.06)	1.08
DS4	1.80 (100)	-	1.07
DS5*	-	-	-
DS6	14.46 (90.63%)	6.14 (9.37%)	1.01
DS7	11.22 (96.55%)	1.44 (3.45%)	1.07
DS8	17.88 (87.59%)	9.21 (12.41%)	1.08

*Good quality micrometer sized crystals cannot be generated for lifetime measurements.

The fluorescence lifetime decay profile showed significant difference in the lifetime of the emitting species in these derivatives. Fluorescence lifetimes of the green emitting derivative (**DS8**) was longer (18 ns, Figure 2.4d), while the derivatives emitting in the bluish green region (**DS6, DS7**) possessed intermediate lifetimes of less than 15 ns (Figure 2.4c) and the derivatives emitting in blue (**DS1-DS4**) have a short lifetime of less than 4 ns (Figure 2.4a,b) for the major emitting species (Table 2.3). It has been shown earlier that the lifetime values can be enhanced substantially when exciton coupling occur between molecules in the solid state [Kumar *et al.* 2009; Davis *et al.* 2008].

2.3.4. Crystal Structures

Single crystals of the dialkoxy-cyano substituted stilbene derivatives (**DS1, DS3, DS4, DS6, DS7** and **DS8**) were developed at room temperature by slow evaporation from their hexane solutions. The X-ray crystallographic refinement data of these derivatives are summarized in Appendix 1.
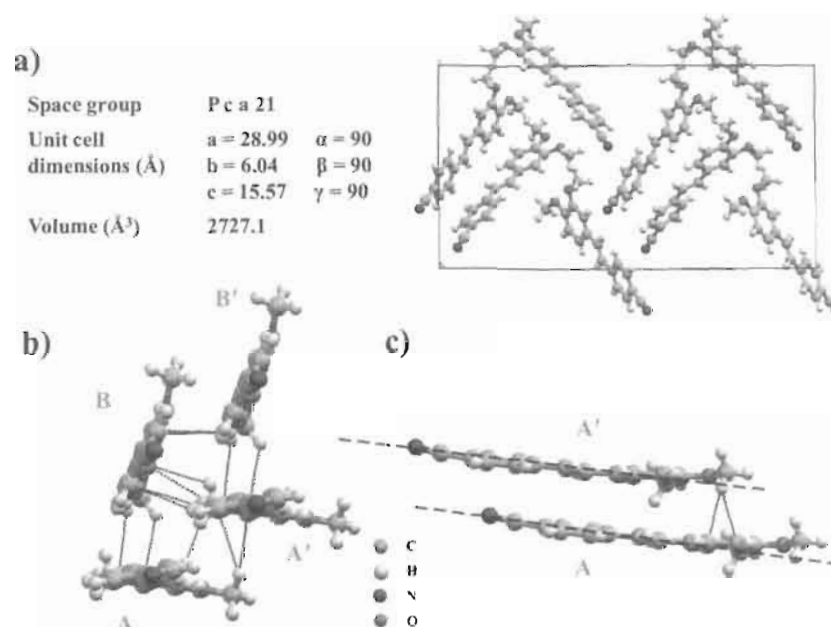
Figure 2.5. a) The unit cell parameters and the organization of **DS1** molecules in the unit cell, b) a tetramer unit of molecules taken from the X-ray structure. An axis passing through the long axis of the molecule is selected for the view. c) short axis view of AA' dimer unit. Molecular interactions below 3Å units are represented in dotted lines.

DS1 has eight molecules per unit cell (Figure 2.5) with the molecules arranged in two non-equivalent stacks, with their long axis pointing in the same

direction in a herringbone fashion. Two different conformational isomers (symmetrically non-equivalent) were observed in the crystal lattice with a dihedral angle of 7.50° and 17.01° between the phenyl rings of the stilbene units, which indicate that the molecules are not significantly distorted from planarity. A tetramer unit of molecules in the crystal lattice was identified for studying the nearest neighbour interaction and is shown in Figure 2.5a. From this figure, two major alignments of the molecules can be identified as i) AB and ii) AA′ with the notations A and B representing molecules of adjacent stacks. The interactions that stabilizes this arrangement are weak C-H...π interactions with a distance of ≤ 3.0 Å. Due to the angular arrangement of AB and A′B′ dimers, the π-π interaction is expected to be weaker compared to that for a cofacial arrangement of the monomer units. Although the distance between the molecules within each stack (i.e., between A and A′ and between B and B′) is 2.69 Å, the π-π stacking interactions between these molecules are minimal as they are slipped along their short axis with respect to each other.

DS3 has four molecules per unit cell (Figure 2.6) with the molecules arranged in two non-equivalent stacks, with their long axis pointing in the same direction. In the crystal lattice, a dihedral angle of 29.15° was observed between the phenyl rings of the stilbene units, indicating that the molecules are significantly distorted from planarity. In a tetramer unit of nearest neighbouring molecules, the molecules are arranged in a herringbone fashion and the major

interactions stabilizing the herringbone organization were the C-H...π interactions. Due to the angular arrangement of AB and A'B' dimers and the slipped stacking along the short molecular axis of AA' and BB' dimers, the π-π overlap between the molecules was negligible.

Figure 2.6. a) The unit cell parameters and the organization of **DS3** molecules in the unit cell, b) a tetramer unit of molecules taken from the X-ray structure. An axis passing through the long axis of the molecule is selected for the view, c) short axis view of AA' dimer unit. Molecular interactions below 3Å units are represented in dotted lines. Alkyl chains are omitted for clarity in b.

a)

Space group	P 2₁/c

Space group: $P\,2_1/c$

Unit cell dimension (Å)	a = 24.90	α = 90
	b = 8.33	β = 90.36
	c = 9.94	γ = 90

Volume (Å³): 2061.22

b)

A'

A

B'

B

○ C
○ H
● N
● O

c)

A'

A

Figure 2.7. a) The unit cell parameters and the organization of **DS4** molecules in the unit cell, b) a tetramer unit of molecules taken from the X-ray structure. An axis passing through the long axis of the molecule is selected for the view, c) short axis view of AA' dimer unit. Molecular interactions below 3Å units are represented in dotted lines. Alkyl chains are omitted for clarity in b.

The crystal structure of **DS4** indicates four molecules per unit cell (Figure 2.7) with the molecules arranged in two non-equivalent stacks, with their long axis pointing in the same direction. In the crystal lattice, a dihedral angle of 41.32° was observed between the phenyl rings of the stilbene units, indicating that the molecules are significantly distorted from planarity. In the tetramer unit, the molecules are arranged in a herringbone fashion and the major interactions stabilizing the herringbone organization were the C-H...π interactions, almost similar to that observed for the **DS3** derivative. Due to the angular arrangement of

AB and A'B' dimers and the slipped stacking along the short molecular axis of AA' and BB' dimers, the π-π overlap between the molecules was negligible.
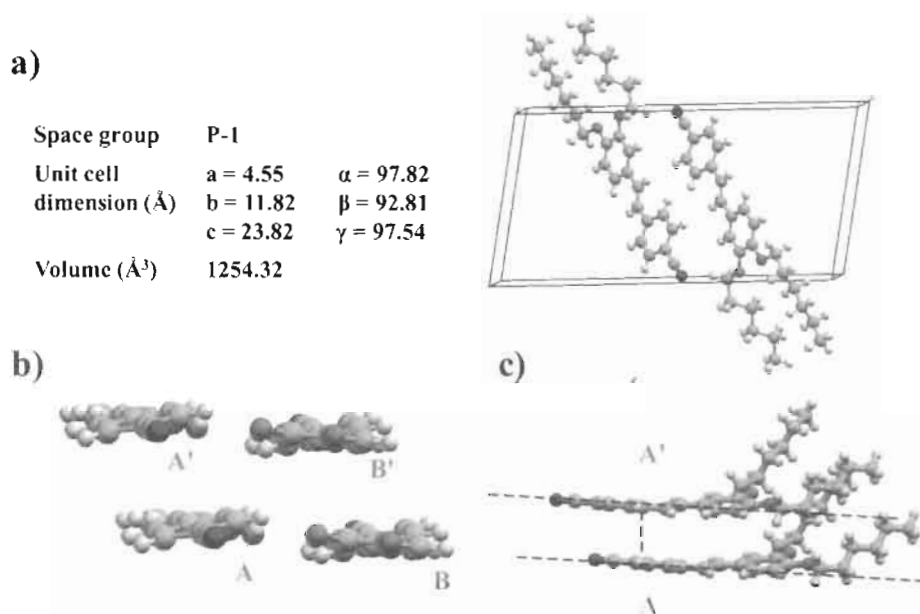
Figure 2.8. a) The unit cell parameters and the organization of **DS6** molecules in the unit cell, b) a tetramer unit of molecules taken from the X-ray structure. An axis passing through the long axis of the molecule is selected for the view, c) short axis view of AA' dimer unit. Molecular interactions below 3Å units are represented in dotted lines. Alkyl chains are omitted for clarity in b.

DS6 has two molecules per unit cell (Figure 2.8), with their long axis pointing in opposite direction. In the crystal lattice, a dihedral angle of 17.88° was observed between the phenyl rings of the stilbene units, indicating that the molecules are nearly planar. The relative alignment of molecules in a tetramer unit of nearest neighbouring molecules is significantly different from that of the

derivatives with shorter alkyl chain lengths (**DS1-DS4**). The molecules are arranged in a brick stone fashion, with the molecules arranged anti-parallel (AB) to each other and this arrangement was stabilized by C-H...N interactions. The C-H...π interactions are conspicuous by their absence compared to the molecular arrangement in the derivatives with shorter alkyl chain lengths (**DS1-DS4**). Even though the A and A' molecules are translated along the short axis relative to each other by a short distance, considerable degree of π-overlap between them is maintained.

a)

| Space group	P-1	
Unit cell dimension (Å)	a = 4.55	α = 97.82
	b = 11.82	β = 92.81
	c = 23.82	γ = 97.54
Volume (Å³)	1254.32	

b)

c)
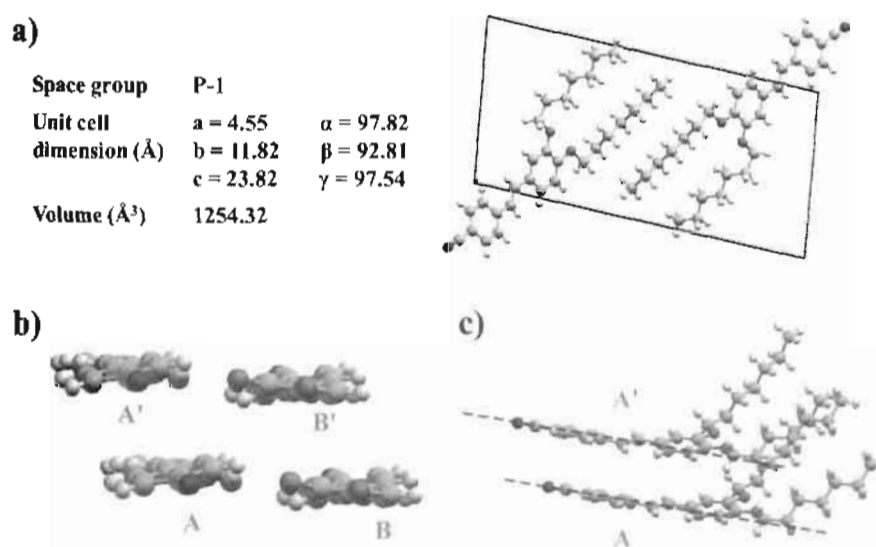
Figure 2.9. a) The unit cell parameters and the organization of **DS7** molecules in the unit cell, b) a tetramer unit of molecules taken from the X-ray structure. An axis passing through the long axis of the molecule is selected for the view, c) short axis view of AA' dimer unit. Molecular interactions below 3Å units are represented in dotted lines. Alkyl chains are omitted for clarity in b.

The crystal structure of **DS7** indicated two molecules per unit cell (Figure 2.9), with the long axis of the molecules pointing in opposite direction. In the crystal lattice, a dihedral angle of $18.16°$ was observed between the phenyl rings of the stilbene units, indicating that the molecules are reasonably planar. In a tetramer unit of nearest neighbouring molecules, the molecules are arranged in a brick stone fashion almost similar to that in **DS6**. Substantial π-overlap between the molecules was maintained, even though the molecules in same stacks (AA' and BB') were the slipped along the short molecular axis, similar to that observed in the **DS6** derivatives.
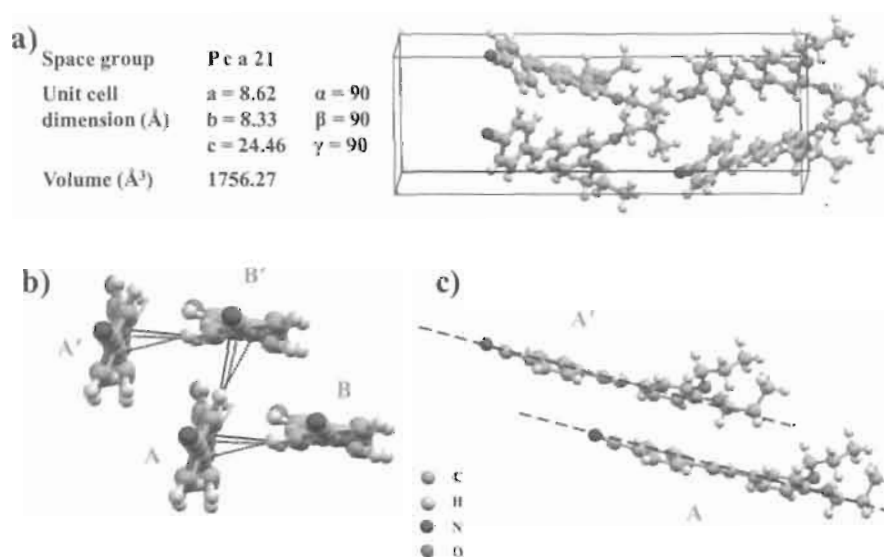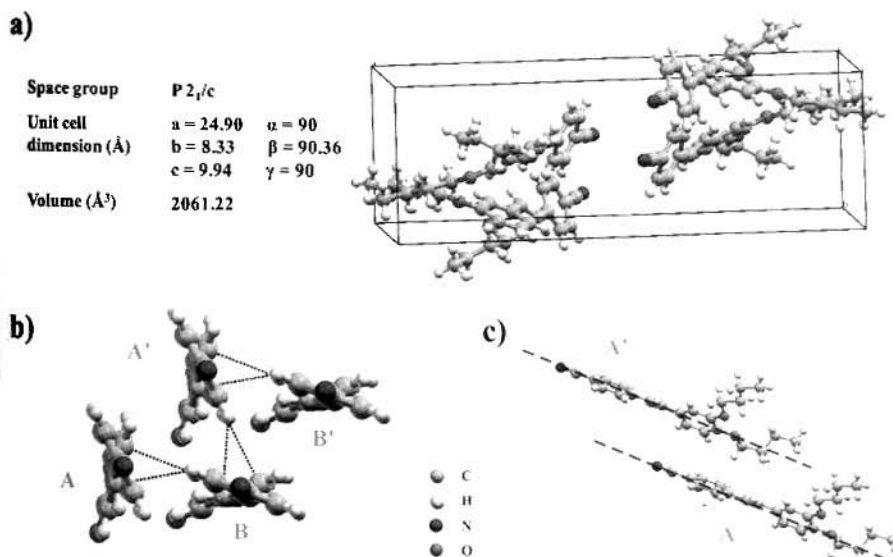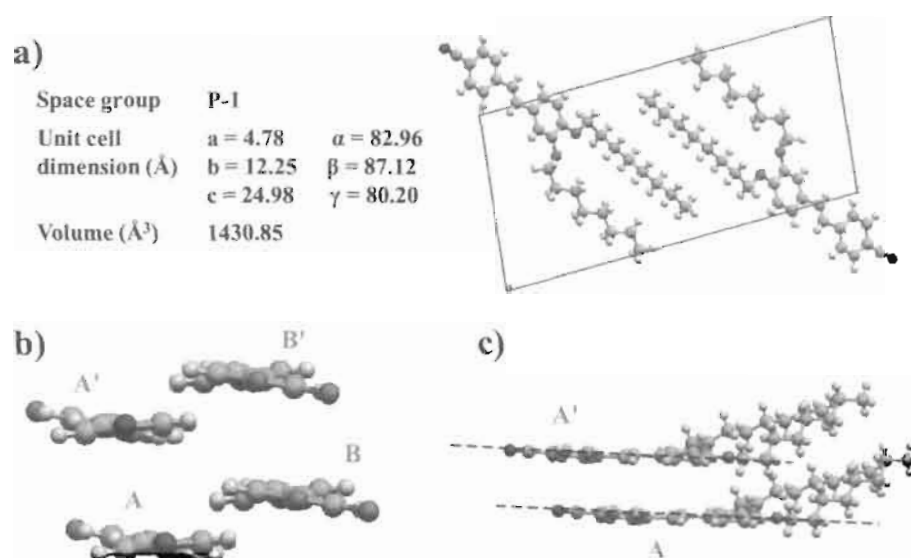

Figure 2.10. a) The unit cell parameters and the organization of **DS8** molecules in the unit cell, b) a tetramer unit of molecules taken from the X-ray structure. An axis passing through the long axis of the molecule is selected for the view, c) short axis view of AA' dimer unit. Alkyl chains are omitted for clarity in b.

The crystal structure of **DS8** indicates two molecules per unit cell (Figure 2.10), with the long axis of the molecules pointing in opposite directions, similar to that observed in **DS6** and **DS7**. In the crystal lattice, a dihedral angle of 15.85° was observed between the phenyl rings of the stilbene units, indicating the molecules are not significantly distorted from planarity. In a tetramer unit of nearest neighbouring molecules, the molecules are arranged in a brick stone fashion and the only interaction (below 3Å) that stabilizes the alignment of the molecules was the C-H...N interaction. Within the same stack, the molecules are arranged one on top of the other with the slip along the long molecular axis and in the neighbouring stacks the molecules are arranged antiparallel to each other. Such an arrangemnet leads to substantial π-overlap between the molecules.

The crystal structure analysis of these derivatives showed that the alignment as well as the conformation of the chromophoric unit (stilbene) was substantially altered by varying the length of the alkyl chains. For the derivatives with short alkyl chain lengths (**DS1-DS4**), the molecules align in an edge to face fashion. Such an arrangement is facilitated by C-H...π interactions between the molecules. It may be noted that in **DS3** and **DS4** derivatives, the chromophoric unit was twisted to accomodate the alkyl chains with substantial C-H...π interactions between the molecules. With increasing length of the alkyl chains (**DS6-DS8**), steric crowding of the alkyl groups restricts the C-H...π interactions resulting in a tranformation from a edge to face herringbone structure to a face to face

brickstone type of arrangement. The derivatives with longer alkyl chain lengths (**DS5-DS8**) were found to be substantially planar compared to the lower derivatives (**DS3, DS4**).

2.3.5. Discussion

In solutions, the optical properties of dialkoxy-cyano substituted stilbene derivatives were similar to that commonly observed in the donor-acceptor substituted polyenes. The absorption spectra of these stilbene derivatives were unaffected by solvent polarity indicating that there is not much difference between the dipole moments of their ground and excited states, while their emission spectra underwent a bathochromic shift on increasing solvent polarity. The red shift in emission spectra with increase in solvent polarity suggests that there exist a significant enhancement in the dipole moment of the excited state compared to the ground state. In order to explain this contradiction it must be assumed that the Franck-Condon (FC) excited state and the emitting states are different. Direct excitation of these molecules leads to locally excited (LE) state, which subsequently transforms into a more polar intramolecular charge transfer (ICT) state [Singh *et al*. 2001; Rettig *et al*. 1994; Davis *et al*. 2001]. These derivatives were weakly fluorescent in solution and the nature of their emission spectra was independent of the length of the alkyl substituent.

In the solid state, the fluorescence emission quantum yields of these derivatives were considerably enhanced. The enhanced emission in the solid state may be attributed to restricted molecular motion as well as to the formation of exciton coupled aggregates. The optical properties of these dialkoxy-cyano substituted stilbene derivatives were observed to be very sensitive to the length of the alkyl substituents. The photophysical properties of these materials could be classified into three distinct types and a clear correlation between the photophysical properties and crystal packing could be observed. The dialkoxy stilbene derivatives with short alkyl chain length (**DS1-DS4**) emitted in the blue region, the stilbene derivatives with intermediate alkyl chain lengths (**DS5-DS7**) emitted in the bluish-green region, while with a longer alkyl chain lengths (**DS8**) emitted in the green region (Figure 2.2). Since the chromophoric part of these stilbene derivatives remains essentially the same and modifications were made only in the length of the alkyl groups, the observed changes in the optical properties can be attributed to the changes in the molecular packing, which in turn are controlled by the weak interactions between the neighbouring molecules.

Since the photophysical properties of π-conjugated materials in solid state are decided by relative orientations and the extent of π-overlap between nearest neighbours, these interactions are described in more detail (Table 2.4). In order to geometrically define the extent of π-stacking, dimer units of nearest neighbour molecules were identified from the crystal data and have been reoriented, such that

both the molecules lie in planes parallel to an xy plane of a coordinate system, where x denotes the direction of the short axis of the molecule and y denotes the direction of its long axis. The z direction is maintained as the stacking direction of the molecules (Figure 2.11).
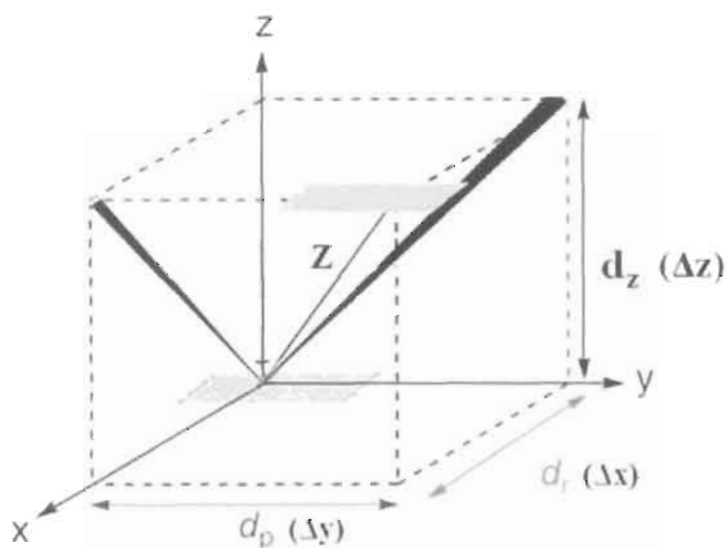
Figure 2.11. Schematic representation of the deviation from a perfect cofacial arrangement of molecules is defined in terms of pitch P (Δy) and roll R (Δx). The labels *x* and *y* refers to the direction of the short and long molecular axes, respectively.

The π-conjugated region of the molecule has a length of ~13 Å. For convenience in describing the system, the centroid (i. e., the midpoint of the π-conjugated region of the molecules) of any one of the molecule of the dimer unit is considered as the origin of the cartesian coordinate system. If the neighbouring molecules are stacked exactly one on top of the other, the (x,y) coordinates of the

centroids would be identical and such an arrangement can be considered as an ideal H-type stacking arrangement. Deviations of the coordinates of the centroids in the X-direction ($\Delta x = x1-x2$), Y-direction ($\Delta y = y1-y2$) and Z-direction ($\Delta z = z1-z2$) gives a measure of the extent of stacking where (x1, y1) and (x2, y2) are the coordinates of the centroids of the chromophore of the dimer units. The Δx and Δy gives the measures of deviation from the ideal H-type stacking, while the Δz value describes the vertical distance between the stacked molecules. The Δx, Δy and Δz parameters for each of the derivatives investigated are shown in Table 2.4. The Δx and Δy values relate respectively to the "roll" and "pitch" displacement of neighbouring molecules as defined by Curtis *et al.* [Curtis *et al.* 2004]. The crystallographic stacking distance is the distance between two identical parts of two adjacent molecules and is defined as Z. The value of Z can be calculated trigonometrically using the equation $Z_{calc} = (\mathbf{d_p}^2 + \mathbf{d_r}^2 + \mathbf{d_z}^2)^{1/2}$ and should be within the error limit of 1% to ensure the quality of the calculated pitch and roll distances [Chung *et al.* 2010; Chang *et al.* 2008; Dautel *et al.* 2008].

It may be noted that when the Δx value ("roll" displacement) is significantly higher than width of a benzene ring (~3.0 Å), the neighbouring molecules would be nearly slipped out from each other with very little π-overlap between them [Kumar *et al.* 2009]. For a similar slip in the y-direction ("pitch" displacement), π-overlap between molecules would be partially retained until Δy

approaches ~13 Å which corresponds to the length of the conjugated part of the chromophore.

Table 2.4. Δx, Δy, and Δz values for the nearest neighbour dimers of the stilbene derivatives.

Code	$\Delta x/Å$	$\Delta y/Å$	$\Delta z/Å$	$Z_{Obs}/Å$	$Z_{calc}/Å$
DS1	4.178	3.439	2.686	6.041	6.041
DS3	3.325	7.327	3.083	8.616	8.617
DS4	3.499	8.685	3.332	9.938	9.939
DS6	1.685	2.442	3.396	4.510	4.509
DS7	1.692	2.511	3.392	4.547	4.547
DS8	1.466	2.853	3.546	4.781	4.782

The deviations of Z values obtained from crystallographic stacking distance (Z_{Obs}) and calculated (Z_{calc}) using equation ($Z = (d_p^2 + d_r^2 + d_z^2)^{1/2}$) were within the error limit of 1% to ensure the quality of the calculated pitch and roll distances.

In **DS8** derivative, the molecules are stacked with their planes arranged parallel to each other with an interplanar distance of 3.546 Å (Δz). The neighbouring molecules are slipped along the short axis of 1.466 Å (Δx), which is significantly less than the width of the molecule. Similarly, the molecules are

slipped along the long molecular axis by 2.853 Å (Δy) which again is significantly lesser than the length of the chromophoric part of the molecule. As a result, significant extent of π-overlap is retained between the neighbouring molecules. Such an arrangement is typical of *J*-type aggregates, and according to exciton coupling theory, the oscillator strength of the electronic transition is concentrated at the bottom of the exciton band resulting in an optically allowed red-shifted emission with respect to the isolated molecules [Kasha *et al.* 1963; Whitten *et al.* 1993; Como *et al.* 2006; Oelkrug *et al.* 1998]. Thus the green emission (λ_{max}=500 nm) observed for this crystal can clearly be attributed to such a *J*-type aggregate.

For **DS7**, the molecules are stacked with their planes arranged parallel to each other with an interplanar distance of 3.392 Å (Δz). The molecules are slipped out along the short axis of about 1.692 Å (Δx) and along the long molecular axis by a distance of 2.511 Å (Δy) both of which are significantly lesser than the chromophore dimension. Thus considerable π-overlap still remains in this dimer system. This type of slipped arrangement is typical of that seen for *J*-type dimers. Even though the dimer structures indicated *J*-type of arrangement in both **DS7** and **DS8**, the slip along the short molecular axis in **DS7** (Δx=1.69 Å) is more compared to that of **DS8** (Δx=1.466 Å) which reduces relatively the π-overlap between the molecules. This reduction in the π-overlap resulted in a relative blue shift of the emission (λ_{max}=472 nm) compared to that of **DS8**. The molecular

alignment in **DS6** was very similar to that of **DS7,** both of which emit in the same region (Figure 2.2, Table 2.2).

Herringbone type of arrangement was observed in the derivatives with lower alkyl chain substituent (**DS3** and **DS4**). The slip along the short molecular axis (Δx) for **DS3** and **DS4** dimers were 3.325 Å and 3.499 Å respectively. Since the Δx values are higher than 3Å, the conjugated part of the chromophore is completely slipped out sideways from one on top of the other resulting in negligible π-overlap between the molecules. In both the derivatives, the conjugated part of the molecules were significantly in a non-planar conformation with a dihedral angle between the phenyl rings of the stilbene unit of 29.15° for **DS3** and 41.32° for **DS4**. Both the derivatives emitted in the blue region with an emission maxima of ~340 nm and this blue shift in emission compared to the derivatives which emitted in the green region (**DS8, DS7** and **DS6**) can be attributed either to twisting of the chromophoric unit of the molecule or due to lack of excitonic interactions between the neighbouring molecules.

A better understanding of the underlying reasons for the changes in the emission behaviour of **DS3** and **DS4** compared to that of **DS6-DS8** derivative was obtained by analyzing the crystal structure of **DS1**. The molecular packing of **DS1** indicated a herringbone arrangement of molecules in the crystal lattice, with a slip along the short axis of about 4.178 Å (Δx) and the slip along the long axis of 3.439 Å (Δy). Since the molecules were slipped out sideways totally from one on top of

the other, there was no π-overlap between the molecules. Two different conformational isomers (symmetrically non-equivalent) were observed in the crystal lattice with a dihedral angle of 7.50° and 17.01° between the phenyl rings of the stilbene units indicating that the molecules are reasonably planar. Even though the molecules are planar, the emission was observed to be in the blue region (λ_{max}=440 nm). Thus the red shift observed with increase in alkyl chain lengths in solid state of these class of molecules cannot be attributed simply to planarization of the molecules. It is clear from the example of **DS1** that planarization dose not lead to such a red shift. The absence of π-overlap between the neighbouring molecule means, exciton coupling between the neighbouring molecules is not possible. This leads to monomer emission [Xie *et al.* 2005]. Thus the large red shift seen in some of the derivatives can clearly be attributed to exciton coupling and not to planarization.

2.3.6. Thermally Induced Polymorphs

An interesting thermochromic behaviour was observed for the dialkoxy-cyano substituted stilbene derivatives with longer alkyl chain lengths (**DS10** and **DS12**). Upon heating, these materials exhibited significant changes in their colour and fluorescence emission. Figure 2.12 summarizes these observations for **DS12** and emission characteristics of both the derivatives (**DS10** and **DS12**) are summarized in Table 2.5. Transparent white crystals of **DS12** exhibiting blue

fluorescence which were obtained on slow crystallization from solvents underwent a transformation to bright green translucent solid on heating to 55 °C at a rate of 5 °C/min. This transformation was accompanied by a change in fluorescence of the crystals from blue to green (Figure 2.13b). Both the blue and green fluorescent polymorphs were highly stable. The thermally induced green fluorescent polymorph which was stable for more than a period of two years, could however be reverted back to the blue form by exposure to hexane vapour or by slow recrystallization from solvents.
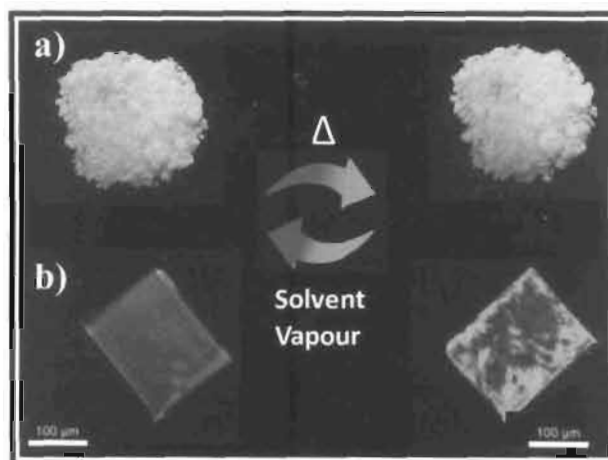
Figure 2.12. Photographs of blue and green fluorescent polymorphs of **DS12** under a) ordinary light and b) UV light of wavelength 365 nm (right).

Both the absorption and the excitation spectra showed a red shift in absorption of the thermally induced green polymorphic form compared to that of the blue polymorph (Figure 2.13). These changes could be visualized directly as

change in the colours of the polymorphs. The blue emitting species was a white transparent solid while the green emitting polymorphs appeared yellow in colour.
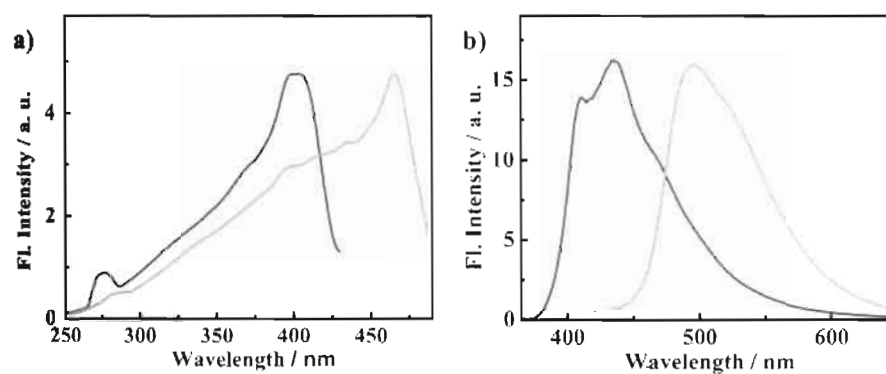
Figure 2.13. a) Fluorescence excitation and b) emission spectra of both the blue (blue line) and the green (green line) polymorphs of **DS12**.

Table 2.5. Photophysical properties of **DS12** and **DS10** derivatives.

	λ_{abs} [nm]	λ_{em} [nm]	FWHM [nm]	Φ_F
DS12				
Hexane	345	404	62	0.01
Blue form	400[a]	440	88	0.59
Green form	465[a]	500	60	0.45
DS10				
Hexane	345	404	63	0.01
Blue form	395[a]	435	80	0.69
Green form	464[a]	498	74	0.61

[a] Obtained from excitation spectrum.
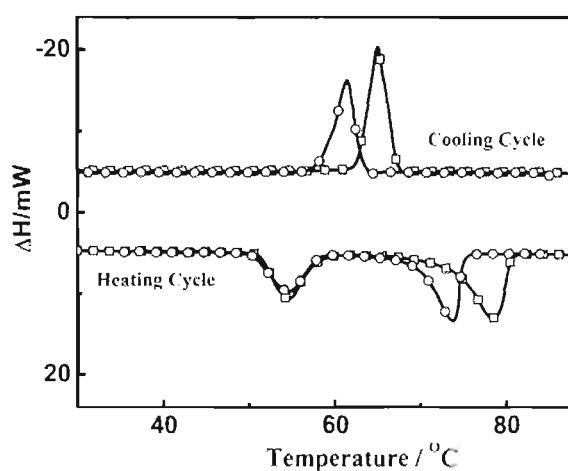
Figure 2.14. DSC thermogram of **DS12** (□) and **DS10** (○) in the first heating/cooling cycle at a scan rate of 5 °C/min.

The thermally induced formation of the green fluorescent polymorphs could also be monitored by differential scanning calorimetry (DSC). The DSC thermograms (Figure 2.14) showed an endothermic peak at 55 °C in the heating cycle corresponding to the formation of the green polymorphs as observed visually. The enthalpy change for this transformation was 27.5 kJ/mol for **DS12** and 31.5 kJ/mol for **DS10**. A second endothermic peak was observed at higher temperatures corresponding to the melting point of **DS12** (78 °C, ΔH= 41.4 kJ/mol) and **DS10** (74 °C, ΔH= 44.9 kJ/mol). In the cooling cycle, peaks corresponding to crystallization were observed at 65 °C (ΔH= 47 kJ/mol) and 61.5 °C (ΔH= 49.1 kJ/mol) for **DS12** and **DS10** respectively. Additional peaks were not observed in the cooling cycle with further decrease in temperature indicating that

the thermally induced green fluorescent polymorphs do not revert to the original form without any external stimulus.

It is interesting to note that whereas the temperatures for melting and crystallization showed slight variations for **DS12** and **DS10**, the temperatures for transformation from one polymorph to the other were identical. This strongly suggests that the mechanism of transformation from one polymorph to the other was similar for the two derivatives. Since the chromophores in the two polymorphic forms are the same, the variations in their optical properties can be attributed to variations in their molecular packing.
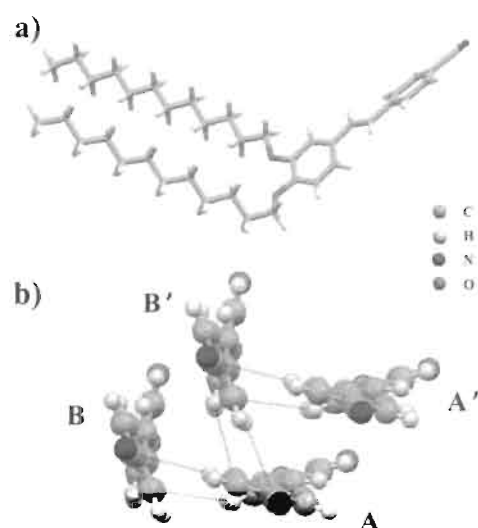
Figure 2.15. a) Crystal structure of **DS12**; b) A tetramer unit viewed along the long molecular axis, dotted lines indicate interactions less than 3 Å (alkyl chains have been omitted for clarity).

X-ray analysis of the single crystals of these derivatives was conducted in order to gain an understanding on the role of molecular packing in determining the

optical properties of these polymorphs. Single crystals of **DS12** suitable for X-ray analysis was obtained by slow evaporation from hexane solutions. **DS12** formed white transparent crystals belonging to the monoclinic space group ($P2_1/c$) with four molecules in the unit cell. The most notable conformational feature obtained from single crystal X-ray analysis of this molecule was the dihedral angle of 33.95° between the phenyl rings of the stilbene units, which indicated the molecules to be significantly distorted from planarity (Figure 2.15a). Analysis of its molecular packing indicated two types of nearest neighbour interactions which are assigned as AA' and AB in Figure 2.15b. In the AA' type interaction, the molecules are aligned in a face to face manner with an interplanar distance of 3.55 Å and a slip of 3.30 Å along the short molecular axis. As a result of this slip, which is larger than the width of a phenyl ring (~3 Å) the π-overlap between them is negligible [Kumar *et al.* 2009; Chung *et al.* 2010; Chang *et al.* 2008; Dautel *et al.* 2008]. For the AB type alignment, the planes of the neighbouring molecules are twisted with respect to each other by an angle of 51.86° in an edge to face configuration, and this alignment is stabilized by C-H...π interactions as well as by strong interactions between alkyl groups of the neigbouring molecules. Such an alignment also results in minimal π-overlap between the neighbouring molecules. As a result, excitonic interactions between the neighbouring molecules are minimal and the structure of the emission spectrum of the crystals was similar to that observed in hexane solutions. The emission maximum was at 435 nm which

was the same as that observed in a solvent of medium polarity such as tetrahydrofuran.
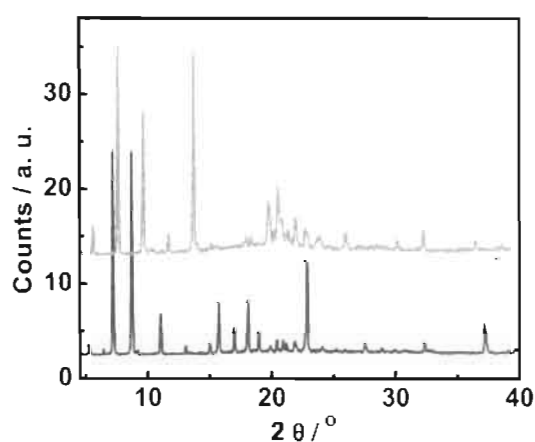
Figure 2.16. Powder XRD spectra of both the blue (blue line) and the green (green line) polymorphs of **DS12**.

X-ray single crystal analysis could not be carried out on the thermally induced polymorph because of the poor quality of crystals obtained on heating. Indication of significant changes in the molecular packing in the two forms could however be obtained by monitoring the variations in their powder X-ray diffraction patterns, especially in the wide angle region. The crystalline nature of both the blue and the green fluorescent forms of **DS12** were evident from the sharp peaks in the powder XRD patterns [Figure 2.16]. In the lower angle region (i.e., $2\Theta = 5\text{-}15$), the XRD patterns are nearly the same except for the appearance of a new sharp peak at 6.47 Å in thermally induced green polymorph. This suggests that the long distance packing parameters are not significantly altered. The major

changes between the XRD spectra of the two forms were in the wide angle region which correspond to shorter distance alignments around 3-6 Å. This, along with the fact that the transformation is from one crystalline state to the other without melting, strongly suggests that major changes in the alignment were in the short distances and in the longer distances, the molecular alignment remains almost unperturbed.

The difference in optical properties of the thermally induced green polymorph, compared to the recrystallized material can be attributed either to planarization of the molecule or to enhanced excitonic interactions as a result of the altered molecular packing. Based on the investigations of the optical properties and correlating them to the molecular packing of the lower homologues (as discussed earlier), the reason for the thermally induced transformation could be unravelled. It is clear from the earlier discussion that the derivatives with strong exciton interaction emitted in the green region and the derivatives lacking exciton interactions emitted in the blue region. The optical properties (emission, excitation and lifetime values) of the thermally induced green polymorph of **DS12** were exactly similar to that of the lower homologues **DS8**. This would strongly suggest that heating of **DS12** leads to planarization of the molecules, resulting in the realignment in such a way to the formation of excitonically coupled *J*-aggregates similar to that observed in **DS8**. Thus the green emission observed for the

thermally induced polymorph can clearly be attributed to the formation of *J*-type aggregates.
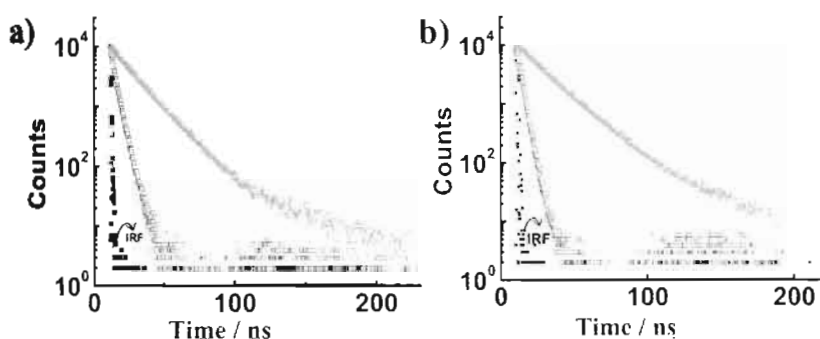
Figure 2.17. Fluorescence lifetime decay profile of a) **DS1** (■) and **DS8** (●) and that of the b) **DS12** blue (■) and green (●) polymorphs.

Evidence for aggregate formation could also obtained from the fluorescence lifetime data measured in the crystals. Figure 2.17 shows the fluorescence lifetime decay profiles of the crystals of **DS1** and **DS8** as well as that of the blue and green polymorphic forms of **DS12**. A biexponential decay with lifetime of 3.87 ns (73.29%) and 1.57 (26.71%) was observed for **DS1**, whereas for **DS8** it was 17.88 ns (87.59%) and 9.21 ns (12.41%) respectively. As described above, crystal structure analyses indicated isolated monomers in **DS1** and J-type aggregates in **DS8**. The nearly four fold enhancement in fluorescence lifetime of the major component in **DS8** compared to **DS1** can be attributed to this difference. Similar differences were observed between the fluorescence lifetimes of the blue and green polymorphic forms of **DS12**. While the fluorescence of the blue polymorphic form of **DS12** showed a monoexponential decay with a lifetime of

about 3.16 ns. the decay profile of the fluorescence of the green form of **DS12** showed a biexponential decay with lifetimes of 20.97 ns (88%) and a shorter component of 8.9 ns (12%). These studies clearly shows that fluorescence lifetime of the major component of the green emitting species is significantly longer than that of the blue emitting species. Comparison of these results with that of **DS1** and **DS8** suggests that heating of **DS12** leads to realignment of the isolated monomers leading to the formation of excitonically coupled J-aggregates similar to that observed in **DS8**. This would suggest that the molecular alignment of **DS12** shown in Figure 2.15b would transform to one that would be similar to the molecular packing observed in **DS8** crystals (Figure 2.10). Such a transformation can occur if the molecules of **DS12** undergo planarization followed by an angular twist of the molecule as a whole along the short axis as shown schematically in Figure 2.18.
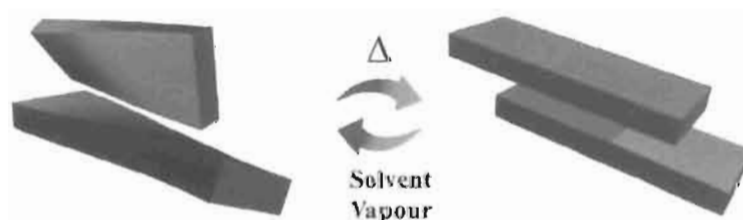
Figure 2.18. Schematic representation of molecular alignment of a) blue polymorph and that of the b) green polymorph of **DS12**.

2.4. Conclusion

The solid state photophysical properties of a series of donor-acceptor substituted stilbene derivatives with dialkoxy groups as donors and cyano group as acceptor has been investigated. By varying the length of the alkyl substituent, it has been possible to fine-tune the solid state fluorescence of these materials over a wide range of wavelengths. On the basis of the analysis of molecular packing in the single crystals and correlating to the optical properties, we have shown the solid state fluorescence of this series of stilbene based molecules depends on various factors such as rigidization, planarization and more importantly the nature of the relative alignment of neighbouring molecules which decides whether exciton coupling will or will not occur. The derivatives with longer alkyl chains (DS10 and DS12) showed thermally induced crystal to crystal transition with significantly different fluorescence emission and colour. The observed thermochromic transitions could be attributed to the planarization of the molecules and the resulting changes in the relative orientations of the neighbouring molecules, which in turn facilitated strong excitonic coupling between them. A detailed understanding of the relative orientation of molecules in the solid state of conjugated materials and its correlation with optical properties has significant implications in the tailoring and fine-tuning of the properties of such materials for various optoelectronic applications.

2.5. Experimental Section

2.5.1. Synthesis and Characterization

Alkoxy-cyano substituted stilbene derivatives were synthesized according to the standard procedure as shown in Scheme 2.1 and were unambiguously characterized.

General Procedure for the Synthesis of Stilbene Derivatives (1)

A suspension of sodium hydride (5.0 equiv.) in dry THF was prepared and diethyl 4-cyanobenzylphosphonate (2) (1.1 equiv.) was added at 0 °C. After stirring for 10 minutes, alkoxy substituted aldehyde (3) (1.0 equiv.) was added drop wise and the reaction mixture stirred for 3 h under argon atmosphere. Solvent was distilled off and cold water was added drop wise and neutralized with 1:1 HCl. It was then extracted with dichloromethane and dried over anhydrous sodium sulphate. The product was purified by column chromatography using 2% ethyl acetate/hexane as eluent and silica as packing material.

(E)-4-(3,4-dimethoxystyryl)benzonitrile (DS1)

Yield: 85 %; m. p.: 103 °C ; IR ν_{max} (KBr): 549.7, 970.19, 1022.27, 1238.30, 1251.80, 1276.88, 13338.60, 1417.68, 1452.40, 1465.90, 1517.98, 1593.20, 2225.85, 2839.22, 2935.66, 3020.53
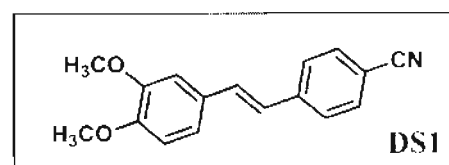
cm^{-1}.: ^{1}H NMR (500MHz, CDCl$_3$, TMS) :δ 7.61-7.60 (d, J – 8.5 Hz, 2H,

aromatic), 7.56-7.54 (d, *J* ~ 8 Hz, 2H, aromatic), 7.17-7.14 (d, *J* – 16.5 Hz, 1H, allylic), 7.08 (s, 1H, aromatic), 7.06-7.04 (d, *J* – 8 Hz, 1H, aromatic), 6.94-6.91 (d, *J* = 16.5 Hz, 1H, allylic), 6.88-6.86 (d, *J* – 8.5 Hz, 1H, aromatic), 3.95 (s, 3H, -OCH$_3$), 3.91(s, 3H, -OCH$_3$); ^{13}C NMR (125 MHz, CDCl$_3$, TMS) δ: 149.66, 149.12, 141.99, 132.35, 132.10, 129.26, 126.47, 124.62, 120.63, 119.03, 111.11, 109.98, 108.82, 55.86, 55.81 ppm; FAB MS: m/z calcd for C$_{17}$H$_{15}$NO$_2$, 265.31; found 266.22 [M+H].

(E)-4-(3,4-diethoxystyryl)benzonitrile (DS2)

Yield: 86 %; m. p.: 108 °C ; IR υ$_{max}$ (KBr): 1039, 1139, 1269, 1512, 2218, 2884, 2980, 3067 cm^{-1}; ^{1}H NMR (500MHz, CDCl$_3$, TMS): δ 7.62-7.60 (d, *J* = 8.5 Hz, 2H, aromatic), 7.55-7.54 (d, *J* – 8
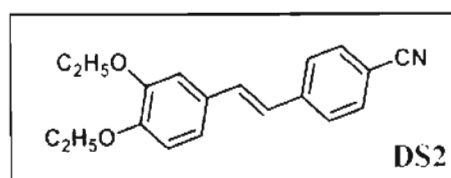
Hz, 2H, aromatic), 7.16-7.12 (d, *J* – 16.5 Hz, 1H, allylic), 7.088 (s, 1H, aromatic), 7.067-7.051 (d, *J* – 8 Hz, 1H, aromatic), 6.943- 6.910 (d, *J* – 16.5 Hz, 1H, allylic), 6.885-6.868 (d, *J* – 8.5 Hz, 1H, aromatic), 4.178-4.106 (m, 4H, -OCH$_2$-), 1.503-1.457(m, 6H, -CH$_3$); ^{13}C NMR (125 MHz, CDCl$_3$, TMS) δ: 149.62, 148.89, 142.19, 132.46, 132.33, 129.31, 126.56, 124.58, 120.79, 119.16, 113.12, 111.34, 110.05, 64.70, 64.53, 14.87, 14.79 ppm; FAB MS: m/z calcd for C$_{19}$H$_{19}$NO$_2$, 293.36; found 294.22 [M+H].

(E)-4-(3,4-dipropoxystyryl)benzonitrile (DS3)

Yield: 82 %; m.p.: 96 °C ; IR υ_{max} (KBr): 1138.00, 1240.23, 1253.73, 1280.73,

1309.67, 1325.10, 1338.60, 1390.66, 1425.40, 1465.90, 1519.91, 1593.20, 2223.92, 2848.86, 2920.23, 2953.02
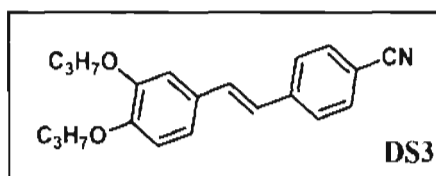
cm^{-1}.; ^{1}H NMR (500MHz, CDCl$_3$, TMS): δ 7.603-7.587 (d, J = 8 Hz, 2H, aromatic), 7.541-7.524 (d, J = 8.5 Hz, 2H, aromatic), 7.145-7.112 (d, J = 16.5 Hz, 1H, allylic), 7.084 (s, 1H, aromatic), 7.052-7.035 (d, J = 8.5 Hz, 1H, aromatic), 6.933- 6.901 (d, J = 16 Hz, 1H, allylic), 6.873-6.856 (d, J = 8.5 Hz, 1H, aromatic), 4.067-4.009 (m, 4H, -OCH$_2$-), 1.846-1.487 (m, 4H, -CH$_2$-), 1.011-0.967 (m, 6H, -CH$_3$) ppm; ^{13}C NMR (125 MHz, CDCl$_3$, TMS) δ: 150.00, 149.23, 142.14, 132.35, 132.72, 129.25, 126.470, 124.44, 120.76, 119.09, 113.40, 111.69, 109.90, 69.05, 68.81, 31.30, 31.19, 19.18, 19.15, 13.82, 13.80 ppm; FAB MS: m/z calcd for C$_{21}$H$_{23}$NO$_2$, 321.41; found 322.23 [M-H$^-$]

(E)-4-(3,4-dibutoxystyryl)benzonitrile (DS4)

Yield: 81 %; m.p.: 70 °C ; IR υ_{max} (KBr): 1175, 1467, 1595, 2222, 2870, 2933,

2953, 3053 cm^{-1}; ^{1}H NMR (500MHz, CDCl$_3$, TMS) :δ 7.603-7.587 (d, J = 8 Hz, 2H, aromatic), 7.541-7.524 (d, J =
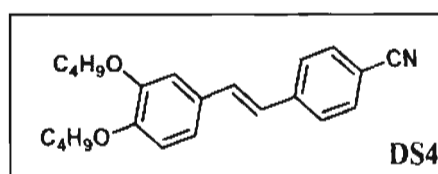
8.5 Hz, 2H, aromatic), 7.145-7.112 (d, J = 16.5 Hz, 1H, allylic), 7.084 (s, 1H, aromatic), 7.052-7.035 (d, J = 8.5 Hz, 1H, aromatic), 6.933- 6.901 (d, J = 16 Hz,

1H, allylic), 6.873-6.856 (d, J = 8.5 Hz, 1H, aromatic), 4.067-4.009 (m, 4H, -OCH$_2$-), 1.846-1.487 (m, 8H, -CH$_2$-), 1.011-0.967 (m, 6H, -CH$_3$) ppm; ^{13}C NMR (125 MHz, CDCl$_3$, TMS) δ: 150.00, 149.23, 142.14, 132.35, 132. 72, 129.25, 126.470 124.44, 120.76, 119.09, 113.40, 111.69, 109.90, 69.05, 68.81, 31.30, 31.19, 19.18, 19.15, 13.82, 13.80 ppm; FAB MS: m/z calcd for C$_{23}$H$_{27}$NO$_2$, 349.47; found 350.43 [M+H$^+$].

(E)-4-(3,4-bis(pentyloxy)styryl)benzonitrile (DS5)

Yield: 80 %; m.p.:69 °C ; IR υ$_{max}$ (KBr): 1138, 1267, 1514, 1595, 2224, 2855, 2953, 3024 cm^{-1}; ^{1}H NMR (500MHz, CDCl$_3$, TMS) :δ 7.615-7.598 (d, J =

8.5 Hz, 2H, aromatic), 7.551-7.534 (d, J = 8.5 Hz, 2H, aromatic), 7.152-7.119 (d, J = 16.5 Hz, 1H, allylic), 7.084 (s, 1H, aromatic), 7.058-7.041 (d, J = 8.5 Hz, 1H, aromatic), 6.939- 6.907 (d, J = 16 Hz, 1H, allylic), 6.876-6.859 (d, J = 8.5 Hz, 1H, aromatic), 4.064-4.008 (m, 4H, -OCH$_2$-), 1.885-1.373 (m, 12H, -CH$_2$-), 0.959-0.921 (m, 6H, -CH$_3$) ppm.; ^{13}C NMR (125 MHz, CDCl$_3$, TMS) δ: 150.01, 149.25, 142.18, 132.40, 132.32, 129.26, 126.50, 124.47, 120.78, 119.12, 113.38, 111.65, 109.95, 69.36, 69.13, 28.96, 28.87, 28.19, 28.16, 22.43, 14.01 ppm; FAB MS: m/z calcd for C$_{25}$H$_{31}$NO$_2$, 377.52; found 378.43 [M+H$^+$].
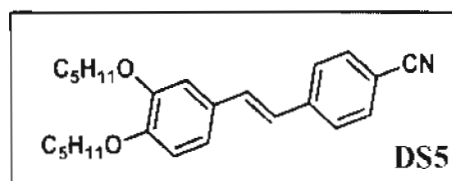
(E)-4-(3,4-bis(hexyloxy)styryl)benzonitrile (DS6)

Yield: 82 %; m.p.: 68 °C ; IR υ_{max} (KBr): 1044, 1138, 1250, 1514, 2224, 2853,

2951, 3022 cm^{-1}; ^{1}H NMR (500MHz, CDCl$_3$, TMS) :δ 7.604-7.588 (d, J = 8 Hz, 2H, aromatic), 7.542-7.525 (d, J =
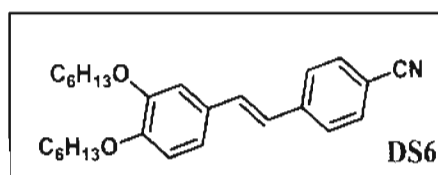
8.5 Hz, 2H, aromatic), 7.146-7.113 (d, J = 16.5 Hz, 1H, allylic), 7.082 (s, 1H,

aromatic), 7.051-7.035 (d, J = 8 Hz, 1H, aromatic), 6.934-6.902 (d, J = 16 Hz, 1H,

allylic), 6.869-6.853 (d, J = 8 Hz, 1H, aromatic), 4.059-4.000 (m, 4H, -OCH$_2$-),

1.859-1.332 (m, 16 H, -CH$_2$-), 0.927-0.894 (m, 6H, -CH$_3$) ppm.; ^{13}C NMR (125

MHz, CDCl$_3$, TMS) δ: 150.00, 149.23, 142.16, 132.37, 132.30, 129.25, 124.44,

120.77, 119.10, 113.37, 111.65, 109.92, 69.35, 69.11, 31.54, 29.23, 29.13, 25.67,

25.63, 22.55, 13.97 ppm; FAB MS: m/z calcd for C$_{27}$H$_{35}$NO$_2$, 405.57; found 406.22

[M+H$^+$].

(E)-4-(3,4-bis(heptyloxy)styryl)benzonitrile (DS7)

Yield: 86 %; m.p.: 66 °C ; IR υ_{max} (KBr): 1138, 1236, 1251, 1514, 2224, 2851,

2920, 2953 cm^{-1}.; ^{1}H NMR (500MHz, CDCl$_3$, TMS) :δ 7.609-7.592 (d, J = 8.5 Hz, 2H, aromatic), 7.545-7.529 (d,
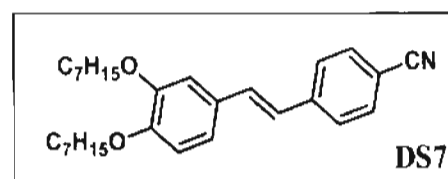
J = 8 Hz, 2H, aromatic), 7.149-7.116 (d, J = 16.5 Hz, 1H, allylic), 7.082 (s, 1H,

aromatic), 7.054-7.037 (d, J = 8.5 Hz, 1H, aromatic), 6.936- 6.904 (d, J = 16 Hz,

1H, allylic), 6.871-6.855 (d, J = 8 Hz, 1H, aromatic), 4.059-4.001 (m, 4H, -OCH$_2$.

), 1.861-1.297 (m, 20H, -CH$_2$-), 0.907-0.894 (m, 6H, -CH$_3$) ppm.; ^{13}C NMR (125 MHz, CDCl$_3$, TMS) δ: 150.01, 149.24, 142.16, 132.38, 132.31, 129.25, 126.48, 124.45, 120.78, 119.10, 113.38, 111.67, 109.94, 69.36, 69.12, 31.76, 29.28, 29.18, 29.03, 25.96, 25.93, 22.56, 14.04 ppm; FAB MS: m/z calcd for C$_{29}$H$_{39}$NO$_2$, 433.63; found 434.72 [M+H$^+$].

(E)-4-(3,4-bis(octyloxy)styryl)benzonitrile (DS8)

Yield: 80 %; m.p.: 65 °C ; IR ν$_{max}$ (KBr): 1138.00, 1240.23, 1253.73, 1280.73, 1309.67, 1325.10, 1338.60, 1390.66, 1425.40, 1465.90, 1519.91, 1593.20, 2223.92, 2848.86, 2920.23, 2953.02
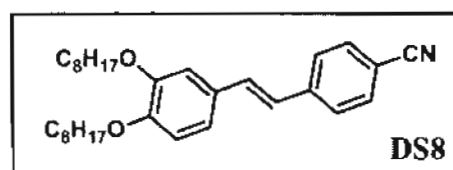
cm^{-1}.; ^{1}H NMR (500MHz, CDCl$_3$, TMS) :δ 7.61-7.7.60 (d, *J* = 8.5 Hz, 2H, aromatic), 7.55-7.54 (d, *J* = 8 Hz, 2H, aromatic), 7.15-7.12 (d, *J* = 16 Hz, 1H, allylic), 7.08 (s, 1H, aromatic), 7.06-7.04 (d, *J* = 8 Hz, 1H, aromatic), 6.94- 6.91 (d, *J* = 16.5 Hz, 1H, allylic), 6.88-6.86 (d, *J* = 8.5 Hz, 1H, aromatic), 4.06-4.00 (m, 4H, -OCH$_2$.), 1.88-1.26 (m, 24H, -CH$_2$-), 0.90-0.87 (m, 6H, -CH$_3$) ppm.; ^{13}C NMR (125 MHz, CDCl$_3$, TMS) δ: 150.04, 149.28, 142.20, 132.42, 132.34, 129.29, 126.51, 124.49, 120.80, 119.13, 113.43, 111.72, 109.98, 69.41, 69.17, 31.80, 29.35, 29.30, 29.26, 29.21, 26.03, 26.00, 22.65, 14.08 ppm; FAB MS: m/z calcd for C$_{31}$H$_{43}$NO$_2$; found 461.58 [M$^-$].

(E)-4-(3,4-bis(decyloxy)styryl)benzonitrile (DS10)

Yield: 90 %; m.p.: 74 °C ; IR υ_{max} (KBr): 819.75, 1138, 1249.87, 1273.02, 1330.88, 1423.47, 1463.97, 1475.54, 1517, 1591.27, 2227.78, 2870.08, 2852.72, 2920.33, 2956.87 cm^{-1}.; ^{1}H
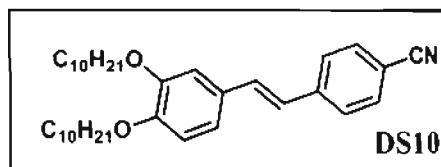
NMR (500MHz, CDCl$_3$, TMS) :δ 7.62-7.60 (d, J = 8.5 Hz, 2H, aromatic), 7.55-7.54 (d, J = 8.5 Hz, 2H, aromatic), 7.15-7.12 (d, J = 16.5 Hz, 1H, allylic), 7.08 (s, 1H, aromatic), 7.06-7.04 (d, J = 8.5 Hz, 1H, aromatic), 6.94- 6.91 (d, J = 16.5 Hz, 1H, allylic), 6.88-6.86 (d, J = 8.5 Hz, 1H, aromatic), 4.06-4.00 (m, 4H, -OCH$_2$-), 1.88-1.27 (m, 32H, -CH$_2$-), 0.90-0.87 (m, 6H, -CH$_3$) ppm.; ^{13}C NMR (125 MHz, CDCl$_3$, TMS) δ: 150.01, 149.24, 142.18, 132.40, 132.32, 129.26, 126.50, 124.46, 120.79, 119.12, 113.39, 111.66, 109.95, 69.38, 69.14, 31.88, 29.59, 29.55, 29.38, 29.32, 29.18, 26.01, 25.98, 22.65, 14.08 ppm; FAB MS: m/z calcd for C$_{35}$H$_{51}$NO$_2$ 517.78; found 517.56 [M].

(E)-4-(3,4-bis(dodecyloxy)styryl)benzonitrile (DS12)

Yield: 86 %; m. p.: 79 °C; IR υ_{max} (KBr): 545.85, 605.65, 723.31, 788.89, 812.03, 835.18, 846.75, 862.18, 914.26, 950.91, 987.55, 999.13, 1016.49, 1058.92, 1066.64, 1109.07, 1138.00,

1170.79, 1213.23, 1228.66, 1240.23, 1249.87, 1269.16, 1278.81, 1315.45, 1325.10, 1336.67, 1377.17, 1390.68, 1423.47, 1454.33, 1463.97, 1514.12,
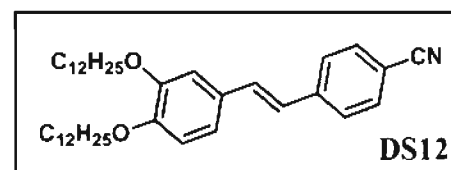
1581.63, 1595.13, 1633.71, 2223.92, 2848.86, 2922.16, 2953.02, 3022.45, 3045.60, 3061.03; ^{1}H NMR (500MHz, CDCl$_3$, TMS) :δ 7.60-7.58 (d, J = 8.5 Hz, 2H, aromatic),7.53-7.51 (d, J = 8.5 Hz, 2H, aromatic), 7.13-7.10 (d, J = 16.5 Hz, 1H, allylic), 7.06 (s, 1H, aromatic), 7. 04-7.02 (d, J = 8.5 Hz, 1H, aromatic), 6.92-6.89 (d, J = 16.5 Hz, 1H, allylic), 6.85-6.84 (d, J = 8.5 Hz, 1H, aromatic), 4.04-3.98(m, 4H, -OCH$_2$-), 1.84-1.32 (m, 40H, -CH$_2$-), 0.88-0.82 (m, 6H, -CH$_3$) ppm; ^{13}C NMR (125 MHz, CDCl$_3$, TMS) δ: 150.06, 149.29, 142.21, 132.43, 132.36, 129.30, 126.52, 124.49, 120.82, 119.13, 113.45, 111.74, 110.00, 69.42, 69.18, 31.92, 30.02, 29.69, 29.64, 29.41, 29.36, 29.22, 26.05, 26.02, 22.68, 14.10 ppm.; FAB MS: m/z calcd for C$_{39}$H$_{59}$NO$_2$, 573.89; found 574.43 [M+H$^+$].

Synthesis and Study of Liquid Crystalline and Photophysical Properties of Pyridine Cored Mesogens
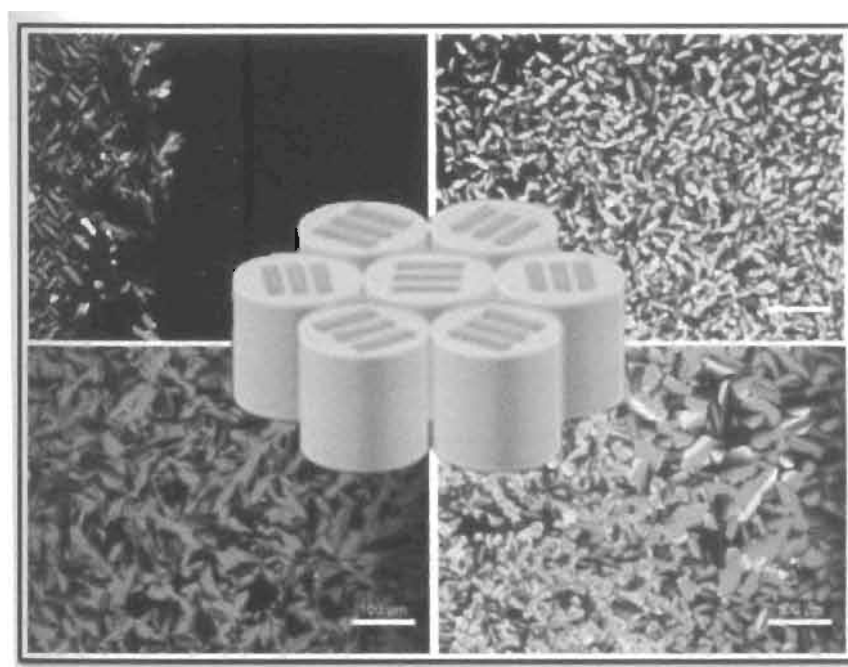
Objective: To synthesize and investigate the liquid crystalline behaviour of rod shaped molecules forming discotic mesophases and to understand their photophysical properties in solution and in their condensed phases.

3.1. Abstract

Two series of pyridine cored donor-acceptor-donor systems, specifically designed to exhibit polycatenar discotic liquid crystalline phases were synthesized and characterized. The chemical structure of the molecules consists of two alkoxy stilbenoid units attached to a central pyridine core through 1,3,4-oxadiazoles linkers in the 2,6 (PS) and 2,5 (PSL) positions of the pyridine ring to form a rigid rod π-conjugated back bone resulting in donor-acceptor-donor architecture. The alkyl chains were grafted in the terminal ends in order to induce liquid like property leading to the formation of mesophases. The extended π-conjugated core and the alkoxy substitution at the terminal ends were expected to facilitate a close packing of the calamitic cores in their bulk states. A few of these derivatives exhibited polycatenar discotic liquid crystalline phases at elevated temperatures and the polarized optical microscopic studies indicated that the phase possessed hexagonal symmetry. These derivatives were found to be luminescent in solution as well as in the solid state. The synthesis of these derivatives, investigation of their liquid crystalline phases and fluorescence properties in solution as well as in the solid state are described in this Chapter.

3.2. Introduction

Liquid crystals (LCs) constitute a unique class of condensed state materials wherein the constituent molecules possess a degree of long range order in between that of highly ordered crystals and isotropic liquids [Sluckin *et al.* 2004; Demus *et al.* 1998; Gennes *et al.* 1995]. As a result, these materials possess anisotropic electrical, magnetic and optical properties similar to crystals and at the same time can flow like liquids. The unique self-organizing ability, fluidity and the ease of formation of defect-free oriented films of liquid crystals make them useful for application in high efficiency organic electro-optic devices [O'Neill *et al.* 2003; Grimsdale *et al.* 2005; Kato *et al.* 2006; Kumar *et al.* 2006; Laschat *et al.* 2007]. They also serve as model compounds for investigating the connection between chemical structure and physical property of self-assembled materials [Yasuda *et al.* 2006; Kimura *et al.* 2006; Levitsky *et al.* 2000; Das *et al.* 2008].

Liquid crystals can be broadly classified as lyotropic, when the mesophase formation is solvent induced and thermotropic, when the mesophase formation is thermally induced. Rod like thermotropic liquid crystals have been known for more than a century and the first report was of cholesteryl benzoate by Reinitzer in 1888. Thermotropic LC phases are predominantly observed in organic compounds, which are rod-, disc- or board shaped anisotropic molecular structures. According to their microscopic organization, liquid crystalline phases are broadly grouped into four major classes namely nematics, cholesterics,

smectics, and discotics (Figure 3.1). In the nematic mesophase, the molecules are aligned with their long axes parallel to each other. Cholesteric or chiral nematic phases are observed in optically active molecules or by nematic liquid crystals containing optically active dopants. In this phase the director (a unit vector signifying the average direction of the molecular long axis) of an individual layer is twisted through a small angle with respect to the director of the adjacent layer resulting in a helical arrangement of the layers. The thickness required for the director to turn through $360°$ represents the pitch length (p) of the helical arrangement in cholesterics. In a smectic mesophase, the molecules are not only aligned parallel but are also arranged in such a way that the centers of adjacent molecules lie in a plane. Smectic phases can be further differentiated depending upon the packing arrangement of the molecules within the layers and the variation in the angle of the directors with respect to the layer plane [Dierking 2003].
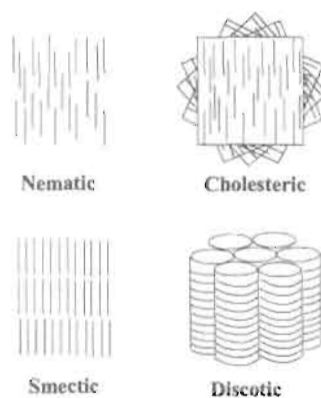
Figure 3.1. Pictorial representations of the molecular shapes and orientations of the major liquid crystalline phase types.

Discotic liquid crystals are a comparatively newer group of liquid crystals discovered by S. Chandrasekhar and co-workers in 1977 [Chandrasekhar *et al.* 1977; 1992]. Originally it was thought that mesomorphism could be observed only in molecules possessing a rod like structure. Later it was shown that many other molecular architectures, particularly disc like structures, were also capable of generating mesophases. Discotic mesophases are usually formed from molecules possessing a disc like core and flexible alkyl periphery, which induces ordering and flow property respectively. The two basic types of discotic mesophases which have been widely recognized are the columnar and nematic phases (Figure 3.2). Nematic phases are anisotropic fluids with the discs having a tendency to align in a parallel manner, where as the columnar phases are characterized by stacked columns of the molecules, with the columns being packed together to form a two dimensional crystalline array [Kumar *et al.* 2006; Laschat *et al.* 2007].

Nematic Discotic   Hexagonal Columnar
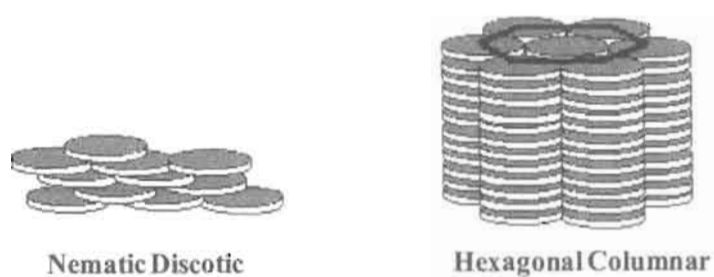
Figure 3.2. Pictorial representations of the orientations of the major discotic liquid crystalline phase types.

There is also a small number of rod like molecular structures capable of generating columnar phases analogous to that observed for discotic molecules. Molecules possessing an elongated linear polyaromatic core with aliphatic chains grafted on the two terminal ends are known to exhibit discotic liquid crystals. Such mesogens are generally termed as 'Catenar' (Figure 3.3). Depending on the number of terminal alkyl chains they are termed as hexacatenar, tetracatenar and so on [Nguyen *et al.* 1997; Rais *et al.* 2001; Smirnova *et al.* 2003; He *et al.* 2007; Yasuda *et al.* 2006]. This molecular architecture which is situated between the rod-like and disc-like mesogenic compounds gives rise to a rich poly-mesomorphism which may present nematic (N), lamellar, cubic (Cub) and columnar (Col) mesophases in the same series of compounds or even in a single compound [Yasuda *et al.* 2009].
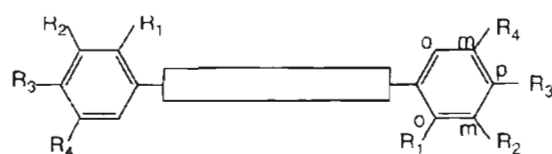
a   Hexacatenars *3mpm-3mpm* or phasmids: R_1 = H; R_2 = R_3 = R_4
b   Tetracatenars *2mp-2mp* or biforked mesogens: R_1 = R_4 = H; R_2 = R_3

Figure 3.3. Schematic representation of polycatenar mesogens.

Over the last decade, π-conjugated LCs have attracted a great deal of attention because of their potential for applications in flexible electronic devices [Hoeben *et al.* 2005; Adam *et al.* 1994; Dodabalapur *et al.* 1995; McCulloch *et al.*

2006; Fichou *et al.* 2000; Sergeyev *et al.* 2007; Otsubo *et al.* 2002; Boden *et al.* 1993; Funahashi *et al.* 2000; Funahashi *et al.* 2005; Bushby *et al.* 2002]. π-Conjugated discotic liquid crystals, which self-assemble into columnar structures with a strong π-orbital overlap can result in forming one dimensional semiconductors with much better performance than that observed for conjugated polymers. High charge carrier mobilities comparable to that of amorphous silicon could be attained in such materials. Using such dynamic and anisotropic LC structures, anisotropic conduction of charge [Adam *et al.* 1994; Boden *et al* 1993; Funahashi *et al.* 2000; Funahashi *et al.* 2005;], ion [Yoshio *et al.* 2004; Ichikawa *et al.* 2007; Kishimoto *et al.* 2005; Cho *et al.* 2004] and mass-transporting [Zhou *et al.* 2005] materials have been reported.

1,3,4-Oxadiazole derivatives have enjoyed widespread use as electron transporting/hole blocking (ET/HB) materials and as emitting layers in electroluminescent diodes due to their electron deficient nature, high photoluminescence quantum yield, good thermal and chemical stabilities and also for their ease of synthesis. In view of this much effort has been devoted to the synthesis of 1,3,4-oxadiazole based liquid crystals [Zhang *et al.* 2003; Tokuhisa *et al.* 1998; Qu *et al.* 2008].

In this Chapter, we describe the synthesis, liquid crystalline and photophysical properties of two series of pyridine cored quadrupolar systems. (Chart 3.1) The chemical structure of the molecules consists of two alkoxy

stilbenoid units attached to a central pyridine core through 1,3,4-oxadiazoles linkers in the 2,5 and 2,6 positions of the pyridine ring to form a rigid rod π-conjugated back bone resulting in Donor-Acceptor-Donor architecture. These molecules exhibited stable columnar phases in both the heating and cooling cycles. These aspects as well as the photophysical properties of these molecules in the solution and in the solid state are described in this Chapter.
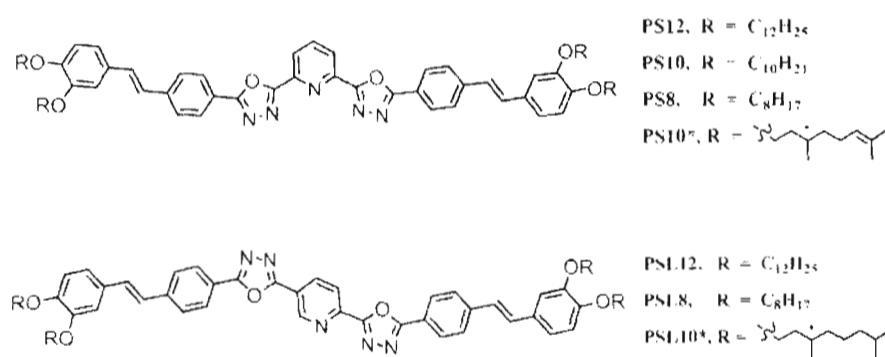
Chart 3.1.

3. 3. Results and Discussion

3.3.1. Synthesis

Two series of polycatenar π-conjugated stilbenoid derivatives shown in Chart 3.1, which differ in the terminal alkyl substitution, have been designed and synthesized. For **PS** series (**PS8, PS10, PS12** and **PS10***) the alkoxy stilbene units are connected through the 1, 3, 4 oxadiazole group at the 2, 6 positions (meta

substitution) of the pyridine unit, whereas in the **PSL** series of compounds (**PSL8**, **PSL12** and **PSL10***) the stilbene units were attached to the 2. 5 positions (para substitution) of the pyridine unit. The dialkoxy benzene groups act as donors and di(1,3,4-oxadiazol-2-yl)pyridine acts as the acceptor to constitute a donor - acceptor-donor quardrupolar system. The extended π-conjugated core and the alkoxy substitution at the terminal ends are expected to facilitate a close packing of the calamitic cores in their bulk states.
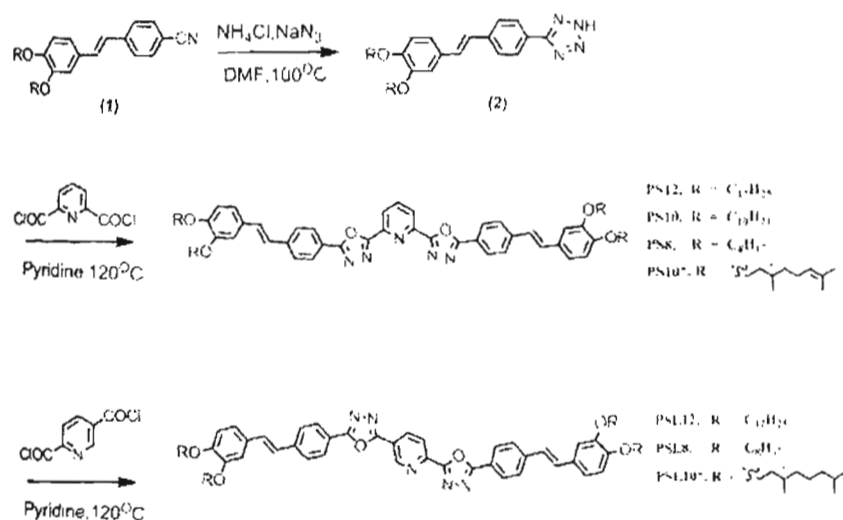
Scheme 3.1.

The synthesis of **PS** and **PSL** derivatives were achieved by two step synthetic procedure as depicted in Scheme 3.1. (E)-4-(3,4-bis(alkoxy)styryl)benzonitrile was converted into the corresponding tetrazole derivatives by 1,3 dipolar addition with sodium azide in presence of ammonium

chloride in DMF as solvent. The conversion of the tetrazole to the 1, 3, 4 oxadiazole derivatives were accomplished via the Huisgen route, in which the tetrazole derivatives were treated with the corresponding acid chloride in pyridine [Bettenhausen *et al.* 1996; Verheyde *et al.* 2001; Cristiano *et al.* 2005].

3.3.2. Liquid Crystalline Properties

The mesomorphic properties of these derivatives were investigated by Polarized Optical Microscopy (POM) and Differential Scanning Calorimetry (DSC). The phase transition temperatures and corresponding enthalpy values of **PS** derivatives are summarized in Table 3.1.

Table 3.1. Phase sequences, phase transition temperatures and corresponding enthalpy changes in the heating and cooling cycles of the **PS** derivatives as observed by DSC analysis.

Sample Code	Transition Temperatures [°C] (ΔH-[kJmol^{-1}])	
	Heating Cycle	Cooling Cycle
PS12	Cr 186 (28.31) Col$_h$ 200 (1.63) I	I 198 (1.95) Col$_h$ 175 (29.67) Cr
PS10	Cr 198(31.53) Col$_h$ 204 (2.69) I	I 203 (2.74) Col$_h$ 185 (34.17) Cr
PS8	Cr 214 (41.10) I	I 198 (35.63) Cr
PS10*	Cr 163 (27.29) I	I 153 (1.26) X 136 (24.26) Cr

Cr - Crystal, Col$_h$ - Columnar Hexagonal, X - Unidentified LC phase and I - Isotropic.

POM studies of **PS12** indicated the presence of an enantiotropic columnar liquid crystalline phase. In the heating cycle. **PS12** underwent a crystal to hexagonal columnar phase transition at 186 °C, as characterized by their typical focal-conic texture (Figure 3.4a) [Yasuda et al. 2009] and undergo isotropization at 200 °C.
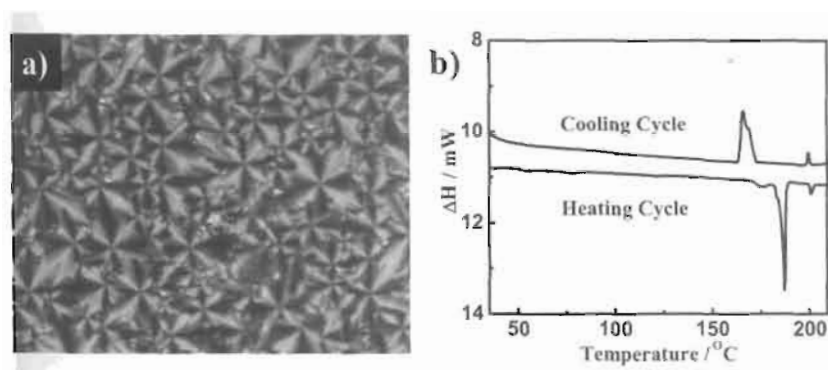
Figure 3.4. a) Focal conic texture observed at 196 °C under polarized optical microscope and b) the DSC trace at a heating/cooling rate of 5 °C/minute of compound **PS12**.

In the cooling cycle, an isotropic to hexagonal columnar phase transition was observed at 198 °C which on further cooling resulted in crystallization of the sample at 175 °C. The phase transition temperatures observed by POM were further confirmed by DSC analysis (Figure 3.4b). Similarly, in the **PS10** derivative, an enantiotropic liquid crystalline behaviour was observed. Crystalline to hexagonal columnar transition was observed at 198 °C which on further heating underwent isotropization at 204 °C. A dendritic texture was observed, on slow cooling from the isotropic state at a rate of 1°C/minute (Figure3.5a). On further

cooling the observed dendritic texture transformed into a focal conic texture (Figure3.5c), confirming the presence of the discotic columnar mesophase. The DSC thermogram of the PS10 derivative is depicted in Figure 3.5d. The transformation from the dendritic texture to the focal conic texture is depicted in Figure 3.5a-c. The **PS8** derivative did not show liquid crystalline behaviour and on heating its crystals simply melted at 214 °C.
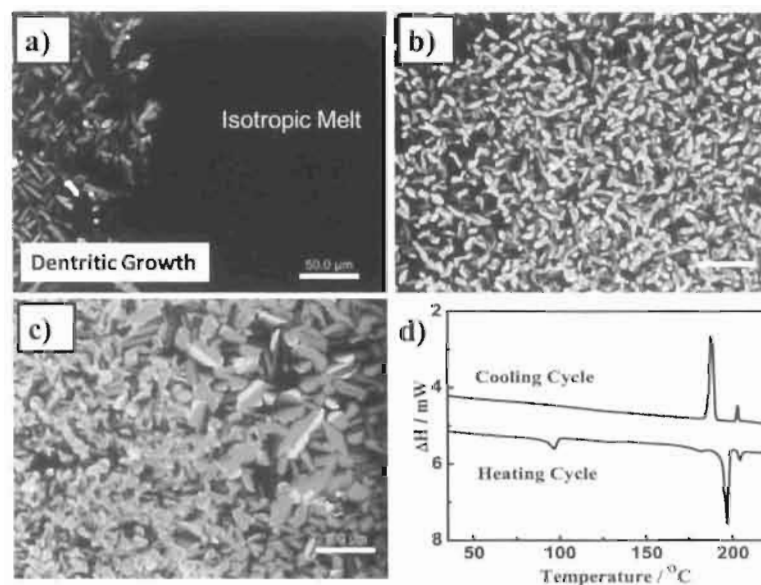
Figure 3.5. Polarized optical micrographs of PS10 at temperature a) 202 °C, b) 200 °C c) 198 °C and d) the DSC trace at a heating/cooling rate of 5 °C per minute for compound **PS10**.

POM studies of the chiral derivative **PS10***, indicated the presence of a monotropic liquid crystalline phase. On heating a solid film of this material, isotropization occurred at 163 °C. Cooling of the isotropic phase resulted in the appearance of birefringent texture at 153 °C which was not characteristic of any of

the known liquid crystalline phases (Figure 3.6a). On further cooling the material underwent crystallization at 136 °C. Phase transitions observed by POM were further confirmed by DSC measurements (Figure 3.6b).
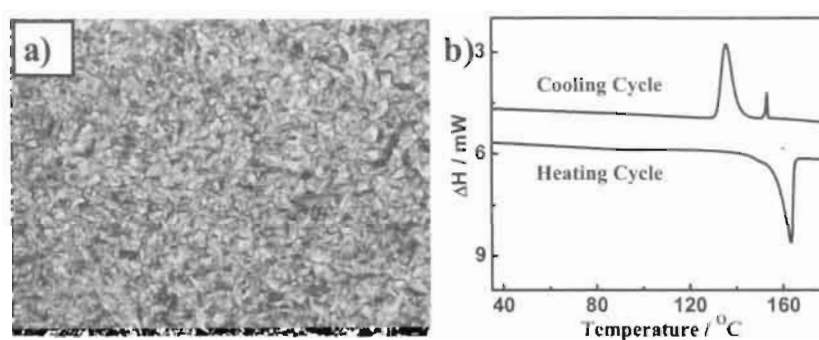
Figure 3.6. Polarized optical micrographs at temperature a) 150 °C and b) the DSC trace at a heating/cooling rate of 5 °C per minute for compound **PS10***.

Table 3.2. Phase sequences, phase transition temperatures and corresponding enthalpy changes in the heating /cooling cycles of the **PSL** derivatives as observed by DSC analysis.

Sample code	Transition Temperatures [°C] (ΔH-[kJmol^{-1}])	
	Heating Cycle	Cooling Cycle
PSL12	Cr 184 (30.91) Col$_h$ 234 (3.51) I	I 232 (3.61) Col$_h$ 174(32.24) Cr
PSL8	Cr 220 (30.90) Col$_h$ 236 (2.39) I	I 233 (2.68) Col$_h$ 212 (33.88) Cr
PSL10*	Cr 180 (32.08) Col$_h$ 213 (2.54) I	I 210 (2.57) Col$_h$ 167 (47.12) Cr

Cr - Crystal, Col$_h$ - Columnar Hexagonal and I - Isotropic.

PSL (**PSL8**, **PSL12** and **PSL10***) derivatives also exhibited thermotropic liquid crystalline behavior. The phase transition temperatures and corresponding enthalpy values of **PSL** derivatives are summarized in Table 3.2.
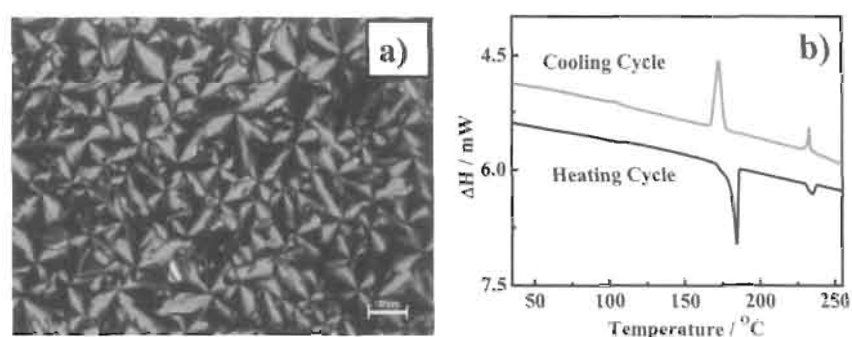
Figure 3.7. a) Focal conic texture observed at 230 °C under polarized optical microscope and b) the DSC trace at a heating/cooling rate of 5 °C per minute of compound **PSL12**.

In the heating cycle, **PSL12** underwent a crystal to hexagonal columnar phase transition at 184 °C, as characterized by their typical focal-conic texture (Figure 3.7a) and underwent isotropization at 234 °C. In the cooling cycle the same sequence of phase transition was observed with a slight temperature hysteresis. An isotropic to hexagonal columnar phase transition was observed at 232 °C which on further cooling resulted in the crystallization of the sample at 174 °C. The phase transitions observed were further confirmed by DSC analysis and are depicted in Figure 3.7b. Similarly in the **PSL8** derivative, an enantiotropic liquid crystalline behaviour was also observed. Crystalline to hexagonal columnar transition was observed at 220 °C which on further heating underwent

isotropization at 236 °C. In the cooling cycle, isotropic to hexagonal columnar transition was observed at 233 °C, as characterized by their typical focal-conic texture (Figure 3.8a) which on further cooling underwent crystallization at 212 °C. Phase transitions observed by POM were further confirmed by DSC measurements (Figure 3.8b) and is summarized in Table 3.2.
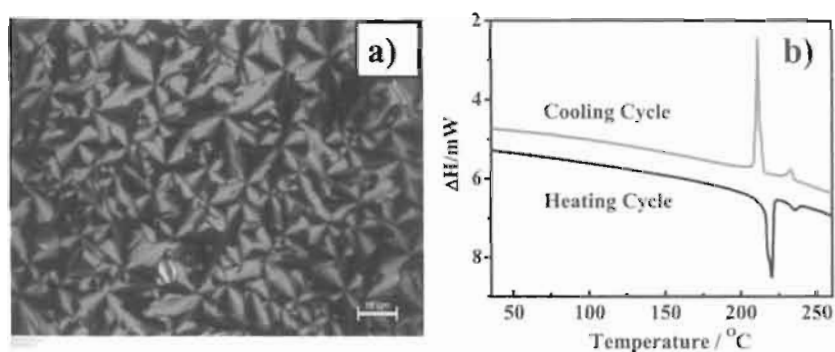
Figure 3.8. a) Focal conic texture observed at 220 °C in the cooling cycle under polarized optical microscope and b) the DSC trace at a heating/cooling rate of 5 °C per minute of compound **PSL8**.

An enantiotropic liquid crystalline behaviour was observed in the chiral derivative **PSL10*** on POM investigations. On heating a solid film of this material, crystalline to hexagonal columnar transition was observed at 180 °C which on further heating underwent isotropization at 213 °C. In the cooling cycle the same phase sequence was observed. An isotropic to hexagonal columnar phase transition was observed at 210 °C which on further cooling underwent crystallization at 167 °C. Dendritic texture was observed on slow cooling from the isotropic melt at a rate of 1°C/ minute at 210 °C, characteristic of the columnar

mesophase (Figure 3.9a). Figure 3.9b depicts the characteristic focal conic texture for the hexagonal columnar phase observed at 200 °C and Figure 3.9c shows the texture observed for the crystalline state at room temperature. Figure 3.9d shows the DSC thermogram of the **PSL10*** at a heating/cooling rate of 5°C/minute.
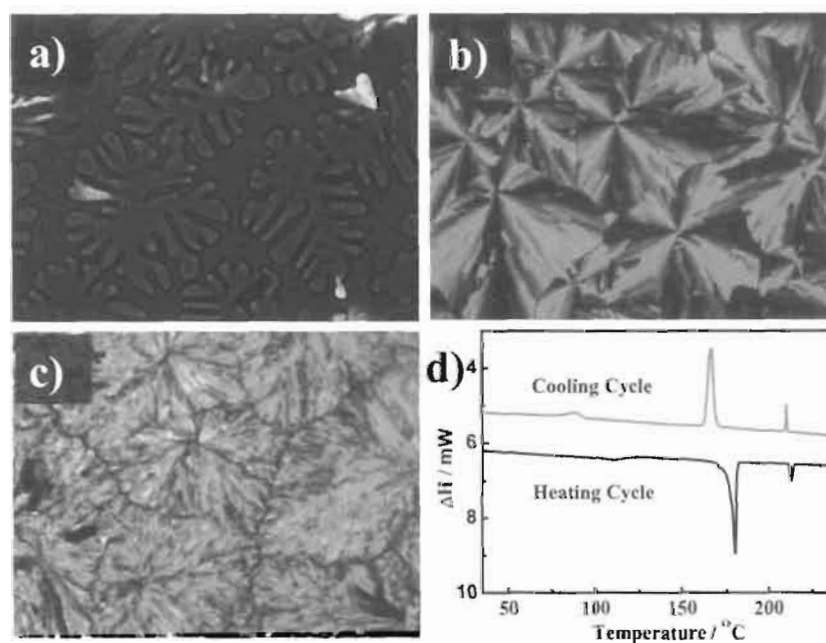
Figure 3.9. a) Dendritic texture observed at 210 °C, b) Focal conic texture observed at 200 °C, c) the texture observed for the crystalline state in the cooling cycle under polarized optical microscope and d) the DSC trace at a heating/cooling rate of 5 °C per minute of compound **PSL10***.

3.3.3. Formation of Liquid crystalline Glasses

The presence of 1,3,4-oxadiazole moieties and the bulky dialkoxy chains were expected to favor formation of liquid crystalline glasses in these class of materials. The liquid crystalline glassy films were obtained by sudden cooling

from the LC phase to ice cold water (~ 0 °C). The derivatives with longer alkyl chains **PS12**, **PSL12** and the chiral derivative (**PSL10***) formed stable transparent glasses, while all the other derivatives underwent crystallization on sudden cooling from their LC phase. POM studies showed, that the texture observed in the liquid crystalline phase (Focal conic texture) was maintained in glassy films indicated the liquid crystalline order was maintained in the glassy state. The focal conic texture was observed for **PS12** (Figure 3.10a) and for **PSL12** (Figure 3.10 b). The pseudo focal conic fan-shaped texture with rectilinear defects observed for **PSL10***in the glassy film is depicted in Figure 3.10c.
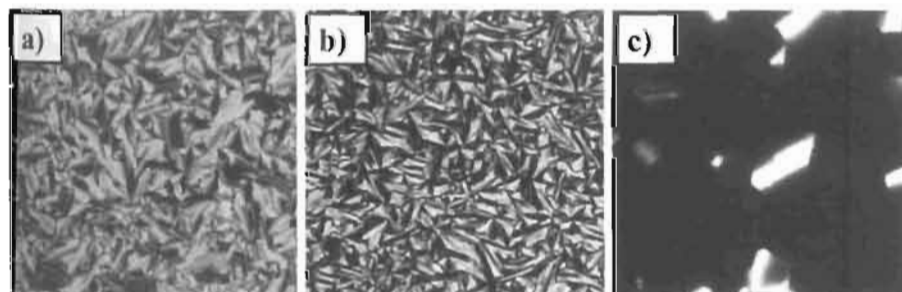
Figure 3.10. Polarized optical micrograph of a) **PS12**, b) **PSL12** and **PSL10*** in liquid crystalline glassy state.

3.3.4. Photophysical Properties

3.3.4.1 Absorption and Emission Properties in Solution

The absorption and emission properties of **PS12** were investigated in various solvents. All the derivatives possess a strong absorption band in the 360 nm region. The absorption spectra were independent of solvent polarity, while the

emission spectra underwent a red shift with increase in solvent polarity.[19] The fluorescence decay of **PS12** was mono-exponential in dilute solutions (Figure 3.11b), with an increase in lifetime being observed on changing from non-polar to polar solvents. The absorption and emission spectral characteristics of **PS12** derivative in a few different solvents are summarized in Table 3.3.
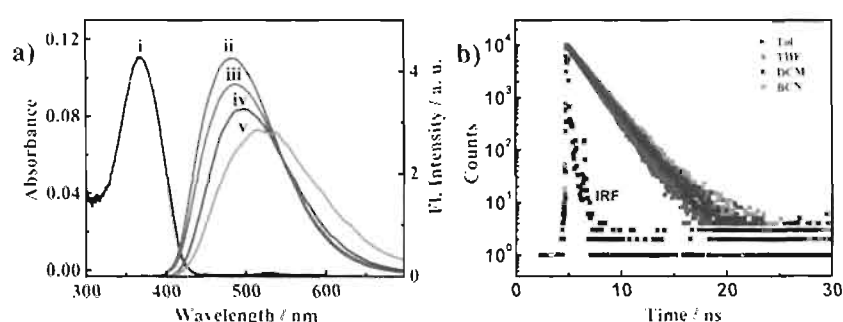
Figure 3.11. a) Absorption and fluorescence spectra of **PS12**; (i) absorption spectrum in toluene. fluorescence spectra in (ii) toluene. (iii) THF. (iv) dichloromethane and (v) benzonitrile (λ_{ex} = 375 nm), b) fluorescence lifetime decay profile (λ_{ex} = 375 nm). emission monitored at their corresponding emission maximum.

The lack of shift in the absorption maxima in solvents of varying polarity indicates a negligible change in the dipole moments between the ground and the excited state of the molecules. The red shift in emission spectrum with increasing solvent polarity indicates however that the polarity of the emitting state is much higher than that of the ground state. These results indicate that the excited state formed via direct excitation is non-fluorescent, and that this state subsequently evolves into a fluorescent excited state via an intra-molecular charge transfer (ICT) process. The ICT state will be increasingly stabilized in solvents of higher

polarity resulting in the observed red shift in the emission spectra [Rettig *et al.* 1994; Davis *et al.* 2001]. Earlier studies on the donor-acceptor substituted stilbenes also showed similar behaviour as discussed in Chapter 2.

Table 3.3. Absorption, emission and fluorescence lifetime characteristics of **PS12** and **PSL12**.

Compound	Solvent	Abs.λ_{max}/nm	Em. λ_{max}/ nm (ϕ_F)	τ/ ns	χ^2
PS12	Toluene	364	484 (0.49)	1.45	1.05
	THF	365	487 (0.55)	1.56	1.09
	DCM	363	499 (0.49)	1.72	1.16
	BCN	367	516 (0.50)	1.77	1.14
PSL12	Toluene	378	554 (0.22)	1.18	1.17
	THF	379	567 (0.11)	0.80	1.13
	DCM	380	582 (0.15)	0.53	1.14

For the **PSL** derivatives, absorption maxima were observed at ~380 nm which were unaffected by varying solvent polarity, while emission spectra underwent a red shift with increasing solvent polarity, similar to that observed for the **PS** derivatives. The fluorescence decay of **PSL12** was mono-exponential in dilute solutions and a decrease in lifetime was observed on changing from non-polar to polar solvents. The absorption and emission spectral characteristics of **PSL12** in a few different solvents are shown in Figure 3.12 and are summarized in Table 3.3.
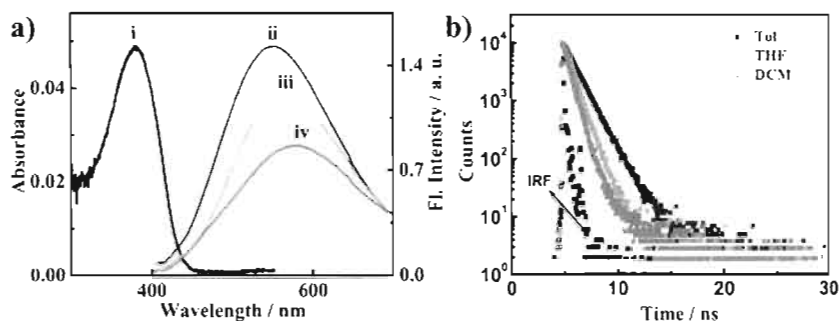
Figure 3.12. a) Absorption and fluorescence spectra of **PSL12**; (i) absorption spectrum in toluene, fluorescence spectra in (ii) toluene (iii) THF and (iv) dichloromethane (λ_{ex} = 375 nm), b) fluorescence lifetime decay profile (λ_{ex} = 375 nm), emission monitored at their corresponding emission maximum.

A red shift of about 20 nm in the absorption maximum and of about 80 nm in the emission maximum was observed in **PSL12** derivative compared that of the **PS12** derivative. The substitution of the stilbene arms in the 2, 5, positions (Para) of the pyridine ring in **PSL** derivatives, results in an enhanced effective conjugation between the donor and acceptor compared to that of **PS** derivatives, where in the later the substitution was at the 2, 5, positions of the pyridine ring.

3.3.4.2. Absorption and Emission Properties in the Solid State.

Both the **PS** and **PSL** series investigated in the present study were found to be fluorescent in the solid state. In most cases aggregation of molecules in the solid state usually leads to self-quenching of the excited state resulting in the formation of non-fluorescent materials. In several stilbene derivatives, as also in the present case, aggregation has been observed to result in enhancement in fluorescence and this may be attributed due to the rigidization as well as the

formation of emissive aggregates in solid state. The absorption, emission and the fluorescence lifetimes of these derivatives were not significantly different in their thin film and in the powder state, except for a slight blue shift observed in the absorption and emission maximum of the thin films compared to that of powder state.

Table 3.4. Absorption, emission and fluorescence lifetime characteristics of **PS** derivatives in solid state.

Sample	State	Abs. λ_{max} (nm) [a]	Em. λ_{max} (nm)	τ_1/ ns ($F_1\%$)	τ_2/ ns ($F_1\%$)	τ_3/ ns ($F_1\%$)	χ^2
PS12	Powder	438	488	7.94 (21.11)	1.96 (36.91)	0.51 (41.98)	1.15
	Thin Film	427	467	8.31 (28.84)	1.87 (37.25)	0.51 (33.91)	1.11
PS10	Powder	460	506	9.04 (41.92)	2.57 (37.65)	0.62 (20.43)	1.06
	Thin Film	429	468	10.48 (45.46)	2.23 (30.35)	0.50 (24.20)	1.13
PS8	Powder	431	479	8.10 (24.69)	2.10 (43.79)	0.62 (31.52)	1.10
	Thin Film	419	469	9.30 (27.34)	2.30 (72.66)	-	1.02
PS10*	Powder	436	488	7.27 (43.46)	2.34 (44.02)	0.62 (12.52)	1.08
	Thin Film	431	487	7.57 (38.18)	2.46 (52.29)	0.82 (9.53)	1.14

[a] Obtained from excitation spectrum.

Figure 3.13a depicts the excitation and emission maxima of **PS12** in thin film and powder form. The fluorescence decay profile of **PS12** derivative showed a slight increase in the lifetime of the longer lifetime species in the thin film compared to that of the powder form and is generally observed in the other derivatives. The fluorescence lifetime decay profiles of **PS12** in the film and powder form are shown in Figure 3.13b.
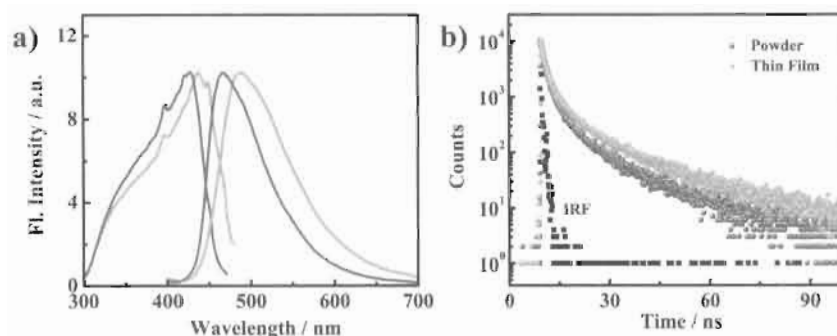
Figure 3.13. a) Fluorescence excitation, emission spectra and b) lifetime decay profile of **PS12** derivative (Blue and green curves represents the powder and film states respectively.

A red shift in absorption and in the emission maximum was observed in **PSL** derivatives compared that of the **PS** derivatives and is attributed to the enhanced effective conjugation between the donor and acceptor in **PSL** derivatives compared to that of **PS** derivatives. The absorption, emission and fluorescence lifetime characteristics of **PSL** in the film and powder form are shown in are depicted in Table 3.5.

Table 3.5. Absorption, emission and fluorescence lifetime characteristics of **PSL** derivatives in solid state.

Sample	State	Abs. λ_{max} (nm) [a]	Em. λ_{max} (nm)	τ_1/ns (F1%)	τ_2/ns (F1%)	τ_3/ns (F1%)	χ^2
PSL12	Powder	470	548	8.90 (47.42)	2.87 (42.18)	0.61 (10.40)	1.11
	Thin Film	486	524	7.84 (72.70)	3.98 (25.19)	0.82 (2.11)	1.00
PSL8	Powder	467	533	7.25 (68.15)	3.16 (28.93)	0.44 (2.92)	1.05
	Thin Film	467	535	7.97 (91.00)	1.99 (7.82)	0.97 (1.18)	1.12
PSL10*	Powder	535	470	5.77 (43.73)	2.30 (43.73)	0.62 (12.55)	1.12
	Thin Film	528	479	5.09 (38.78)	2.41 (52.88)	0.82 (8.33)	1.14

[a] Obtained from excitation spectrum.

3.3.5. Discussion

Polycatenar compounds, with their special molecular structure made up of a long aromatic core and several terminal aliphatic chains, can present different mesogenic properties depending on the characteristics of the molecular core and especially on the number of side chains substituents. The molecular structure of polycatenars can be placed between that of mesogenic discs and mesogenic rods (Figure 3.14), and the observed poly-mesomorphism for this class of molecules is very similar to that observed in lyotropic systems. As a result, much effort has

been spent on polycatenar liquid crystals in terms of understanding structure property relationships and also for investigating its potential applications. For all the polycatenars, the textures of their columnar mesophases observed under the polarizing microscope are generally the characteristic focal conic texture or fan type texture, similar to that observed in disc shaped molecules.
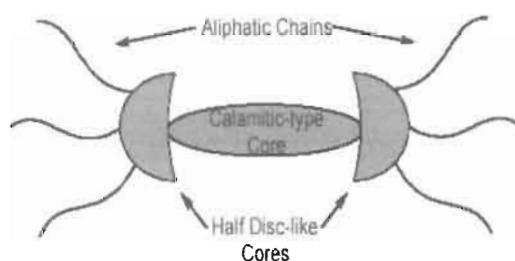
Figure 3.14. Representation of the central core of polycatenar LCs comprises a calamitic region, with half-discs on the extremities.

The general description of molecular packing in the columnar phase of polycatenar molecules is based on a model previously proposed for a hexacatenar compounds. This model considers the transverse section of the columns to be constituted by several calamitic rigid cores disposed side by side and surrounded by the corresponding disorganised aliphatic end chains. The number of molecules in a slice of a column depends upon the number and the length of the terminal aliphatic chains and generally, three molecules are found for six-chain phasmids, and four to five molecules for biforked mesogens [Ribeiro *et al.*2003; Cardinaels *et al.*2008; Nguyen *et al.* 1997]
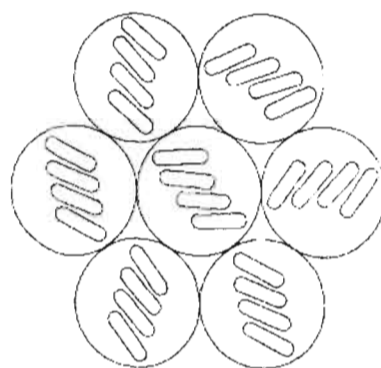
Figure 3.15. Schematic representation of the molecular organization in the hexagonal columnar phase of biforked mesogens.

The chemical structures of the molecules designed for the present study consists of two alkoxy stilbenoid units attached to a central pyridine core through 1,3,4-oxadiazoles linkers in the 2,6 (**PS**) and 2,5 (**PSL**) positions of the pyridine ring to form a rigid rod π-conjugated back bone with two alkyl chains grafted on the either sides of the rigid rod structure resulting in a biforked (teracatenar) architecture. In concurrence with the characteristic focal conic texture observed in the mesophase, it is reasonable to assume that the rigid-rod π-conjugated back bone self-assemble into a one dimensional domain and the outer part of the columns are filled with the molten alkoxy segments, similar to the previously reported polycatenar mesogens [Yasuda *et al.* 2009].

3.4. Conclusion

The synthesis, thermotropic liquid crystalline behaviour and photophysical properties of two series of pyridine cored donor-acceptor-donor systems have been

described. The molecules in which two alkoxy stilbenoid units were attached to the central pyridine core through 1,3,4-oxadiazoles linkers in the 2,6 (**PS**) and 2,5 (**PSL**) positions of the pyridine ring to form a rigid rod π-conjugated back bone. Both these series of derivatives exhibited stable discotic LC phases in the heating and cooling cycles. Chiral discotic LC phases were obtained by introducing chiral groups in the alkyl periphery. A few of these derivatives were observed to form stable glasses on sudden cooling from the LC phase, where the liquid crystalline order was maintained. These materials were found to be fluorescent in their solid state as well as in glassy state. The ability of these materials to form stable liquid crystalline glass and their fluorescent nature, along with the semiconducting properties of 1,3,4-oxadiazole derivatives may make them applicable as active elements in the emerging field of organic electronics.

3.5. Experimental Section

3.5.1. Synthesis and Characterization

All the derivatives were synthesized according to the general procedure as shown in Scheme 3.2. and the structural characterization data are provided below.

General Procedure for the Synthesis of PS and PSL Derivatives

Pyridine-2,6-dicarbonyl dichloride/Pyridine-2,5-dicarbonyl dichloride (1 equiv.) was taken in a dry two necked R.B. under argon atmosphere, dry pyridine (5mL) added and was stirred for two minutes. Compound **2** (2.4 equiv.) dissolved

in dry pyridine (15 mL) was added to the above acid chloride drop wise with constant stirring. The reaction mixture was then refluxed at 115 °C for 12h and was poured into ice cold water and then neutralized with 2N HCl. The precipitate was washed with water, filtered and extracted with dichloromethane. The compound was then concentrated and dissolved in minimum amount of dichloromethane and was precipitated using methanol to give pure product.

PS12: Yield: 76 %; IR υ_{max} (KBr): 521, 963, 1142, 1251, 1520, 1593, 2849, 2918, 2955 cm^{-1}.; ^{1}H NMR (500MHz. CDCl$_3$, TMS)
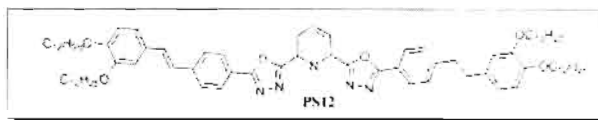
:δ 8.498-8.482 (d, J = 8 Hz, 2H, aromatic), 8.262-8.245 (d, J = 8.5 Hz, 4H, aromatic), 8.152-8.121 (t, 1H, aromatic), 7.697-7.680 (d, J = 8.5 Hz , 4H, aromatic), 7.225-7.193 (d, J = 16 Hz, 2H, allylic), 7.125 (s, 2H, aromatic), 7.094-7.077 (d, J = 8.5 Hz, 2H, aromatic), 7.035-7.003 (d, J = 16.5 Hz, 2H, allylic), 6.897-6.880 (d, J = 8.5 Hz, 2H, aromatic), 4.084-4.020 (m, 8H, -OCH$_2$-), 1.875-1.268 (m, 80H, -CH$_2$-), 0.898-0.863 (m, 12H, -CH$_3$); ^{13}C NMR (125 MHz, CDCl$_3$, TMS) δ: 165.89, 163.01, 149.71, 149.22, 144.30, 141.58, 138.58, 131.26, 129.72, 127.79, 126.75, 125.18, 121.54, 120.56, 113.44, 111.56, 69.35, 69.21, 31.90, 29.65, 29.60, 29.48, 29.33, 29.25, 26.05, 26.02, 22.70, 14.08; FAB MS: m/z calcd for C$_{85}$H$_{121}$N$_5$O$_6$, 1307.93; found 1308.67 [M+H$^+$].

PS10: Yield: 74 %; IR υ_{max} (KBr): 962, 1020, 1141, 1252, 1518, 1593, 2851, 2920, 2953 cm^{-1}; ^{1}H NMR (500MHz. CDCl$_3$, TMS) : δ 8.495-8.479 (d, J = 8 Hz,

2H, aromatic), 8.260- 8.243 (d, *J* = 8.5 Hz, 2H,
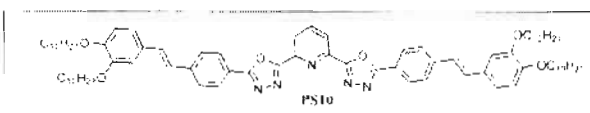
aromatic), 8.148-8.117 (t, 1H, aromatic), 7.695-7.678 (d, *J* = 8.5 Hz , 4H, aromatic), 7.223-7.191 (d, *J* = 16 Hz, 2H, allylic), 7.123 (s, 2H, aromatic), 7.092-7.075 (d, *J* = 8.5 Hz, 2H, aromatic), 7.033-7.001 (d, *J* = 16.5 Hz, 2H, allylic), 6.895-6.878 (d, *J* = 8.5 Hz, 2H, aromatic), 4.083-4.019 (m, 8H, -OCH$_2$-), 1.875-1.268 (m, 64H, -CH$_2$-), 0.898-0.863 (m, 12H, -CH$_3$); ^{13}C NMR (125 MHz, CDCl$_3$, TMS) δ: 165.99, 163.08, 149.81, 149.28, 144.33, 141.64, 138.56, 131.30,129.72, 127.83, 126.75, 125.20, 121.63, 120.63, 113.49, 111.61, 69.39, 69.21, 31.93, 29.65, 29.60, 29.44, 29.37, 29.25, 26.07, 26.04, 22.70, 14.13; FAB MS: m/z calcd for C$_{77}$H$_{105}$N$_5$O$_6$, 1195.81; found 1196.44 [M+H$^+$].

PS8: Yield: 72 %; IR υ$_{max}$ (KBr): 854, 1138, 1251, 1267, 1512, 2853, 2922, 2953cm^{-1}; ^{1}H NMR (500MHz, CDCl$_3$, TMS)
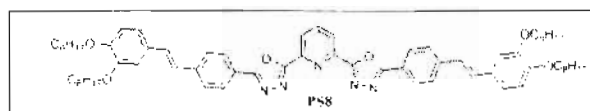
: δ 8.412-8.396 (d, *J* = 8 Hz, 2H, aromatic), 8.181-8.164 (d, *J* = 8.5 Hz, 4H, aromatic), 8.068-8.036 (t, 1H, aromatic), 7.617-7.600 (d, *J* = 8.5 Hz, 4H, aromatic), 7.144-7.112 (d, *J* = 16 Hz, 2H, allylic), 7.048 (s, 2H, aromatic), 7.016-6.999 (d, *J* = 8.5 Hz, 2H, aromatic), 6.954-921(d, *J* = 16.5 Hz, 2H, allylic), 6.821-6.804 (d, *J* = 8.5 Hz, 2H, aromatic), 4.011-3.946 (m, 8H, -OCH$_2$-), 1.783-1.218 (m, 48H, -CH$_2$-), 0.834-0.807 (m, 12H, -CH$_3$); ^{13}C NMR (125 MHz, CDCl$_3$, TMS) δ: 165.89, 163.07, 149.91, 149.32, 144.30, 141.62, 138.56, 131.32,129.73,

127.84, 126.75, 125.21, 121.63, 120.61, 113.49, 111.61, 69.39, 69.21, 31.93,

29.64, 29.62, 29.44, 29.38, 29.24, 26.08, 26.04, 22.69, 14.12; FAB MS: m/z calcd

for $C_{69}H_{89}N_5O_6$, 1083.68; found 1084.32 [M+H$^+$].

PS10*: Yield: 78 %; IR υ_{max} (KBr): 962, 1016, 1265, 1433, 1492, 1595, 2870,

2913, 2959 cm^{-1}; ^{1}H

NMR (500MHz, CDCl$_3$,
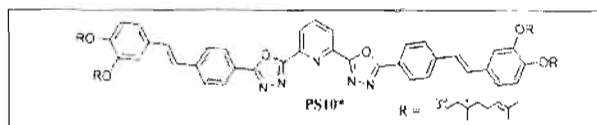
TMS) : δ 8.493-8.478 (d, J = 7.5 Hz, 2H, aromatic), 8.260-8.245 (d, J = 8.5 Hz,

4H, aromatic), 8.150-8.119 (t, 1H, aromatic), 7.697-7.681 (d, J = 7.5 Hz , 4H,

aromatic), 7.225-7.193 (d, J = 16 Hz, 2H, allylic), 7.123 (s, 2H, aromatic), 7.092-

7.075 (d, J = 8.5 Hz, 2H, aromatic), 7.036-7.004(d, J = 16 Hz, 2H, allylic), 6.900-

6.884 (d, J = 8 Hz, 2H, aromatic), 5.124-5.113(d, J = 5.5 Hz, 4H, allylic), 4.126-

4.050 (m, 8H, -OCH$_2$-), 2.054-1.230 (m, 28H, -CH$_2$-), 1.004-0.972 (m, 36H, -

CH$_3$); ^{13}C NMR (125 MHz, CDCl$_3$, TMS) δ: 165. 09, 163.07, 149.92, 149.32,

144.30, 141.62, 138.55, 131.32,129.72, 127.84, 126.73, 125.21, 121.63, 120.61,

113.43, 111.61, 69.35, 69.24, 31.93, 29.64, 29.60, 29.41, 29.38, 29.24, 26.08,

26.05, 22.68, 14.12; FAB MS: m/z calcd for $C_{77}H_{97}N_5O_6$, 1187.74; found 1188.44

[M+H$^+$].

PSL12: Yield: 64 %; IR υ_{max} (KBr): 845, 951, 1138, 1251, 1265, 1514, 2849,

2918, 2953 cm^{-1}; ^{1}H

NMR (500MHz, CDCl$_3$,
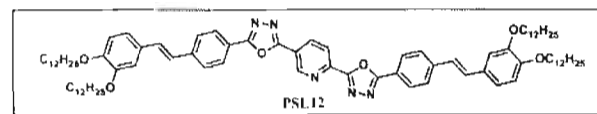
TMS) :δ 9.543 (s, 1H, aromatic), 8.637-8.621 (d, J = 8.5 Hz, 1H, aromatic), 8.511-

8.495 (d, $J = 8.5$ Hz, 1H, aromatic), 8.222-8.206 (d, $J = 8.5$ Hz, 2H, aromatic), 8.152-8.136 (d, $J = 8.5$ Hz, 2H, aromatic), 7.679-7.651 (dd, 4H, aromatic), 7.211-7.178 (d, $J = 16$ Hz, 2H, allylic), 7.115 (s, 2H, aromatic), 7.085-7.069 (d, $J = 8.5$ Hz, 2H, aromatic), 7.017-6.985(d, $J = 16$ Hz, 2H, allylic), 6.890-6.874 (d, $J = 8$ Hz, 2H, aromatic), 4.069-4.028 (m, 8H, -OCH$_2$-), 1.861-1.269 (m, 80H, -CH$_2$-), 0.897-0.870 (m, 12H, -CH$_3$); ^{13}C NMR (125 MHz, CDCl$_3$, TMS) δ: 165.90,165.36, 163.05, 161.60, 149.89, 149.83, 149.29, 145.43, 141.68, 141.62, 131.37, 131.26, 129.60, 127.72, 127.47, 126.77, 126.69, 125.01, 124.94, 121.08, 121.83, 121.33, 120.62, 113.49, 111.71, 69.43, 69.40, 9.20, 31.94, 29.73, 29.72, 29.68, 29.65, 29.48, 29.45, 29.38, 29.27, 26.09, 26.04, 22.70, 14.12: FAB MS: m/z calcd for C$_{85}$H$_{121}$N$_5$O$_6$, 1307.93; found 1308.67 [M+H$^+$].

PSL8: Yield: 68 %; IR υ_{max} (KBr): 963, 1139, 1251, 1265, 1512, 2853, 2918, 2963 cm^{-1}; ^{1}H NMR (500MHz, CDCl$_3$, TMS) : δ 9.541
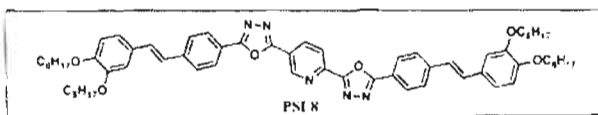
(s, 1H, aromatic), 8.635-8.619 (d, $J = 8.5$ Hz, 1H, aromatic), 8.509-8.493 (d, $J = 8.5$ Hz, 1H, aromatic), 8.220-8.204 (d, $J = 8.5$ Hz, 2H, aromatic), 8.150-8.134 (d, $J = 8.5$ Hz, 2H, aromatic), 7.677-7.649 (dd, 4H, aromatic), 7.209-7.176 (d, $J = 16$ Hz, 2H, allylic), 7.115 (s, 2H, aromatic), 7.083-7.067 (d, $J = 8.5$ Hz, 2H, aromatic), 7.015-6.983(d, $J = 16$ Hz, 2H, allylic), 6.888-6.872 (d, $J = 8$ Hz, 2H, aromatic), 4.067-4.026 (m, 8H, -OCH$_2$-), 1.859-1.220 (m, 48H, -CH$_2$-), 0.895-0.868 (m, 12H, -CH$_3$);^{13}C NMR (125 MHz, CDCl$_3$, TMS) δ: 165.79, 165.25,

149.87, 149.81, 149.27, 148.03, 141.57, 131.27, 131.16, 129.58, 127.66, 127.41, 126.71, 126.62, 124.82, 123.00, 120.66, 120.61, 113.42, 111.61, 69.41, 69.38, 31.86, 31.84, 29.44, 29.41, 29.38, 29.32, 29.29, 29.28, 26.09, 26.04, 22.70, 22.68, 14.11; FAB MS: m/z calcd for $C_{69}H_{89}N_5O_6$, 1084.47; found 1085.27 [M+H].

PSL10*: Yield: 70 %; IR υ_{max} (KBr): 962, 1049, 1138, 1251, 1512, 2843, 2868, 2927, 2953 cm^{-1}; ^{1}H NMR (500MHz, CDCl$_3$,

NMR (500MHz, CDCl$_3$,

TMS) :δ 9.535 (s, 1H, aromatic), 8.629-8.613 (d, J – 8.5 Hz, 1H, aromatic), 8.503-8.487 (d, J – 8.5 Hz, 1H, aromatic), 8.214-8.198 (d, J = 8.5 Hz, 2H, aromatic), 8.144-8.128 (d, J = 8.5 Hz, 2H, aromatic), 7.671-7.643 (dd, 4H, aromatic), 7.203-7.170 (d, J = 16 Hz, 2H, allylic), 7.107 (s, 2H, aromatic), 7.077-7.061 (d, J – 8.5 Hz, 2H, aromatic), 7.009-6.977(d, J = 16 Hz, 2H, allylic), 6.882-6.866 (d, J = 8 Hz, 2H, aromatic), 4.061-4.020 (m, 8H, -OCH$_2$-), 1.853-1.250 (m, 40H, -CH$_2$-), 0.891-0.862 (m, 36H, -CH$_3$); ^{13}C NMR (125 MHz, CDCl$_3$, TMS) δ: 165.79, 165.25, 149.89, 149.32, 127.77, 127.53, 126.83, 126.74, 125.05, 120.61, 113.42, 111.58, 67.76, 67.57, 39.30, 39.27, 37.40, 37.37, 36.31, 36.21, 29.96, 28.01, 28.00, 24.76, 24.73, 22.72, 22.71, 22.62, 19.76, 19.71; FAB MS: m/z calcd for $C_{77}H_{105}N_5O_6$, 1195.81; found 1196.64 [M+H$^-$].

Synthesis and Study of Liquid Crystalline, Aggregation and Photophysical Properties of Trigonal Octupolar Oxadiazole Derivatives

Luminescent Discotics with Columnar Order

Hierarchical Self-Assembly in Solution
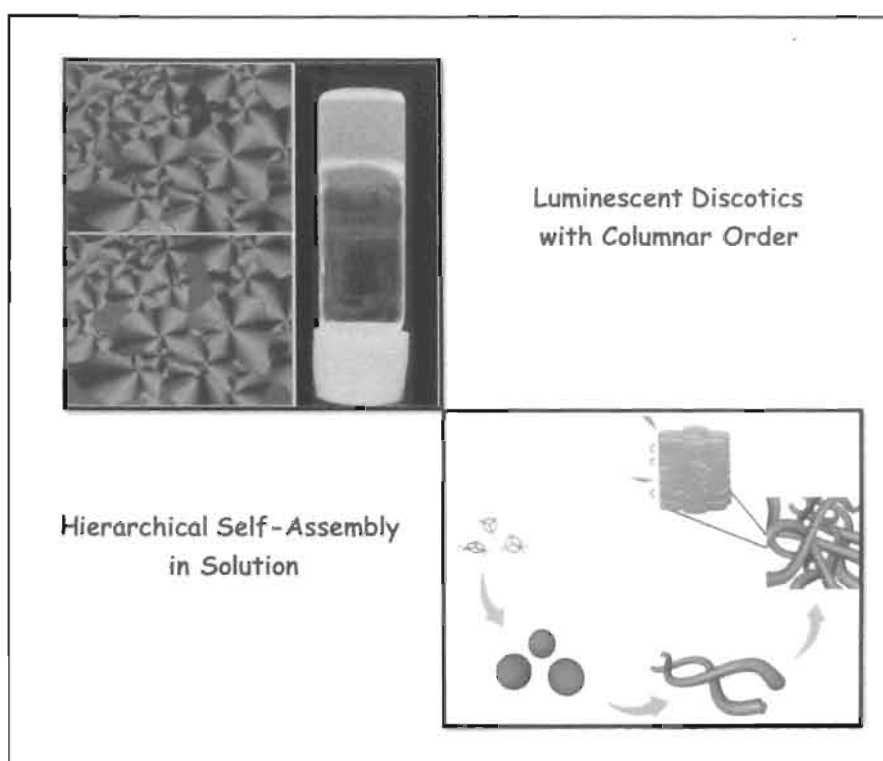
Objective: To investigate the hierarchical self-assembly and related changes in photophysical behaviour of trigonal octupolar derivatives in solution and in condensed phases.

4.1. Abstract

A series of novel trigonal octupolar 1,3,4-oxadiazole derivatives exhibiting discotic liquid crystalline phases were designed and synthesized. The self-assembly of these materials in their mesophase and within their aggregates in solution and the resultant changes in their photophysical properties are described in this Chapter. A few of the derivatives exhibited enantiotropic columnar discotic liquid crystalline phases with hexagonal as well as rectangular two dimensional lattices. Their concentration dependent hierarchical self-assembly in non-polar solvents from spheres to nano-fibers wherein the hexagonal columnar order observed in their mesophases was retained has been investigated. The derivatives with longer alkyl chain lengths formed stable, highly luminescent transparent gels in non-polar solvents such as decane and toluene. The gelation process was slow and it took few days for complete immobilization of the solvent. The high sensitivity of the luminescence properties of these molecules to their state of aggregation provided an effective method to monitor the nature of the molecular packing involved in the various stages of the hierarchical self-assembly. Incorporation of stereogenic groups into these self-assembling molecular units led to the induction of chirality in the columnar stacks of these molecules in their mesophase. A similar induction of chirality was observed in the self-assembled stacks in solution. An interesting concentration dependent reversal of chirality, attributed to the formation of coiled-coil aggregates in solution was also observed.

Section A

Hierarchical Self-Assembly from Nanospheres to Fibrous Gels

4.2. Introduction

The realization that π-conjugated organic molecules can behave as electrical conductors has given rise to the field of organic electronics [Chiang *et al.* (a) 1977; Chiang *et al.* (b) 1977]. Currently this field is attracting significant attention in view of the tremendous commercial potential based on such materials [Tang *et al.* 1987; Tang *et al.* 1989; Tsumura *et al.* 1988; Clar 1972]. Although organic electronics is clearly in its infancy, significant advances are being made across a broad range of activities for understanding the fundamental phenomena underlying the factors determining device performance. In the area of organic electronics, two distinct approaches are being pursued for the construction of organic semiconducting materials. In the late 1970's, it was demonstrated that polymers can be made to conduct electricity by manipulating their molecular structure. Conjugated polymers possess the inherent ability to conduct electric charges along their backbone [Heeger *et al.* 1988; Skotheim *et al.* 1988; Cao *et al.* 1988]. Significant advances have been made on polymer material based organic electronics, many of which have reached the second phase of commercialization

[Tullo *et al.* 2000; Friend *et al.* 1999]. However, efficiencies in many of these devices are not satisfactory and there is considerable room for improvement. One of the reasons for the lack of efficiencies is poor long range order. This has led the interest in the second approach which is a relatively newer one, which tries to make use of principles of self-assembly [Hoeben *et al.* 2005]. Making use of weak intermolecular interactions, it is possible to develop materials with enhanced molecular order resulting in improved device efficiencies. A wide variety of such well defined π-conjugated materials have been synthesized and studied. Although precise control over the structure and electronic properties has been achieved at the molecular level, a major challenge now is to obtain control of the supramolecular ordering over long ranges and to understand and manipulate the resultant optical and electronic properties.

An interesting field that is rapidly developing is the so called area of "Supramolecular Electronics". This is a term recently coined by Schenning and Meijer to describe the construction of supramolecular assemblies of π-conjugated systems in the 5–100 nm length scale which can act as conducting wires of electronic components in the nanometer range [Meijer *et al.* 2002; Van Der Auweraer *et al.* 2004]. This field is expected to bridge the gap between the organic electronics and molecular electronics. Use of bulk materials as active elements in devices have limitations due to the difficulty of obtaining long range ordered domains [Brunsveld *et al.* 2001].

The challenge of constructing bulk materials with long range highly ordered π-conjugated elements with anisotropic electronic properties for use in organic electronics remains unmet. In this context, disc shaped molecules are particularly interesting since they can form one-dimensional supramolecular architectures with strong π-π interactions over macroscopic scales [Palermo *et al.* 2007; De Luca *et al* 2008; Grimsdale *et al.* 2005; Samori *et al.* 2005; Zang *et al.* 2008; Hasegawa *et al.* 2007]. The long range self-assembled structures in such materials results from a delicate balance of various non-covalent interactions involving hydrogen bonding, van der Waals', dipolar, π-π, solvatophilic and solvatophobic forces [Sagara *et al.* 2008; Chen *et al.* 2007; Hennrich *et al.* 2007; Camerel *et al.* 2006; Camerel *et al.* 2007; Yagai *et al.* 2007; Fernandez *et al.* 2007; Nakanishi *et al.* 2008; Nakanishi *et al.* 2007; Terech *et al.* 1997; van Esch *et al.* 2000]. Understanding the nature of such interactions is essential for harnessing them for the construction of supramolecular architectures with desired molecular organization [Keizer *et al.* 2005; Lee *et al.* 2001; Wurthner *et al.* 2003; Lehn *et al.* 2003]. With a few exceptions [Lee *et al.* 2008; Haino *et al.* 2008; Palma *et al.* 2008], most of the discotic molecules hitherto reported to form such self-assembled superstructures possess hydrogen bonding functionalities incorporated into the molecule [Ikeda *et al.* 2003; Bao *et al.* 2006; Sakajiri *et al.* 2008; Li *et al.* 2006; Alvarez *et al.* 2006]. With regard to improving charge and exciton transport properties in discotic materials, it would be of interest to develop discotic

molecules wherein self-assembly is governed mainly by π-π stacking and dipole-dipole interactions. Moreover, most discotic molecules investigated possess cores such as triphenylenes, hexabenzenocoronenes and phthalocyanines with p-type semiconducting properties. Systems containing electron withdrawing moieties have been less explored [Pieterse *et al.* 2001; Lehmann *et al.* 2005; Wurthner *et al.* 2004].

Sample Code	R
SA1	CH₃
SA4	C₄H₉
SA6	C₆H₁₃
SA8	C₈H₁₇
SA12	C₁₂H₂₅
SA16	C₁₆H₃₃
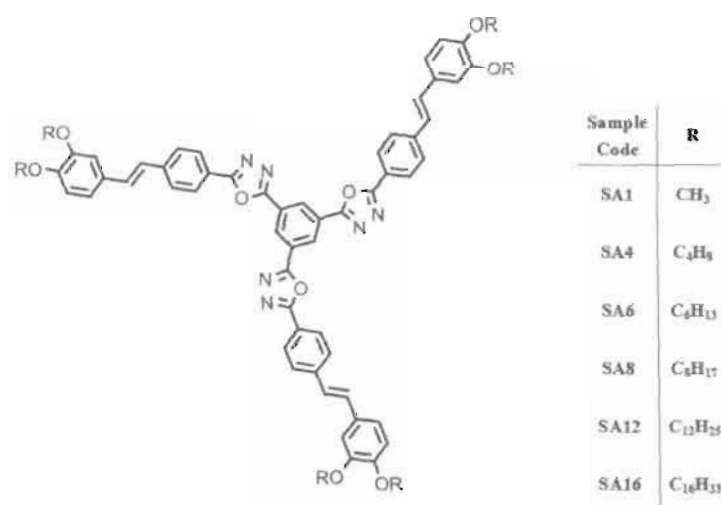
Chart 4.1

Herein, we report a novel class of highly luminescent octupolar 1,3,4-oxadiazole derivatives (Chart 4.1) with few of the derivatives (**SA12** and **SA16**) exhibiting columnar mesophases. 1,3,4-Oxadiazoles were incorporated in the core of the discotic molecules in view of their excellent electron transporting and luminescent properties as well as their ability to undergo efficient π-stacking [Zhang *et al.* 2003; Tokuhisa *et al.* 1998; Qu *et al.* 2008]. These molecules were

capable of spontaneous concentration dependent hierarchical self-assembly leading from spheres to fibers possessing columnar organization in non-polar solvents. Few of the derivatives (**SA8, SA12** and **SA16**) formed stable, highly luminescent transparent gels in non-polar solvents such as decane and toluene. The high sensitivity of the luminescence properties of these materials to their state of aggregation provided an effective method to monitor the nature of the molecular packing involved in the various stages of the hierarchical self-assembly [Kumar *et al.* 2006; Yagai *et al.* 2007; Kaiser *et al.* 2007; Kamikawa *et al.* 2007; Seo *et al.* 2008; Chen *et al.* 2009; Kozhevnikov *et al.* 2008]. Detailed studies on their liquid crystalline, self-aggregating and luminescence properties are discussed here.

4.3. Results and Discussion

4.3.1. Synthesis of the 1,3,4-Oxadiazole Derivatives

The 1,3,4-oxadiazole derivatives (Chart 4.1) were synthesized by a multistep process (Scheme 4.1), in which the final step involved the conversion of a tetrazole to 1,3,4-oxadiazole by the Huisgen mechanism [Sauer *et al.* 1960]. Tetrazole derivatives were obtained by the reaction between sodium azide and (E)-4-(3,4-bis(alkoxy)styryl)benzonitrile, which was prepared by the Wittig-Horner reaction of diethyl 4-cyanobenzylphosphonate and 3,4-bis(alkoxy)benzaldehyde. The products were characterized by FT-IR, NMR, MALDI-TOF and elemental analysis. The details of the synthetic procedure and spectral characterization of these derivatives are provided in the Experimental Section 4.8.
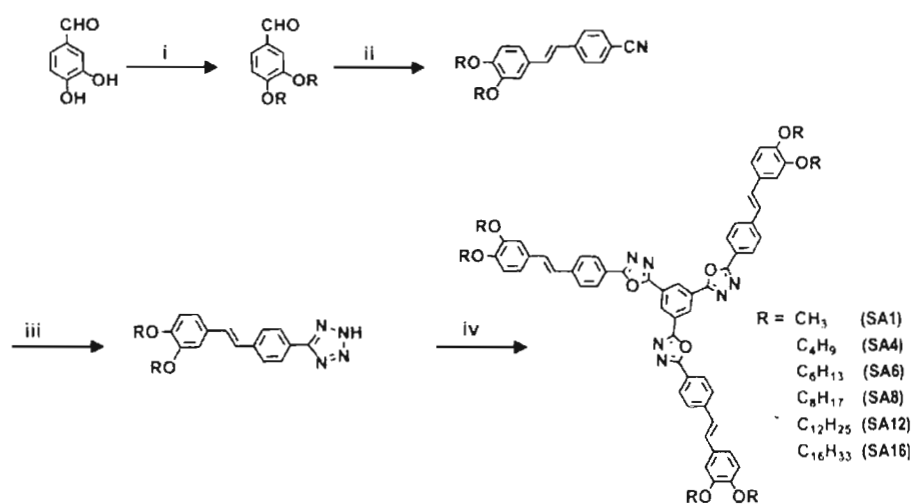
Reagents and conditions: (i) *n*-RBr, K₂CO₃, DMF, 100 °C, 12 h, (ii) diethyl-4-cyanobenzylphosphonate, NaH, THF, 25 °C, 3 h, (iii) NaN₃, NH₄Cl, DMF, 100 °C, 12 h (iv) benzene-1,3,5-tricarbonyl trichloride, pyridine, 115 °C. 12 h.

Scheme 4.1

4.3.2. Liquid Crystalline Properties

The thermotropic liquid crystalline phase behaviour of these materials were investigated by polarized light optical microscopy (POM), differential scanning calorimetry (DSC) and small-angle X-ray diffractometry (XRD). The 1,3,4-oxadiazole derivatives with long alkyl substituents (**SA12** and **SA16**) exhibited enantiotropic liquid crystalline behaviour while those with short alkyl chains (**SA1, SA4, SA6** and **SA8**) did not exhibit LC properties and melted sharply. The phase transition temperatures and corresponding enthalpy values of transitions are summarized in Table 4.1.

Table 4.1. Phase transition characteristics as observed from DSC in the heating/cooling cycles of the **SA12 and SA16**.

Sample Code	Heating cycle, °C (ΔH. kJmol^{-1})	Cooling cycle, °C (ΔH, kJmol^{-1})
SA12	Cr 165 (13.15)Col$_h$ 233 (1.14) I	I 228 (1.08) Col$_h$ 158 (9.21) Col$_{ob}$ [a]
SA16	Cr 44 (47.31) Col$_r$ 158 (16.40) Col$_h$ 235 (2.23) I	I 233 (2.52) Col$_h$ 151 (15.01) Col$_r$ 31 (38.63) Cr

[a] Material glassified on subsequent cooling; Cr – Crystalline phase, Col$_h$ - Hexagonal Columnar phase, Col$_{ob}$ - Columnar Oblique phase, Col$_r$ - Columnar Rectangular phase and I – Isotropic liquid.

POM studies of **SA12** indicated the presence of an enantiotropic columnar liquid crystalline behaviour. In the heating cycle, **SA12** underwent a crystal to hexagonal columnar phase transition at 165 °C, as characterized by their typical focal-conic texture (Figure 4.1a) and isotropizes at 233 °C [Laschat *et al.* 2007; Dierking 2003]. In the cooling cycle, an isotropic to hexagonal columnar phase transition was observed at 228 °C. Further cooling resulted in the appearance of crossed striations on the arms of the focal conic texture at 158 °C, which remained unchanged down to room temperature (Figure 4.1b). The appearance of the striations on the arms of the focal conic texture suggested a transformation from the hexagonal columnar phase to an oblique columnar phase [Laschat *et al.* 2007]. The striated texture observed at the higher temperatures was retained on cooling to

room temperature by which time the sample had solidified into a glass. The identical texture observed in the solid state indicates that the columnar arrangement had been frozen into a supercooled LC state [Abraham *et al.* 2006; Chen *et al.* 2003; Seo *et al.* 2007]. Phase transitions observed by POM were further confirmed by DSC measurements (Figure 4.1c).
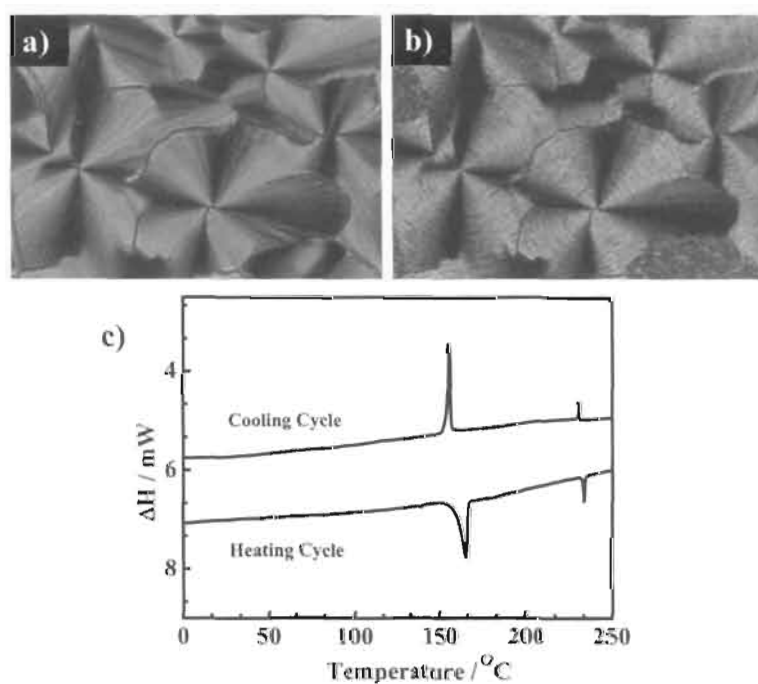
Figure 4.1. POM images of compound **SA12** a) hexagonal columnar phase at 220 °C, b) oblique columnar phase at 30 °C and c) DSC trace of compound **SA12** in the cooling/heating cycle at a rate of 5 °C per minute.

Similarly, for **SA16** in the cooling cycle an isotropic to hexagonal columnar transition was observed at 233 °C as indicated by the formation of a focal conic texture under POM (Figure 4.2a). On further cooling, transition to a rectangular columnar mesophase was observed at 151 °C as indicated by the formation of a striated focal conic texture (Figure 4.2b). Unlike in the case of **SA12**, further cooling did not lead to glass formation and a clear LC to crystal transformation was observed at 31 °C (Figure 4.2c). Phase transitions observed by POM were further confirmed by DSC analysis (Figure 4.2d).
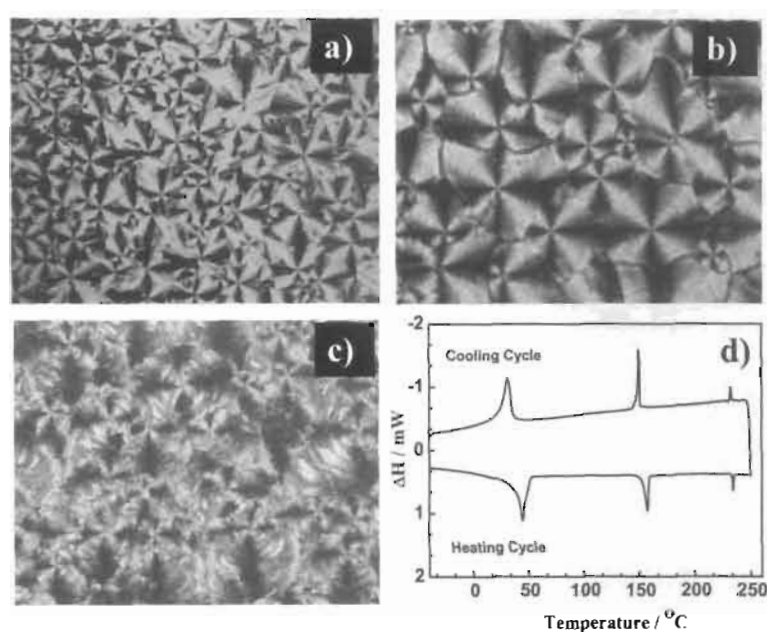
Figure 4.2. POM images of compound **SA16** a) hexagonal columnar phase at 220 °C, b) rectangular columnar phase at 90 °C, c) crystalline phase at 25 °C and d) DSC trace of compound **SA16** in the cooling/heating cycle at a rate of 5 °C per minute.

4.3.3. X-ray Diffraction Studies

X-ray diffraction analysis of these compounds confirmed the LC phase assignments observed by POM and results are summarized in Table 4.2 and 4.3. The samples were filled in Lindemann capillaries and were found to generally undergo spontaneous orientation in the capillaries, with the quality of alignment being as good as for monodomain samples. The X-ray diffraction pattern for compound SA12 at 220 °C showed a strong sharp peak at low angle (with a d-spacing of 48 Å) and broad and diffuse one in the wide angle region (Figure 4.3a). Although qualitatively this could suggest a lamellar structure, considering the molecular dimension of 60 Å, this would require substantial folding of the chains. Therefore in conjunction with the observed texture (Figure 4.1a) this result is indicative of a hexagonal columnar (Col_h) arrangement with a lattice spacing of 55.6 Å, a value which is closer to the molecular dimension (Figure 4.3b). At 158 °C striations appeared on the arms of the focal conic texture which remained unchanged down to room temperature (Figure 4.1b). The X-ray diffraction pattern obtained at 120 °C indicates a columnar structure, which can be mapped to an oblique lattice (Col_{ob}) with a = 57.9 Å, b = 45.6 Å and γ = 83° (Figure 4.3c). At room temperature, the mesophase was extremely viscous and XRD studies showed that the structure continues to be that of Col_{ob} with a small increase in the lattice dimensions (a = 59.2 Å, b = 48.7 Å and γ = 83°) but with a fluid-like wide angle peak indicating that the liquid crystalline state had frozen into a supercooled

glassy state, while retaining the columnar order [Abraham *et al.* 2006; Chen *et al.* 2003; Seo *et al.* 2007].

Table 4. 2. X-ray diffraction characterization of the mesophase of **SA12**.

Sample code	Phase Characteristics	d_{meas} [Å]	hk	d_{calc} [Å]	Lattice parameters measured at indicated temperatures
	Hexagonal Columnar LC Phase	48.1	10	48.1	T – 220 °C
		4.8			a – 55.6 Å
	Oblique Columnar LC Phase	57.4	11	57.4	T ≈ 120 °C
		45.2	01	45.2	a – 57.9 Å
		25.8	21	25.7	b ≈ 45.6 Å
SA12		4.7			γ – 83 °
	Oblique Columnar Liquid Crystalline Glassy Phase	58.7	10	58.8	T = 30 °C
		48.4	01	48.3	a = 59.2 Å
		26.8	21	26.6	b = 48.7 Å
		16.7	32	16.2	γ = 83 °
		4.5			
		3.4			
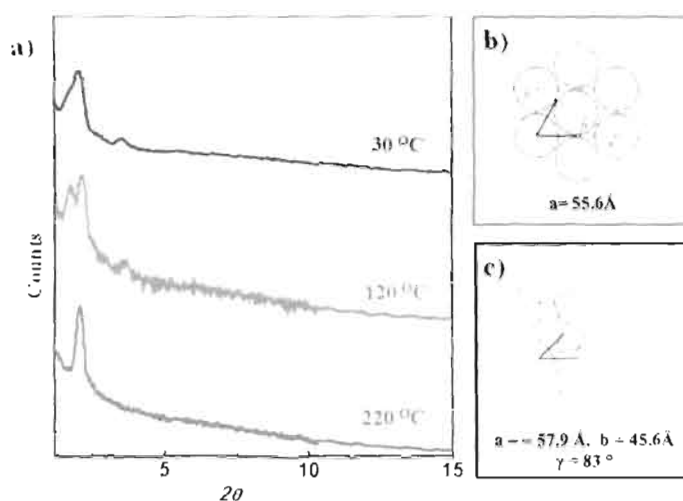
Figure 4.3. X-ray diffraction pattern of **SA12** at a) 220 °C (corresponds to hexagonal columnar lattice), 120 °C (corresponds to oblique columnar lattice); 30 °C (corresponds to oblique columnar lattice); b) & c) represent the schematics of hexagonal and oblique lattices respectively.

For the higher homologue i.e., compound **SA16,** the high temperature mesophase is the same as that of compound **SA12,** namely, a hexagonal columnar phase, with a lattice parameter of 59.8 Å (at 220 °C) (Figure 4.4a and Table 4.3). At low temperatures this phase transforms to a columnar phase whose reflections index to a rectangular lattice of a = 63.5 Å, b = 61.2 Å dimensions (at 130 °C) (Figure 4.4a). These numbers indicate a large increase in the lattice dimension with decrease in temperature. Such a negative thermal expansion (α) is commonly observed in columnar phases [Prasad *et al.* 2003]. However, the magnitude of α = 2.1×10^{-3} K^{-1} seen for compound **SA16** is larger than what is usually observed, for example, in triphenylene core molecules, the archetypal discotic systems. The

reason for this is the large free space available around the core for compound **SA16**, which permits the chains to fold up and occupy the volume between the arms at high temperatures, a feature that would be more difficult in the case of larger cores, such as triphenylenes. This view point is supported by the fact that a nearly doubles for compound **SA16**, in comparison to compound **SA12**. The change from a Col_h to Col_{ob} or Col_r phases requires strong interaction between the cores of neighbouring columns, since the core of one column has to selectively tilt with respect to the others. The tilted column reduces the interactions between bulky side chains and allows closer contact between the cores, as also suggested by the appearance of a wide angle peak corresponding to core-core interactions [Laschat *et al*. 2007].

Table 4.3. X-ray diffraction characterization of the mesophase of **SA16**.

Sample code	Phase Characteristics	d_{meas} [Å]	hk	d_{calc} [Å]	Lattice parameters measured at indicated temperatures
SA16	Hexagonal Columnar LC Phase	51.8 4.8	10	51.8	T = 220 °C a – 59.8 Å
	Rectangular Columnar LC Phase	63.6 61.3 44.1 4.7	10 01 11	63.5 61.2 44.1	T = 130 °C a – 63.5 Å b = 61.2 Å
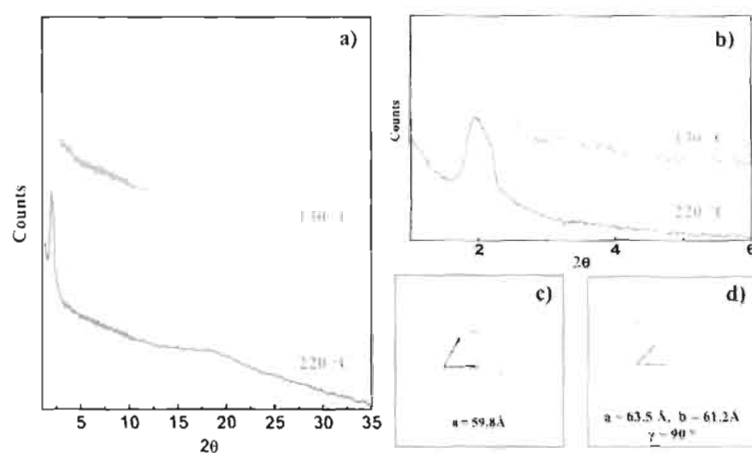
Figure 4.4. X-ray diffraction pattern of **SA16** at a) 220 °C (corresponds to hexagonal columnar lattice) and 130 °C (corresponds to rectangular columnar lattice), b) corresponding zoomed images of the XRD spectra. c) & d) represent the schematics of hexagonal and the oblique lattices respectively.

4.3.4. Gelation Studies

The strong core–core interactions observed in the mesophase studies prompted us to study the self-assembly behaviour of the molecules in solution, which revealed an interesting hierarchical build-up of supramolecular assemblies leading to the formation of highly luminescent gels. The oxadiazole derivatives with long alkyl substituents (**SA8**, **SA12** and **SA16**) are capable of forming gels in non-polar solvents like decane and toluene, while the derivatives with shorter alkyl chain length (**SA1**, **SA4** and **SA6**) did not undergo gelation. The critical gelation concentrations of these derivatives in decane and toluene solvents were determined in glass vials of 1 cm diameter and the gel formation was confirmed by

the failure of the contents of the vials to flow on inverting the glass vials. The critical gelator concentrations of these derivatives are summarized in Table 4.4.

Table 4.4. Critical gelator concentration in decane and toluene of oxadiazole derivatives. All the gels formed were transparent and highly stable.

Solvent	SA12 mg/mL (mM)	SA12 mg/mL (mM)	SA16 mg/mL (mM)
Decane	9.2 (6.5)	28 (14.5)	18.6 (8.2)
Toluene	14 (9.6)	32 (16.6)	24.18 (10.7)

In derivatives with longer alkyl chains (**SA12** and **SA16**), the gelation process was found to be very slow and it took few days for complete immobilization of the solvent. The gels were prepared by dissolving small amounts of the oxadiazole derivatives in decane or toluene by heating and keeping them at room temperature in a closed vial for 2 days, following which clear transparent gels were formed.

Rheological studies on the decane gel of **SA12** indicated the gel to be fairly stable. Frequency-sweep measurements showed that the elastic modulus (G') and the loss modulus (G'') were almost independent over a wide range of frequency at 25 °C at a shear strain of 5%. A strain-sweep experiment was performed at constant angular frequency of 1 rad/s for the strain range 0.1 to 100. The strain-

sweep experiment shows the non-linearity in viscoelastic behaviour leading to the collapse of the gel. The critical strain calculated was 56% at the applied frequency of 1 rad/s. These results are indicative of the viscoelastic nature of the gel (Figure 4.5) [Yao *et al.* 2004; Babu *et al.* 2008; Menger *et al.* 2004; Huang *et al.* 2005; Wang *et al.* 2006].
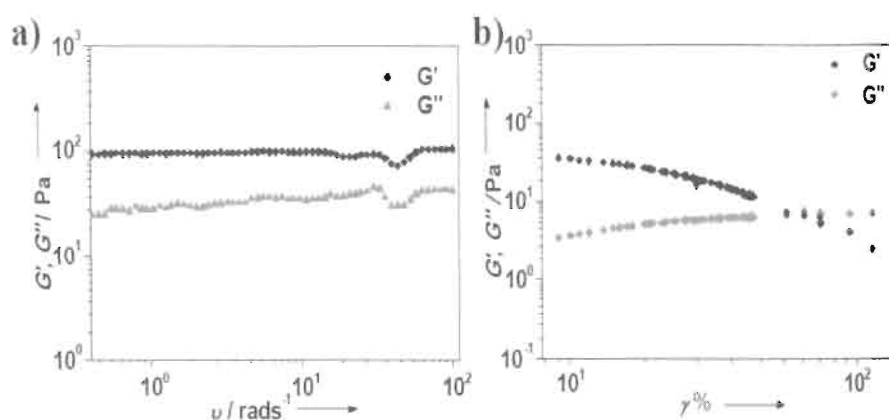
Figure 4.5. Rheology measurements of **SA12** gel in decane at 25 °C a) Frequen sweep measurements, Dynamic moduli, G', G'' vs angular frequency on doul logarithmic scale at a shear strain of 5%. b) Strain sweep measurements, Dynan moduli, G', G'' vs strain on double logarithmic scale; frequency, υ – 1 rad/s.

Scanning electron microscopy (SEM) of the xero gel indicated t formation of interlocked fibrillar structures (Figure 4.6a). Most of the molecu organogelators reported, especially those containing a discotic core, conti hydrogen bonding motifs, which play a major role in the self-assembly process Since these discotic molecules do not possess specific hydrogen bonding moieti

the self-assembly of these molecules would most likely occur *via* π-π and dipole-dipole interactions.
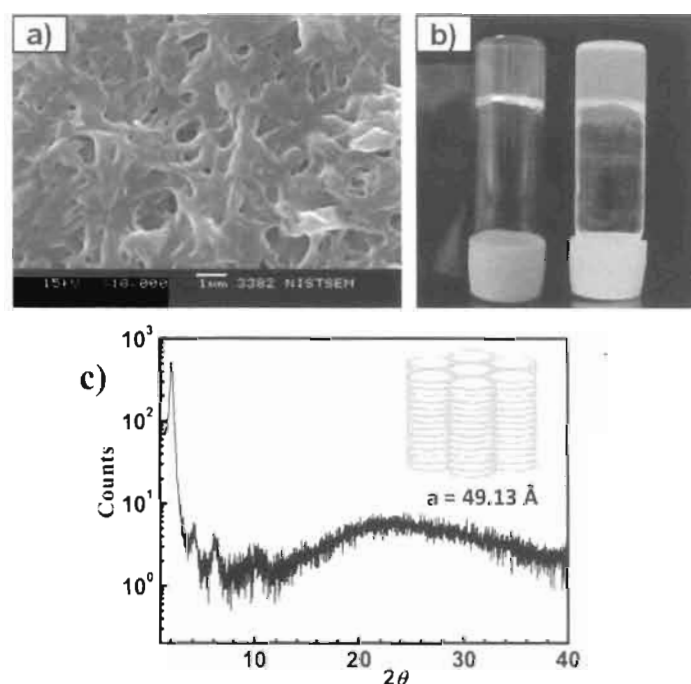
Figure 4.6. a) SEM images of entangled fibrous network in the xero gel state derived from decane at its critical gelation concentration. b) Photographs of decane gel; under ordinary light and on 365 nm illumination. c) X-ray diffraction pattern of xero gel of **SA12**.

X-ray diffraction studies were carried out on the xero gels in order to gain further insight into the nature of self-assembly of the molecules in the gel state. X-ray patterns showed reflection peaks at 42.49, 21.25 and 14.3 Å in the small angle region (Figure 4.6c). Although the ratios of the spacings are integers, a feature which is characteristic of lamellar structures, it may be noted that the ratios can also be represented as $1:\sqrt{4}:\sqrt{9}$. Additionally a very weak signal near 2θ ~10°.

which can be fitted to two peaks provides additional values of the ratios as √19 and √25, which would be absent in lamellar structure. These features and the fact that the mesophase shows a hexagonal phase strongly indicate hexagonal columnar organization in the fibers of the gel with a lattice spacing of 49.13 Å, a value that is closer to the molecular dimension. The compound **SA16** exhibited almost similar gelation behaviour but required less amount of material for the immobilization of the solvent.

For derivative containing a shorter alkyl chain (**SA8**), the gelation process was found to be instantaneous. The dissolution of small amounts of **SA8** in decane (1 mL), by heating followed by cooling of the solution, resulted in the spontaneous immobilization of the solvent. The gels obtained were transparent and stable and the glass vial could be turned upside down without perturbing the gel structure (Figure 4.7a). An unusual phase transition was observed in the gelled material with time. Shrinkage of the gel resulting in a small cylindrical mass occurred on letting the gel to stand for a period of twelve hours. Nearly 75% of the trapped solvent was squeezed out of the original gel. The shrunken gel was self-supporting and highly stable (Figure 4.7b).

Gels formed by the self-assembly of small molecules, making use of non-covalent interactions are relatively unstable compared to those formed from covalently linked polymers. The former is susceptible to breakage with the course of time or slight perturbation. In contrast, the shrunken gel was found to be highly

stable. The SEM images of the freshly prepared gel and the shrunken gel indicated transformation from a smooth fibrous arrangement to a more aligned and densely packed fibrous arrangement.
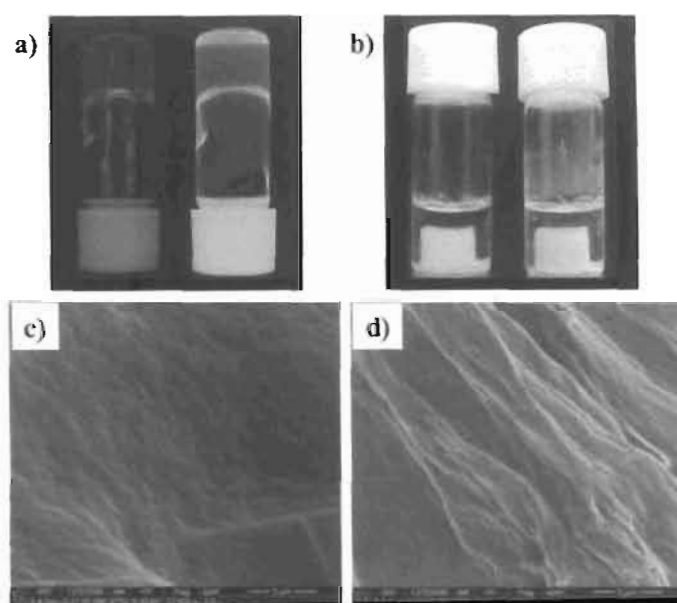
Figure 4.7. Photographs of decane gel a) freshly prepared, b) after a time interval of 12 h; (right side under ordinary light and left side on 365 nm illumination). SEM images of c) freshly prepared gel and d) after a time period of 12 h of **SA8** in decane.

X-ray diffraction studies were carried out on the freshly prepared and the shrunken gel after twelve hours in order to gain insight into the nature of self-assembly of the molecules in both the states. The X-ray diffraction pattern for the freshly prepared gel showed only two peaks, a broad reflection peak at 2.93° (33.98 Å) in the small angle region and a broad diffuse hallow in the wide angle

region (Figure 4.8a). The broad small angle peak qualitatively suggests the formation of a disordered lamella in the freshly prepared gel and the broad diffuse hallow in the wide angle region indicates the disordered alkyl packing. The XRD pattern of the shrunken gel however showed reflection peaks at 35.02, 17.58, 10.51 and 7.89 Å in the small angle region (Figure 4.8b). The ratios of the spacings were well in agreement with the features which are characteristic of hexagonal columnar structures.
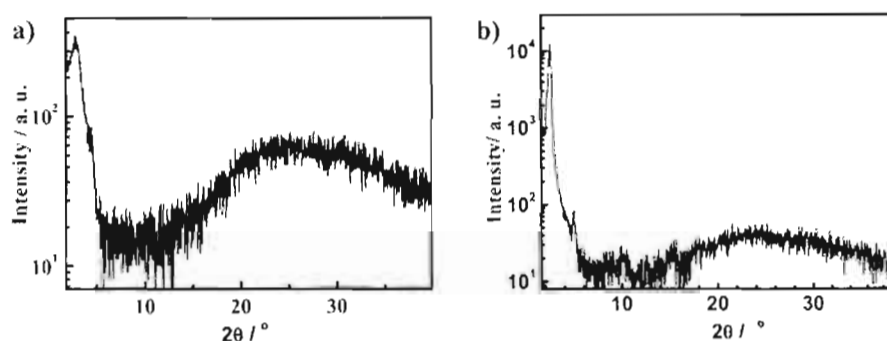
Figure 4.8. X-ray diffraction pattern of a) freshly prepared gel and b) the shrunken gel of **SA8** in decane.

Comparison of the XRD investigations of the freshly prepared gel and the shrunken gel indicate significant changes in the nature of packing of the molecules in both these forms. In the freshly prepared gels, the molecules are randomly arranged into a lamellar structure. This arrangement can be attributed to a kinetically organized (trapped) form. Over a period of time, the molecular alignment changes to the thermodynamically more stable hexagonal columnar

arrangement. In the process of formation of the more densely packed structure significant amount of the trapped solvent (~75%) was squeezed out of the gel.

Unlike conventional organogelators, disk shaped molecules have to self-organize in a manner so as to maximize π π interactions which can result in the formation of columnar superstructures leading to formation of fibers and eventually to entangled network of fibers wherein the solvent molecules are immobilized. The large core size of the disk shaped molecules and absence of strong hydrogen bonding interactions can lead to a slowing down of the self-assembly process, since the molecules have to sort themselves into hexagonally columnar lattices purely by π–π and dipole–dipole interactions. The various stages of these transformations were clearly visible in the lower homologues (**SA8**), where the randomly organized lamellar structure resulted in the immobilization of solvent in the fibrillar network but with course of time get transformed into the more stable hexagonal columnar arrangement resulted in the shrinkage of the gel.

4.3.5. Hierarchical Self-Assembly in Solution

The gelling process was extremely slow for **SA12** compared to most organogelators reported in the literature [Sangeetha *et al.* 2005]. In order to obtain a better insight into the self-assembly process, microscopic studies of the superstructures formed in aged solutions of **SA12** at different concentrations were investigated. The studies revealed an interesting hierarchical build-up of supramolecular assemblies with the increase in concentrations, leading from

spheres to fibers and finally resulting in the formation of highly luminescent transparent gels.
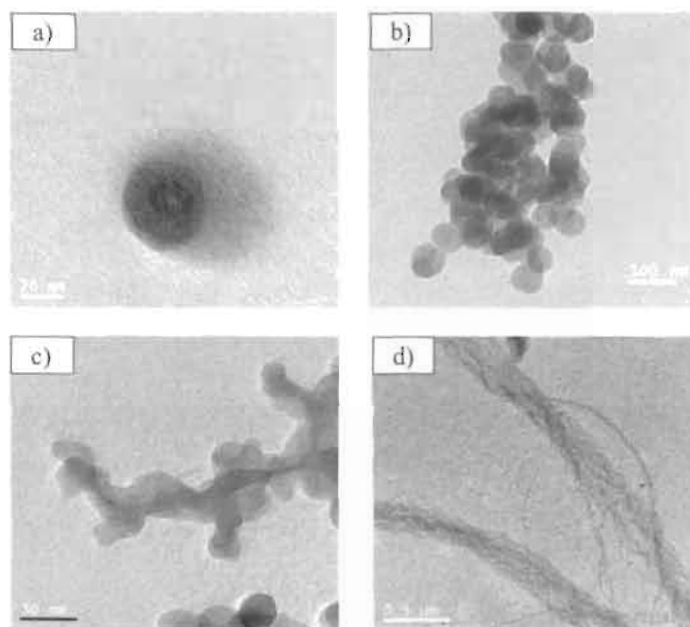
Figure 4.9. TEM images showing hierarchical build-up of supramolecular assemblies of **SA12** at a) 10^{-6} M concentration shows individual sphere with ~30 nm in diameter b)10^{-6} M shows the clusters of individual spheres, c) 10^{-5} M, d) 10^{-4} M solutions in decane.

The hierarchical build up of supramolecular assemblies was investigated by high resolution transmission electron (HR-TEM) and field emission-scanning electron microscopic (FE-SEM) experiments. TEM analysis was carried out on solutions aged for a week by drop casting them on copper grids. TEM micrographs of samples prepared from 10^{-6} M solution of **SA12** in decane showed clusters of spheres dispersed with a size distribution ranging from 10-60 nm in diameter

(Figure 4.9a & b). TEM images obtained from 10^{-5} M solutions indicated that these nanometer sized spheres had fused together constructing a framework somewhat like the back bone of a fiber while retaining the spherical morphology on the surface (Figure 4.9c). In the concentration range of 10^{-4} M, these joined spheres fused together to form fibrous aggregates with diameter ranging from 20 nm to 100 nm (Figure 4.9d).
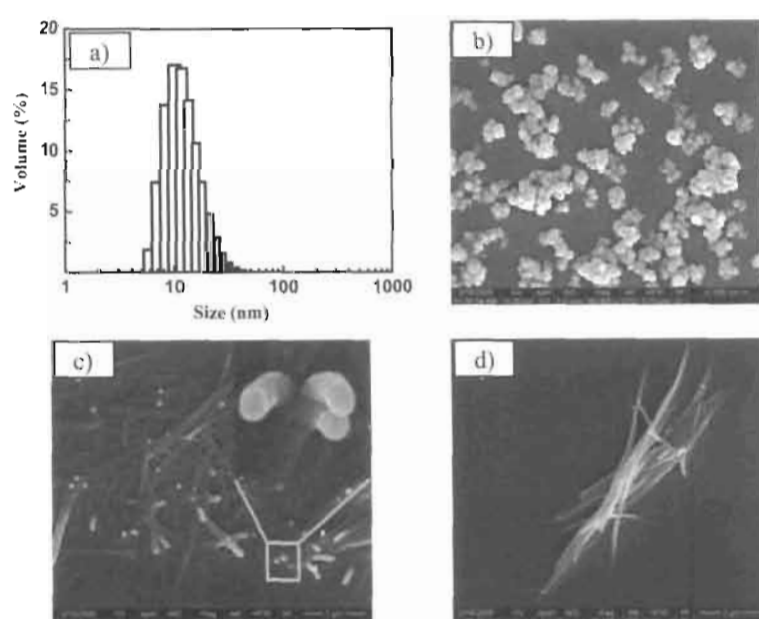
Figure 4.10. Dynamic light scattering analysis of **SA12** in decane; a) at 10^{-6} M concentration and FE-SEM images of self-assembled structures of **SA12** drop casted from b) 10^{-6} M, c) 5×10^{-5} M; Inset shows the zoomed image of the growing end of the fibrous aggregates and d) 10^{-4} M solutions in decane.

Dynamic light scattering investigations were carried out to confirm the spherical texture in the lower concentrations. The dynamic light scattering studies

also confirmed the formation of nanometric spheres with diameters ranging from 7-50 nm in size at 10^{-6} M solution in decane (Figure 4.10a). Further evidence for the concentration dependent hierarchical build–up of nanometric spheres to fibrous aggregates was obtained from FE-SEM experiments on samples prepared by drop casting aged solutions on aluminum stubs. A 10^{-6} M solution showed clusters of spheres (Figure 4.10b) similar to that observed by TEM. The SEM analysis of 5×10^{-5} M solutions showed the formation of fibrous aggregates (Figure 4.10c) with the spherical morphology being clearly visualized near the growing end of the fibers. In 10^{-4} M solutions, the spheres merged to form fibrous aggregates with an average diameter of ~80 nm, with no remnant indication of the spherical texture (Figure 4.10d).
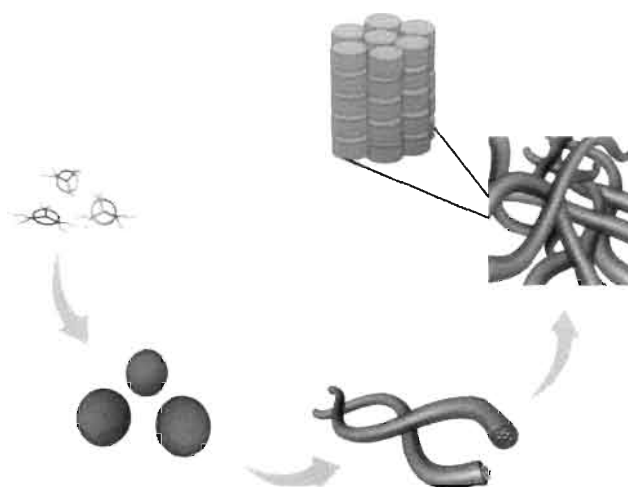
Figure 4.11. Schematic representation of the hierarchical self-assembly of SA12. Columnar arrangement of the molecules within the fibers is also depicted.

A schematic representation of the concentration dependent hierarchical self-assembly of **SA12** in decane, starting from nanometric spheres to fibrous morphology resulting in the formation of gels, which is consistent with the microscopic studies is depicted in Figure 4.11.
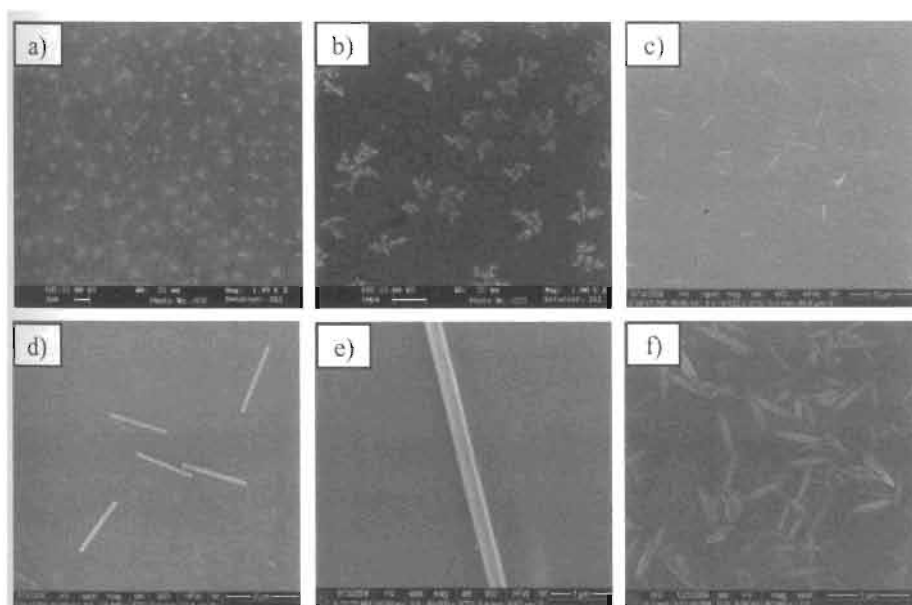
Figure 4.12. FE-SEM images of self-assembled structures of **SA8** drop casted from a) and b) 10^{-7} M showing spherical aggregates, c) 10^{-6} M showing nano rods, c) and d) shows the magnified image of the nano-rods at 10^{-6} M solution in decane, f) shows the spindles formed at 10^{-5} M solutions in decane.

Self-assembly of **SA8** in decane solution showed significantly different aggregation behaviour. Microscopic investigation revealed the hierarchical self-assembly leading from spheres to nano-rods which finally transformed into spindle like structures. SEM experiments were carried out on the samples prepared by

drop casting aged (12 h) solutions on aluminium stubs. Solutions of **SA8** in decane of lower concentrations (10^- M) showed the formation spherical aggregates (Figure 4.12a & b). Samples prepared from the solution with higher concentration (10^{-6} M), however showed the formation of nanorods (Figure 4.12c-e) with the high aspect ratio. The nanorods formed possessed an average dimension of ~50 nm (width) and ~2.5 μM (length). The nanorod surface was unusually smooth and straight (Figure 4.12e) Samples prepared from solutions of even higher concentration (>10^{-5} M) showed the formation of the spindle like structures (Figure 4.12f).

The formation of the nanorods at 10^{-6} M solution of **SA8** in decane was further confirmed by TEM analysis. The nanorods formed were approximately 40 nm in width and few micrometers in length (Figure 4.13a), almost similar to that observed in the SEM analysis. Figure 4.13b showed the formation of the spindles at 10^{-5} M solution. It was evident from the TEM images (Figure 4.13a) that the spindles are formed by the joining of the nanorods. Fluorescence microscopic images at 0.4 x 10^{-5} M solution showed that the nano-rods formed are highly fluorescent and emit in the green region (Figure 4.13c) The large area image of the clusters of nanorods are depicted in Figure 4.13d.
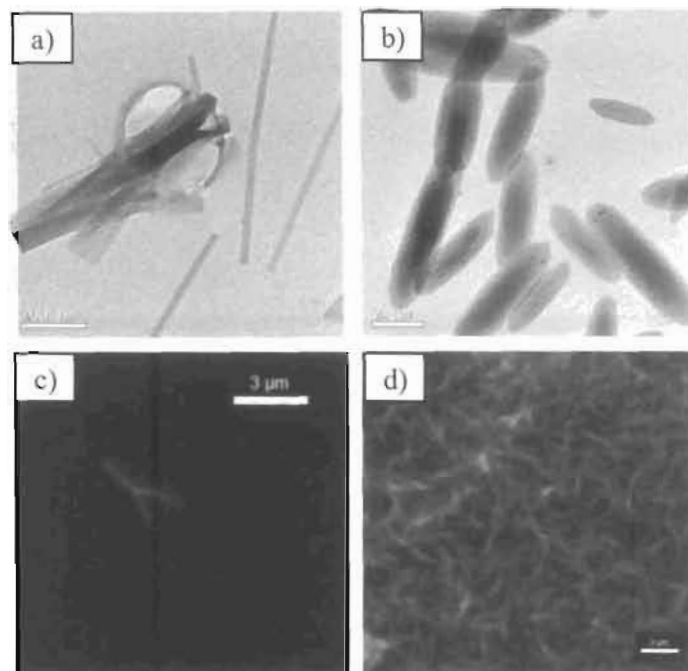
Figure 4.13. TEM images of self-assembled structures of **SA8** drop casted from a) 10^{-6} M and b) 10^{-5} M, c) and d) fluorescence microscopy images of the nano-rods drop casted from decane solution of **SA8** ($c = 0.4 \times 10^{-4}$ M)

4.3.6. Photophysical Properties

The absorption and emission properties of compound **SA12** in a few different solvents are summarized in Table 4.5. Its absorption maximum was independent of solvent polarity, indicating that the dipole moments of its ground and excited states are nearly the same. The fluorescence spectra however showed a significant red shift with increasing solvent polarity. This is suggestive of the direct excitation of these molecules leading to a non-emissive locally excited state (LE) possessing nearly the same dipole moment as the ground state, which

subsequently transforms into a more polar emissive state *via* an intramolecular charge transfer (ICT) process [Rettig 1994; Demeter *et al.* 2000]. It has been shown earlier that some donor–acceptor substituted butadienes exhibit the unusual phenomenon of dual emission, with emissions emanating both from the Frank-Condon state (FC) and the ICT states [Davis *et al.* 2001; 2008]. The fluorescence decay of **SA12** was mono-exponential in dilute solution in most of the solvents investigated (Table 4.5) at low concentrations with a slight increase in lifetime being observed on going from non-polar to polar solvents.

Table **4.5.** Absorption, emission and fluorescence lifetime characteristics of compound **SA12**

SA12	Abs. λ_{max} (nm)	Em. λ_{max} (nm)	Φ_f	τ (ns)	χ^2
Decane	363	410, 432, 460	0.05	0.82	1.09
Toluene	372	440	0.52	0.88	1.03
DCM	369	493	0.96	1.60	1.04
THF	369	484	0.99	1.72	1.07
Ethylacetate	365	475	0.98	1.57	1.01

Figure 4.14 shows the normalized absorption spectra of **SA12** in ethylacetate and decane. In ethyl acetate, the sharp absorption spectrum and mono-exponential fluorescence decay indicated that **SA12** existed in its monomeric form. In decane, however, the shape of the absorption spectrum was observed to

be highly dependent on the concentration of **SA12**. Curve a in Figure 4.14 shows the absorption spectrum of 10^{-5} M solution of **SA12** in decane. A clear broadening in the absorption spectrum and a blue shift in the absorption maximum could be observed compared to that of the monomer band observed in ethyl acetate. The spectrum obtained at higher concentration in decane (10^{-4} M) is also very broad however the enhancement of absorption in the red region is significantly higher. Since as described above the absorption spectrum of **SA12** was fairly independent of solvent polarity, the significant changes in absorption spectra observed in decane and its dependence on concentration clearly point to the formation of aggregates. The presence of aggregates in decane solutions was also confirmed by studying the effect of temperature on the absorption spectrum.
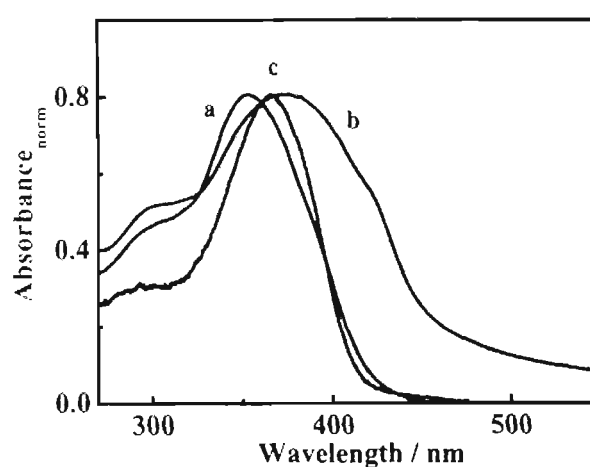
Figure 4.14. Normalized absorption spectra of **SA12** in a) decane (10^{-5} M), b) decane (10^{-4} M) and c) ethyl acetate.

Temperature dependent absorption spectra of **SA12** in decane at 10^{-5} M solution and 10^{-4} M solutions were carried out to know the nature of molecular packing in the aggregates (Figure 4.15). For a 10^{-5} M solution of **SA12** in decane, increase in temperature led to an increase in intensity and a 10 nm red shift of the peak at 353 nm which was accompanied by a decrease of absorption in the 300 and 415 nm regions (Figure 4.15a). These changes were marked by the presence of two isosbestic points at 320 and 398 nm. Aggregation of molecules can result in *H*- or *J*-aggregates and their optical properties can be explained by exciton coupling theory. *H*-aggregates possess a high energy allowed transition and a low-energy forbidden band, and their absorption is therefore blue-shifted compared to that of the monomer. In contrast, for *J*-aggregates the low energy transitions are allowed giving rise to a red-shifted absorption. For 10^{-4} M solutions of **SA12** in decane (Figure 4.15b) increase in temperature resulted in an increase in intensity and blue shift of the main peak at 373 nm, and a concomitant decrease of intensity of absorption at 425 nm. These changes indicate the existence of mainly *J*-aggregates in this concentration range, where TEM and SEM studies indicated formation of fibrous aggregates.
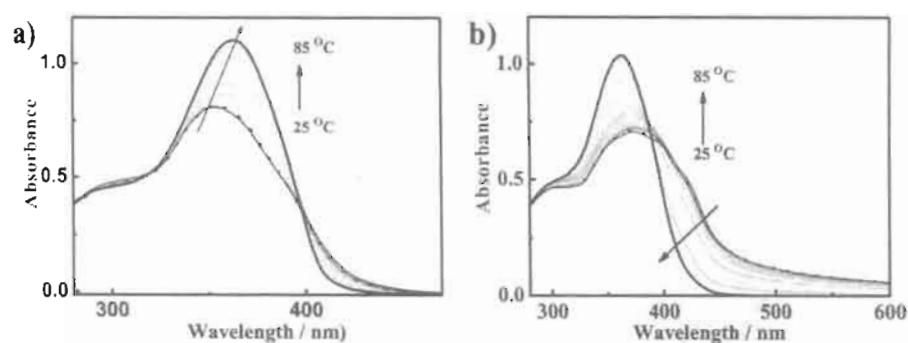
Figure 4.15. Temperature dependent changes in absorption spectra of aged solutions of **SA12** in decane at a) 10^{-5} M measured in 10 mm cuvette and b) 10^{-4} M measured in 1 mm cuvette.

Self-assembly of molecules can result in *H*- or *J*- aggregates and their optical properties can be explained by exciton coupling theory [Kasha *et al.* 1965; Kaiser *et al.* 2007], wherein the excited state of aggregates splits into two energy levels (Davydov splitting). The transition to the upper state is allowed in the case of *H*-aggregates, characterized by a hypsochromically shifted absorption band, and that to the lower state for *J*-aggregates marked by a bathochromically shifted absorption band compared to the isolated monomer. In the present study, at the lower concentration (10^{-5} M) a blue shift in the absorption spectrum is therefore indicative of formation of the *H*-type aggregates. For 10^{-4} M solutions of **SA12** in decane, where, a significant enhancement of absorption in the long wavelength region compared to that of the monomer indicated predominant formation of *J*-type aggregates.
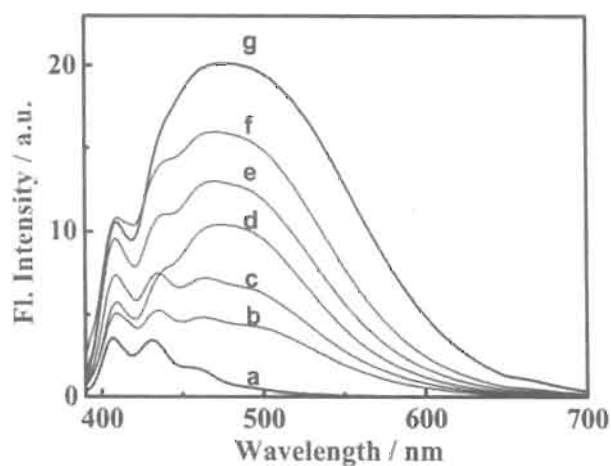
Figure 4.16. Concentration dependent changes in emission (λ_{ex} = 370 nm) of SA12 in a) 10^{-7} M, b) $8\times10^{-}$ M, c) 2×10^{-6} M, d) 6×10^{-6} M, e) 8×10^{-6} M, f) 10^{-5} M and g) 2×10^{-5} M solutions in decane.

Further information on the nature of aggregates formed could be obtained by monitoring changes in the fluorescence spectra of the solutions as a function of concentration (Figure 4.16). For a 10^{-7} M solution, the emission occurred solely from the molecularly dissolved species as indicated by the structured band in the 400 to 470 nm region. At higher concentrations, a new peak at 500 nm was observed whose intensity relative to that of the monomer emission band increased significantly with increasing concentration. The formation of the new band which was considerably red shifted compared to that of the molecularly dissolved species, indicated the formation of exciton coupled aggregates.
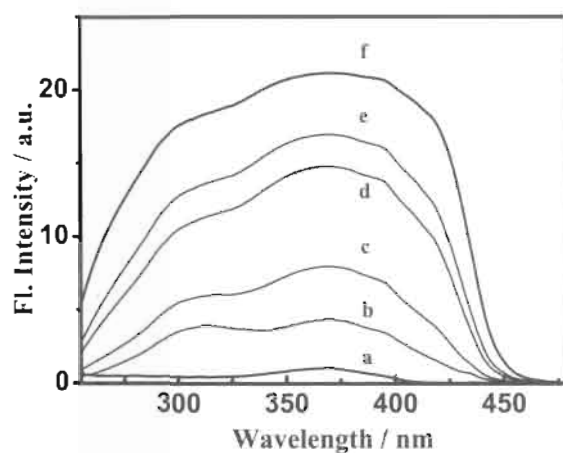
Figure 4.17. Concentration dependent changes in excitation spectra (λ_{em} – 500 nm) of **SA12** in decane at concentrations; a = 6×10^{-7} M, b = 10^{-6} M, c – 2×10^{-6} M, d = 8×10^{-6} M, e = 10^{-5} M, f = 2×10^{-5} M.

The changes in the excitation spectra as a function of concentration were studied in order to understand the nature of the emitting species (Figure 4.17). At lower concentrations (10^{-7} M), the excitation spectrum indicated a main peak at 367 nm which could be attributed to the molecularly dissolved species. With increasing concentration, a significant broadening of the spectrum was observed indicating formation of aggregates. The nature of the aggregates formed could be clearly visualized by subtracting the contribution of the monomer band (obtained from excitation spectra measured in 10^{-7} M decane solutions where molecule exists mainly in the molecularly dissolved state) from the excitation spectra obtained at the higher concentrations. Figure 4.18 shows the spectra obtained by subtracting the contribution of the monomer band from spectra normalized at 367 nm for 10^{-6} M and 2×10^{-5} M solutions of **SA12** in decane. Two new bands, one

in the blue and red shifted region compared to that of the monomer, clearly point to the formation of both *H*- and *J*-type aggregates in both solutions. A significant increase in the relative contribution of the red shifted *J*-aggregate could be seen at the higher concentration. These results are in agreement with the changes in absorption spectra as a function of concentration described earlier. It may be mentioned here that microscopic studies had indicated formation of spheres in the 10^{-6} M solutions whereas fibers were observed in 2×10^{-5} M solutions.
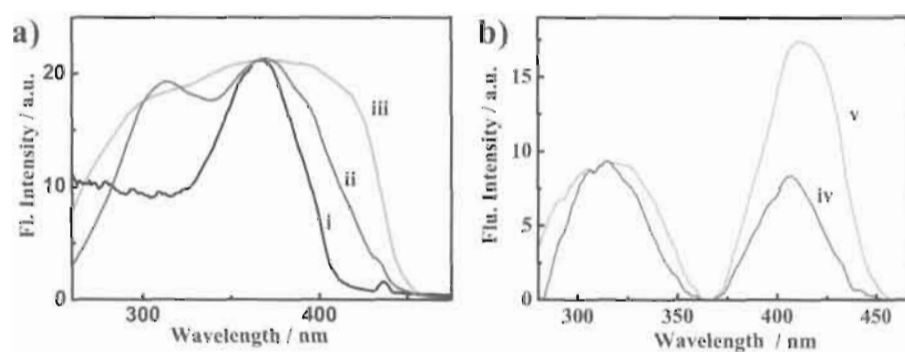
Figure 4.18. a)Normalized excitation spectra of i) 10^{-7} M ii) 10^{-6} M, iii) 2×10^{-5} M, solutions of **SA12** in decane. b) difference spectra obtained by subtracting the normalized excitation spectra of a) 10^{-7} M from 10^{-6} M and b) 10^{-7} M from 2×10^{-5} M solutions, emission monitored at 500 nm.

The gel state of **SA12** in decane exhibited a strong emission ($\Phi_F = 0.3$) in the 450-700 nm region with a emission maximum at 500 nm (Figure 4.19a). The excitation spectra of **SA12** in the gel state showed a broad band with maxima at 280, 370 and 445 nm, indicating the presence of monomer, *H*- and *J*-aggregates (Figure 4.19a). Excitation at all these wavelengths led to emission form the *J*-

aggregate indicating efficient energy transfer from the monomer and *H*-aggregates to the *J*-aggregates. *H*-aggregates are generally known to be non-luminescent. The appearance of the *H*-aggregate band in the excitation spectra monitored at a wavelength where the *J*-aggregate emits (500 nm) therefore indicates an efficient transfer of light energy harvested by the *H*-aggregate to the *J*-aggregate. This can be attributed to the columnar organization of the disc shaped chromophores within the fibers, with the strong $\pi-\pi$ interactions resulting in exciton migration from the *H*- to the *J*-type aggregates and subsequent emission from the *J*-traps. Evidence for energy transfer was also obtained by monitoring the fluorescence lifetimes of the gels which indicated a triexponential decay profile with the longest lifetime being 17 ns which was significantly higher than the 0.82 ns lifetime observed for the monomeric form (Figure 4.19b) [Bayer *et al.* 2001; Chen *et al.* 2007; Ajayaghosh *et al.* 2007]. Time resolved fluorescence anisotropy decay profile of compound **SA12** in the gel state showed an extremely fast depolarization of emission taking place from an initial anisotropic value of 0.25 (r_0) to a plateau value of 0.04 . The rate of anisotropic decay in the gel state was found to be faster than that of the monomeric species, where the initial anisotropic value of 0.36 (r_0) reached a plateau value of 0.04. Fluorescence depolarization in a system can occur either by rotational displacement of the chromophores or by an energy migration process. Since rotational motion of the molecules in the gel state will be largely restricted, the fast depolarization in the gel state, even faster than

that in solution can mainly attributed to energy transfer between the molecules of different orientation [Herz *et al.* 2003; Gierschner *et al.* 1997; Watanabe *et al.* 1997; Egelhaaf *et al.* 1996; Westenhoff *et al.* 2006].
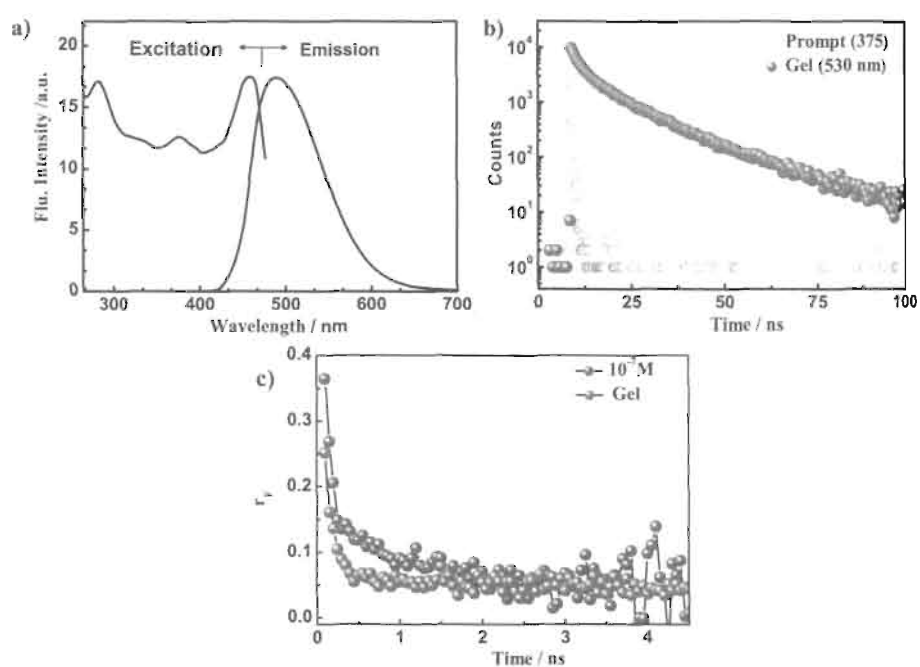
Figure 4.19. a) Excitation (λ_{em} = 500 nm) and emission spectra (λ_{ex} − 375 nm), b) fluorescence lifetime decay profile (λ_{ex} = 375 nm), emission monitored at 500 nm and c) fluorescence anisotropic decay profile of compound **SA12** in the gel state (λ_{ex} = 375 nm , λ_{em} = 500 nm) and in 10^{-7}M solution (λ_{em} = 410 nm) in decane.

As discussed above, the XRD spectral analysis indicated hexagonal columnar organization of molecule in the gel fibers. The presence of *H-* and *J-*type aggregates in the gel state, as indicated in emission and excitation spectra strongly suggests substantial overlap between the conjugated arms of the

neighbouring trigonal discotic molecules within the columnar stacks. A schematic representation of the molecular level organization within the fibers of the gel based on the above mentioned studies is shown in Figure 4.20. The discotic molecules can form co-facial π-stacks as shown in the figure resulting in the formation of the *H*-type aggregates. Since the angle between the molecular plane and the aggregation direction decides the nature of the aggregates (*H*- or *J*-type), the results suggest that within the stacks some of the molecules can be tilted with respect to each other (Figure 4.20), giving rise to the *J*-type aggregates [Wurthner *et al* 2001; Ghosh *et al.* 2008]. As a result, emission from the *J*-type aggregates can occur either due to direct excitation or *via* efficient exciton migration from the *H*- to the *J*-type aggregates as a result of the columnar π-stacked arrangement.
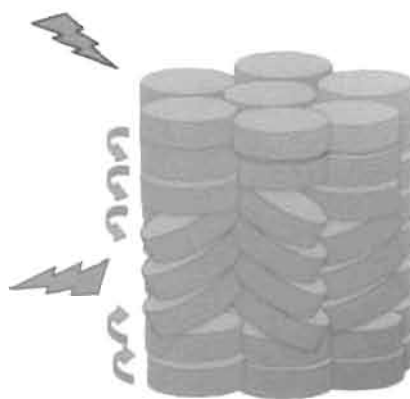
Figure 4.20. Model of chromophore packing in the fibers of the gel of **SA12** in decane.

4.4. Conclusion

A novel class of octupolar oxadiazole derivatives (**SA1-16**) has been synthesized and their mesophase properties and ability to self-assemble in non-polar solvents have been examined. Few of the derivatives exhibited enantiotropic columnar mesophases over a wide temperature range. One of the derivatives (**SA12**) could be cooled from its liquid crystalline state into a glassy state at room temperature wherein the columnar order was retained. Microscopic investigations provided clear evidence for the hierarchical self-assembly of these molecules in non-polar solvents leading to gel formation. Spheres of nanometric dimensions were observed at lower concentrations which merged together to form nanoscopic fibers at higher concentrations resulting in an extended network of interlocked fibrils which immobilize the solvent to form the gel. As a result of the absence of strong hydrogen bonding motifs, the self-organization process is purely driven by π-π stacking interactions and occurs slowly over a long period of time. While XRD spectral analysis revealed a hexagonal columnar organization of the molecules in the fibers of the gel, spectroscopic studies indicated the formation of *H*-and *J*-type aggregates in the self-assembled structures. At lower concentrations where the nanospheres were seen, predominantly *H*-type aggregates were observed whereas in the fibers *J*-type aggregates were found to predominate. The columnar stacking of the molecules in the fibers provided an efficient pathway for the excitation energy migration between *H*- and *J*-type aggregates of the same

chromophore. Unusual phase transition behaviour was observed in the derivative posessing shorter alkyl chain lengths (**SA8**), where the gelation process was rapid but underwent shrinkage over a period of time (12 h). These changes could be attributed to the molecules which were originally kinetically trapped into a lamellar arrangement, slowly reorganizing into the thermodynamically stable hexagonal columnar stacking. The more tightly packed organization of the molecules resulted in squeezing out of almost 75 % of the trapped solvent in the original gel matrix. Microscopic investigations revealed concentration dependent transformation from nanospheres to nanorods and finally to spindle like aggregates for the **SA8** derivative. The nanorods formed possessed high aspect ratio and an unusually smooth surface. The ability to form fluorescent nano fibers/rods wherein these n-type molecules self-assemble into π-stacked columns makes them potentially useful as candidates for investigation as molecular wires and emitters in the emerging area of supramolecular electronic devices.

Section B

Induction of Chirality into Columnar Stacks

4.5. Introduction

Helicity is an inevitable structural feature of various biological systems. Nature makes use of the intriguing phenomenon of supramolecular chirality for the construction of complex helical structures with specific shape, size and functions, such as single stranded RNA for replication, DNA double helix for genetic data storage and collagen triple helix for structural integrity [Luisi 2006; Mason 1985; Cintas 2002; Watson 1954]. The elegance and complexity in their structural features and specificity in functions has interested chemists to construct such superstructures [Service 2005]. Self-assembly is proven to be the most effective method for the creation of complex structures from simpler building blocks and can be achieved by interplay of various weak non covalent interactions such as hydrogen bonding, $\pi-\pi$ stacking, solvophobic effects and so on [Lehn 1995]. Precise control of molecular arrangements at the supramolecular level is essential to obtain well-defined nanoscopic architectures with desired shape and specific functionalities [Rowan *et al.* 1998]. In complex self-assembled helical architectures, helical sense is generally induced by the transfer of chiral

information from the molecular to the supramolecular level and is amplified due to the high co-operativity between the building units [Palmans *et al.* 2007; George *et al.* 2007; Rosaria *et al.* 2008]. Incorporating stereogenic groups into the self-assembling molecular units is a general strategy for constructing supramolecular helices and there have been several efforts directed towards designing materials exhibiting supramolecular helical architectures making use of supramolecular design principles [Maeda *et al.* 2006; Schmuck *et al.* 2003; Lelkema *et al.* 2006; Brizard *et al.* 2003; Mateos-Timoneda *et al.* 2003; Serrano *et al.* 2003]. Self-assembly of discotic molecules into helical architectures in particular is important, since the shape anisotropy of the discotic molecules tends to favour a face to face stacking geometry, resulting in one dimensional columnar aggregates which in turn facilitates strong π-π interaction [Jin *et al.* 2005; Dehm *et al.* 2007; Klosterman *et al.* 2009; Chen *et al.* 2009]. Helical organization of the discoid molecules facilitates condensed packing between the molecules, which is an essential feature for the enhanced transport of charges and photons within the stacks [Chen *et al.* 2007; Adam *et al.* 1994; Herz *et al.* 2003].

Here, we describe our investigation on the unique aggregation behaviour of discoid molecules leading to the formation of helical fibers with right handed helicity at lower concentrations. At higher concentrations, the helices further wind around each other leading to a superhelix secondary structure which exhibits left handed chirality. The formation of the superhelix secondary structure and the

associated reversal of chirality in the supramolecular level could be monitored by circular dichroism (CD) spectroscopy as well as SEM and TEM microscopic techniques.
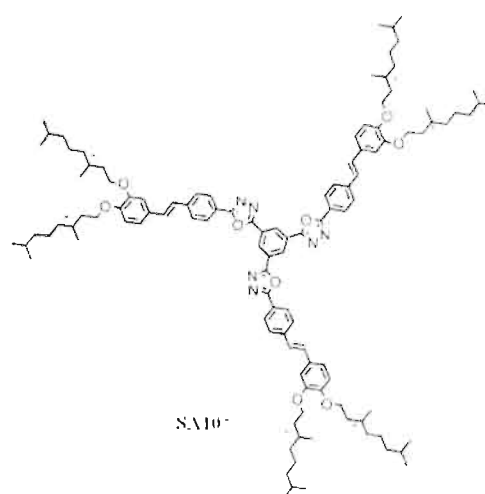
Chart 4.2

4.6. Results and Discussion

4.6.1. Synthesis of the Chiral Oxadiazole Derivative

The 1,3,4-oxadiazole derivatives (Chart 4.2) were synthesized as per Scheme 4.1. The final product was characterized by FTIR, NMR, MALDI-TOF and elemental analysis. The details of the synthetic procedure and spectral characterization data are provided in the Experimental Section 4.8.

4.6.2. Liquid Crystalline Properties

The thermotropic liquid crystalline behaviour of these materials was investigated by polarized light optical microscopy (POM), differential scanning

calorimetry (DSC) and X-ray diffractometry (XRD). Phase transitions temperatures and corresponding enthalpy values of transitions are summarized in Table 4.6.

Table 4.6. Phase transition characteristics as observed from DSC in the heating/cooling cycles.

Sample Code	Heating cycle, °C (ΔH, kJmol^{-1})	Cooling cycle, °C (ΔH, kJmol^{-1})
SA10*	Cr 160 (24.8) Col$_h$ 218 (0.82) I	I 216.56 (0.67) Col$_h$ 121.90 (21.56) Cr

Cr - Crystalline phase, Col$_h$ - Hexagonal Columnar phase, and I - Isotropic liquid.
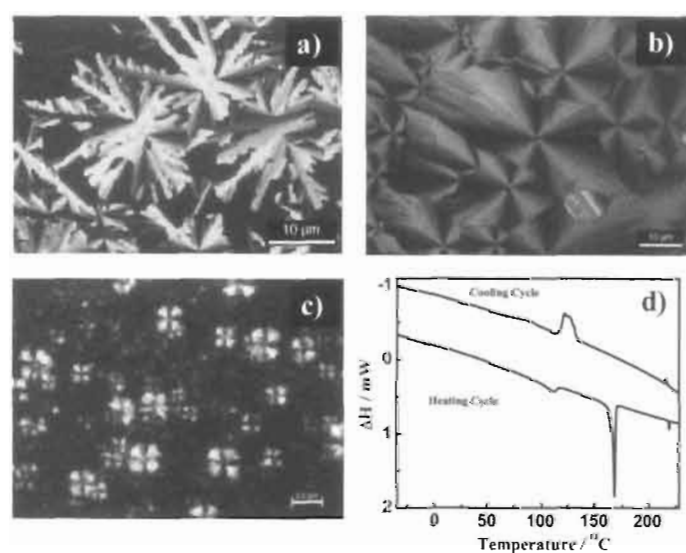
Figure 4.21. POM images of compound SA10* a) dendritic growth texture at 215 °C, b) focal conic texture at 200 °C, c) spherulite growth crystalline texture at 30 °C and d) DSC trace of compound SA16 in the cooling/heating cycle at a rate of 5 °C per minute.
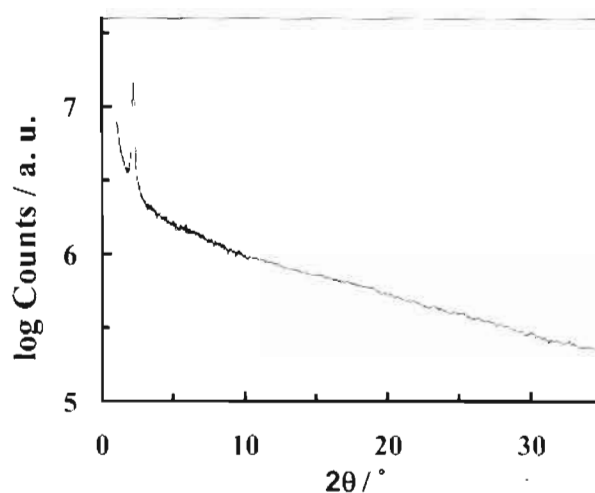
Figure 4.22. X-ray diffraction pattern of **SA10*** at 180 °C.

Enantiotropic liquid crystalline behaviour was observed for compound **SA10***, similar to that observed for the achiral octupolar 1,3,4-oxadiazole derivative. In the cooling cycle, an isotropic to hexagonal columnar transition was observed in the POM at 216 °C as indicated by the dendritic texture (Figure 4.21a) which further transformed into a focal conic texture (Figure 4.21b) under POM [Dierking 2003]. On further cooling, transition from the liquid crystalline state to a crystalline phase was observed at 122 °C as indicated by formation of a spherulite texture (Figure 4.21c). Phase transitions observed by POM were further confirmed by DSC analysis (Figure 4.21d). The X-ray diffraction pattern at 180 °C showed a strong sharp peak at low angle (with a d-spacing of 44 Å) and a diffuse peak in the wide angle region (Figure 4.22). Although qualitatively this would

suggest a lamellar structure, in conjunction with the observed dendritic texture (Figure 4.1a) is indicative of a hexagonal columnar (Col$_h$) arrangement.
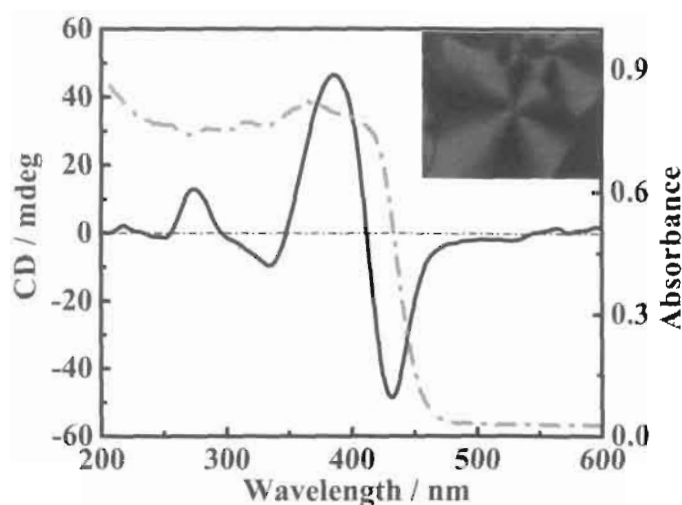
Figure 4.23. Absorption and CD spectrum recorded for a liquid crystalline glassy film obtained for **SA10*** by sudden cooling of films from the hexagonal columnar phase (200 °C). Inset showed the Polarized optical micrographs of **SA10*** in the liquid crystalline glassy state.

XRD analysis failed to give any reminiscent indication of chirality in the columnar stacks, but CD investigations on the liquid crystalline glassy film obtained by sudden cooling of films from the hexagonal columnar phase (200 °C) clearly indicated the formation of chiral columns. The POM textures (focal conic) remains unperturbed on sudden cooling of the thin film, indicating that the molecular arrangement (hexagonal columnar) observed in the high temperature phase and the glassy films at room temperature were identical in nature (Figure 4.23 Inset). A bisignated CD spectrum was observed for the glassy film,

exhibiting a negative Cotton effect at higher and a positive Cotton effect at lower wavelengths (Figure 4.23). According to the exciton chirality theory, these observations are characteristics of exciton coupled chromophores with a preferential left handed chiral orientation [Berova *et al.* 2000; Dehm *et al.* 2007]. The zero cross over point ($\lambda - 412$nm) was observed at the absorption maximum of the red shifted aggregate band of the chromophore, indicating the formation of strong exciton coupled *J*-type aggregates in the columnar stacks [Simonyi *et al.* 2003; Zsila *et al.* 2001; Spano 2009] .

4.6.3. Hierarchical Self-Assembly in Solution

The chiral derivative **SA10*** self-assembles to form well defined helical aggregates in non-polar solvents (Decane). Microscopic investigations of aggregates of **SA10*** at different concentrations revealed an intriguing two stage self-assembly process, initially forming helices which further wound around each other along the molecular axis at higher concentrations resulting in the formation of superhelix secondary structure. The morphology of the aggregates was examined by transmission electronic microscopy (TEM) and field emission scanning electron microscopy (FE-SEM). Samples were prepared by drop casting an aged (3 h) decane solutions onto the substrate and allowing the excess solvent to evaporate under mild vacuum conditions.

TEM micrographs of 10^{-6} M solution of **SA10*** in decane indicated the formation of nanofibers with the helical twist in the fibers being clearly discernible (Figure 4.24a). Clustering of helical fibers was observed in film formed from 6×10^{-6} M solution as shown in Figure 4.24b. At a concentration greater than 10^{-5} M, networks of fibers were observed. Figure 4.24c shows the networks of fibers formed in a 4×10^{-5} M solution of **SA10*** in decane. Careful analysis of the fibers showed the formation of coiled coil ropelike structures with left handed chirality, where the ropelike structures are formed by the twisting together of few helical fibers along the fiber axis. (Figure 4.24d).
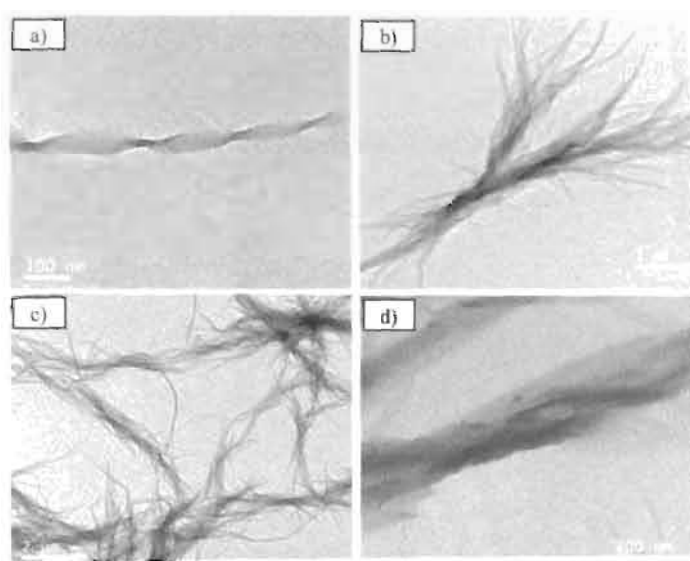
Figure 4.24. TEM images showing helical assemblies of **SA10*** drop casted from a) 10^{-6} M concentration shows individual helices, b) clusters of helices at 6×10^{-6} M, c) networks of fibers at 4×10^{-5} M and the magnified image showed the formation of a coiled coil aggregates at 4×10^{-5} M solutions in decane.
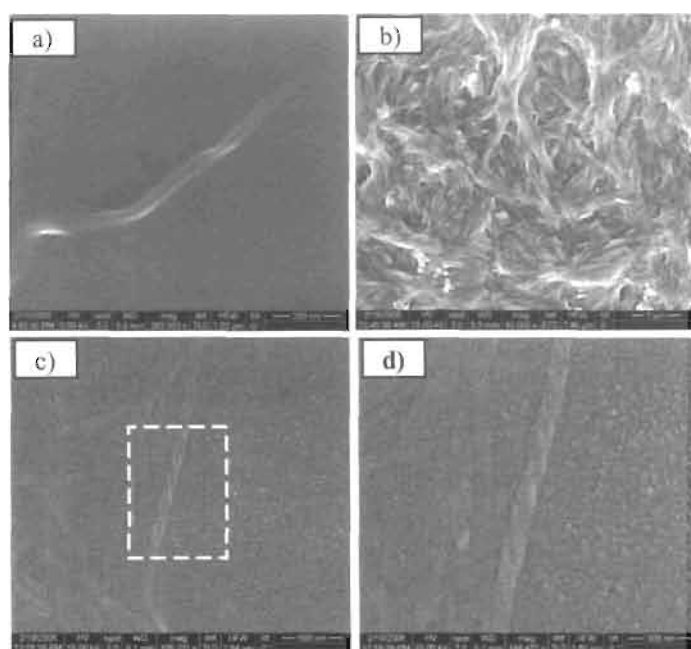
Figure 4.25. FE-SEM images of self-assembled structures of **SA10*** drop casted from a) 10^{-6} M, b) 4×10^{-5} M; c) and d) shows the magnified images of the coiled coil fibrous aggregates with left handed chirality at 4×10^{-5} M solution in decane.

Unequivocal evidence for the concentration dependent transformation of helices to coiled coil super helices and the reversal of chirality was obtained from FE-SEM experiments in samples prepared by drop casting aged (3 h) solutions on aluminum stubs. Film cast from a 10^{-6} M solution showed the individual helices (Figure 4.25a) similar to that observed by TEM, with the fibrillar morphology posessing right handed helical organization. SEM analysis of film cast from a 4×10^{-5} M solutions showed the formation of extended network of fibrous aggregates (Figure 4.25b). Figure 4.25c shows a typical image of the fibrous

aggregates in film formed from 4×10^{-5} M solution, which clearly indicates the formation of the coiled coil aggregates. The magnified image of the fibrous aggregates (Figure 4.25d) showed that the coiled coil rope like aggregate possess left handed chirality.

Investigations of the morphology of the aggregates in film formed from decane solution of **SA10*** of increasing concentration provided the evidence for the hierarchical self-assembly leading from helical tapes with right handed chirality and super coiled helical structure with left handed chirality at higher concentrations. It is important to note that the chirality in these aggregates is getting transmitted from the alkyl periphery of the molecule to the primary structure and to the secondary structure through molecular assembly. It has been reported earlier that helical fibers can give rise to super coiled helical structures with opposite helicity through a stepwise hierarchical self-assembly process [Lohr *et al.* 2005; Engelkamp *et al.* 1999; Sommerdijk *et al.* 1998].

4.6.4. Photophysical Properties

4.6.4.1. Photophysical Properties in Solution

Table 4.7 summarizes the absorption and fluorescence properties of the chiral octupolar 1,3,4-oxadiazole derivative (**SA10***) in different solvents. It may be noted that in a particular solvent, introducing chirality to alkoxy group did not bring about substantial changes in its absorption or

emission properties in comparison with the achiral derivatives, which was as expected. The absorption and fluorescence spectra of **SA10*** are shown in Figure 4.26. Whereas the absorption spectrum (λ_{max} ~370 nm) was found to be practically independent of the nature of the solvent, a bathochromic shift in the fluorescence band was observed with increase in solvent polarity. The fluorescence maximum was observed to shift from ~448 nm in toluene to ~500 nm in benzonitrile. The fluorescence decay of dilute solutions of **SA10*** were mono-exponential in the solvents investigated (Table 4.7) with a slight increase in lifetime being observed from non-polar to polar solvents.
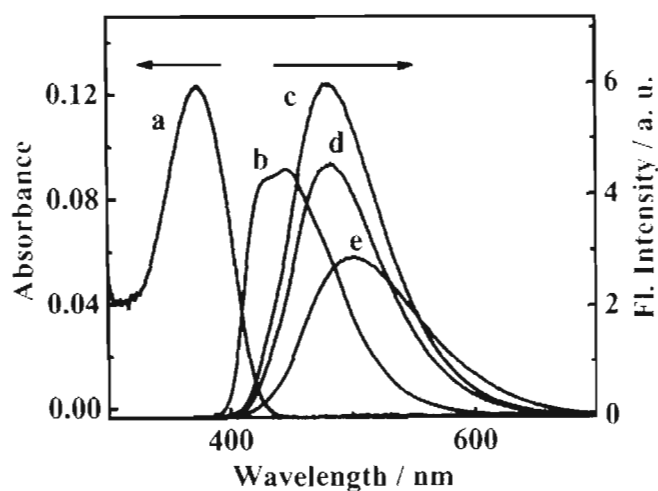
Figure 4.26. Absorption and fluorescence spectra of **SA10***; (a) absorption spectrum in benzonitrile, fluorescence spectra in (b) toluene, (c) tetrahydrofuran, (d) dichloromethane and (e) benzonitrile (Excitation: 360 nm).

Table 4.7. Absorption, emission and fluorescence lifetime characteristics of compound **SA10***.

SA12	Abs. λ_{max} (nm)	Em. λ_{max} (nm)	Φ_f	τ (ns)	χ^2
Toluene	374	448	0.45	0.76	1.02
DCM	372	483	0.92	1.58	1.07
THF	371	480	0.99	1.66	1.08
BCN	374	502	0.44	1.99	1.02

4.6.4.2. Photophysical Properties in the Aggregates

UV/Vis absorption and fluorescence spectroscopy. Aggregation behaviour of the molecule in decane solution was studied using UV-visible and fluorescence spectroscopy. Figure 4.27a shows changes in the absorption spectra as a function of concentration. A 10^{-7} M solution of **SA10*** in decane showed a UV-vis absorption spectrum typical for that of molecularly dissolved species with an absorption maximum at 370 nm. With increasing concentration, a clear broadening in the absorption spectrum and the appearance of new blue and red shifted bands compared to that of the monomer band could be observed (Figure 4.27b).
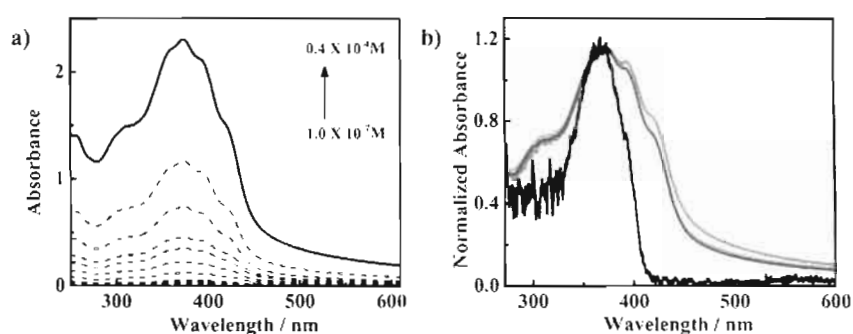
Figure 4.27. a) Concentration dependent changes in absorption spectra of **SA10*** and b) normalized absorption spectra at 10^{-7}M (black line), 10^{-6} M (blue line), 10^{-5}M (green line) and 4 x 10^{-5}M (red Line) solutions in decane.

Aggregation of molecules also brought about significant changes in the fluorescence, as shown in Figure 4.28. In a 10^{-7} M solution of **SA10*** the emission occurred solely from the molecularly dissolved species as indicated by the structured band with an emission maximum at 407 nm with vibronic progressions at 456, 433 nm. At higher concentrations, a new peak at about 500 nm was observed whose intensity relative to that of the monomer emission band increased significantly with increasing concentration. The formation of the new band which was considerably red shifted compared to that of the molecularly dissolved species, indicated the formation of exciton coupled aggregates.
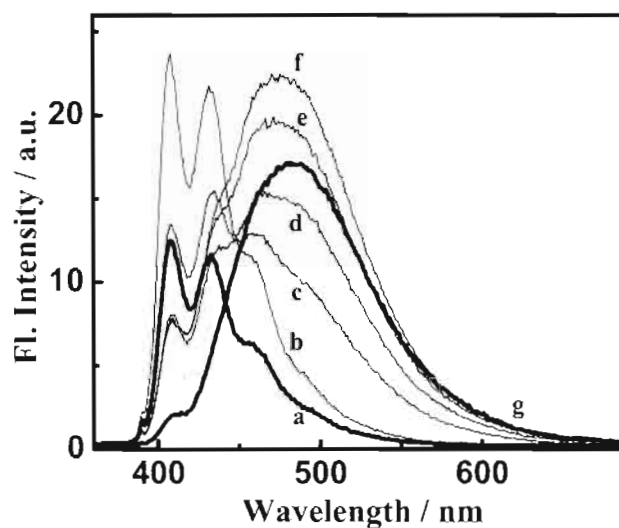
Figure 4.28. Concentration dependent changes in emission (λex = 350 nm) of **SA10*** in a) 2 x 10⁻⁷ M, b) 4 x 10⁻⁷ M, c) 4 x 10⁻⁶ M, d) 6 x 10⁻⁶ M, e) 8 x 10⁻⁶ M, f) 10⁻⁵ M, g) 4 x 10⁻⁵ M solutions in decane.
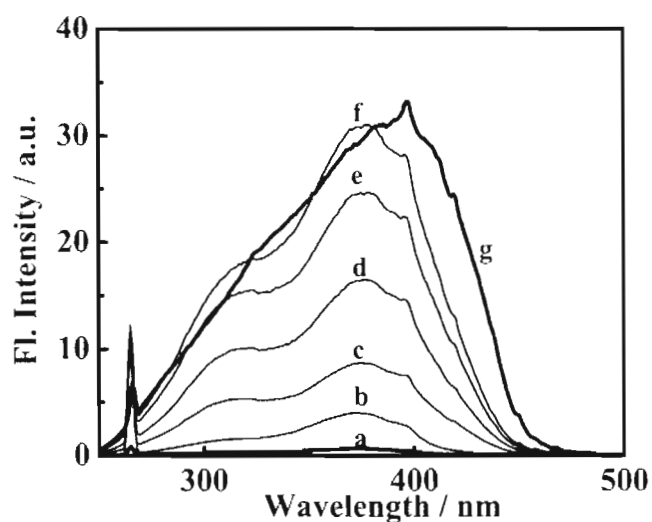
Figure 4.29. Concentration dependent changes in excitation spectra (λ_{cm} = 500 nm) of **SA10*** in decane at concentrations; a = 2×10^{-7} M, b = 4×10^{-7} M, c = 2×10^{-6} M, d = 4×10^{-6} M, e = 6×10^{-6} M, f = 8×10^{-6} M, g = 4×10^{-5} M.
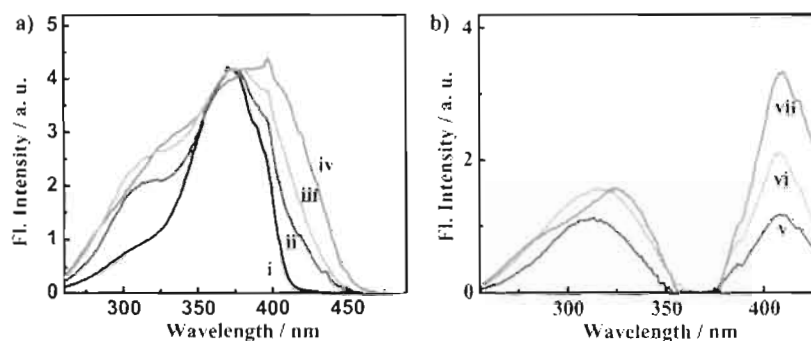
Figure 4.30. a)Normalized excitation spectra of i) 10^{-7}M ii) 10^{-6} M. iii) 10^{-5} M, iv) 4×10^{-5} M solutions of **SA10*** in decane. b) difference spectra obtained by subtracting the normalized excitation spectra of v) 10^{-7} M from 10^{-6} M. vi) 10^{-7} M from 10^{-5} M and vii) 10^{-7} M from 10^{-5} M solutions (emission monitored at 500 nm).

The concentration dependent change in the fluorescence excitation spectra of **SA10*** is shown in Figure 4.29 and this was consistent with the change observed in the UV/vis absorption spectra at lower concentrations (10^{-7} M). the excitation spectrum indicated a main peak at 370 nm which could be attributed to the molecularly dissolved species. With increasing concentration, a significant broadening of the spectrum was observed indicating formation of aggregates. The nature of the aggregates formed could be clearly visualized by subtracting the contribution of the monomer band (obtained from excitation spectra measured in 10^{-7} M decane solutions where molecule exists mainly in the molecularly dissolved state) from the excitation spectra obtained at the higher concentrations. Figure 4.30b shows the spectra obtained by subtracting the contribution of the monomer band from spectra normalized at 370 nm (Figure 4.30a) for 10^{-6} M,

10^{-5}M and 4 x10^{-5} M solutions of **SA10*** in decane. Two new bands were observed, one in the blue and the other in the red shifted region compared to that of the monomer, which is consistent with the concentration dependent changes observed in the UV/vis absorption spectra.

Circular Dichroism Spectroscopy. CD spectra of 10^{-7}M solution of **SA10*** indicated a very weak bisignated CD effect with a negative Cotton effect at short and a positive Cotton effect at longer wavelengths (Figure 4.31a). The CD intensity increased with increase in concentration up to 2 x 10^{-6} M solution (Figure 4.31a). Upon further increase in concentration, a total inversion of the CD spectra was observed, with a positive Cotton effect at short and a negative Cotton effect at longer wavelengths (Figure 4.31b). A well-defined isodichroic point was observed at about 360 nm almost near to the zero cross over point. Figure 4.31c and 4.31d showed a near mirror image spectra observed at lower and higher concentration with changes in the CD intensity. This is in accordance with the observed changes in the morphology, where with increasing concentration an inversion in chirality was observed due to the formation of coiled coil aggregates in TEM and SEM investigations (Figure 4.24 &4.25).
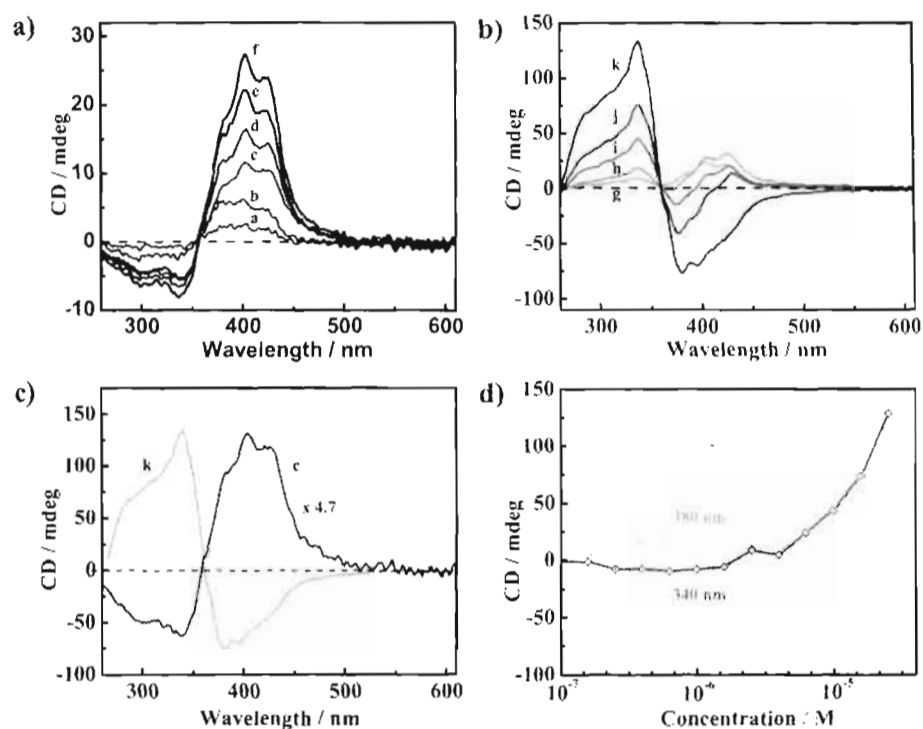
Figure 4.31 Spectra a). b) depicts the changes in CD spectra with concentration of **SA10*** a) 10^{-7} M, b) 2×10^{-7} M, c) 4×10^{-7}M, d) 6×10^{-7}M, e) 10^{-6} M, f) 2×10^{-6} M, g) 4×10^{-6} M, h) 6×10^{-6}M, i) 10^{-5} M. j) 2×10^{-5} M and k) 4×10^{-5}M solutions in decane, c) normalized CD spectra of 4×10^{-5}M and 4×10^{-7}M solutions in decane. showed the near mirror image relationship. d) plots of variation in CD intensity monitored at 380 nm and 340 nm against the concentrations of **SA10***solution in decane.

The UV/vis absorption and excitation spectra indicated the broadening in the main absorption band along with the appearance of blue shifted and red shifted shoulders with increasing concentrations. Even though the blue- and red-shifted features of the absorption spectra are generally assigned for *H* or *J* type aggregates, such spectral features are also observed in the chiral aggregates due to

the twisted stacking of molecules on one on top of the other [Westenhoff *et al.* 2006; Schenning *et al.*2002; Lohr *et al.* 2005]. The observed circular dichroism effects and the fact that the self-assembled structures exhibited supramolecular chirality, suggests that these properties arise out of the formation of twisted conformation of the C_3 symmetric molecules in the chiral stacks as addressed by SEM and TEM. The blue shifted zero cross over point in the CD spectra compared to that of monomer absorption is expected on preferential formation of *H*-aggregates. These observations are fully consistent with the spectral observations reported earlier for linear oligomeric thiophene and phyneylenevinylene derivatives [Westenhoff *et al.* 2006; Schenning *et al.*2002; Lohr *et al.* 2005]. The spectral features of the UV/Vis absorption and fluorescence excitation spectra remained almost unchanged in the chirality inversion regime as observed in the CD spectra (except for an increase in intensity), indicating the mode of chromophore packing in the helical aggregates at lower concentrations and the coiled coil aggregates at higher concentrations were nearly the same.

4.7. Conclusion

We have investigated the influence of peripheral chiral alkyl chains on the liquid crystalline and the self-assembling behaviour of trigonal octupolar oxadiazole derivative (**SA10***). This derivative exhibited discotic liquid crystalline phase with a helical ordering as observed by CD investigations at elevated temperatures and can be super cooled into liquid crystalline glassy films on sudden

cooling from the LC phase. Investigation of the morphology of the aggregates in decane solutions showed a unique aggregation behaviour leading to the formation of helical fibers at lower concentrations with right handed helicity. These helices further wound around their molecular axes resulting in the formation of a superhelix (secondary structure) at higher concentrations exhibited left handed chirality in decane solvent. The formation of the helical primary structure and superhelix secondary structure and the associated reversal of chirality in the supramolecular level could be well monitored by microscopic techniques such as TEM and SEM as well as by circular dichroism (CD) spectroscopy.

4.8. Experimental Section

4.8.1. Synthesis of Trigonal Octupolar 1,3,4-Oxadiazole Derivatives (SA1, SA4, SA6, SA8, SA12, SA16 and SA10*)

The synthetic route adopted for the synthesis of these derivatives is shown in scheme 4.1.

General Procedure for the Synthesis of 1,3,4-Oxadiazole Derivatives (SA1, SA4, SA6, SA8, SA12, SA16 and SA10*)

Benzene-1,3,5-tricarbonyl trichloride (1 equiv.) was taken in a dry two necked R.B. under argon atmosphere, dry pyridine (5mL) added and stirred for two minutes. Corresponding tetrazole derivative (3.9 equiv.) was dissolved in dry pyridine (15 mL) and was added to the above acid chloride drop wise with constant stirring. The reaction mixture was then refluxed at 115 °C for 12 h and

was poured into ice cold water and washed with 2N HCl to remove pyridine. The precipitate was washed with water, filtered and extracted with dichloromethane. The compounds were purified by column chromatography using silica as stationary phase and gradient elution with a mixture of ethyl acetate-hexane as the eluent to yield the pure product. The compounds were then further purified by dissolving in minimum amount of dichloromethane and precipitated using methanol to give pure product.

1,3,5-tris(5-(4-(3,4-dimethoxystyryl)phenyl)-1,3,4-oxadiazol-2-yl) benzene (SA1)

Yield - 56 %; m.p: >260 °C (decomposed); IR υmax (KBr): 712, 959, 1026, 1252, 1269, 1516, 1597, 2837, 2951, 2999 cm^{-1}; ^{1}H NMR (500 MHz, CDCl$_3$, TMS) δ: 8.991 (s, 3H, aromatic), 8.093-8.077 (d, J = 8 Hz, 6H, aromatic), 7.596-7.579 (d, J = 8.5 Hz, 6H, aromatic), 7.116-7.084 (d, J = 16 Hz,

SA1

3H, allylic), 7.034 (s, 3H, aromatic), 6.999-6.982 (d, J = 8.5 Hz, 3H, aromatic), 6.918- 6.886 (d, J = 16 Hz, 3H, allylic), 6.804-6.787 (d, J = 8.5 Hz, 6H, aromatic), 3.984 (s, 9H, -OCH$_3$) 3.919 (s, 9H, -OCH$_3$) ppm; ^{13}C NMR (125 MHz, CDCl3, TMS) δ: 165.27, 162.48, 162.44, 149.90, 149.77, 149.37, 149.24, 141.52, 141.47, 131.20, 131.15, 129.69, 129.55, 127.50, 126.70, 126.04, 125.95, 124.96,
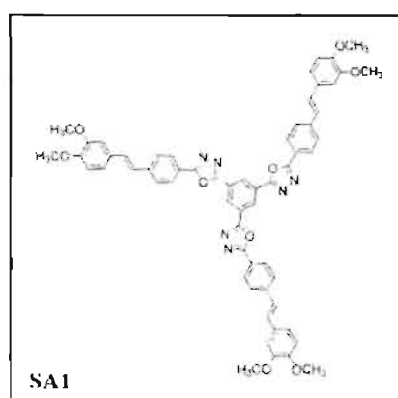
124.86, 121.42, 121.33, 120.62, 113.64, 113.35, 111.88, 111.51, 69.48, 69.35 ppm; MALDI-TOF: m/z calcd for $C_{35}H_{51}NO_2$ $C_{60}H_{48}N_6O_9$, 996.35, found: 996.06.

1,3,5-tris(5-(4-(3,4-dibutoxystyryl)phenyl)-1,3,4-oxadiazol-2-yl)benzene (SA4)

Yield - 58 % ; m.p: 210 °C: IR ʋmax (KBr): 961, 1182, 1230, 1249, 1492, 1510, 2870, 2934, 2955 cm⁻¹; ¹H NMR (500 MHz, CDCl3, TMS) δ: 8.909 (s, 3H, aromatic), 8.093-8.077 (d, J - 8 Hz, 6H, aromatic), 7.596-7.579 (d, J = 8.5 Hz, 6H, aromatic), 7.116-7.084 (d, J = 16 Hz, 3H,

SA4

allylic), 7.034 (s, 3H, aromatic), 6.999-6.982 (d, J = 8.5 Hz, 3H, aromatic), 6.918-6.886 (d, J = 16 Hz, 3H, allylic), 6.804-6.787 (d, J = 8.5 Hz, 3H, aromatic), 4.08-4.05 (t, 6H, -OCH2-), 4.03-4.00 (t, 6H, -OCH₂-), 1.87-1.27 (m, 24H, -CH₂-), 0.90-0.86 (m, 18H) ppm; ¹³C NMR (125 MHz, CDCl3, TMS) δ: 164.38, 161.54, 148.77, 148.25, 140.57, 130.24, 128.62, 126.54, 125.75, 125.12, 123.99, 120.38, 119.60, 112.44, 110.58, 30.38, 30.28, 18.26, 18.22, 12.92, 12.88 ppm; MALDI-TOF: m/z calcd for $C_{78}H_{84}N_6O_9$, 1248.63 found: 1249.87.

1,3,5-tris(5-(4-(3,4-bis(hexyloxy)styryl)phenyl)-1,3,4-oxadiazol-2-yl)benzene (SA6)

Yield - 69 %; mp: 190 °C; IR (KBr) v_{max}: 960, 1010, 1138, 1250, 1267, 1510, 2860, 2931, 2953 cm⁻¹; ¹H NMR (300 MHz, CDCl₃, TMS) : δ 8.93 (s, 3H,
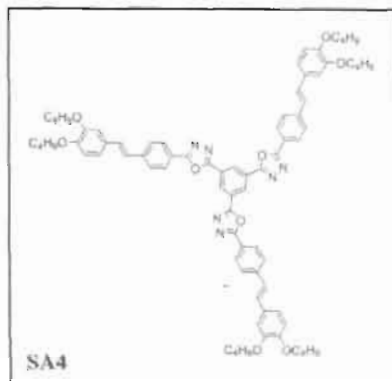
aromatic), 8.13-8.12 (d, *J* = 7.5 Hz, 6H, aromatic), 7.63-7.61 (d, *J* = 7.5 Hz, 6H, aromatic), 7.15-7.12 (d, *J* = 16.5 Hz, 3H, allylic), 7.07 (s, 3H, aromatic), 7.03-7.02 (d, *J* = 8 Hz, 3H, aromatic), 6.95- 6.92 (d, *J* = 16.5 Hz, 3H, allylic), 6.84-6.82 (d, *J* = 8.5 Hz, 3H, aromatic), 4.05-4.03 (t, 6H, -
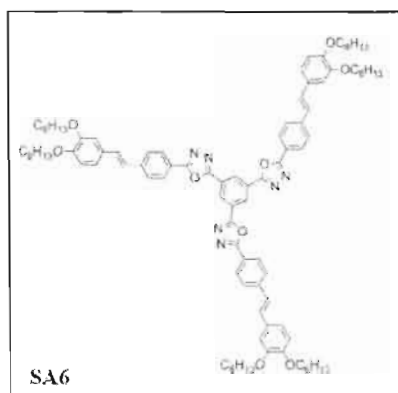
OCH$_2$-), 3.97-3.92 (t, 6H, -OCH$_2$-), 1.84-1.26 (m, 48H, -CH2-). 0.89-0.86 (m, 18H, -CH3) ppm; ^{13}C NMR (75 MHz, CDCl$_3$, TMS): δ 165.25, 162.45, 149.75, 149.22, 141.47, 131.15, 129.55, 127.49, 126.69, 125.96, 124.87, 121.33, 120.60, 113.32, 111.45,31.66, 31.64, 29.33, 29.24, 25.76, 25.72, 22.66, 22.64, 14.08, 14.06 ppm; MALDI-TOF: m/z calcd for C$_{90}$H$_{108}$N$_6$O$_9$, 1416.82 found: 1417.65.

1,3,5-tris(5-(4-(3,4-bis(octyloxy)styryl)phenyl)-1,3,4-oxadiazol-2-yl) benzene (SA8)

Yield - 68 %; mp: 194 °C; IR (KBr) ν$_{max}$: 2926, 2852, 1597, 1510, 1467, 1427, 1267, 1249, 1138, 1022, 1010, 960, 842, 826, 783, 711, 621, 599, 520 cm^{-1}; ^{1}H NMR (500 MHz, CDCl$_3$, TMS) δ: 9.011 (s, 3H, aromatic), 8.185-8.168 (d, *J* = 7.5 Hz, 6H, aromatic), 7.675-7.659 (d, *J* = 8 Hz, 6H,
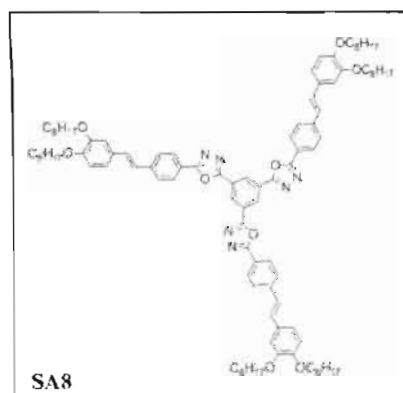
aromatic), 7.199-7.167 (d, J = 16 Hz, 3H, allylic), 7.105 (s, 3H, aromatic), 7.075-7.058 (d, J = 8.5 Hz, 3H, aromatic), 7.003- 6.971 (d, J = 16 Hz, 3H, allylic), 6.876-6.860 (d, J = 8 Hz, 3H, aromatic), 4.079-4.052 (t, 6H, -OCH_2-), 4.030-4.003 (t, 6H, -OCH_2-), 1.875-1.109 (m, 72H, -CH_2-), 0.911-0.883 (m, 18H, -CH_3) ppm; ^{13}C NMR (125 MHz, CDCl3, TMS) δ:165.27, 162.48, 162.44, 149.90, 149.77, 149.37, 149.24, 141.52, 141.47, 131.20, 131.15, 129.69, 129.55, 127.50, 126.70, 126.04,125.95, 124.96, 124.86, 121.42, 121.33, 120.62, 113.64, 113.35, 111.88, 111.51, 69.48, 69.35, 69.26, 69.15, 31.86, 29.43, 29.33, 29.31, 26.01, 26.06, 22.71, 22.67, 14.13, 14.07 ppm; MALDI-TOF MS: m/z calcd for $C_{102}H_{132}N_6O_9$, 1586.17, found: 1587.35 [M+H$^+$].

1,3,5-tris(5-(4-(3,4-bis(dodecyloxy)styryl)phenyl)-1,3,4-oxadiazol-2-yl)benzene (SA12)

Yield - 65 %; m.p: 228 °C; IR vmax (KBr): 518.85, 599.86, 617.22, 677.01, 711.73, 721.38, 740.67, 785.03, 798.53, 823.60, 842.89, 862.18, 894.97, 914.26, 960.55, 1010.70, 1068.56, 1083.99, 1138.00, 1168.86, 1182.36, 1228.66, 1249.87, 1267.23, 1305.81, 1336.67,

SA12

1377.17, 1427.32, 1456.26, 1467.83, 1494.83, 1510.26, 1546.91, 1573.91, 1597.06, 2852.72, 2922.16, 3024.38 cm-1; 1H NMR (500 MHz, CDCl3, TMS) δ:
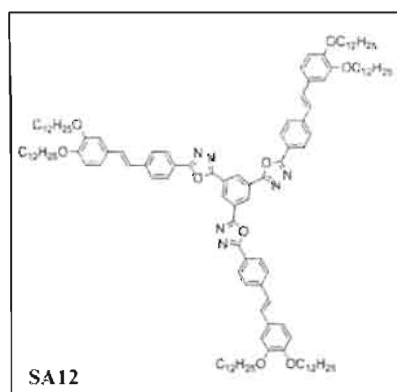
8.93 (s, 3H, aromatic), 8.13-8.12 (d, J = 7.5 Hz, 6H, aromatic), 7.63-7.61 (d, J =

7.5 Hz, 6H, aromatic), 7.15-7.12 (d, J = 16.5 Hz, 3H, allylic), 7.07 (s, 3H,

aromatic), 7.03-7.02 (d, J = 8 Hz, 3H, aromatic), 6.95- 6.92 (d, J = 16.5 Hz, 3H,

allylic), 6.84-6.82 (d, J = 8.5 Hz, 3H, aromatic), 4.05-4.03 (t, 6H, -OCH$_2$-), 3.97-

3.40 (t, 6H, -OCH$_2$-), 1.84-1.26 (m, 120H, -CH$_2$-), 0.89-0.86 (m, 18H, -CH$_3$) ppm;

^{13}C NMR (125 MHz, CDCl$_3$, TMS) δ:165.33, 162.52, 149.87, 149.35, 141.56,

131.24, 129.68, 127.53, 126.88, 126.73, 126.09, 124.98, 121.42, 120.62, 113.58,

111.78, 69.44, 69.23, 31.93, 29.67, 29.47, 29.37, 29.32, 26.10, 26.06, 22.68,14.09

ppm; MALDI-TOF: [M+H]+ m/z calcd for C$_{126}$H$_{180}$N$_6$O$_9$, 1922.81 found: 1924.8.

1,3,5-tris(5-(4-(3,4-bis(hexadecyloxy)styryl)phenyl)-1,3,4-oxadiazol-2-yl) benzene (SA16)

Yield - 63 % ; m.p: 234 °C; IR v_{max} (KBr):

522.71, 607.58, 711.73, 783.10, 842.89,

960.55, 1010.70, 1138.00, 1226.73,

1249.87, 1267.23, 1307.74, 1386.82,

1427.32, 1467.83, 1510.26, 1597.06,

2850.79, 2920.23 cm^{-1}; ^{1}H NMR (500

MHz, CDCl$_3$, TMS) δ: 9.02 (s, 3H,

aromatic), 8.19-8.17 (d, J = 8 Hz, 6H, aromatic), 7.68-7.66 (d, J = 8 Hz, 6H,

aromatic), 7.20-7.17 (d, J = 16 Hz, 3H, allylic), 7.11 (s, 3H, aromatic), 7.07-7.06

(d, J = 8 Hz, 3H, aromatic), 7.00- 6.97 (d, J = 16.5 Hz, 3H, allylic), 6.87-6.86 (d,
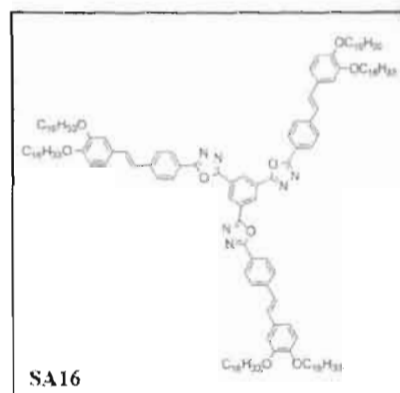
J = 8 Hz, 3H, aromatic), 4.08-4.05 (t, 6H, -OCH$_2$-), 4.03-4.00 (t, 6H, -OCH$_2$-), 1.87-1.27 (m, 168H, -CH$_2$-), 0.90-0.86 (m, 18H, CH$_3$) ppm; ^{13}C NMR (125 MHz, CDCl$_3$, TMS) δ: 165.46, 162.62, 149.88, 149.36, 141.66, 131.34, 129.72, 127.59, 127.06, 126.80, 126.24, 125.08, 124.98, 121.49, 120.64, 113.60, 111.77, 69.44, 69.25, 31.93, 29.73,29.68, 29.49, 29.38, 29.31, 26.10, 26.06, 22.69,14.11 ppm; MALDI-TOF: [M+H]˙ m/z calcd for C$_{150}$H$_{228}$N$_6$O$_9$, 2258.45 found: 2259.8;

1,3,5-tris(5-(4-(3,4-bis(3,7-dimethyloctyloxy)styryl)phenyl)-1,3,4-oxadiazol-2-yl)benzene (SA10*)

Yield: 72%; m.p: 228 °C; IR vmax (KBr): 518.85, 617.22, 711.73, 740.67, 960.55, 1138.00, 1249.87, 1267.23, 1382.96, 1427.32, 1469.76, 1514.12, 1595.13, 2926.01, 2953.02 cm-1; 1H NMR (500 MHz, CDCl3, TMS) δ: 8.948 (s, 3H, aromatic), 8.153-8.136 (d, J = 8.5 Hz, 6H,

SA10*
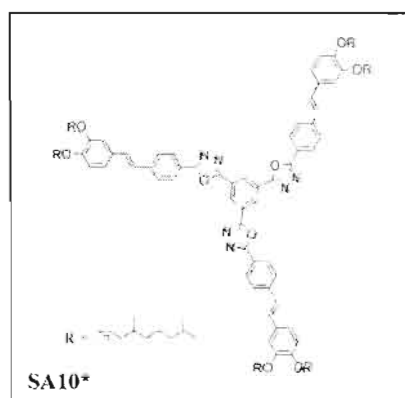
aromatic), 7.649-7.632 (d, J = 8.5 Hz, 6H, aromatic), 7.174-7.142 (d, J = 16 Hz, 3H, allylic), 7.090 (s, 3H, aromatic), 7.054-7.037 (d, J = 8.5 Hz, 3H, aromatic), 6.975- 6.943 (d, J = 16 Hz, 3H, allylic), 6.864-6.847 (d, J = 8.5 Hz, 3H, aromatic), 4.099-4.034 (t, 12H, -OCH2-), 1.902-1.156 (m, 54H, -CH2-), 0. 993-0.969 (m, 18H, -CH3), 0.892-0.875 (m, 36H, -CH$_3$) ppm; ^{13}C NMR (125 MHz, CDCl3, TMS) δ:165.38, 162.56, 149.78, 149.26, 141.57, 131.27, 129.60, 127.56, 126.96,

126.76, 126.12, 124.98, 121.42, 120.59, 113.29, 111.40, 67.65,67.51 39.29,39.28, 37.41, 36.31, 36.21, 29.96, 28.02, 28.00, 24.77, 24.74, 22.74, 22.64, 22.63, 19.76 ppm; MALDI-TOF MS: m/z calcd for $C_{114}H_{150}N_6O_9$, 1747.15, found: 1748.19 [M+H'].

Bibliography

Abraham, S.; Mallia, V. A.; Ratheesh, K. V.; Tamaoki, N.; Das, S. 'Reversible thermal and photochemical switching of liquid crystalline phases and luminescence in diphenylbutadiene-based mesogenic dimers' *J. Am. Chem. Soc.* 128 (**2006**) 7692.

Abrash, S.; Repinec, S.; Hochstrasser, R. M. 'The viscosity dependence and reaction coordinate for isomerization of *cis*-stilbene' *J. Chem. Phys.* 93 (**1990**) 1041.

Adam, P.; Schuhmacher, J.; Simmerer, L.; Haussling, K.; Siemensmeyer, K.; Etzbach, H.; Ringsdorf, H.; Haarer, D. 'Fast photoconduction in the highly ordered columnar phase of a discotic liquid crystal' *Nature* 371(**1994**) 141.

Ajayaghosh, A.; George, S. J. 'First phenylenevinylene based organogels: Self-assembled nanostructures via cooperative hydrogen bonding and π-stacking' *J. Am. Chem. Soc.* 123 (**2001**) 5148.

Ajayaghosh, A.; Praveen, V. K. 'π-organogels of self-assembled p-phenylenevinylenes: Soft materials with distinct size, shape, and functions' *Acc. Chem. Res.* 40 (**2007**) 644.

Ajayaghosh, A.; Praveen, V. K.; Vijayakumar, C. 'Organogels as scaffolds for excitation energy transfer and light harvesting' *Chem. Soc. Rev.* 37 (**2008**) 109.

Ajayaghosh, A.; Praveen, V. K.; Vijayakumar, C.; George, S. J. 'Organogels as scaffolds for excitation energy transfer and light harvesting' *Chem. Soc. Rev.* 37 **(2008)** 109.

Alvarez, L.; Barbera, J.; Puig, L.; Romero, P.; Serrano, J. L.; Sierra, T. 'Supramolecular chirality of columnar mesophases consisting of H-bonded complexes of melamine and polycatenar benzoic acids' *J. Mater. Chem.* 16 **(2006)** 3768.

Alves, H.; Molinari, A. S.; Xie, H.; Morpurgo, A. F. 'Metallic conduction at organic charge-transfer interfaces' *Nature Mater.* 7 **(2008)** 574.

Anthony, J. E.; Gierschner, J.; Landis, C. A.; Parkin, S. R.; Shermana, J. B.; Bakus, R. C. 'A new functionalization strategy for pentacene' *Chem. Commun.* **(2007)** 4746.

Antony, J. E. 'Functionalized acenes and heteroacenes for organic electronics' *Chem. Rev.* 106 **(2006)** 5028.

Babu, S. S.; Praveen, V. K.; Prasanthkumar, S.; Ajayaghosh, A. 'Self-assembly of oligo(para-phenylenevinylene)s through arene-perfluoroarene interactions: π gels with longitudinally controlled fiber growth and supramolecular exciplex-mediated enhanced emission' *Chem. Eur. J.* 14 **(2008)** 9577

Bao, C. Y.; Lu, R.; Jin, M.; Xue, P. C.; Tan, C. H.; Liu, G. F.; Zhao, Y. Y. 'Helical stacking tuned by alkoxy side chains in π-conjugated triphenylbenzene discotic derivatives' *Chem. Eur. J.* 12 **(2006)** 3287.

Bayer, A.; Hubner, J.; Kopitzke, J.; Oestreich, M.; Ruhle, W.; Wendorff, J. H. 'Time-resolved fluorescence in 3-dimensional ordered columnar discotic materials' *J. Phys. Chem.* B 105 **(2001)** 4596.

Berova, N.; Nakanishi, K.; Woody, R. W. Circular dichroism: Principles and applications; *Wiley-VCH*: New York, **2000**.

Bettenhausen, J.; Strohriegl, P. 'Efficient synthesis of starburst oxadiazole compounds' *Adv. Mater.* 8 **(1996)** 507.

Boden, N.; Bushby, R. J.; Clements, J. 'Mechanism of quasi-one-dimensional electronic conductivity in discotic liquid crystals' *J. Chem. Phys.* 98 **(1993)** 5920.

Brizard, A.; Oda, R.; Huc, I. 'Chirality effects in self-assembled fibrillar networks' *Top. Curr. Chem.* 256 **(2005)** 167.

Brocklehurst, B.; Bull, D. C.; Evans, M.; Scott, P. M.; Stanney, G. 'Excimer fluorescence of trans-stilbene and diphenylacetylene' *J. Am. Chem. Soc.* 97 **(1975)** 2977.

Brunsveld, L.; Folmer, B. J. B.; Meijer, E. W.; Sijbesma, R. P. 'Supramolecular polymers' *Chem. Rev.* 101 **(2001)** 4071.

Burroughes, J. H.; Bradley, D. D. C.; Brown, A. R.; Marks, R. N.; Mackay, K.; Friend, R. H.; Burn, P. L.; Holmes, A. B. 'Light-emitting diodes based on conjugated polymers' *Nature* 347(**1990**), 359.

Bushby, R. J.; Lozman, O. R. 'Photoconducting liquid crystals' *Curr. Opin. Solid State Mater. Sci.* 6 (**2002**) 569.

Caldwell, R. A.; Mizuno, K.; Hansen, P. E.; Vo, L. P.; Frentrup, M.; Ho, C. D. 'Photochemistry of the phenanthrene-stilbene system. Cycloaddition and singlet-sensitized isomerization' *J. Am. Chem. Soc.* 103 (**1981**) 7263.

Camerel, F.; Bonardi, L.; Schmutz, M.; Ziessel, R. 'Highly luminescent gels and mesogens based on elaborated borondipyrromethenes' *J. Am. Chem. Soc.* 128 (**2006**) 4548.

Cao, Y.; Smith, P.; Heeger, A. J. 'Counter ion induced processibility of conducting polyaniline and of conducting polyblends of polyaniline in bulk polymers' *Synth. Met.* 48 (**1992**) 91.

Cardinaels, T.; Ramaekers, J.; Nockemann, P.; Driesen, K.; Hecke, K. V.; Meervelt, L.V.; Wang, G.; De Feyter, S.; Iglesias, E. F.; Guillon, D.; Donnio, B.; Binnemans, K.; Bruce, D. W. 'Rigid tetracatenar liquid crystals derived from 1,10-phenanthroline' *Soft Matter*, 4 (**2008**) 2172.

Chandrasekhar, S. 'Liquid crystals' *Cambridge University Press*, **1992**.

Chandrasekhar, S.; Sadashiva, B. K.; Suresh, K. A. 'Liquid crystals of disc-like molecules' *Pramana* 9 (**1977**) 471.

Chandrasekharan, N.; Kelly, L. A. 'A dual fluorescence temperature sensor based on perylene/exciplex interconversion' *J. Am. Chem. Soc. 123* (**2001**) 9898.

Chang, Y. -C.; Chen, Y. -D.; Chen, C. -H.; Wen, Y. -S.; Lin, J. T.; Chen, H. -Y.;
Kuo, M. -Y.; Chao. I. 'Crystal engineering for π -π stacking via interaction
between electron-rich and electron-deficient heteroaromatics' *J. Org.*
Chem. *73* **(2008)** 4608.

Che, Y.; Datar, A. X. Y.; Naddo, T.; Zhao, J.; Zang, L. Enhancing one-
dimensional charge transport through cofacial π-electronic delocalization:
Conductivity improvement for organic nanobelts. *J. Am. Chem. Soc.* 129
(2007) 6354.

Chen, S. H.; Chen, H. M. P.; Geng, Y.; Stephen, D. J.; Marshall, K. L.; Blanton. T.
N. 'Novel Glassy Nematic Liquid Crystals for Non-destructive Rewritable
Optical Memory and Photonic Switching' *Adv. Mater.* 15 **(2003)** 1061.

Chen, Z.; Baumeister, U.; Tschierske, C.; Wurthner, F. 'Effect of core twisting on
self-assembly and optical properties of perylene bisimide dyes in solution
and columnar liquid crystalline phases' *Chem. Eur. J.* 13 **(2007)** 450.

Chen, Z.; Lohr, A.; Saha-Möller, C. R.; Würthner, F. 'Self-assembled π-stacks of
functional dyes in solution: Structural and thermodynamic features' *Chem.*
Soc. Rev. 38 **(2009)** 564.

Chen, Z.; Stepanenko, V.; Dehm, V.; Prins, P.; Siebbeles, L. D. A.; Seibt, J.;
Marquetand, P.; Engel, V.; Wurthner, F. 'Photoluminescence and
conductivity of self-assembled π-π stacks of perylene bisimide dyes' *Chem.*
Eur. J. 13 **(2007)** 436.

Chiang, C. K.; Druy, M. A.; Gau, S. C.; Heeger, A. J.; E. J. Louis, E. J.; MacDiarmid, A. G.; Park, Y. W.; Shirakawa. H. 'Synthesis of highly conducting films of derivatives of polyacetylene-$(CH)_x$' *J. Am. Chem. Soc.* 100 (**1977**) 1013.

Chiang, C. K.; Fischer, C. R.; Park, Y.W.; Heeger, A. J.; Shirakawa, H.; Louis, E. J.; Gau, S. C.; MacDiarmid, A. G. 'Electrical conductivity in doped polyacetylene' *Phys. Rev. Lett.* 39 (**1977**) 1096.

Cho, B. -K.; Jain, A.; Gruner, S. M.; Wiesner, U. 'Mesophase structure-mechanical and ionic transport correlations in extended amphiphilic dendrons' *Science* 305 (**2004**) 1598.

Chung, D. S.; Park, J. W.; Park, J. -H.; Moon, D.; Kim, G. H.; Lee, H. -S.; Lee, D. H.; Shim, H. -K.; Kwon, S. -K.; Park, C. E. 'High mobility organic single crystal transistors based on soluble triisopropylsilylethynyl anthracene derivatives' *J. Mater. Chem.* 20 (**2010**) 524.

Chung, J. W.; You, Y.; Huh, H. S.; An, B. -K.; Yoon, S. -J.; Kim, S. H.; Lee, S. W.; Park, S. Y. 'Shear- and UV-induced fluorescence switching in stilbenic π-dimer crystals powered by reversible [2 + 2] cycloaddition' *J. Am. Chem. Soc.* 131 (**2009**) 8163.

Cintas P. 'Chirality of living systems: a helping hand from crystals and oligopeptides' *Angew. Chem. Int. Ed.* 41 (**2002**) 1139.

Clar, E. 'The Aromatic Sextet' Wiley: New York, **1972**.

Collings, P. J.; Hird, M. 'Introduction to liquid crystals chemistry and physics' Taylor & Francis, **1997**.

Como, E. D.; Loi, M. A.; Murgia, M.; Zamboni, R.; Muccini, M. '*J*-Aggregation in α-sexithiophene submonolayer films on silicon dioxide' *J. Am. Chem. Soc. 128* (**2006**) 4277.

Cornelissen, J. J. L. M.; Rowan, A. E. ; Nolte, R. J. M.; Sommerdijk, N. A. J. M. 'Chiral architectures from macromolecular building blocks' *Chem. Rev.* 101 (**2001**) 4039.

Cornil, J.; Beljonne, D.; Calbert, J. -P.; Brédas, J. -L. 'Interchain interactions in organic π-conjugated materials: Impact on electronic structure, optical response, and charge transport' *Adv. Mater.* 13 (**2001**) 1053.

Cornil, J.. Beljonne, D.; dos Santos, D. A.; Calbert, J. P.; Bredas, J. L. 'Intermolecular interactions in electroluminescent conjugated materials' *Thin Solid Films* 363 (**2000**) 72.

Courtney, S. H.; Balk, M. W.; Philips, L. A.; Webb, S. P.; Yang, D.; Levy, D. H.; Fleming, G. R. 'Unimolecular reactions in isolated and collisional systems: Deuterium isotope effect in the photoisomerization of stilbene' *J. Chem. Phys.* 89 (**1988**) 6697.

Crenshaw, B. R.; Weder, C. 'Phase separation of excimer-forming fluorescent dyes and amorphous polymers: A versatile mechanism for sensor applications' *Adv. Mater.* 17 (**2005**) 1471.

Cristiano, R.; Santos, D. M. P. O.; Gallardo, H. 'Synthesis and characterization of low molecular mass luminescent liquid crystalline materials with 1,3,4-oxadiazole units' *Liq. Cryst.* 32 **(2005)** 7.

Curtis, M. D.; Cao, J.; Kampf, J. W. 'Solid-state packing of conjugated oligomers: from π-stacks to the herringbone structure' *J. Am. Chem. Soc.* 126 **(2004)** 4318.

Das, S.; Gopinathan, N.; Abraham, S.; Jayaraman, N.; Singh, M. K.; Prasad, S. K.; Rao, D. S. S. 'Manifestation of a chiral smectic C phase in diphenylbutadiene-cored bolaamphiphilic sugars' *Adv. Funct. Mater.* 18 **(2008)** 1632.

Dautel, O. J.; Robitzer, M.; Flores, J. -C.; Tondelier, D.; Serein-Spirau, F.; Lere-Porte, J. -P.; Guerin, D.; Lenfant, S.; Tillard, M.; Vuillaume, D.; Moreau, J. J. E. 'Electroactive nanorods and nanorings designed by supramolecular association of -conjugated oligomers' *Chem. Eur. J.* 14 **(2008)** 4201.

Davis, R.; Das, S.; George, M.; Druzhinin, S.; Zachariasse K. A. 'Intramolecular charge transfer and photochemical isomerization in donor/acceptor-substituted butadienes' *J. Phys. Chem. A* 105 **(2001)** 4790.

Davis, R.; Kumar, N. S. S.; Abraham, S.; C. H. Suresh, Rath, N. P.; Tamaoki, N.; Das, S. 'Molecular packing and solid-state fluorescence of alkoxy-cyano substituted diphenylbutadienes: Structure of the luminescent aggregates' *J. Phys. Chem. C* 112 **(2008)** 2137.

Davis, R.; Rath, N. P.; Das, S. 'Thermally reversible fluorescent polymorphs of alkoxy-cyano-substituted diphenylbutadienes: role of crystal packing in solid state fluorescence' *Chem. Commun.* (**2004**) 74.

De Luca, G.; Liscio, A.; Nolde, F.; Scolaro, L. M.; Palermo, V.; Müllen, K.; Samori, P. 'Self-assembly of discotic molecules into mesoscopic crystals by solvent-vapour annealing' *Soft Matter* 4 (**2008**) 2064.

De Mello, J. C.; Wittmann, H. F.; Friend, R. H. 'An improved experimental determination of external photoluminescence quantum efficiency' *Adv. Mater.* 9 (**1997**) 230.

Dehm, V.; Chen, Z.; Baumeister, U.; Prins, P.; Siebbeles, L. D. A.; Würthner, F. 'Helical growth of semiconducting columnar dye assemblies based on chiral perylene bisimides' *Org. Lett.* 9 (**2007**) 1085.

Demeter, A.; Druzhinin, S.; George, M.; Haselbach, E.; Roulin, J. -L.; Zachariasse, K. A. 'Dual fluorescence and fast intramolecular charge transfer with 4-(diisopropylamino)benzonitrile in alkane solvents' *Chem. Phys. Lett.* 323 (**2000**) 351.

Demus, D. 'Physical properties of liquid crystals' *Wiley-VCH*, **1999**.

Desiraju, G. R. 'Designer crystals: intermolecular interactions, network structures and supramolecular synthons' *Chem. Commun.* (**1997**) 1475.

Dierking, I. 'Textures of liquid crystals' *Wiley-VCH*, **2003**.

Dilling, W. L. 'Organic photochemistry. XVII. Polymerization of unsaturated compounds by photocycloaddition reactions' *Chem. Rev.* 83 (**1983**) 1.

Dodabalapur, A.; , Katz, H. E.; , Torsi, L.; Haddon, R. C. 'Organic heterostructure field-effect transistors' *Science* 269 (**1995**) 1560.

Dong, J.; Solntsev, K. M.; Tolbert, L. M. 'Activation and tuning of green fluorescent protein chromophore emission by alkyl substituent-mediated crystal packing' *J. Am. Chem.Soc.* 131 (**2009**) 662.

Dugave, C., Demange, L. 'Cis-trans isomerization of organic molecules and biomolecules: Implications and applications' *Chem. Rev.* 103 (**2003**) 2475.

Eelkema, R.; Feringa, B. L. 'Amplification of chirality in liquid crystals' *Org. Biomol. Chem.* 4 (**2006**) 3729.

Egelhaaf, H. -J.; Gierschner, J.; Oelkrug, D. 'Characterization of oriented oligo(phenylenevinylene) films and nano-aggregates by UV/Vis-absorption and fluorescence spectroscopy' *Synth. Met.* 83 (**1996**) 221.

Engelkamp, H.; Middelbeek, S.; Nolte, R. J. M. 'Self-assembly of disk-shaped molecules to coiled-coil aggregates with tunable helicity' *Science* 284 (**1999**) 785.

Fei, Z.; Kocher, N.; Mohrschladt, C. J.; Ihmels, H.; Stalke, D. 'Single crystals of the disubstituted anthracene 9,10-$(Ph_2P=S)_2C_{14}H_8$ selectively and reversibly detect toluene by solid-state fluorescence emission' *Angew. Chem. Int. Ed.* 42 (**2003**) 783.

Fernandez, G.; Perez, E. M.; Sanchez, L.; Martin, N. 'Self-organization of electroactive materials: A head-to-tail donor-acceptor supramolecular Polymer' *Angew. Chem. Int. Ed.* 47 (**2008**) 1094.

Fichou, D. 'Structural order in conjugated oligothiophenes and its implications on opto-electronic devices' *J. Mater. Chem.* 10 (**2000**) 571.

Forrest, S. R. 'The path to ubiquitous and low-cost organic electronic appliances on plastic' *Nature* 428 (**2004**) 911.

Friend, R. H.; Gymer, R. W.; Holmes, A. B.; Burroughes, J. H.; Marks, R. N.; Taliani, C.; Bradley, D. D. C.; dos Santos, D. A.; Logdlund, M.; Salaneck, W. R. 'Electroluminescence in conjugated polymers' *Nature* 397 (**1999**) 121.

Funahashi, M.; Hanna, J. 'High ambipolar carrier mobility in self-organizing terthiophene derivative' *Appl. Phys. Lett.* 76 (**2000**) 2574.

Funahashi, M.; Hanna, J. 'High carrier mobility up to 0.1 cm^2 V^{-1} s^{-1} at ambient temperatures in thiophene-based smectic liquid crystals' *Adv. Mater.* 17 (**2005**) 594.

Geiger, C.; Stanescu, M.; Chen, L.; Whitten, D. G. 'Organogels resulting from competing self-assembly units in the gelator: structure, dynamics, and photophysical behavior of gels formed from cholesterol stilbene and cholesterol squaraine gelators' *Langmuir* 15 (**1999**) 2241.

Gennes, P. G.; Prost, J. 'The physics of liquid crystals' *Oxford University Press*, **1995**.

George, S. J.; Ajayaghosh, A. 'Self-assembled nanotapes of oligo(p-phenylene vinylene)s: sol–gel-controlled optical properties in fluorescent p-electronic gels' *Chem. Eur. J.* 11 (**2005**) 3217.

George, S. J.; Tomovic, Z.; Smulders, M. M. J.; De Greef, T. F. A.; Leclere, P. E. L. G.; Meijer, E. W., Schenning, A. P. H. J. 'Helicity induction and amplification in an oligo(p-phenylenevinylene) assembly through hydrogen-bonded chiral acids' *Angew. Chem. Int. Ed.* 46 (**2007**) 8206.

Ghosh, S.; Li, X. -Q.; Stepanenko, V.; Wurthner, F. 'Control of H- and J-type π stacking by peripheral alkyl chains and self-sorting phenomena in perylene bisimide homo- and heteroaggregates' *Chem. Eur. J.* 14 (**2008**) 11343.

Gierschner, J.; Egelhaaf, H. -J.; Oelkrug, D. 'Absorption, fluorescence and light scattering of oligothiophene and oligophenylenevinylene nanoaggregates' *Synth. Met.* 84 (**1997**) 529.

Gierschner, J.; Ehni, M.; Egelhaaf, H. -J.; Medina, B. M.; Beljonne, D.; Benmansour, H.; Bazan, G. C. 'Solid-state optical properties of linear polyconjugated molecules: π-stack contra herringbone' *J. Chem. Phys.* 123 (**2005**) 144914.

Grabowski, Z. R.; Rotkiewicz, K.; Rettig, W. 'Structural changes accompanying intramolecular electron transfer: focus on twisted intramolecular charge-transfer states and structures' *Chem. Rev.* 103 (**2003**) 3899.

Grimsdale, A. C.; Müllen, K. 'The Chemistry of Organic Nanomaterials' *Angew. Chem. Int. Ed.* 44 (**2005**) 5592

Haino, T.; Tanaka, M.; Fukazawa, Y. 'Self-assembly of tris (phenylisoxazolyl) benzene and its asymmetric induction of supramolecular chirality' *Chem. Commun.* (**2008**) 468.

Hasegawa, M.; Enozawa, H.; Kawabata, Y.; Iyoda, M. 'Hexagonally ordered nanostructures comprised of a flexible disk-like molecule with high self-assembling properties at neutral and cationic states' *J. Am. Chem. Soc.* 129 (**2007**) 3072.

He, C. F.; Richards, G. R.; Kelly, S. M.; Contoret, A. E. A.; O'Neill, M. 'Heterocyclic polycatenar liquid crystals' *Liq. Cryst.* 34 (**2007**), 1249.

Heeger, A. J.; Kivelson, S.; Schrieffer, J. R.; Su, W. -P. 'Solitons in conducting polymers, *Rev. Mod. Phys.* 60 (**1988**), 781.

Hennrich, G.; Omenat, A.; Asselberghs, I.; Foerier, S.; Clays, K.; Verbiest, T.; Serrano, J. L. 'Liquid crystals from C_3-symmetric mesogens for second-order nonlinear optics' *Angew. Chem. Int. Ed.* 45 (**2006**) 4203.

Herz, L. M.; Daniel, C.; Silva, C.; Hoeben, F. J. M.; Schenning, A. P. H. J.; Meijer, E. W.; Friend, R. H.; Phillips, R. T. 'Fast exciton diffusion in chiral

stacks of conjugated p-phenylene vinylene oligomers' *Phys. Rev.* B 68 **(2003)** 045203.

Hide, F.; Diaz-Garcia, M. A.; Schwartz, B. J.; Heeger, A. J. 'New developments in the photonic applications of conjugated polymers' *Acc. Chem. Res.* 30 **(1997)** 430.

Hoeben, F. J. M.; Jonkheijm, P.; Meijer, E. W.; Schenning, A. P. H. J. 'About supramolecular assemblies of π-conjugated systems' *Chem. Rev.* 105 **(2005)** 1491.

^hHoeben, F. J. M.; Schenning, A. P. H. J.; Meijer, E. W. 'Energy-transfer efficiency in stacked oligo(p-phenylene vinylene)s: Pronounced effects of order' *Chem. Phys. Chem.* 6 **(2005)** 2337.

Huang, X.; Terech, P.; Raghavan, S. R.; Weiss, R. G. 'Kinetics of 5α-cholestan-3β-yl N-(2-naphthyl)carbamate/n-alkane organogel formation and its influence on the fibrillar networks' *J. Am. Chem. Soc.* 127 **(2005)** 4336.

Ichikawa, T.; Yoshio, M.; Hamasaki, A.; Mukai, T.; Ohno, H.; Kato, T. 'Self-organization of room-temperature ionic liquids exhibiting liquid-crystalline bicontinuous cubic phases: Formation of nano-ion channel networks' *J. Am. Chem. Soc.* 129 **(2007)** 10662.

Ikeda, M.; Takeuchi, M.; Shinkai, S. 'Unusual emission properties of a triphenylene-based organogel system' *Chem. Commun.* **(2003)** 1354.

Ito, H.; Saito, T.; Oshima, N.; Kitamura, N.; Ishizaka, S.; Hinatsu, Y.; Wakeshima, M.; Kato, M.; Tsuge, K.; Sawamura, M. 'Reversible mechanochromic luminescence of [(C$_6$F$_5$Au)2(μ-1,4-diisocyanobenzene)]' *J. Am. Chem. Soc.* 130 (**2008**) 10044.

Jayanty, S.; Radhakrishnan, T. P. 'Spontaneous resolution through helical assembly of a conformationally chiral molecule with an unusual zwitterionic structure' *Chem. Eur. J.* 10 (**2004**) 2661.

Jin, W.; Fukushima, T.; Niki, M.; Kosaka, A.; Ishii, N.; Aida, T. 'Self-assembled graphitic nanotubes with one-handed helical arrays of a chiral amphiphilic molecular graphene' *Proc. Natl. Acad. Sci. USA* 102 (**2005**) 10801.

Jonkheijm, P.; Hoeben, F. J. M.; Kleppinger, R.; van Herrikhuyzen, J.; Schenning, A. P. H. J.; Meijer, E. W. 'Transfer of π-conjugated columnar stacks from solution to surfaces' *J. Am. Chem. Soc.* 125 (**2003**) 15941.

Kaiser, T. E.; Wang, H.; Stepanenko, V.; Wurthner, F. 'Supramolecular construction of fluorescent *J*-aggregates based on hydrogen-bonded perylene dyes' *Angew. Chem. Int. Ed.* 46 (**2007**) 5541.

Kamikawa, Y.; Kato, T. 'Color-tunable fluorescent organogels: Columnar self-assembly of pyrene-containing oligo(glutamic acid)s' *Langmuir* 23 (**2007**) 274.

Kasha, M. 'Energy transfer mechanism and the molecular exciton model for molecular aggregate' *Radiat. Res.* 20 (**1963**) 55.

Kasha, M.; Rawls, H. R.; El-Bayoumi, M. A. 'The exciton model in molecular spectroscopy' *Pure Appl. Chem.* 11 (**1965**) 371.

Kato, T.; Mizoshita, N.; Kishimoto, K. 'Functional liquid-crystalline assemblies: self-organized soft materials' *Angew. Chem. Int. Ed.* 45 (**2006**) 38.

Kelley T.W.; Baude P. F.; Gerlach C.; Ender D. E.; Muyres D.; Haase, M. A.; Vogel, D. E.; Theiss, S. D. 'Recent progress in organic electronics: materials, devices, and processes' *Chem. Mater.* 16 (**2004**) 4413.

Kimura, M.; Narikawa, H.; Ohta, K.; Hanabusa, K.; Shirai, H.; Kobayashi, N. 'Star-Shaped Stilbenoid Phthalocyanines' *Chem. Mater.* 14 (**2002**) 2711.

Kimura, M.; Yasuda, T.; Kishimoto, K.; Gotz, G.; Bauerle, P.; Kato, T. Oligothiophene-based liquid crystals exhibiting smectic A phases in wider temperature ranges' *Chem. Lett.* 35 (**2006**) 1150.

Kishimoto, K.; Suzawa, T.; Yokota, T.; Mukai, T.; Ohno, H.; Kato, T. 'Nano-segregated polymeric film exhibiting high ionic conductivities' *J. Am. Chem. Soc.* 127 (**2005**) 15618.

Klosterman, J. K.; Yamauchi, Y.; Fujita, M. 'Engineering discrete stacks of aromatic molecules' *Chem. Soc. Rev.*, 38 (**2009**) 1714.

Koutecky, V. B.; Koutecky, J.; Michl, J. 'Neutral and charged biradicals, zwitterions, funnels in S_1, and proton translocation: Their role in photochemistry, photophysics, and vision' *Angew. Chem. Int. Ed.* 26 (**1987**) 170.

Kozhevnikov, V. N.; Donnio, B.; Bruce, D. W. 'Phosphorescent, terdentate, liquid-crystalline complexes of platinum (ii): Stimulus-dependent emission' *Angew. Chem Int. Ed.* 47 (**2008**) 6286.

Kumaki, J.; Kawauchi, T.; Okoshi, K.; Kusanagi, H.; Yashima, E. 'Supramolecular helical structure of the stereo complex composed of complementary isotactic and syndiotactic poly(methyl methacrylate)s as revealed by atomic force microscopy' *Angew. Chem. Int. Ed.* 46 (**2007**) 5348.

Kumar, N. S. S.; Varghese, S.; Narayan, G.; Das, S. 'Hierarchical self-assembly of donor-acceptor-substituted butadiene amphiphiles into photoresponsive vesicles and gels' *Angew Chem. Int. Ed.* 45 (**2006**) 6317.

Kumar, N. S. S.; Varghese, S.; Rath, N. P.; Das, S. 'Solid state optical properties of 4-alkoxy-pyridine butadiene derivatives: reversible thermal switching of luminescence' *J. Phys. Chem. C.* 112 (**2008**) 8429.

Kumar, N. S. S.; Varghese, S.; Suresh, C. H.; Rath, N. P.; Das, S. 'Correlation between solid-state photophysical properties and molecular packing in a series of indane-1,3-dione containing butadiene derivatives' *J. Phys. Chem. C* 113 (**2009**) 11927.

Kumar, S. 'Self-organization of disc-like molecules: chemical aspects' *Chem. Soc. Rev.* 35 (**2006**) 83.

Kunzelman, J.; Chung, T.; Matherx, P. T.; Weder, C. 'Shape memory polymers with built-in threshold temperature sensors' *J. Mater. Chem.* 18 (**2008**) 1082.

Kunzelman, J.; Kinami, M.; Crenshaw, B. R.; Protasiewicz, J. D.; Weder, C. 'Oligo(p-phenylene vinylene)s as a "new" class of piezochromic fluorophores' *Adv. Mater.* 20 (**2008**) 119.

Lapouyade, R.; Czeschka, K.; Majenz, W.; Rettig, W.; Gilabert, E.; Rulliere, C. 'Photophysics of donor-acceptor substituted stilbenes. A time-resolved fluorescence study using selectively bridged dimethylamino cyano model compounds' *J. Phys. Chem.*, 96 (1**992**) 9643.

Laschat, S.; Baro, A.; Steinke, N.; Giesselmann, F.; Hagele, C.; Scalia, G.; Judele, R.; Kapatsina, E.; Sauer, S.; Schreivogel, A.; Tosoni, M. 'Discotic liquid crystals: From tailor-made synthesis to plastic electronics' *Angew. Chem. Int. Ed.* 46 (**2007**) 4832.

Lee, C.C.; Grenier, C.; Meijer, E.W.; Schenning, A. P. H. J. 'Preparation and characterization of helical self-assembled nanofibers' *Chem. Soc. Rev.* 38 (**2009**) 671.

Lee, D. -C.; McGrath, K. K.; Jang, K. 'Nanofibers of asymmetrically substituted bisphenazine through organogelation and their acid sensing properties' *Chem. Commun.* (**2008**) 3636.

Lehmann, M.; Kestemont, G.; Gomez Aspe, R.; Buess-Hermann, C.; Koch, M. H. J.; Debije, M. G.; Piris, J.; de Haas, M. P.; Warman, J. M.; Watson, M. D.; Lemaur, V.; Cornil, J.; Geerts, Y. H.; Gearba, R.; Ivanov, D. A. 'High Charge-Carrier Mobility in π-Deficient Discotic Mesogens: Design and Structure–Property Relationship' *Chem. Eur. J.* 11 (2005) 3349.

Lehn, J. -M. 'Supramolecular chemistry, concepts and perspectives' VCH, Weinheim, 1995.

Letsinger, R. L.; Wu, T. 'Control of Excimer emission and photochemistry of stilbene units by oligonucleotide hybridization' *J. Am. Chem. Soc.* 116 (1994) 811.

Levitsky, I. A.; Kishikawa, K.; Eichhorn, S. H.; Swager, T. M. 'Exciton coupling and dipolar correlations in a columnar liquid crystal: photophysics of a bent-rod hexacatenar mesogen' *J. Am. Chem. Soc.* 122 (2000) 2474.

Lewis, F. D.; Yang, J. S. 'Solid-state fluorescence of aromatic dicarboxamides. dependence upon crystal packing' *J. Phys. Chem.* B 101 (1997) 1775.

Lewis, F. D.; Yang, J. -S.; Stern, C. L. 'Crystal structures of secondary arenedicarboxamides. an investigation of arene-hydrogen bonding relationships in the solid state' *J. Am. Chem. Soc.* 118 (1996) 12029.

Lewis, F. D.; Yang, J. -S.; Stern, C. L. 'Ground and excited state aromatic–aromatic interactions with distance control by hydrogen bonding' *J. Am. Chem. Soc.* 118 (1996) 2772.

Li, X.; Stepanenko, V.; Chen, Z.; Prins, P.; Siebbeles, L. D. A.; Wurthner, F. 'Functional organogels from highly efficient organogelator based on perylene bisimide semiconductor' *Chem. Commun.* **(2006)** 3871.

Likhtenshtein, G. 'Stilbenes: Applications in chemistry, life sciences and materials science' 1st ed.; *Wiley-VCH*: New York, **2009**.

Lim, J. A.; Lee, H. S.; Lee, W. H.; Cho, K. 'Control of the morphology and structural development of solution-processed functionalized acenes for high-performance organic transistors' *Adv. Funct. Mater.* 19 **(2009)** 1515.

Liu, R. S. H.; Browne, D. T. 'A bioorganic view of the chemistry of vision: H.T.-n and B.P.-m,n mechanisms for reactions of confined, anchored polyenes' *Acc. Chem. Res.* 19 **(1986)**, 42.

Liu, R. S. H.; Hammond, G. S. 'Reflection on medium effects on photochemical reactivity' *Acc. Chem. Res.* 38 **(2005)** 396.

Lohr, A.; Lysetska, M.; Wurthner, F. 'Supramolecular stereomutation in kinetic and thermodynamic self-assembly of helical merocyanine dye nanorods' *Angew. Chem. Int. Ed.* 44 **(2005)** 5071.

Luisi, P. L. 'The emergence of life: From chemical origins to synthetic biology' *Cambridge University Press*, Cambridge, **2006**.

Maeda, K.; Yashima, E. 'Detection and amplification of chirality by helical polymers' *Top. Curr. Chem.* 265 **(2006)** 47.

Mason, S. 'Chemical evolution: Origin of biomolecular chirality' *Nature* 314 (1985) 400.

Mateos-Timoneda, M. A.; Crego-Calama, M.; Reinhoudt, D. N. 'Supramolecular chirality of self-assembled systems in solution' *Chem. Soc. Rev.* 33 (2004) 363.

Mathies, R. A. Photons, 'Femtoseconds and dipoler interactions: a molecular picture of the primary events in vision. in rhodopsins and phototransduction' *John Wiley & Sons*: New York, 1999.

McCulloch, I.; Heeney, M.; Bailey, C.; Genevicius, K.; MacDonald, I.; Shkunov, M.; Sparrowe, D.; Tierney, S.; Wagner, R.; Zhang, W.; Chabinyc, M. L.; Kline, R. J.; McGehee, M. D.; Toney, M. F. 'Liquid-crystalline semiconducting polymers with high charge-carrier mobility' *Nat. Mater.* 5 (2006) 328.

Meier, H. 'The photochemistry of stilbenoid compounds and their role in materials technology' *Angew. Chem. Ind. Ed.* 31 (1992) 3399.

Meier, H.; Lifka, T.; Seus, P.; Oehlhof, A.; Hillmann, S. 'Photochemistry of 3, 6-bis(styryl)pyridazines in solution and in neat liquid crystalline phase-optical switching and imaging techniques' *Tetrahedron* 64 (2008) 10754.

Meijer, E.W.; Schenning, A. P. H. J. 'Chemistry: Material marriage in electronics' *Nature* 419 (2002) 353.

Menger, F. M.; Peresypkin, A. V. 'Strings of vesicles: Flow behavior in an unusual type of aqueous gel' *J. Am. Chem. Soc.* 125 (2003), 5340.

Mizobe, Y.; Tohnai, N.; Miyata, M.; Hasegawa, Y. 'A tunable solid-state fluorescence system consisting of organic salts of anthracene-2,6-disulfonic acid with primary amines' *Chem. Commun.* (2005) 1839.

Mizuguchi, J.; Tanifuji, N.; Kobayashi, K. 'Electronic and structural characterization of a piezochromic indigoid: 11-(3'-oxodihydro benzothiophen -2'-ylidene) cyclopenta[1,2-b:4,3-b'] dibenzothiophene' *J. Phys. Chem.* B 107 (2003) 12635.

Mizukami, S.; Houjou, H.; Sugaya, K.; Koyama, E.; Tokuhisa, H.; Sasaki, T.; Kanesato, M. 'Fluorescence color modulation by intramolecular and intermolecular π-π interactions in a helical zinc(ii) complex' *Chem. Mater.* 17 (2005) 50.

Montali, A.; Bastiaansen, C.; Smith, P.; Weder, C. 'Polarizing energy transfer in photoluminescent materials for display applications' *Nature* 392 (1998), 261.

Mutai, T.; Satou, H.; Araki, K. 'Reproducible on-off switching of solid-state luminescence by controlling molecular packing through heat-mode interconversion' *Nat. Mater.* 4 (2005) 685.

Mutai, T.; Tomoda, H.; Ohkawa, T.; Yabe, Y.; Araki, K. 'Switching of polymorph-dependent ESIPT luminescence of an imidazo [1, 2-a] pyridine derivative' *Angew. Chem. Int. Ed.* 47 (**2008**) 9522.

Nakanishi, T.; Ariga, K.; Michinobu, T.; Yoshida, K.; Takahashi, H.; Teranishi, T.; Mchwald, H.; Kurth, D. G. 'Flower-shaped supramolecular assemblies: Hierarchical organization of a fullerene bearing long aliphatic chains' *Small* 3 (**2007**) 2019.

Nakanishi, T.; Michinobu, T.; Yoshida, K.; Shirahata, N.; Ariga, K.; Möhwald, H.; Kurth, D. G. 'Nanocarbon superhydrophobic surfaces created from fullerene-based hierarchical supramolecular assemblies' *Adv. Mater.* 20 (**2008**) 443.

Nguyen, H. T.; Destrade, C.; Malthete, J. 'Phasmids and polycatenar mesogens' *Adv. Mater.* 9 (**1997**) 375.

O'Neill, M.; Kelly, S. M. 'Liquid crystals for charge transport, luminescence, and photonics' *Adv. Mater.* 15 (**2003**) 1135.

Oelkrug, D.; Tompert, A.; Gierschner, J.; Egelhaaf, H. -J.; Hanack, M.; Hohloch, M.; Steinhuber, E. 'Tuning of fluorescence in films and nanoparticles of oligophenylenevinylenes' *J. Phys. Chem.* B 102 (**1998**) 1902.

Ota, A.; Yamochi, H.; Saito, G. A novel metal–insulator phase transition observed in (EDO-TTF)₂PF₆, *J. Mater. Chem.* 12 (**2002**) 2600.

Palermo, V.; Samori, P. 'Molecular self-assembly across multiple length scales' *Angew. Chem. Int. Ed.* 46 (**2007**) 4428.

Palma, M.; Levin, J.; Debever, O.; Geerts, Y.; Lehmann, M.; Samori, P. 'Self-assembly of hydrogen-bond assisted supramolecular azatriphenylene architectures' *Soft Matter* 4 (**2008**) 303.

Palmans, A. R. A.; Meijer, E. W. 'Amplification of chirality in dynamic supramolecular aggregates' *Angew. Chem. Int. Ed.* 46 (**2007**) 8948.

Papaefstathiou, G. S.; Zhong, Z.; Geng, L.; MacGillivray, L. R. 'Coordination-driven self-assembly directs a single-crystal to single-crystal transformation that exhibits photocontrolled fluorescence' *J. Am. Chem. Soc.* 126 (**2004**) 9158.

Paulsson, L. -O.; Monkman, A. P. 'Measurements of solid-state photoluminescence quantum yields of films using a fluorimeter' *Adv. Mater.* 14 (**2002**) 757.

Pieterse, K.; van Hal, P. A.; Kleppinger, R. F.; Vekemans, J. A. J. M.; Janssen, R. A. J.; Meijer, E. W. 'An electron-deficient discotic liquid-crystalline material' *Chem. Mater.* 13 (**2001**) 2675.

Pines, D.; Pines, E.; Rettig, W. J. 'Dual Fluorescence and Excited-State Structural Relaxations in Donor Acceptor Stilbenes' *J. Phys. Chem. A* 107 (**2003**) 236.

Prakash, M. J., Radhakrishnan, T. P. 'SHG active crystals of a remote functionalized achiral NLO-phore assembled through zinc(II) complexation' *Inorg. Chem.* 45 (**2006**) 9758.

Prasad, S. K.; Rao, D. S. S.; Chandrasekhar, S.; Kumar, S. 'X-ray studies on the columnar structures of discotic liquid crystals' *Mol. Cryst. Liq. Cryst.* 396 (**2003**) 121.

Qu, S.; Chen, X.; Shao, X.; Li, F.; Zhang, H.; Wang, H.; Zhang, P.; Yu, Z.; Wu, K.; Wang, Y.; Li, M. 'Self-assembly of highly luminescent bi-1,3,4-oxadiazole derivatives through electron donor-acceptor interactions in three-dimensional crystals, two-dimensional layers and mesophases' *J. Mater. Chem.* 18 (**2008**) 3954.

Radhakrishnan, T. P. 'Molecular structure, symmetry and shape as design elements in the fabrication of molecular crystals for second harmonic generation and the role of molecules-in-materials' *Acc. Chem. Res.* 41 (**2008b** 367.

Rais, K.; Daoud, M.; Gharbia, M.; Gharbi, A.; Nguyen, H. T. 'Column correlation in polycatenar mesophases' *Chem. Phys. Chem.* (**2001**) 1439.

Ramamurthy, V. 'Photochemistry in organized and constrained media' Ramamurthy, V., Ed.; *VCH* Publishers: New York, **1991**.

Repinec, S. T.; Sension, R. J.; Szarka, A. Z. Hochstrasser, R. M. 'Femtosecond laser studies of the cis-stilbene photoisomerization reactions. The cis-

stilbene to dihydrophenanthrene reaction' *J. Phys. Chem. A* 95 (**1991**) 10380.

Rettig, W. 'In Topics of Current Chemistry' Vol. 169, Electron Transfer 1; Springer: Berlin, **1994**, 253.

Rettig, W.; Maus, M. 'In conformational analysis of molecules in excited states' Waluk, J., Ed.; Wiley-VCH: New York, **2000**; Chapter 1.

Ribeiro, A. C.; Heinrich, B.; Cruz, C.; Nguyen, H. T.; Diele, S.; Schröder. M.W.; Guillon, D. 'Rectangular to hexagonal columnar phase transition exhibited by a biforked mesogen' *Eur. Phys. J. E* 10 (**2003**) 143.

Rosaria, L.; D'Urso, A.; Mammana, A.; Purrello, R. 'Chiral memory: Induction, amplification, and switching in porphyrin assemblies' *Chirality* 20 (**2008**) 411.

Rothenberger, G.; Negus, D. K.; Hochstrasser, R. M. 'Solvent influence on photoisomerization dynamics' *J. Chem. Phys.* 79 (**1983**) 5360.

Rowan, A. E.; Nolte, R. J. M. 'Helical Molecular Programming' *Angew. Chem. Int. Ed.* 37 (**1998**) 63.

Russell, J. C.; Costa, S. B.; Seiders, R. P.; Whitten, D. G. 'Photochemistry of a surfactant stilbene in organized media: A probe for hydrophobic sites in micelles, vesicles, and other assemblies' *J. Am. Chem. Soc.* 102 (**1980**) 5678.

Sagara, Y.; Kato, T. 'Mechanically induced luminescence changes in molecular assemblies' *Nature Chem.* 1 (**2009**) 605.

Sagara, Y.; Kato, T. 'Stimuli-responsive luminescent liquid crystals: Change of photoluminescent colors triggered by a shear-induced phase transition' *Angew. Chem. Int. Ed.* 47 (**2008**) 5175.

Sagara, Y.; Mutai, T.; Yoshikawa, I.; Araki, K. 'Material design for piezochromic luminescence: hydrogen-bond-directed assemblies of a pyrene derivative' *J. Am. Chem. Soc.* 129 (**2007**) 1520.

Sakajiri, K.; Sugisaki, T.; Moriya, K. 'Stable supramolecular helical structure of C_6-symmetric hydrogen-bonded hexakis(phenylethynyl)benzene derivatives with amino acid pendant groups and their unique fluorescence properties' *Chem. Commun.* (**2008**) 3447.

Saltiel, J., Waller, A. S.; Sears Jr. D. F. 'Dynamics of cis-stilbene photoisomerization: The adiabatic pathway to excited trans-stilbene' *J. Photochem. Photobiol. A* 65 (**1992**) 29.

Samori, P.; Engelkamp, H.; de Witte. P. A. J.; Rowan, A. E. R. J. M. Nolte, Rabe J. P. 'Self-organization of semiconducting polysiloxane-phthalocyanine on a graphite surface' *Adv. Mater.* 17 (**2005**) 1265.

Sangeetha, N. M.; Maitra, U. 'Supramolecular gels: Functions and uses' *Chem. Soc. Rev.*, 34 (**2005**) 821.

Sauer, J.; Huisgen, R.; Sturm H. J. 'Zur acylierung von 5-aryl-tetrazolen; ein duplikationsverfahren zur darstellung von polyarylen' *Tetrahedron* 11 (**1960**) 241.

Schenning, A. P. H. J.; ;Jonkheijm. P.; Peeters, E.; Meijer, E.W. 'Hierarchical Order in Supramolecular Assemblies of Hydrogen-Bonded Oligo(p-phenylene vinylene)s' *J. Am. Chem. Soc.* 123 (**2001**) 409.

Schenning, A. P. H. J.; Kilbinger, A. F. M.; Biscarini, F.; Cavallini, M.; Cooper, H. J.; Derrick, P. J.; Feast, W. J.; Lazzaroni, R.; Leclerc, Ph.; McDonell, L. A.; Meijer, E. W.; Meskers S. C. J. 'Supramolecular organization of α,α'-disubstituted Sexithiophenes' *J. Am. Chem. Soc.* 124 (**2002**) 1269.

Schenning, A. P. H. J.; Meijer, E. W. 'Supramolecular electronics; nanowires from self-assembled π-conjugated systems' *Chem. Commun.*, (**2005**) 3245.

Schmuck, C. 'Helical Structure: How to build a molecular spiral staircase *Angew. Chem. Int. Ed.* 42 (**2003**) 2448.

Segura, C.; Parella, T.; Ferrando, F. S.; Laurent, H. B.; Desvergne, J. P. 'Stilbene to Phenanthrene' Type Photocyclization of a Bis-(4-Anthryl) Ethylene. A New Access to the Dibenzopicene Skeleton' *Bull. Soc. Chimi. Belg.* 101 (**1992**) 513.

Sension, R. J.; Repinec, S. T.; Hochstrasser, R. M. 'Femtosecond laser study of energy disposal in the solution phase isomerization of stilbene' *J. Chem. Phys.* 98 (**1993**) 6291.

Seo, J.; Chung, J. W.; Jo, E. -H.; Park, S. Y. 'Highly fluorescent supramolecular gels with chirality transcription through hydrogen bonding' *Chem. Commun.* (**2008**) 2794.

Seo, J.: Kim, S.; Gihm, S. H.; Park, C. R.; Park, S. Y. 'Highly fluorescent columnar liquid crystals with elliptical molecular shape: oblique molecular stacking and excited-state intramolecular proton-transfer fluorescence' *J. Mater. Chem.* 17 (**2007**) 5052.

Sergeyev, S.; Pisula, W.; Geerts, Y. H. 'Discotic liquid crystals: a new generation of organic semiconductors' *Chem. Soc. Rev.* 36 (**2007**) 1902.

Serrano, J. L.; Sierra, T. 'Helical supramolecular organizations from metal-organic liquid crystals' *Coord. Chem. Rev.* 242 (**2003**) 73.

Service, R. F. 'How far can we push chemical self-assembly' *Science* 309 (**2005**) 95.

Sheikh-Ali, B. M.; Weiss, R. G. 'Effects of aggregation and mesomorphic order on the photophysical properties of 4-alkyl-n-(p-cyanophenyl)piperidines. molecules capable of forming intramolecular charge transfer states' *J. Am. Chem. Soc.* 116 (**1994**) 6111.

Shinar, J. 'Organic light-emitting devices- A survey' Springer-Verlag, New York, **2004**.

Siddiqui. S.; Spano, F. C. 'H- and J-aggregates of conjugated polymers and oligomers: A theoretical investigation' *Chem. Phys. Lett.* 308 (**1999**) 99.

Simonyi, M.; Bikadi, Z.; Zsila, F.; Deli, J. Supramolecular exciton chirality of carotenoid aggregates. *Chirality* 15 (**2003**) 680.

Singh, A. K.; Kanvah, S. 'Photophysical studies of substituted 1,2-diarylethenes: twisted intramolecular charge transfer fluorescence in dimethoxycyano-substituted 1,2-diarylethene' *J. Chem. Soc., Perkin Trans. 2* (**2001**) 395.

Skotheim, T. A.; Reynolds, J. R. 'Handbook of conducting polymers' CRC Press, **2007**.

Sluckin, T. J.; Dunmur, D. A.; Stegemeyer, H. 'Crystals that flow: Classic papers from the history of liquid crystals' *Taylor & Francis*, **2004**

Sommerdijk, N. A. J. M.; Buynsters, P. J. J. A.; Akdemir, H.; Geurts, D. G.; Feiters, M. C.; Nolte, R. J. M.; Zwanenburg, B. 'Expression of supramolecular chirality in aggregates of chiral amide-containing surfactants' *Chem. Eur. J.* 4 (**1998**) 127.

Song, X.; Perlstein, J.; Whitten D. G. 'Self-assembly of styrylthiophene amphiphiles in aqueous dispersions and interfacial films: aggregate structure, assembly properties, photochemistry, and photophysics' *J. Phys. Chem.* A 102 (**1998**) 5440.

Spano, F. C. 'The fundamental photophysics of conjugated oligomer herringbone aggregates' *J. Chem. Phys.* 118 (**2003**) 981.

Spano, F. C. Analysis of the UV/Vis and CD Spectral Line Shapes of Carotenoid assemblies: Spectral Signatures of Chiral H-Aggregates. *J. Am. Chem. Soc.* 131 (**2009**) 4267.

Sumitani, M.; Nakashima, N.; Yoshihara, K. 'Direct measurement of the reaction rate for cis-trans photoisomerization of stilbene' *Chem. Phys. Lett.* 68 (**1979**) 255.

Sun, H.; Zhao, Z.; Spano, F. C.; Beljonne, D.; Cornil, J.; Shuai, Z.; Brédas, J.-L. 'Absorption and emission in quaterthienyl thin films' *Adv. Mater.* 15 (**2003**) 818.

Syage, J. A.; Felker, P. M.; Zewail, A. H. 'Picosecond dynamics and photoisomerization of stilbene in supersonic beams: Spectra and mode assignments' *J. Chem. Phys.* 81 (**1984**) 4685.

Tang, C. W.; Van Slyke, S. A. 'Organic electroluminescent diodes' *Appl. Phys. Lett.* 51 (**1987**) 913.

Tang, C.W.; Van Slyke, S. A. 'Electroluminescence of doped organic thin films' *Appl. Phys. Lett.* 65 (**1989**) 3610.

Terech, P.; Weiss, R. G. 'Low molecular mass gelators of organic liquids and the properties of their gels' *Chem. Rev.* 97 (**1997**) 3133.

Todd, D. C.; Fleming, G. R. 'Cis-stilbene isomerization: Temperature dependence and the role of mechanical friction' *J. Chem. Phys.* 98 (**1993**) 269.

Tokuhisa, H.; Era, M.; Tsutsui, T. 'Novel liquid crystalline oxadiazole with high electron mobility' *Adv. Mater.* 10 (**1998**) 404.

Tsumura, A.; Koezuka, H.; Ando, Y. 'Polythiophene field effect transistor: Its characteristics and operation mechanism' *Synth. Meth.* 25 (**1988**) 11.

Tullo, A. H. 'Diode developers: A bright future' *Chem. Eng. News* J26 (**2000**) 20.

Vaday, S.; Geiger, H. C.; Cleary, B.; Perlstein, J.; Whitten, D. G. 'Structure of aggregates of trans-4-alkoxy-4'-carboxystilbenes in the solid state and in microheterogeneous media. A link between the "Unit Aggregate" and extended arrays' *J. Phys. Chem. B* 101 (**1997**) 321.

Van Der Auweraer, M.; De Schryver, F. C. 'Organic electronics: Supra solutions' *Nat. Mater.* 3 (**2004**) 507.

van Esch, J. H.; Feringa, B. L. 'New functional materials based on self-assembling organogels: From serendipity towards design' *Angew. Chem. Int. Ed.* 39 (**2000**) 2263.

Venema, L. 'Organic electronics: On the border' *Nature* 453 (**2008**) 996.

Verheyde, B.; Dehaen, W. 'Synthesis of dendrimers containing 1,3,4-oxadiazoles' *J. Org. Chem.* 66 (**2001**) 4062.

Waldeck, D. H. 'Photoisomerization dynamics of stilbenes' *Chem. Rev.* 91 (**1991**) 415.

Wang, R.; Geiger, C.; Chen, L.; Swanson, B.; Whitten, D. G. 'Direct observation of sol gel conversion: The role of the solvent in organogel formation' *J. Am. Chem. Soc.* 122 (**2000**) 2399.

Wang, R.; Liu, X. -Y.; Xiong, J.; Li, J. 'Real-time observation of fiber network formation in molecular organogel: Supersaturation-dependent microstructure and its related rheological property' *J. Phys. Chem.* B 110 (**2006**) 7275.

Watanabe, A.; Kodaira, T.; Ito, O. 'Time-resolved emission spectra of poly(3-octylthiophene): Energy migration in the π-conjugated polymer chain' *Chem. Phys. Lett.* 273 (**1997**) 227.

Watson, J. D. 'The structure of tobacco mosaic virus. I. X-ray evidence of a helical arrangement of sub-units around the longitudinal axis' *Biochim. Biophys. Acta.* 13 (**1954**) 10.

Weigel, A.; Ernsting, N. P. 'Excited stilbene: Intramolecular vibrational redistribution and solvation studied by femtosecond stimulated raman spectroscopy' *J. Phys. Chem.* B 114 (**2010**) 7879.

Westenhoff, S.; Abrusci, A.; Feast, W. J.; Henze, O.; Kilbinger, A. F. M.; Schenning, A. P. H. J.; Silva, C. 'Supramolecular electronic coupling in chiral oligothiophene nanostructures' *Adv. Mater.* 18 (**2006**) 1281.

Whitten, D. G. 'Photochemistry and photophysics of *trans*-stilbene and related alkenes in surfactant assemblies' *Acc. Chem. Res.* 26 (**1993**) 502.

Whitten, D. G.; Chen, L.; Geiger, H. C.; Perlstein, J.; Song, X. 'Self-assembly of aromatic-functionalized amphiphiles: The role and consequences of aromatic aromatic noncovalent interactions in building supramolecular aggregates and novel assemblies' *J. Phys. Chem. B* 102 (**1998**) 10098.

Wu, J.; Pisula, W.; Muellen, K. 'Graphenes as potential material for electronics' *Chem. Rev.* 107 (**2007**) 718.

Wurthner, F. 'Perylene bisimide dyes as versatile building blocks for functional supramolecular architectures' *Chem. Commun.* (**2004**) 1564.

Wurthner, F.; Thalacker, C.; Diele, S.; Tschierske, C. 'Fluorescent J-type aggregates and thermotropic columnar mesophases of perylene bisimide dyes' *Chem. Eur. J.* 7 (**2001**) 2245.

Xie, Z.; Yang, B.; Li, F.; Cheng, G.; Liu, L.; Yang, G.; Xu, H.; Ye, L.; Hanif, M.; Liu, S.; Ma, D.; Ma, Y. 'Cross dipole stacking in the crystal of distyrylbenzene derivative: the approach toward high solid-state luminescence efficiency' *J. Am. Chem. Soc.* 127 (**2005**) 14152.

Yagai, S.; Ishii, M.; Karatsu, T.; Kitamura, A. 'Supramolecular assembly of zinc salphen complexes: Access to metal-containing gels and nanofibers' *Angew. Chem. Int. Ed.* 46 (**2007**) 8005.

Yagai, S.; Kinoshita, T.; Higashi, M.; Kishikawa, K.; Nakanishi, T.; Karatsu, T.; Kitamura, A. 'Diversification of self-organized architectures in supramolecular dye assemblies' *J. Am. Chem. Soc.* 129 (**2007**) 13277.

Yang, J. S.; Liau, K. L.; Hwang, C. Y.; Wang, C. M. 'Photoinduced single- versus double-bond torsion in donor acceptor substituted trans-stilbenes' *J. Phys. Chem.* A 110 (**2006**) 8003.

Yang, L.; Harigai, M.; Imamoto, Y.; Kataoka, M.; Ho, T.; Andrioukhina, E.; Federova, O.; Shevyakova, S.; Liu, R. S. H. 'Stilbene analogs in Hula-twist photoisomerization' *Photochem. Photobiol. Sci.*, 5 (**2006**) 874.

Yao, S.; Beginn, U.; Gress, T.; Lysetska, M.; Würthner, F. 'Supramolecular polymerization and gel formation of bis(merocyanine) dyes driven by dipolar aggregation' *J. Am. Chem. Soc.* 126 (**2004**) 8336.

Yasuda, T.; Kishimoto, K.; Kato, T. 'Columnar liquid crystalline p-conjugated oligothiophenes' *Chem. Commun.* (**2006**) 3399.

Yasuda, T.; Ooi, H.; Morita, J.; Akama, Y.; Minoura, K.; Funahashi, M.; Shimomura, T.; Kato, T. 'π-Conjugated oligothiophene-based polycatenar liquid crystals: self-organization and photoconductive, luminescent and redox properties' *Adv. Funct. Mater.* 19 (**2009**) 411.

Yoon, S. J.; Chung, J. W.; Gierschner, J.; Kim, K. S.; Choi, M. G.; Kim, D., Park S. Y. 'Multistimuli two-color luminescence switching via different slip-stacking of highly fluorescent molecular sheets' *J. Am. Chem. Soc.*, 132 (**2010**) 13675.

Yoshio, M.; Mukai, T.; Ohno, H.; Kato, T. 'One-Dimensional Ion Transport in Self-Organized Columnar Ionic Liquids' *J. Am. Chem. Soc.* 126 (2004) 994.

Zachariasse, K. A. 'Pseudo-Jahn-Teller and TICT-models: A photophysical comparison of meta- and para-DMABN derivatives' [Chem. Phys. Lett. 305 (1999) 8]: The PICT model for dual fluorescence of aminobenzonitriles' *Chem. Phys. Lett.* 320 (2000) 8.

Zachariasse, K. A.; Grobys, M.; von der Haar, T.; Hebecker, A.; Ilichev, Y. V.; Jiang, Y. B.; Morawski, O.; Kuhnle, W. 'Intramolecular charge transfer in the excited state. Kinetics and configurational changes' *J. Photochem. Photobiol. A* 102 (1996) 5970.

Zang, L.; Che, Y.; Moore, J. S. 'One-dimensional self-assembly of planar π-conjugated molecules: Adaptable building blocks for organic nanodevices' *Acc. Chem. Res.* 41 (2008) 1596.

Zhang, Y. D.; Jespersen, K. G.; Kempe, M.; Kornfield, J. A.; Barlow, S.; Kippelen, B.; Marder, S. R. 'Columnar discotic liquid-crystalline oxadiazoles as electron-transport materials' *Langmuir* 19 (2003) 6534.

Zhou, M.; Kidd, T. J.; Noble, R. D.; Gin, D. L. 'Supported lyotropic liquid-crystal polymer membranes: Promising materials for molecular-size-selective aqueous nanofiltration' *Adv. Mater.* 17 (2005) 1850.

Zsila, F.; Bikadi, Z.: Keresztes. Z.; Deli, J.; Simonyi, M. 'Investigation of the self-organization of lutein and lutein diacetate by electronic absorption, circular dichroism spectroscopy, and atomic force microscopy' *J. Phys. Chem.* B 105 (**2001**) 9413.

Description of Instrumental Techniques

1) Chemical Structure Characterization

All intermediates and final products were characterized by FTIR, NMR and FAB-MS. MALDI-TOF and elemental analysis were also conducted in few of the derivatives to ascertain the purity. FT-IR spectra were recorded on a Shimadzu IR Prestige-21 Fourier Transform Infrared Spectrophotometer. ^{1}H (500 MHz) and ^{13}C NMR (125 MHz) spectral analysis were performed on a Brucker Advance DPX spectrometer with TMS as internal standard. MALDI-TOF mass spectrometry was conducted on a Perspective Biosystems Voyager DE PRO MALDI-TOF mass spectrometer using α-cyano-4-hydroxy cinnamic acid as the matrix. FAB-MS spectra were recorded on a JEOL JM AX 505 HA mass spectrometer. Elemental analysis was performed on a Perkin Elmer Series II CHN analyzer.

2) Electronic Spectral Measurements

Electronic absorption spectra were recorded on a Shimadzu UV-3101 PC NIR scanning spectrophotometer the emission spectra were recorded on a SPEX-Fluorolog F112x spectrofluorimeter. The absorption measurements and fluorescence measurements were carried out using 1 x 1 cm cuvette (unless otherwise mentioned) with a thermistor directly attached to the wall of the cuvette holder for controlling the temperature. In crystalline samples and in aggregates the emission was measured in a front face configuration. Fluorescence quantum yields

in solutions were determined by comparison with standard dyes such as quinine sulfate in 0.1 N H_2SO_4 ($\Phi_f = 0.53$) or 10-methyl acridinium trifluorthane sulfonate in water ($\Phi_f = 1$). Solid-state fluorescence quantum efficiency was measured using a calibrated integrating sphere in the spectrofluorimeter. The Xe-arc lamp was used to excite the thin-film/crystalline samples placed in the sphere. The quantum yield was determined by comparing the spectral intensities of the lamp and the sample emission as reported in the literature [De Mello *et al.* 1997; Paulsson *et al.* 2002]. Using this experimental set-up and the integrating sphere system, solid-state fluorescence quantum yield of thin film of the standard green emitting OLED material tris-8-hydroxyquinolinolato Aluminum (Alq3) was determined to be 0.19, which is consistent with previously reported values.

3) Fluorescence Lifetime Measurements

Fluorescence lifetimes were measured using IBH (FluoroCube) time-correlated picosecond single photon counting (TCSPC) system. Solutions were excited with a pulsed diode laser (<100 ps pulse duration) at a wavelength of 375 nm (NanoLED-11) with a repetition rate of 1 MHz. The detection system consisted of a micro channel plate photomultiplier (5000U-09B, Hamamatsu) with a 38.6 ps response time coupled to a monochromator (5000M) and TCSPC electronics (Data station Hub including Hub-NL, NanoLED controller and preinstalled fluorescence Measurement and Analysis Studio (FMAS) Software).

The fluorescence lifetime values were obtained using DAS6 decay analysis software. Fluorescence lifetime measurements in solutions were carried out using 1 x 1 cm cuvette with the emission collected at perpendicular configuration, while in solid samples and in aggregates lifetime measured in a front face configuration.

4) Polarized Optical Microscopy (POM)

Phase transitions were observed using a LEICA DM 2500P polarized light optical microscope with a crossed polarizer configuration, equipped with Mettler Toledo FP900 Thermosystem heating/cooling stage. Samples were kept between untreated glass slides to obtain the POM textures on heating.

5) Differential Scanning Calorimetery (DSC)

DSC experiments were performed using a Perkin-Elmer Pyris 6 DSC instrument. Samples were kept in a sealed aluminum pans under nitrogen flow and the experiments were carried out at a heating/cooling rate of 5 °C min^{-1}.

6) X-Ray Diffractometry (XRD)

Single Crystal X-ray Diffractometry

Single crystal analyses were carried out in a Bruker SMART-CCD diffractometer. structure determination and refinement was carried out with SAINT (SAINTPLUS Version 6.22, Bruker AXS, Madison, WI, USA) and SHELXTL software packages and the empirical absorption correction with the

SADABS program. For crystal structure visualization, MERCURY (CSD software), chemcraft and ChemBio 3D ultra 11 were used.

Powder X-ray Diffractometry

X-ray diffraction studies were carried out using X'pert Pro 1710, Phillips X ray diffractometer with monochromator on the diffraction beam side (CuKα radiation, λ = 1.54 A). X-ray diffraction studies of xero-gel was carried out on samples coated in glass slide and variable temperature X-ray diffraction studies at liquid crystalline phases were carried out on samples filled in Lindemann capillaries and were held at required temperatures using a Mettler hot stage and irradiated with CuKα radiation (λ= 1.5418A [9]).

7) Rheological Measurements

The rheological measurements were carried out using Physica Modular Compact (MCR 150) stress controlled rheometer from Anton Paar with a Cone-and-plate geometry (CP 50-1). The gelled samples were carefully transferred into the Peltier kept at 20 °C and was allowed to form a uniform layer. A strain-sweep experiment was performed at constant angular frequency of 1 rads^{-1} for the strain range 0.001 to 100[8a,27] and a frequency-sweep experiment was performed at a constant shear stress of 1 Pa with an angular frequency(ω) varying from 0.1 to 100 rads^{-1}.

8) Dynamic Light Scattering Measurements (DLS)

Dynamic light scattering measurements were made, using the Nano ZS Malvern instrument employing a 4mW He-Ne laser (λ = 632.8 nm). The measurements were carried out using quartz cuvette with 1 cm path length.

9) Scanning Electron Microscopy (SEM)

For SEM measurements, the samples were drop cast and air dried on one flat surface of cylindrical brass stubs and subjected for thin gold coating using JOEL JFC-1200 fine coater. The probing side was inserted into JEOL JSM-5600 LV Scanning electron microscope for taking photographs. FE-SEM images were recorded with an FEI-Nova NanoSEM600.

10) Transmission Electron Microscopy (TEM)

TEM measurements were carried on an FEI-Technai $30G^2$ S-Twin, 300 kV HR-TEM microscope with an accelerating voltage of 100 kV. Samples were prepared by drop casting the solution on to a formvar coated copper grid (400 mesh) and allowing the excess solvent to evaporate under mild vaccum conditions.

SUMMARY

The work described in the thesis entitled "**Exploring Self-Assembled Stilbenoid Architectures in the Pathway from Molecules to Materials**" explores the use of donor-acceptor substituted stilbene derivatives for the construction of functional self-assembled materials and the changes in their photophysical properties brought about by their self-assembly. Stilbenoid compounds have been extensively investigated from the theoretical and experimental standpoint, in view of their importance both as model compounds for polyenes and as functional materials for technological applications. The photochemical properties of stilbenoid units have been exploited for the construction of photoresponsive smart materials. The high sensitivity of their photophysical properties to the state of molecular organization provides an effective method to monitor the nature of the molecular packing involved in these materials. However, to tailor-make stilbene based materials suitable for a particular application, a better fundamental understanding of the structure-property relationships is needed.

The thesis consists of four chapters. Chapter 1 provides a brief overview on the photochemical and photophysical properties of stilbenoid compounds and on their use in the construction of photoresponsive soft materials. The role of molecular packing in controlling the photophysical properties of these materials in the self-assembled and solid state are also discussed.

Chapter 2 describes the synthesis and investigation of photophysical properties of a series of donor-acceptor substituted stilbene derivatives with alkoxy group as the donor and the cyano group as the acceptor. The solid state photophysical properties of these stilbene derivatives were fine tuned effectively by bringing in subtle modifications in their molecular packing by varying the length of the alkyl chains. A clear correlation between the molecular packing and the fluorescence properties in this class of materials was obtained by investigating their molecular packing in their single crystals. The formation of thermally induced polymorphs and role of the modification of molecular packing induced by heating in controlling optical properties of these materials has also been investigated. Our studies have shown, the solid state fluorescence of this series of stilbene based molecules depend on various factors such as rigidization, planarization and more importantly the nature of the relative alignment of neighbouring molecules which decide whether exciton coupling will or will not occur.

In Chapter 3, the design, synthesis, thermotropic liquid crystalline behaviour and the photophysical properties of two series of pyridine cored donor-acceptor-donor quardrupolar systems are described. The molecules consist of two alkoxy stilbenoid units attached to a central pyridine core through 1,3,4-oxadiazoles linkers in the 2,6 (**PS**) and 2,5 (**PSL**) positions of the pyridine ring to form a rigid rod π-conjugated back bone. Both these series of derivatives exhibited

stable discotic LC phases in the heating and cooling cycles. Chiral discotic LC phases were obtained by introducing chiral groups in the alkyl periphery. A few of these derivatives were observed to form stable glasses on sudden cooling from the LC phase, where the liquid crystalline order was maintained. These materials were found to be fluorescent in their solid state as well as in glassy state. The ability of these materials to form stable liquid crystalline glasses, their strong fluorescence and the electron transporting property of the oxadiazole moiety can make these materials useful as active elements in the emerging field of organic electronics.

In Chapter 4, design, synthesis and discotic liquid crystalline properties of a series of novel trigonal octupolar 1,3,4-oxadiazole derivatives are described. The self-assembly behaviour of these materials in their mesophase as well as in their aggregates in solution and the resultant changes in their photophysical properties have been investigated. A few of these derivatives exhibited enantiotropic columnar mesophases over a wide temperature range. The derivatives with longer alkyl chains were observed to self-assemble in non-polar solvents leading to gel formation. Microscopic investigations of the gels provided clear evidence for the hierarchical self-assembly of these molecules in non-polar solvents leading to gel formation. Filled spheres of nanometric dimensions were observed at lower concentrations which merged together to form nanoscopic fibers at higher concentrations resulting in an extended network of interlocked fibrils which immobilize the solvent to form the gel. The high sensitivity of the luminescence

properties of these materials to their state of aggregation provided an effective method to monitor the nature of the molecular packing involved in the various stages of self-assembly.

We have also investigated the influence of peripheral chiral alkyl chains on the liquid crystalline and the self-assembling behaviour of trigonal octupolar oxadiazole derivative (SA10*). This derivative exhibited discotic liquid crystalline phase with a helical ordering as observed in CD investigations at elevated temperatures. The LC phase could be fixed into liquid crystalline glassy films by sudden cooling from their LC phase. Investigation of the morphology of the aggregates in decane solutions showed a unique aggregation behaviour resulting in the formation of helical fibers at lower concentrations with right-handed helicity. These helices further wound around the molecular axes resulting in the formation of superhelix secondary structure at higher concentrations exhibiting left handed chirality in decane.. The formation of the helical primary structure and superhelix secondary structure and the associated reversal of chirality in the supramolecular level could be monitored by microscopic techniques such as TEM and SEM as well as by circular dichroism (CD) spectroscopy.

Appendix - 1

A. X- ray Crystallographic and Structure Refinement Data of DS1

Empirical formula	$C_{17} H_{15} N O_2$
Formula weight	265.30
Temperature	100(2) K
Wavelength	0.71073 Å
Crystal system	Orthorhombic
Space group	$Pca2_1$
Unit cell dimensions	a = 28.9910(18) Å $\quad \alpha = 90°$.
	b = 6.0408(3) Å $\quad \beta = 90°$.
	c = 15.5719(10) Å $\quad \gamma = 90°$.
Volume	2727.1(3) Å^3
Z	8
Density (calculated)	1.292 Mg/m^3
Absorption coefficient	0.085 mm^{-1}
F(000)	1120
Crystal size	0.37 x 0.30 x 0.25 mm^3
Theta range for data collection	2.81 to 26.43°.
Index ranges	$-36 \leq h \leq 36, -7 \leq k \leq 7, -19 \leq l \leq 19$
Reflections collected	45774
Independent reflections	5473 [R(int) = 0.041]
Completeness to theta = 26.43°	99.7 %
Absorption correction	Semi-empirical from equivalents
Max. and min. transmission	0.9791 and 0.9693
Refinement method	Full-matrix least-squares on F^2
Data / restraints / parameters	5473 / 1 / 365

Goodness-of-fit on F^2	1.034
Final R indices [I>2sigma(I)]	R1 = 0.0358, wR2 = 0.0838
R indices (all data)	R1 = 0.0418, wR2 = 0.0875
Absolute structure parameter	1.4(8)
Largest diff. peak and hole	0.382 and -0.212 e.A^{-3}

B. X- ray Crystallographic and Structure Refinement Data of DS3

Empirical formula	$C_{21} H_{23} N O_2$	
Formula weight	321.40	
Temperature	100(2) K	
Wavelength	0.71073 Å	
Crystal system	Orthorhombic	
Space group	$Pca2_1$	
Unit cell dimensions	a = 8.6162(3) Å	$\alpha = 90°$.
	b = 8.3332(3) Å	$\beta = 90°$.
	c = 24.4604(8) Å	$\gamma = 90°$.
Volume	1756.27(11) $Å^3$	
Z	4	
Density (calculated)	1.216 Mg/m^3	
Absorption coefficient	0.078 mm^{-1}	
F(000)	688	
Crystal size	0.37 x 0.31 x 0.30 mm^3	
Theta range for data collection	2.44 to 30.12°.	
Index ranges	$-12 \leq h \leq 11, -11 \leq k \leq 11, -31 \leq l \leq 34$	
Reflections collected	33655	
Independent reflections	5063 [R(int) = 0.0318]	

Completeness to theta = 25.00°	99.9 %
Absorption correction	Semi-empirical from equivalents
Max. and min. transmission	0.9774 and 0.9721
Refinement method	Full-matrix least-squares on F^2
Data / restraints / parameters	5063 / 1 / 219
Goodness-of-fit on F^2	1.042
Final R indices [I>2sigma(I)]	R1 = 0.0332, wR2 = 0.0856
R indices (all data)	R1 = 0.0349, wR2 = 0.0870
Absolute structure parameter	0.6(6)
Largest diff. peak and hole	0.301 and -0.205 e.Å^{-3}

C. X- ray Crystallographic and Structure Refinement Data of DS4

Empirical formula	$C_{23}H_{27}NO_2$	
Formula weight	349.46	
Temperature	296(2) K	
Wavelength	0.71073 Å	
Crystal system	Monoclinic	
Space group	P2$_1$/c	
Unit cell dimensions	a = 24.8991(16) Å	$\alpha = 90°$.
	b = 8.3297(5) Å	$\beta = 90.363(4)°$.
	c = 9.9385(7) Å	$\gamma = 90°$.
Volume	2061.2(2) Å^3	
Z	4	
Density (calculated)	1.126 Mg/m^3	
Absorption coefficient	0.071 mm^{-1}	
F(000)	752	
Crystal size	0.53 x 0.35 x 0.15 mm^3	

Theta range for data collection	2.94 to 25.00°.
Index ranges	$-29 \leq h \leq 29, -9 \leq k \leq 9, -11 \leq l \leq 11$
Reflections collected	45485
Independent reflections	3612 [R(int) = 0.0441]
Completeness to theta = 25.00°	99.8 %
Absorption correction	Semi-empirical from equivalents
Max. and min. transmission	0.9896 and 0.9635
Refinement method	Full-matrix least-squares on F^2
Data / restraints / parameters	3612 / 0 / 238
Goodness-of-fit on F2	1.014
Final R indices [I-2sigma(I)]	R1 = 0.0659, wR2 = 0.1819
R indices (all data)	R1 = 0.1275, wR2 = 0.2462
Extinction coefficient	0.006(3)
Largest diff. peak and hole	0.306 and -0.140 e.$Å^{-3}$

D. X- ray Crystallographic and Structure Refinement Data of DS6

Empirical formula	$C_{27} H_{35} N O_2$	
Formula weight	405.56	
Temperature	100(2) K	
Wavelength	0.71073 Å	
Crystal system	Triclinic	
Space group	P-1	
Unit cell dimensions	a = 4.5096(13) Å	$\alpha = 77.883(15)°$.
	b = 11.728(3) Å	$\beta = 89.722(16)°$.
	c = 22.810(6) Å	$\gamma = 81.944(15)°$.
Volume	1167.5(5) $Å^3$	
Z	2	

Density (calculated)	1.154 Mg/m3
Absorption coefficient	0.071 mm-1
F(000)	440
Crystal size	0.50 x 0.22 x 0.19 mm3
Theta range for data collection	2.18 to 25.00°.
Index ranges	$-4 \le h \le 5, -13 \le k \le 13, -27 \le l \le 27$
Reflections collected	14809
Independent reflections	4036 [R(int) = 0.147]
Completeness to theta = 25.00°	97.8 %
Absorption correction	Semi-empirical from equivalents
Max. and min. transmission	0.9868 and 0.9655
Refinement method	Full-matrix least-squares on F2
Data / restraints / parameters	4036 / 0 / 274
Goodness-of-fit on F2	1.024
Final R indices [I>2sigma(I)]	R1 = 0.1094, wR2 = 0.2717
R indices (all data)	R1 = 0.2281, wR2 = 0.3265
Extinction coefficient	0.012(7)
Largest diff. peak and hole	0.370 and -0.371 e.Å-3

E. X- ray Crystallographic and Structure Refinement Data of DS7

Empirical formula	$C_{29} H_{39} N O_2$	
Formula weight	433.61	
Temperature	100(2) K	
Wavelength	0.71073 Å	
Crystal system	Triclinic	
Space group	P-1	
Unit cell dimensions	a = 4.5469(10) Å	$\alpha = 97.824(13)°$.

	b = 11.818(3) Å	β = 92.805(13)°.
	c = 23.823(5) Å	γ = 97.539(14)°.
Volume	1254.3(5) Å^3	
Z	2	
Density (calculated)	1.148 Mg/m^3	
Absorption coefficient	0.071 mm^{-1}	
F(000)	472	
Crystal size	0.32 x 0.32 x 0.10 mm^3	
Theta range for data collection	2.64 to 25.00°.	
Index ranges	$-5 \le h \le 5$, $-14 \le k \le 13$, $-28 \le 1 \le 28$	
Reflections collected	23474	
Independent reflections	4276 [R(int) = 0.155]	
Completeness to theta = 25.00°	96.4 %	
Absorption correction	Semi-empirical from equivalents	
Max. and min. transmission	0.9930 and 0.9776	
Refinement method	Full-matrix least-squares on F^2	
Data / restraints / parameters	4276 / 0 / 291	
Goodness-of-fit on F^2	1.037	
Final R indices [I>2sigma(I)]	R1 = 0.1025, wR2 = 0.2440	
R indices (all data)	R1 = 0.2099, wR2 = 0.2906	
Largest diff. peak and hole	0.494 and -0.354 e.Å^{-3}	

F. X- ray Crystallographic and Structure Refinement Data of DS8

Empirical formula	C$_{31}$H$_{43}$NO$_2$
Formula weight	461.68
Temperature	273 (2) K

Wavelength	0.71073 Å
Crystal system:	Triclinic
Space group	P-1

Unit cell dimensions	a = 4.7814(4) Å	$\alpha = 82.963(4)°$.
	b = 12.2533(12) Å	$\beta = 87.120(4)°$.
	c = 24.983(2) Å	$\gamma = 80.202(4)°$.

Volume	1430.9(2) $Å^3$
Z	2
Density (calculated)	1.069 Mg/m^3
Absorption coefficient	0.065 mm^{-1}
F(000)	502
Crystal size	0.30 x 0.20 x 0.20 mm^3
Theta range for data collection	2.4 to 17.60°.
Index ranges	$-4 \le h \le 4, -11 \le k \le 11, -22 \le l \le 22$
Reflections collected	14233
Independent reflections	2240 [R(int) = 0.155]
Completeness to theta = 25.00°	96.4 %
Absorption correction	Semi-empirical from equivalents
Max. and min. transmission	0.9930 and 0.9776
Refinement method	Full-matrix least-squares on F^2
Data / restraints / parameters	4276 / 0 / 291
Goodness-of-fit on F^2	1.109
Final R indices [I>2sigma(I)]	R1 = 0.1066, wR2 = 0.2503
R indices (all data)	R1 = 0.0788, wR2 = 0.2004
Largest diff. peak and hole	0.306 and -0.140 $e.Å^{-3}$

G. X- ray Crystallographic and Structure Refinement Data of DS12

Empirical formula	$C_{39}H_{59}NO_2$
Formula weight	573.89
Temperature	100 K
Wavelength	0.71073 Å
Crystal system	Monoclinic
Space group	P 21/c
Unit cell dimensions	a = 45.929(3) Å α= 90.00 °.
	b = 8.1824(6) Å β = 95.409(4)°.
	c = 9.1005(6) Å γ = 90.00°.
Volume	3404.8(4) $Å^3$
Z	4
Density (calculated)	1.120 Mg/m^3
Absorption coefficient	0.067 mm^{-1}
F(000)	1264
Crystal size	0.47 x 0.14 x 0.06 mm^3
Theta range for data collection	3.12 to 25.06 °.
Index ranges	$-54 < h \leq 54, -9 \leq k \leq 9, -10 \leq l \leq 10$
Reflections collected	52955
Independent reflections	4276 [R(int) = 0.155]
Completeness to theta = 25.00°	99.5 %
Absorption correction	Semi-empirical from equivalents
Max. and min. transmission	0.9692 and 0.9960
Refinement method	Full-matrix least-squares on F^2
Data / restraints / parameters	4276 / 0 / 291
Goodness-of-fit on F^2	1.017

Final R indices [I>2sigma(I)]	R1 = 0.0942, wR2 = 0.1247
R indices (all data)	R1 = 0.0539, wR2 = 0.1097
Largest diff. peak and hole	0.494 and -0.354 e. $Å^{-3}$

Curriculum Vitae

Shinto Varghese was born on 18 August, 1981, in Kerala, India. He had his early education at De-Paul English Medium High School, Choondal and completed his schooling in 1997. He obtained the degrees of Bachelor of Science and Master of Science from the Department of Chemistry, St. Thomas College, Thrissur, affiliated to The University of Calicut, in 2002 and 2005 respectively. Subsequently he qualified CSIR (JRF) and joined for the Ph. D. programme in Photosciences and Photonice section of National Institute for Interdisciplinary Science and Technology (CSIR) in April, 2005. Under the guidance of Dr. Suresh Das, he investigated the photophysical and materials aspects of functionalized stilbene based soft materials until November 2010. The results of his research are described in this thesis.

List of Publications

1. Formation of highly luminescent supramolecular architectures possessing columnar order from octupolar oxadiazole derivatives: Hierarchical self-assembly from nanospheres to fibrous gels. **Shinto Varghese**, N. S. S. Kumar, A. Krishna, D. S. Shankar Rao, S. K. Prasad, S. Das, *Adv. Funct. Mater.* **2009**, *19*, 2064.

2. Butadiene-based photoresponsive soft materials. S. Das, **Shinto Varghese**, N. S. S. Kumar, *Langmuir (Feature Article)* **2010**, 26, 1598.

3. Correlation between solid-state photophysical properties and molecular packing in a series of indane-1, 3-dione containing butadiene derivatives. N. S. Saleesh Kumar, **Shinto Varghese**, C. H. Suresh, N. P. Rath, S. Das, *J. Phys. Chem. C.* **2009**, *113*, 11927.

4. The influence of crystal packing on the solid state fluorescence behavior of alkyloxy substituted phenyleneethynylenes. R. Thomas, **Shinto Varghese**, G. U. Kulkarni, *J. Mater. Chem.*, **2009**, 19, 4401.

5. Solid state optical properties of 4-Alkoxy-pyridine butadiene derivatives: reversible thermal switching of luminescence. N. S. Saleesh Kumar, **Shinto Varghese**, Nigam P. Rath, S. Das, *J. Phys. Chem. C.* **2008**, *112*, 8429.

6. Hierarchical self-assembly of donor-acceptor substituted butadiene amphiphiles into photoresponsive vesicles and gels, N. S. Saleesh Kumar, **Shinto Varghese**, G. Narayan, S. Das. *Angew. Chem. Int. Ed.* **2006**, *45*, 6317.

Manuscripts to be communicated.

7. Thermally driven crystal to crystal transition and associated fluorescence changes in dialkoxy-cyano-substituted stilbenes, **Shinto Varghese**, Remyamol T., Aneesh P. S., Deepak D. Prabhu, Nigam P. Rath, S. Das.

8. Molecular packing and solid-state fluorescence of alkoxy-cyano substituted diphenylstilbenes, **Shinto Varghese**, Aneesh P. S., Nigam P. Rath, S. Das.

9. Correlation between molecular packing and solid-state fluorescence in organic π-conjugated materials, **Shinto Varghese** and Suresh Das (Perspective).

10. Concentration depended self-assembly from nano spheres to helices to multi-stranded nanofibers, **Shinto Varghese**, S. Das.

11. One-dimensional Nanorods with High Aspect Ratio and Shrinkage of Gel in a Trigonal Octupolar Derivative, **Shinto Varghese**, Aneesh P. S., S. Das.

Posters/Oral Presentations at Conferences

Oral presentations:

1. Self-assembling behaviour of trigonal oxadiazole derivatives, Shinto Varghese and Suresh Das, JNC Research conference on 'Chemistry of Materials' held at Cochin, 2-4, October, **2010**.

2. Hierarchical self-assembly from nanospheres to fibrous gels possessing columnar order from trigonal oxadiazole derivatives, Shinto Varghese and Suresh Das, Asian science seminar-2009 on frontiers in the 'Photocatalysis and Photochemistry of Advanced Materials' held at the Kanagawa Science Park (KSP) Hall in Kawasaki, Japan, 2-6 March, **2009**.

3. Luminescent discotics and gels from C_3-symmetric donor-acceptor oxadiazole derivative, ShintoVarghese, N. S. Saleesh Kumar, Anjali Krishna and Suresh Das, JNC Research conference on 'Chemistry of Materials' held at Munnar, 29-31, October, **2007**.

Posters presented:

4. Switching of luminescence in dialkoxy substituted stilbene derivatives, Shinto Varghese and Suresh Das, 11th CRSI National symposium in chemistry held at NCL Pune, India, 6-8, February, **2009**. (Received best poster award)

5. Luminescent discotics and gels from C_3-symmetric donor-acceptor oxadiazole derivatives, Shinto Varghese and Suresh Das, International conference on functional materials held at IIT Madras, Chennai, 27-29, November, **2008**. **(Received best poster award)**

6. Thermal switching of polymorphic forms of dialkoxy substituted cyanostilbene derivatives with distinctly different fluorescence. Shinto Varghese and Suresh Das, JNC Research Conference on 'Chemistry of Materials' held at Allapuzha, 13-15, October, **2008**.

7. Thermotropic liquid crystals and supramolecular aggregates of sugar containing photoresponsive Bolaamphiles, Gopinathan Narayan, Shibu Abraham, N. S. Saleeshkumar, Shinto Varghsese, Narayanaswamy Jayaraman and Suresh Das, JNC Research Conference on 'Chemistry of Materials' held at Quilon, 29-31, October, **2006**.